(MITNE - 83)

COMPUTER SIMULATION OF NEUTRON CAPTURE THERAPY

Arne Peter Olson

August, 1967

DEPARTMENT OF NUCLEAR ENGINEERING
MASSACHUSETTS INSTITUTE OF TECHNOLOGY
CAMBRIDGE, MASSACHUSETTS, 02139

PREPARED FOR
PHYSICS RESEARCH LABORATORY
MASSACHUSETTS GENERAL HOSPITAL
BOSTON, MASSACHUSETTS

Computer Simulation of

Neutron Capture Therapy

Arne Peter Olson

MITNE-83

Department of Nuclear Engineering
Massachusetts Institute of Technology
Cambridge, Massachusetts

August, 1967

Prepared for
Physics Research Laboratory
Massachusetts General Hospital
Boston, Massachusetts

COMPUTER SIMULATION

OF NEUTRON CAPTURE THERAPY

by

Arne Peter Olson

Submitted to the Department of Nuclear Engineering on August 21, 1967 in partial fulfillment of the requirement for the degree of Doctor of Science.

ABSTRACT

Analytical methods are developed to simulate on a large digital computer the production and use of reactor neutron beams for boron capture therapy of brain tumors. The simulation accounts for radiation dose distributions in tissue produced by fast neutrons and by neutron capture reaction products such as gamma rays, α-particles, protons, and heavy particles. These techniques are applied to optimize the effectiveness of the M.I.T. Reactor Medical Therapy Facility through a survey of the effects of neutron filters and of modifications to the beam collimation system. Neutron beams reflected from thin slabs of hydrogenous materials are shown to have an improved ability to effectively irradiate a deep tumor without destroying normal tissue above it because relatively few fast neutrons are reflected. Considerable improvements in thermal neutron distribution in tissue are shown to result from surrounding the head with a neutron-reflecting annulus to reduce lateral neutron leakage.

A new numerical solution is obtained for the problem of neutron transport in finite thickness slabs with isotropic scattering. Gaussian quadratures are used to evaluate the neutron transport integral equations, yielding transmission, absorption, and reflection probabilities, and fluxes, as a function of collision number. Collision history correlations are devised which use only five parameters to predict the fate of neutrons incident on an infinite slab having arbitrary thickness and neutron cross sections. A very fast multigroup neutron spectrum calculation is developed by combining collision history correlations with single-collision group transfer probabilities to directly obtain transmission and reflection matrices for multi-slab shielding problems.

Thesis Supervisor: Gordon L. Brownell
Title: Associate Professor of Nuclear Engineering

ACKNOWLEDGEMENTS

The author is deeply indebted to Professor Gordon L. Brownell for his constant enthusiasm and advice during the conduct of this work. Helpful discussions with Professors K. F. Hansen and N. C. Rasmussen are gratefully acknowledged. Dr. Reddy and Dr. Ayyangar of the Massachusetts General Hospital Physics Research Laboratory have worked in close association with the author to the benefit of all concerned, in order to relate their experimental program to the theoretical studies in this thesis. R. G. Fairchild, of the Medical Physics Division, Brookhaven National Laboratory, has been most helpful in comparing his experimental studies of epithermal neutron beams with a computer simulation by the author. This work would not have been possible without the Gerard Swope Fellowship awarded by M.I.T. for academic year 1964-65. Financial support from June 1965 to September 1967 in the form of a full-time Research Assistantship was provided by the Physics Research Laboratory (M.G.H.). The Physics Research Laboratory also provided computer time at the Harvard Computation Center from June 1965 to September 1966. Computing time since September 1966 has been provided by the Nuclear Engineering Department at the M.I.T. Computation Center.

BIOGRAPHICAL NOTE

The author was born in Kimberley, British Columbia, on August 9, 1939. He attended the University of British Columbia at Vancouver, British Columbia, Canada, from September 1958 to May 1962, and from September 1963 to May 1964. He was graduated in May 1964, with the degree of Bachelor of Applied Science in Engineering Physics. Aerodynamics was the minor program. The author was employed as a Research Technician by the Reactor Physics Division of Atomic Energy of Canada, Ltd., Chalk River, Ontario, from May 1962 to September 1963 and from May 1964 to September 1964. While at Chalk River he wrote two computer codes which have been extensively used for three-dimensional fuel management and lifetime studies of the NPD and CANDU heavy water power reactors. He is the author of three Chalk River Reports on this work:

"APOGEE - A Computer Program to Solve the One-Group Neutron Diffusion Equation in Three Dimensions". A.E.C.L.-1799 (CRRP-1159), July, 1963;

"PERIGEE - Computer Codes for Reactor Simulation in 3 Dimensions, Using 1 or 2 Neutron Velocity Groups". A.E.C.L.-1901 (CRRP-1184), Feb., 1964;

"Appendix I to A.E.C.L.-1901". A.E.C.L.-2095 (CRRP-1184), Sept., 1964.

While at Chalk River he met and married the former Carol Slater, a Second Grade teacher from Toronto. A daughter, Jennifer, is now one year old.

The author was awarded a Gerard Swope Fellowship by the Massachusetts Institute of Technology for academic year 1964-65. Concurrently awarded, but declined, was a National Research Council of Canada Fellowship and a University of Toronto Institute of Aerophysics Fellowship. He was a full-time Research Assistant in the Nuclear Engineering Department under Professor G. L. Brownell at the Massachusetts General Hospital from June 1965 to September 1967. Some of the work performed as a Research Assistant has been reported as follows:

"Computer Prediction of Neutron-Capture Therapy Radiation Dose for the M.I.T.R. Medical Therapy Facility Beam", Trans. Am. Nuc. Soc. 9, 74 (1966).

"Selection of Neutron Beam Characteristics for Neutron Capture Therapy", A. P. Olson and G. L. Brownell, TID-23054. Int. Conf. on the Use of Computers in Therapeutic Radiology, 14-17 June, 1966, Cambridge, England.

The author is a student member of the American Nuclear Society and the Engineering Institute of Canada.

TABLE OF CONTENTS

LIST OF FIGURES

LIST OF TABLES

CHAPTER I

INTRODUCTION

The purpose of this thesis is twofold: to develop analytical methods for simulating, via computer, the production and use of reactor neutron beams for boron capture therapy of brain tumors, and to apply these techniques to survey and optimize the effectiveness of the M.I.T. Reactor Medical Therapy Facility.

1.1 The M.I.T.R. MEDICAL FACILITY

The M.I.T.R. is an enriched uranium, heavy water moderated research reactor which normally operates at a power level of 5MW (thermal). The Medical Therapy Facility is a fully equipped surgical operating room located directly beneath the reactor core, as is shown in Figure 1.1. The room has thick concrete walls, a motor-driven sliding shielded door, and an oil-filled viewing window to allow operating personnel to control, observe, and monitor the irradiation from outside the room with negligible radiation hazard.

The operating table can be elevated hydraulically to position, the patient under the neutron beam port in the ceiling. Sheets of lithium fluoride-loaded plastic serve as a collimator to channel neutrons directly to the tissue to be irradiated, and lead sheets serve as a gamma-ray shield to protect the rest of the body.

The neutron beam passes through a collimator containing three shutters which are opened during irradiations. Radiation levels, with shutters closed, are low enough to permit working inside the room for limited periods of time during full power operation of the reactor.

The primary shield, nearest the reactor core, is a drainable tapered aluminum tank containing a thickness of about three feet of light water. Lead and boral plates located in the ceiling of the medical room comprise the

other two shutters. They shield gamma rays and thermal neutrons, respectively.

With all shutters open, neutrons leaving the core travel through 21.0 inches of heavy water, 9.81 inches of bismuth, 0.625 inches of aluminum, and 56.75 inches of air. Bismuth is used because it combines low neutron absorption with strong gamma ray attenuation. The heavy water, forming the lower reflector for the core, is a strong moderator of fast neutrons. Hence the emergent beam is well thermalized.

FIGURE 1.1
M.I.T. REACTOR

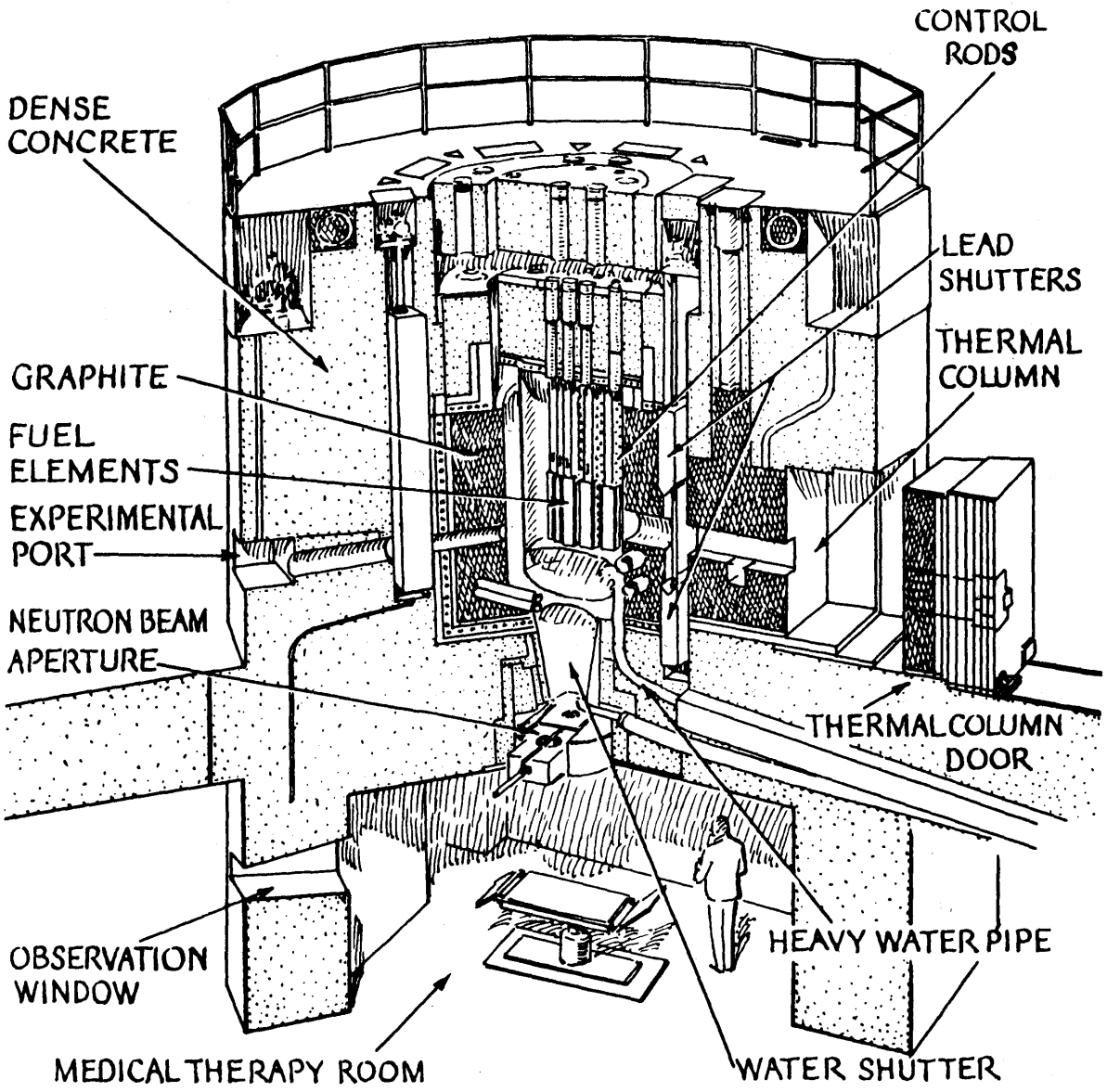

1.1.1 NEUTRON CAPTURE THERAPY

The medical use of thermal neutron beams for capture therapy to destroy tumor tissue was first proposed in 1936 by Locher.[1] If a suitable neutron capturing isotope could be preferentially concentrated in tumor tissue, neutron irradiation will produce a large local radiation dose to the tumor with minimal damage to normal cells. This technique is known as neutron capture therapy. In common with all forms of radiation therapy, it uses the fact that the survival probability of irradiated cells has a marked dose threshold. In order to minimize the damage to normal cells, one must first select an isotope whose neutron absorption reaction products have a short range in tissue. Then a non-toxic compound must be synthesized which strongly concentrates in tumor tissue. Finally, a neutron beam is required which is able to deliver a large thermal neutron flux to the tumor.

Sweet and Javid [2] demonstrated that boron could be preferentially concentrated in human brain tumor tissue to a sufficient degree to warrant attempts at therapy. Clinical trials were carried out at Brookhaven [3] and at the M.I.T.R. and the Massachusetts General Hospital. The disappointing results led to termination of patient irradiations in 1961 although basic chemical, biological, and physical studies have continued to the present time. The clinical trials demonstrated

the need for reduced B^{10} concentration in blood and blood vessels, improved dosimetry to monitor the irradiations, and improved neutron beam characteristics to maximize its effectiveness for neutron capture therapy.

The present status of boron capture therapy has recently been reviewed with particular attention to the properties of boron compounds.[4,5] Many compounds have recently been made and tested for toxicity and pharmacology. Both concentration and localization in tumor have been of particular interest. Three main classes of compounds have been considered:

I Boron-containing Antimetabolites
- A. Amino Acids
- B. Pyrimidines
- C. Purines

II Borono Proteins
- A. Tumor Antibodies

III Alkylating Agents Containing Boron

Group I compounds may interfere with tumor metabolism and replication, thereby inhibiting growth. They may also be capable of mimicking normal biological constituents and become readily incorporated into the tumor cell. Boron-labeled proteins of Group II have been synthesized with 1-3% boron by weight. It has been found that I^{131}-labeled antifibrin antibodies localize in tissues such as brain tumors. Attempts have been made to incorporate boron in such compounds. Group III compounds are known tumor growth inhibitors which have been altered by introducing a boron atom

within the molecule. Alkylating agents interact with tumor nucleic acids. The strategic location of a boron atom at the interaction site followed by neutron irradiation would have a profound effect on tumor growth by destroying its ability to replicate.

Two compounds have recently been synthesized[6] which look very promising.

Compound	Boron Concentration Ratio	
	Tumor/Blood	Tumor/Brain
$CS_2B_{12}H_{11}SH$	6:1	16:1
$Na_2B_{12}H_{11}SH$	8:1	25:1

They will be tested in humans within six months for toxicity and pharmacology. Irradiations will probably take place within a year at the M.I.T. reactor.

1.1.2 COMPUTER SIMULATION OF NEUTRON CAPTURE THERAPY

The need for improvements in neutron beam characteristics for neutron capture therapy has been clearly shown by the results of the clinical trials of several years ago. The enormity and cost of modifying the existing reactor collimator structure and experimentally analyzing the beam characteristics obviously precludes this approach. If, on the other hand, a reasonable physical model of this system could be coded for a large digital computer, the effects of hypothetical modifications to materials and geometrical arrangements could rapidly be surveyed. In addition, the computer studies would be of value both to analyze practical experiments and to suggest new experiments. These ideas form the rationale for this thesis.

1.2 CONTENTS

The physical model for neutron capture therapy involves describing the passage of polyenergetic neutrons from the reactor core through numerous and varied layers until finally the neutrons penetrate tissue - or a tissue-equivalent phantom head. Chapter II begins with a consideration of neutron transmission through infinite slabs in Section 2.1.1. Section 2.1.2 examines a new numerical integration solution to the transport equations based on solving for spatial distributions of neutrons suffering the same number of collisions. Collision history correlations are discussed in Section 2.1.3 to show how the solution for monoenergetic neutrons in a non-absorbing, non-multiplying slab yields solutions for all slabs of the same thickness but different absorption or multiplication. An approach to the problem of polyenergetic neutron transmission through slabs is presented in Section 2.1.4. Simpler approximations which have been used to obtain spectral shapes are discussed in Section 2.1.5.

One-dimensional spatial distributions of thermal neutron flux are obtained by replacing the second-order diffusion equation by a system of three coupled, linear, first-order differential equations, which can be numerically integrated. The derivation of this equation is presented in Section 2.2, along with a discussion of boundary conditions and the method of numerical integration.

Section 2.3 is concerned with the calculation of radiation dose rates from all sources in a tissue-equivalent phantom head of cylindrical shape, when bombarded by a beam of neutrons.

The use of scattered neutrons, rather than a direct beam, for neutron capture therapy, has many promising aspects. Methods used to attack this problem are discussed in Section 2.4.

Test Problem results are given in Chapter 3, Section 3.1, dealing with monoenergetic neutrons incident on thin infinite slabs which scatter neutrons isotropically in the lab. system. Comparisons are made with two other solutions to this problem which are referred to as the Markov Matrix Method and the Invariant Imbedding Method.

Fast Neutron transmission through 30 cm of polyethylene is a more practical, and difficult, test of the methods used to calculate neutron transmission. Section 3.2 deals with this problem, and draws comparisons with Invariant Imbedding results. Section 3.3 gives results for neutron transmission through a 40 cm thick slab of D_2O.

A rather extensive set of experiments was performed by R. G. Fairchild, using the Brookhaven Medical Research Reactor to evaluate the production and use of "epithermal" neutron beams for neutron capture therapy. Chapter IV is devoted to comparisons of this work and results obtained by computer.

Chapter V gives results for the M.I.T.R. Medical Facility, and deals successively with heavy water removal effects, thermal neutron filter effects, fast neutron filter effects, and the use of scattered neutrons.

Conclusions are given in Chapter VI, while Appendix A describes all computer codes used. Appendix B contains the bibliography.

CHAPTER II

MATHEMATICAL AND COMPUTATIONAL METHODS

2.1 EPITHERMAL AND FAST NEUTRON SPECTRA

Many shielding codes and methods have been developed for routine problems in reactor design. Highly accurate results are obtainable if the need justifies the cost in computer time and man-hours. However, for calculations involving numerous variations from a reference condition, such as a parametric survey, it is often easier to perform a few "bench-mark" calculations using the best possible methods, and to explore around the "bench-marks" by less accurate methods. For example, prediction of absolute neutron fluxes transmitted through a complicated shield is extremely difficult, whereas small departures from a given geometry can be predicted, relatively, with much less effort.

It is the purpose of this chapter to present a very fast method for performing polyenergetic neutron transmission and reflection problems, suitable for survey calculations, which has been used in conjunction with a few bench-mark calculations obtained by the method of Invariant Imbedding.

2.1.1 REFLECTION AND TRANSMISSION OF NEUTRONS FROM SLABS

The general problem to be considered is that of neutron reflection, absorption and transmission through a homogeneous plane infinite slab or series of slabs of arbitrary neutron cross sections. For simplicity, the single slab will be considered first.

The Transmission Matrix Method described by Aronson and Yarmush[7] offers a unified approach to the solution of a large variety of neutron transport problems in plane geometry. The formulation in terms of transfer matrices can be thought of as an alternative to the formulation in terms of the differential or integral linearized Boltzmann equations. A brief summary of the mathematical formulation of the Transmission Matrix Method is presented below, because its concepts carry over directly to the simplified treatment developed and used in this thesis.

Let $\vec{X}_1$ and $\vec{X}_2'$ be neutron fluxes incident from the left and right, respectively. They are functions of incident angle and neutron energy for a source-free slab. $\vec{X}_1'$ is the emergent flux on the right and $\vec{X}_2$ on the left. Assuming the problem is linear

$$\begin{aligned} \vec{X}_1' &= \underline{T}\vec{X}_1 + \underline{R}^*\vec{X}_2' \\ \vec{X}_2 &= \underline{R}\vec{X}_1 + \underline{T}^*\vec{X}_2' \end{aligned} \tag{2.1}$$

where $\underline{T}$ and $\underline{R}$ are transmission and reflection operators for neutrons incident from the left, and $\underline{T}^*$ and $\underline{R}^*$ for neutrons incident from the right. If the slab is symmetric, $\underline{T} = \underline{T}^*$, and $\underline{R} = \underline{R}^*$. Equations (2.1) may be solved for $\vec{X}_1'$ and $\vec{X}_2'$ to give in matrix form

$$\begin{bmatrix} \vec{X}_1' \\ \vec{X}_2 \end{bmatrix} = \underline{H} \begin{bmatrix} \vec{X}_1 \\ \vec{X}_2' \end{bmatrix} \tag{2.2}$$

where $\underline{H}$ is a 2 × 2 matrix of operators:

$$\underline{H} = \begin{bmatrix} \underline{T} - \underline{R}^*\underline{U}^*\underline{R} & \underline{R}^*\underline{U}^* \\ -\underline{U}^*\underline{R} & \underline{U}^* \end{bmatrix} \tag{2.3}$$

with

$$\underline{U} = \underline{T}^{-1}, \quad \underline{U}^* = (\underline{T}^*)^{-1} \tag{2.4}$$

Equation (2.2) yields a composition law for $\underline{H}$ matrices:

$$H = \underline{H}_n \cdots \underline{H}_2 \underline{H}_1 \tag{2.5}$$

for n layers, with $\underline{H}_i$ associated with the i-th layer. For a two-layer problem one obtains total transmission $\underline{T}$ and total reflection $\underline{R}$ as follows:

$$\begin{aligned} T &= \underline{T}_2 (\underline{I} - \underline{R}^*_1 \underline{R}_2)^{-1} \underline{T}_1 \\ &= \underline{T}_2 (\underline{T}_1 + \underline{R}^*_1 \underline{R}_2 \underline{T}_1 + (\underline{R}^*_1 \underline{R}_2)^2 \underline{T}_1 + \cdots) \\ &= \underline{T}_2 \sum_{n=o}^{\infty} (\underline{R}^*_1 \underline{R}_2)^n \underline{T}_1 \end{aligned} \tag{2.6}$$

$$\begin{aligned} R &= \underline{R}_1 + \underline{T}_1^* (\underline{I} - \underline{R}_2 \underline{R}_1^*)^{-1} \underline{R}_2 \underline{T}_1 \\ &= \underline{R}_1 + \underline{T}_1^* \underline{R}_2 (\underline{I} - \underline{R}_1^* \underline{R}_2)^{-1} \underline{T}_1 \\ &= \underline{R}_1 + \underline{T}_1^* \underline{R}_2 \sum_{n=o}^{\infty} (\underline{R}_1^* \underline{R}_2)^n \underline{T}_1 \end{aligned} \tag{2.7}$$

The series expansions (2.6) and (2.7) have a simple physical interpretation. For instance, $\underline{T}_1^* \underline{R}_2 (\underline{R}_1^* \underline{R}_2)^n \underline{T}_1$ represents transmission through slabs 1, n pairs of reflections back and forth at the interface, a final reflection from slab 2, and transmission back through slab 1.

The problem is to obtain the $\underline{H}$-matrix in terms of physical properties of the slab. A new matrix $\underline{W}$ depending only on the neutron cross sections can be formulated. For a slab of thickness t:

$$\underline{H} = \exp\ (-\underline{W}t)$$

is the formal relationship required. Up to this point, everything is exact. But to deal with a real problem, a discrete representation of neutron energy and angle must be chosen. This converts integral operators to matrices, and one obtains a mathematical system which can be solved on a large digital computer.

The particular concepts taken from the Transmission Matrix Method and used in this thesis are expressed by Equations (2.6) and (2.7). A method has been developed which directly yields the transmission and reflection matrices $\underline{T}_1$, $\underline{T}_2$, $\underline{R}_1$, $\underline{R}_2$, from which $\underline{T}$ and $\underline{R}$ are obtained by use of (2.6) and (2.7).

The original concept for the calculation of the reflection and transmission operators $\underline{R}_i$, $\underline{T}_i$ (for slab i) stemmed largely from the work of Eaton and Huddleston[8] on a Markov Matrix Method for slab problems. They consider a homogeneous, infinite slab of thickness L with macroscopic absorption, scattering, and total cross sections of Σ_a, Σ_s, and $\Sigma_t = \Sigma_a + \Sigma_s$. The probabilities for scatter and absorption at a collision are $c = \Sigma_s/\Sigma_t$, and $1 - c = \Sigma_a/\Sigma_t$,

respectively. Scattering is assumed to be isotropic in the laboratory system.

In order to apply the Markov chain concept, the slab must be conceptually divided into n discrete layers each of thickness $s = L/n$, where $s \ll 1/\Sigma_t$. Upon including the semi-infinite voids on either side of the slab, one obtains $n + 2$ Markov states. The probability that a neutron incident at polar angle θ_o has its first collision in the i-th state (layer) is

$$P(i) = \int_{(i-1)s}^{is} \sec\theta_o \, \Sigma_t \exp\left(-\Sigma_t \sec\theta_o \, t\right) dt$$

$$= \exp\left[-\Sigma_t \sec\theta_o \, (i-1)s\right] - \exp\left(-\Sigma_t \sec\theta_o \, is\right),$$

$$i = 1, 2, \cdots n \qquad (2.8)$$

and

$$P(0) = 0 \text{ (no impacts in a void)}$$

$$P(n+1) = \int_L^\infty \Sigma_t \sec\theta_o \exp(-\Sigma_t \sec\theta_o \, t) \, dt \qquad (2.9)$$

$$= \exp\left(-\Sigma_t \sec\theta_o \, L\right)$$

$$= \text{uncollided transmission probability.}$$

These probabilities are the ordered elements of the Markov initial state vector $\vec{V}_1$:

$$\vec{V}_1 = \left[P(0),\ P(1),\ \cdots\ P(n),\ P(n+1)\right] \tag{2.10}$$

Now a transition matrix $\underline{M}$ is required such that

$$\vec{V}_{j+1} = \vec{V}_j\ \underline{M}, \qquad j = 1, 2, \cdots \infty \tag{2.11}$$

where the 1-th element in any $\vec{V}_j$ approximates the probability that the neutron will experience a j-th impact in the i-th layer.

Now define the element $M_{\ell k}$ of $\underline{M}$ as approximately the probability that if the last impact was in layer ℓ, the next impact will be in layer k. We need to know the probability distribution of collisions, h(x), as a function of distance, x, measured from a given impact depth (perpendicular to the slab face) to the next impact depth. This problem is identical to finding the neutron flux from an infinite plane isotropic source of unit strength at a perpendicular distance, x, in a medium with total macroscopic cross section Σ_t.

The flux ϕ is given by

$$\begin{aligned}\phi(x) &= \iint \frac{\exp\ (-\Sigma_t\ |x|\ \sec\ \theta)}{4\pi r^2}\ dA \\ &= \frac{1}{2} \int_1^\infty \exp\ (-\Sigma_t\ |x|\ u)\ \frac{du}{u} \\ &= \frac{1}{2}\ E_1\ (\Sigma_t\ |x|)\end{aligned} \tag{2.12}$$

where

$$r = x \tan \theta$$

$$dA = 2\pi r dr = 2\pi x^2 \sin \theta d\theta / \cos^3 \theta \qquad (2.13)$$

$$E_n = (g) = \int_1^\infty \exp(-g u) \frac{du}{u^n}$$

then

$$h(x) = \Sigma_t \phi(x) = \frac{1}{2} \Sigma_t E_1 (\Sigma_t |x|) \qquad (2.14)$$

$$M_{\ell k} = c \int_{(\ell - \frac{1}{2})s - (k-1)s}^{(\ell - \frac{1}{2})s - ks} h(x)\, dx, \quad 1,k \quad 1,2, \cdots n \qquad (2.15)$$

For transitions outside the slab ($k = 0$ or $n + 1$), one of the integration limits becomes infinity.

It is assumed that collisions in a layer occur at its midpoint. Repeating the problem for smaller s and extrapolating to the limit as $s^2 \to o$ removes this inaccuracy. However, this limits the method to thin slabs with $\Sigma_t L \leq 1$.

What one has obtained in this manner is really an approximation to the flux of j-th collision neutrons, as one could write

$$\vec{V}_j = \Sigma_t \vec{\phi}_j \qquad (2.16)$$

with elements of $\vec{\phi}_j$ being approximate fluxes in each state or layer. The method amounts to tabulation of reflection, transmission, and absorption as a function of collision number.

In terms of the j-th collision fluxes, we have

$$\phi_{j+1}(x_o) = \int_o^L \phi_j(x)\, \Sigma_s \frac{E_1}{2} (\Sigma_t |x - x_o|)\, dx \quad (2.17)$$

If the integral is approximated as a sum, assuming some average flux $\hat{\phi}_{jk}(x_k)$ in each state or layer k, then

$$\hat{\phi}_{j+1,\ell}(x_\ell) \simeq \sum_k \hat{\phi}_{jk}(x_k) \int_{x_k - s/2}^{x_k + s/2} \Sigma_s \frac{E_1}{2} (\Sigma_t |x - x_\ell|)\, dx \quad (2.18)$$

$$= \sum_k \hat{\phi}_{jk}(x_k) \frac{\Sigma_s}{\Sigma_t} \int_{x_k - s/2}^{x_k + s/2} \Sigma_t \frac{E_1}{2} (\Sigma_t |x - x_\ell|)\, dx \quad (2.19)$$

or

$$\hat{\phi}_{j+1,\ell}(x_\ell) \simeq \sum_k \hat{\phi}_{jk}(x_k)\, M_{\ell k}, \quad (2.20)$$

using the definition of $M_{\ell k}$. Now forming a vector $\vec{\phi}_{j+1}$ whose ℓ-th element is $\sum_k \hat{\phi}_{jk}(x_k)\, M_{\ell k}$, we find that

$$\vec{\hat{\phi}}_{j+1} = \vec{\hat{\phi}}_j \underline{M} \tag{2.21}$$

and

$$\vec{V}_{j+1} = \vec{V}_j \underline{M}, \quad \text{as} \quad \Sigma_t \vec{\phi}_j = \vec{V}_j \tag{2.22}$$

This analysis indicates that the Markov Matrix Method amounts to numerically integrating the transport equation (2.17), assuming some average flux in each layer. As the sub-layer thickness approaches 0, one obtains the flux at that point. If one numerically integrated the right hand side of (2.17) without assuming some average flux in a sub-layer, then the need for going to many sub-layers could be sidestepped. One then would have a method of solution usable on slabs of several mean free paths thickness.

It will be useful to obtain another distribution function, $g(|x-x_o|)$, similar to $h(x)$ of Equation (2.14), but which gives the uncollided current for a neutron arriving at x_o having last collided at x.

$$g(|x-x_o|) = \iint \frac{\exp(-\Sigma_t |x-x_o| \sec\theta_o) \cos\theta dA}{4\pi r^2} \tag{2.23}$$

$$= \frac{1}{2} E_2(\Sigma_t |x-x_o|),$$

using Equations (2.13).

Now assume that the flux incident on the slab is $S(\mu)$, with $\mu=\cos\theta$, and θ the polar angle. The uncollided flux at depth x in the slab is

$$\phi_o(x) = \int_0^1 S(\mu)\ \exp\ (-\Sigma_t\ x/\mu)\ d\mu \qquad (2.24)$$

For a beam at angle θ_o, $S(\mu) = S'\ \delta(\mu - \mu_o)$, and $\phi_o(x) = S'\ e^{-\Sigma_t\ x/\mu_o}$. If the source emits neutrons such that $S(\mu) = S_m\ \mu^m$, then defining $u = 1/\mu$,

$$\begin{aligned}\phi_o(x_o) &= S_m \int_0^1 \mu^m\ \exp\ (-\Sigma_t\ x/\mu)\ d\mu \\ &= S_m \int_1^\infty \exp\ (-\Sigma_t\ x\ u\ )\ \frac{du}{u^{m+1}} \\ &= S_m\ E_{m+1}\ (\Sigma_t\ x)\end{aligned} \qquad (2.25)$$

Taking $S_m = m$ implies a unit forward-directed current incident on the slab.

At this point, the equations describing the flux of 1st collision neutrons, and transmission and reflection of 1st collision neutrons are:

$$\begin{aligned}\phi_1\ (x_o) &= c' \int_0^L \phi_o\ (x)\ h(|x-x_o|)\ dx, \\ R_1(0) &= c\int_0^L \phi_o\ (x)\ g\ (x)\ dx \\ T_1(L) &= c\int_0^L \phi_o\ (x)\ g\ (|L-x|\ )\ dx\end{aligned} \qquad (2.26)$$

$c' = c/\mu$, for an incident beam at angle $\theta = \cos^{-1}\mu$

$= c$, otherwise

Changing variables to $w = \Sigma_t x$, and writing equations (2.26) for n-th collision fluxes:

$$\phi_n(w_0) = \frac{c}{2}\left\{ \int_0^{\Sigma_t w_0} \phi_{n-1}(w)\, E_1(w_0-w)\, dw + \int_{\Sigma_t w_0}^{\Sigma_t L} \phi_{n-1}(w) E_1(w-w_0)\, dw \right\}$$

$$R_n(0) = \frac{c}{2} \int_0^{\Sigma_t L} \phi_{n-1}(w)\, E_2\,(w)\, dw \qquad (2.27)$$

$$T_h(\Sigma_t L) = \frac{c}{2} \int_0^{\Sigma_t L} \phi_{n-1}\,(w)\, E_2\,(\Sigma_t L - w)\, dw$$

The ϕ-equation may be written

$$\phi_n(w_0) = \frac{c}{2} \int_0^{\Sigma_t w_0} \phi_{n-1}(w_0-z)\, E_1(z)\, dz + \frac{c}{2} \int_0^{\Sigma_t (L-w_0)} \phi_{n-1}(w_0+z) E_1(z) dz \qquad (2.28)$$

For a beam incident at polar angle θ, with $\mu = \cos\theta$, only the calculation of first collision flux requires the factor of $1/\mu$. It arises because the probability of first collision in dx around x is $\Sigma_t dx/\mu$.

2.1.2 NUMERICAL SOLUTION OF TRANSPORT EQUATIONS

It can be seen from Equations (2.27) and (2.28), that the integrals are all of the following form:

$$I_p \Big|_0^v = \int_0^v f(z)\, E_p(z)\, dz, \quad p=1 \text{ or } 2 \tag{2.29}$$

One may approximate this integral to arbitrary accuracy, by the method of Gaussian quadratures. That is,

$$I_p \Big|_0^v = \int_0^v f(z)\, E_p(z)\, dz \simeq \sum_{j=1}^{m} a_j f(z_j) \tag{2.30}$$

where m is the order, a_j are the weights, and z_j are the nodes of the quadrature formula. For the usual Gaussian quadratures, the method is exact for $f(z)$ a polynomial of degree less than or equal to $2m - 1$.

It remains to show how to obtain the a_j and z_j, which are functions of the upper limit of integration v. First the moments of $E_p(z)$ are found:

$$\alpha_p^{\ell}(v) \equiv \int_0^v z^{\ell}\, E_p(z)\, dz, \quad \ell = 0, 1, 2, \cdots 2m - 1 \tag{2.31}$$

$$= \sum_{j=1}^{m} a_j\, z_j^{\ell}, \quad \ell = 0, 1, 2, \cdots 2m - 1 \tag{2.32}$$

Equations (2.32) are a non-linear system of $2m$ equations in $2m$ unknowns, whose solution yields the desired a_j and z_j.

It can be shown[9] that the extremely difficult numerical solution of Equations (2.32) is not necessary, since the problem is equivalent to solving two sets of m linear equations in m unknowns. One writes

$$\alpha_p^{i+\ell} \sum_{j=1}^{m} a_j \, z_j^{i+\ell}, \qquad \ell = 0, 1 \ldots m; \quad 0 \leq i \leq m-1 \tag{2.33}$$

Then

$$\alpha_p^{i+m} + \sum_{\ell=0}^{m-1} c_\ell \, \alpha_p^{i+\ell} = 0, \qquad i = 0, 1, \ldots m-1 \tag{2.34}$$

and the new unknowns c_ℓ introduced here are easily obtained from this linear system. One then has a polynomial

$$F(z) = z^m + \sum_{\ell=0}^{m-1} c_\ell \, z^\ell \tag{2.35}$$

whose m roots occur at the nodes z_j. Extracting the roots numerically and substituting them into any m of Equations (2.32), gives a new set of m linear equations in the m weights a_j. For simplicity, the first m of equations (2.32) are used.

The analytical results for the moments $\alpha_p^{\ell}(v)$ of Equations (2.32) are:

$$\alpha_1^{\ell}(v) = \left\{ v^{\ell+1} E_1(v) - e^{-v}\left[v^{\ell} + \ell v^{\ell-1} + \ldots + \ell!\right] + \ell!\right\}/(\ell+1),$$

$$\alpha_2^{\ell}(v) = \frac{v^{\ell+1}}{\ell+1}\left[E_2(v) + \frac{v}{\ell+2} E_1(v)\right] - \frac{e^{-v}}{(\ell+1)(\ell+2)}$$

$$\times \quad \left[v^{\ell+1} + (\ell+1)v + \ldots + (\ell+1)!\right] + \frac{\ell!}{\ell+2} \tag{2.36}$$

However, it was found that for slabs of a few mean free paths thickness, moments above $\ell \approx 6$ gave highly erroneous results. This was because the moment was a small difference between two large numbers. Consequently Gaussian integration was used.

Kronrod[10] has tabulated 16 place tables of nodes and weights for an improved Gaussian Quadrature which is claimed to be exact for functions of order $3m - 1$ or less. His formula is

$$\int_a^b f(x)dx \simeq (b-a) \sum_{i=1}^{m+1} \left[f(a+(b-a)\, x_i) + f(b-(b-a)x_i)\right] w_i \tag{2.37}$$

where x_i are the nodes and w_i are the weights. The increased accuracy is partly due to the fact that his m-th order formula

uses $2m+1$ points. In any case, for $m=10$, his formula yields a relative error of 10^{-8} for $a=-1$, $b=1$, for $f(x)$ a 36-th degree polynomial. Many of the calculations have been done using this order quadrature. Table 2.1 lists nodes and weights for $m=10$. For slabs several mean free paths thick, some gains in accuracy were obtained by doing the integration over sub-intervals of a mean free path and going to $m=20$. The limiting factor appeared to be the accuracy of obtaining the exponential integral functions E_1 and E_2 not the quadrature formula.

Series expansions and rational approximations were both used to obtain the functions E_1 and E_2, but only about 6 figure accuracy was attained. Ultimately, a Share Library Subroutine [11] was obtained which evaluated

$$E_i(x) = -\int_{-x}^{\infty} e^{-t}\, dt/t \qquad (2.38)$$

from which is found

$$E_1(x) = -E_i(-x); \quad E_2(x) = e^{-x} - xE_1(x) \qquad (2.39)$$

Accuracy was 7 to 8 decimal places, sufficient to handle slabs five mean free paths thick. Thicker slabs can, of course, be made up with several thin slabs, and the Transmission Matrix Method applied.

TABLE 2.1. 10-th Order Improved Gaussian Quadrature Nodes and Weights

I	x_i				w_i			
1	.0021	7141	8487	0960	.0058	4731	9433	6859
2	.0130	4673	5741	4141	.0162	7908	1153	9824
3	.0349	2125	4322	1459	.0273	7794	8287	1760
4	.0674	6831	6655	5077	.0375	1983	7405	4600
5	.1095	9113	6706	7916	.0465	6272	7291	8488
6	.1602	9521	5850	4878	.0546	9357	9401	1488
7	.2186	2143	2665	6977	.0617	4598	8131	0329
8	.2833	0230	2935	3764	.0673	5460	8655	7367
9	.3528	0356	8649	2699	.0713	8796	9288	5300
10	.4255	6283	0509	1844	.0738	6955	2450	6692
11	.5000	0000	0000	0000	.0373	6138	8500	7292

The various systems of linear equations were solved by the Gauss elimination method, using Share Library Subroutine LEQ.[12] Two methods were tried for extracting roots of a polynomial. Share Subroutine RTSCH[13] was very slow, and was abandoned in favor of Share Subroutine MULLER[14] which used a straight-forward Newton's method.

It is necessary to know $\phi_{n-1}(w)$ for all w in order to evaluate the integrals of Equations (2.27). Assume an m-th order Gaussian quadrature. It is convenient to evaluate $\phi_n(w_0)$ at w_{0j} and $\Sigma_t L - w_{0j}$ given by the nodes used for the calculation of the reflection and transmission. Then

$$R_n(0) = \sum_{j=1}^{m} \phi_{n-1}(w_{0j})\, a_j$$

$$T_n(\Sigma_t L) = \sum_{j=1}^{m} \phi_{n-1}(\Sigma_t L - w_{0j})\, a_j \qquad (2.40)$$

Fluxes are also calculated at each surface of the slab. In effect, $2m + 2$ fluxes are calculated, from which fluxes at all other points are obtained by Lagrangian interpolation[15] (usually of order $2m+2$). The fluxes are quite smooth,

changing from exponential behaviour to a symmetrical cosine shape, as the number of collisions increases. Hence, errors in numerical interpolation are not large, even for small m.

Although considerable computing time is involved in obtaining quadrature weights and nodes for each slab thickness desired, once obtained they need not be recalculated in order to deal with the same thickness (mean free paths, $\Sigma_t L$) but for a different neutron source or different ratio of Σ_s to Σ_t.

2.1.3 COLLISION HISTORY CORRELATIONS

Solving equations (2.27) for $c = 1$ gives solutions for all other values of c. Such a happy result can only occur in a method which follows the neutrons, one collision at a time. Evidently, from (2.27)

$$T_n^c(\Sigma_t L) = c^n T_n^1(\Sigma_t L)$$
$$R_n^c(0) = c^n R_n^1(0) \tag{2.41}$$

Now if one defines a quantity TOT_k as the flux of k-th collision neutrons which have neither been absorbed, transmitted, or reflected out of the slab, then

$$TOT_0^c = 1 - T_0; \quad T_0 = \text{transmitted uncollided flux;}$$
$$TOT_1^c = c\,(TOT_0 - R_1^1 - T_1^1)$$
$$\vdots$$
$$TOT_n^c = c^n \left[TOT_0 - \sum_{\ell=1}^{n} (R_\ell^1 + T_\ell^1)\right] \tag{2.42}$$

and the absorption of the n-th collision neutrons is

$$A_n^c = (1 - c)\, c^{n-1} \left\{ TOT_0 - \sum_{\ell=1}^{n-1} (R_\ell^1 + T_\ell^1) \right\} \tag{2.43}$$

Therefore a tabulation of transmission and reflection probabilities, obtained for $c=1$ as a function of number of collisions, can be simply used to solve the same slab problem for arbitrary values of c. Empirical correlations are given in Section 3.1.1 from which only three parameters are required in order to find, for example, the probability of transmission through any slab with any value of c, having undergone any number of collisions.

2.1.4 MULTIGROUP SPECTRA

Generally, shielding problems involve only one source of neutrons. Some simplification results in Equations (2.1) and (2.2) if $\vec{X}_2' = 0$. We want to find the transfer matrix $\underline{T}$. The matrix product of $\underline{T}$ with the neutron source $\vec{X}_1$ gives the output flux vector $\vec{X}_1'$. Contributions to $\underline{T}$ come from neutrons suffering any number of collisions. Section 2.1.3 has shown how to obtain monoenergetic neutron transmission (and reflection) probabilities through slabs, as a function of collision number. If one could combine these probabilities with multigroup transition probabilities, then $\underline{T}$ (or $\underline{R}$) could be found.

The uncollided flux is best handled separately from the collided flux as its attenuation is known analytically. It cannot transfer from group to group. Now define:

$\sigma_{i\to j}$ = Microscopic cross section for transfer of a neutron from group i to group j as a result of a single collision.

σ_{ti} = Total microscopic cross section for group i.

$f_{ij} = \sigma_{i\to j}/\sigma_{ti}$ = Probability of a neutron in group i transferring to group j as a result of a single collision.

The transfer probability f_{ij} depends only on the details of the kinematics of scattering, not on the spatial or

angular distribution of neutron flux. Let matrix $\underline{F}$ have elements f_{ij}. Assuming no upscattering in energy, f_{ij} vanishes for $j < i$, if the lowest numbered neutron group has the highest energy. $\underline{F}$ then is a square upper-triangular matrix of order NG, the number of energy groups. Let diagonal matrix $\underline{P}_n$ have diagonal elements P_{nii} which are the probability of transmission of group i neutrons after n collisions. Then

$$\vec{X}_1' = \underline{T}\,\vec{X}_1 = \left[\underline{P}_1\,\underline{F} + \underline{P}_2\underline{F}^2 + \underline{P}_3\underline{F}^3 + \ldots\right]\,\vec{X}_1 \qquad (2.44)$$

and the transfer matrix is

$$\underline{T} = \left[\underline{P}_1\underline{F} + \underline{P}_2\underline{F}^2 + \underline{P}_3\underline{F}^3 + \ldots\right] \qquad (2.45)$$

where

$$\underline{F}^3 = \underline{F}\,\underline{F}\,\underline{F}, \text{ etc.} \qquad (2.46)$$

Given matrices $\underline{P}_n$ and $\underline{F}$, $\underline{T}$ can be obtained to arbitrary precision by summing terms $\underline{P}_n\underline{F}^n$ to sufficiently high n. The decision as to how high n must be is simply made by ensuring that the diagonal elements of $\underline{T}$ satisfy

$$\left|T_{ii}^{(n)} - T_{ii}^{(n-1)}\right| / T_{ii}^{(n)} < \epsilon, \quad i = 1, 2, \ldots NG \qquad (2.47)$$

Epsilon is an arbitrarily small number usually taken to be about 10^{-3} to 10^{-4}. Numerical results indicate that the accuracy of $\vec{X}_1'$ is of about the same order as ϵ.

Neutron total cross sections as a function of energy need not be flat, as the transmitted neutron flux of k-th collision neutrons is based on transmission probabilities for the groups that the neutrons occupy after k collisions. A more subtle assumption is that the k-th collision flux shapes across the slab are the same for all groups. Transmission (and reflection) probabilities depend mainly on the flux shape near the slab surface. After many collisions, the neutron flux shape becomes symmetrical across the slab, independent of the location of the incident neutron beam. In effect, the neutrons have undergone enough collisions to "forget" where they came from. Section 3.1.1 will present flux shapes for a wide range of total cross sections and a given slab thickness, in order to assess the importance of this effect. Intuitively, one would expect best results for materials with slowly varying total cross sections.

2.1.5 SIMPLER APPROXIMATIONS

Prior to the development of the simplified Transmission Matrix Method described in preceding sections of Chapter II, some success was obtained in predicting spectrum shapes using a more approximate calculation of the Transfer Matrix $\underline{T}$. Experimental information such as fast neutron dose rates was used to normalize the absolute magnitude of the spectrum.

Consider, for example, an infinite, plane isotropic source emitting one neutron/second in the forward direction through a homogeneous, plane, infinite slab with macroscopic total cross section Σ_t. The forward-directed uncollided current fraction is $E_2(\Sigma_t x)$ at a distance x perpendicular to the slab face. The collided fraction is $1 - E_2(\Sigma_t x)$, which is made up of neutrons suffering any number of collisions. However, the probability for survival of a lst-collision neutron is $c(1 - E_2(\Sigma_t x))$. If one assumes that the probability for surviving k collisions is $\left\{c\left[1 - E_2(\Sigma_t x)\right]\right\}^k$ then matrix $\underline{P}_k$ of Equation (2.44) becomes $(\underline{P}_1)^k$. This amounts to assuming that the flux shape of k-th collision neutrons is the same as for lst collision neutrons. The error in this assumption increases with slab thickness, because the flux shapes change more.

Group transfer probabilities f_{ij} can be obtained directly from tabulated neutron cross section sets such as given by Bondarenko [16]. Slowing down cross sections not available in the literature can be approximated in the

following manner. Take the same width, Δu, in lethargy units, for all neutron groups. Let ξ be the average lethargy decrement per scattering collision. Microscopic elastic scattering and total cross sections are σ_{se} and σ_t, respectively. The average number of collisions required to transfer to another group is $\Delta u/\xi$. Then the probability of transfering to the next lethargy group is approximately $\left\{ \frac{\sigma_{se}}{\sigma_t} \left[1 - E_2(\Sigma_t L) \right] \right\}^{\Delta u/\xi}$ for a slab of thickness L. The Bondarenko set gives the elastic slowing-down cross section σ_{de}, obtained by averaging over a flat flux per unit lethargy within the groups for energies less than 1 MeV, and over a fission spectrum for $E > 1$ MeV. Then the more accurate result is

$$f_{i \to i+1} = \sigma_{de}/\sigma_t \tag{2.48}$$

for elastic scattering. Inelastic scattering contributes to f_{ij} as well:

$$f_{i \to j} = \sigma_{in}(i \to j)/\sigma_t \tag{2.49}$$

Transport-corrected cross sections can be obtained which yield improved results. They are

$$\begin{aligned} \sigma_{tr} &= \sigma_t - \mu_e(\sigma_e - \sigma_d) \\ \sigma_{dtr} &= \sigma_d(1 - \mu_e) \end{aligned} \tag{2.50}$$

The average cosine of the elastic scattering angle is given by μ_e. Transport-correcting the inelastic scattering cross sections (or elastic group transfer cross sections for light elements) is also possible, but requires considerable elaboration in order to account for the small-angle scattered neutrons which appear to be uncollided, but in fact have changed energy groups. Inclusion of this effect would undoubtedly lead to further improvements in accuracy.

2.1.6 THE INVARIANT IMBEDDING METHOD

In addition to utilizing experimental data as checks on calculations, a few highly accurate "bench mark" results have been obtained by the Invariant Imbedding Method with the "STAR" code written by Mathews.[17] Bellman et al[18] have described it as a perturbation method, the system size being perturbed. The calculation of reflection and transmission of neutrons through slabs is obtained by a detailed study of particle processes in a differential layer of material added between the source and the slab, from which a first-order coupled set of nonlinear differential equations may be derived and numerically integrated.

Calculations were made using four energy groups in the range of 0.1 to 10 MeV, and two angular groups (equivalent to a P_3-calculation by the Spherical Harmonics Method). Group widths in MeV and unit cosine of the polar angle are selected via Gaussian quadratures, which limits the code to at most a two-decade energy range.

A four-stage process is involved in making best use of STAR. First, angular cross section data must be reduced to Legendre polynomial form. A special code, LPF-LEGENDRE POLYNOMIAL FITS, was written for this task. Appendix A.3 describes it. Second, the companion code to STAR known as CSDP-CROSS SECTION DATA PREPARATION,

takes the angular and energy dependent cross sections from LPF and calculates transfer probabilities between states (a state is defined as any angular and energy group). Appendix A.5 describes modifications made to CSDP, and A.6 describes modifications made to STAR. Third, the output from CSDP is supplies to STAR, and reflection and transmission matrices computed and punched on cards for use by stage four. The final operation of generating reflected and transmitted fluxes for a neutron source of arbitrary energy and angle dependence is performed by another special code called STAR DATA REDUCTION, in Appendix A.4. It combines source information with the transmission and reflection matrices to compute angular fluxes, differential fluxes per unit energy and lethargy and fast neutron dose rates. Similar output comes from STAR, but for a unit, isotropic fission source.

2.2 THERMAL NEUTRON FLUX

Diffusion theory yields the neutron balance equation in a non-multiplying medium with diffusion length L:

$$\nabla^2 \phi - \frac{1}{L^2} \phi = 0 \qquad (2.54)$$

In circular cylindrical geometry this becomes

$$\frac{\partial^2 \phi}{\partial \chi^2} + \frac{1}{r} \frac{\partial}{\partial r} \left(r \frac{\partial \phi}{\partial r} \right) + \frac{1}{r^2} \frac{\partial^2 \phi}{\partial \theta^2} - \frac{1}{L^2} \phi = 0 \qquad (2.55)$$

Assuming $\phi (r, \theta, \chi) = \chi(\chi, \theta) \psi (r)$

$$\frac{1}{r} \frac{\partial}{\partial r} \left(r \frac{\partial \phi}{\partial r} \right) = \frac{1}{r} \frac{d}{dr} \left(r \frac{d\psi}{dr} \right) \chi (\chi, \theta), \text{ etc., and}$$

(2.55) becomes, after dividing by ϕ:

$$\frac{1}{\psi} \frac{1}{r} \frac{d}{dr} \left(r \frac{d\psi}{dr} \right) + \frac{1}{\chi} \left[\frac{\partial^2 \chi}{\partial \chi^2} + \frac{1}{r^2} \frac{\partial^2 \chi}{\partial \theta^2} \right] - \frac{1}{L^2} = 0 \qquad (2.56)$$

Equation (2.56) now separates into

$$\frac{\partial^2 \chi}{\partial \chi^2} + \frac{1}{r^2} \frac{\partial^2 \chi}{\partial \theta^2} = -\alpha^2 \chi$$

$$\frac{1}{r} \frac{d}{dr} \left(r \frac{d\psi}{dr} \right) - \left(\alpha^2 + \frac{1}{L^2} \right) \psi = 0 \qquad (2.57)$$

Here it is seen that the separation constant α^2 represents lateral neutron leakage in the one dimensional diffusion equation for $\psi(r)$. If a source is present of strength S neutrons/cm^3-sec., then the result (2.57) can be expressed in slab, cylindrical, or spherical geometry by taking $p = 0$, 1, or 2:

$$\frac{d^2\psi}{dr^2} + \frac{p}{r}\frac{d\psi}{dr} - \left(\alpha^2 + \frac{1}{L^2}\right)\psi + \frac{S}{D} = 0 \qquad (2.58)$$

Here D is the diffusion coefficient.

Now consider the equation

$$\left(\frac{d}{dr} + w(r)\right)\left(D\frac{d\phi}{dr} + u(r)\,\phi\right) + S = 0 \qquad (2.59)$$

i.e.,

$$D\frac{d^2\phi}{dr^2} + u\frac{d\phi}{dr} + Dw\frac{d\phi}{dr} + \phi\frac{du}{dr} + uw\phi + S = 0 \qquad (2.60)$$

Dx(2.58)

$$D\frac{d^2\phi}{dr^2} + \frac{Dp}{r}\frac{d\phi}{dr} - D\left(\alpha^2 + \frac{1}{L^2}\right)\phi + S = 0$$

Comparing coefficients of $\frac{d\phi}{dr}$, and of ϕ:

$$\frac{Dp}{r} = u + Dw; \therefore w(r) = \frac{p}{r} - \frac{u(r)}{D}$$

(2.61)

$$\frac{du}{dr} + uw = -D(\alpha^2 + \frac{1}{L^2})$$

Substitute for w to get

$$\frac{du}{dr} + \frac{up}{r} - \frac{u^2}{D} = -D(\alpha^2 + \frac{1}{L^2}); \therefore \frac{du}{dr} = \frac{u^2}{D} - \frac{pu}{D} - D(\alpha^2 + \frac{1}{L^2})$$

(2.62)

Now define $v(r) = -D\frac{d\phi}{dr} - u\phi$, so $\frac{dv}{dr} = -D\frac{d^2\phi}{dr^2} - u\frac{d\phi}{dr} - \phi\frac{du}{dr}$.

$$\therefore \frac{d\phi}{dr} = -\frac{v+u\phi}{D} \qquad (2.63)$$

From (2.60),

$$vw = -(D\frac{d\phi}{dr} + u\phi)w = D\frac{d^2\phi}{dr^2} + u\frac{d\phi}{dr} + \phi\frac{du}{dr} + S$$

$$= -\frac{dv}{dr} + S \qquad (2.64)$$

$$\frac{dv}{dr} = \frac{uv}{D} - \frac{pv}{r} + S$$

Equations (2.62), (2.63) and (2.64) comprise a set of

3 non-linear first-order coupled differential equations, which can be solved numerically. A standard library subroutine named RKS3[19] is used, which employs the Runge-Kutta method.

Boundary conditions needed at the core-reflector interface and at the vacuum boundary of the last slab are:

Core-reflector	Last slab
$a_1 D\frac{d\phi}{dr} + a_2\phi + a_3 = 0$ (2.65)	$a_4 D\frac{d\phi}{dr} + a_5\phi + a_6 = 0$ (2.66)

Three different boundary conditions can be obtained:

1. $\phi_o = -a_3/a_2$, if $a_3 = 0$

2. $\left(\frac{d\phi}{dr}\right)_o = -\frac{a_2}{a_1 D}$, if $a_2 = 0$

3. $\left(\frac{1}{\phi}\frac{d\phi}{dr}\right)_o = -\frac{a_2}{a_1 D}$, if $a_3 = 0$.

We select the following values:

$a_1 = 0$	$a_4 = 2.13$
$a_2 = -1$	$a_5 = 1.$
$a_3 = \phi_o$	$a_6 = 0.$

Here ϕ_o = thermal flux at core-reflector interface. The values of a_4, a_5 and a_6 are such that $-\left(\phi \frac{d\phi}{dr}\right)_o = 0.71\lambda_{tr} = 2.13D$ = extrapolation length at the vacuum boundary.

In order to start integrating equations (2.62) and (2.64), initial values U_o and V_o are required. From the a-values,

$$U_o = a_2/a_1 \qquad V_o = a_3/a_1 \quad \text{if} \quad a_1 \neq 0 \qquad (2.67)$$

If the flux is specified, $a_1 = 0$, and it is necessary to expand ϕ about $r_1 = r_o + h$:

$$\phi_o = \phi_1 - h\frac{d\phi_1}{dr} + \frac{h^2}{2}\frac{d^2\phi_1}{dr^2} \qquad (2.68)$$

From (2.57), $\frac{d^2\phi}{dr^2} = -\frac{p}{r_1}\frac{d\phi_1}{dr} + (\alpha^2 + \frac{1}{L^2})\phi_1 - \frac{S_1}{D}$

$$\therefore \phi_o = \phi_1 - \left(h + \frac{ph^2}{2r_1}\right)\frac{d\phi_1}{dr} + \frac{h^2}{2}(\alpha^2 + \frac{1}{L^2})\phi_1 - \frac{h^2}{2}\frac{S_1}{D}$$

By (2.63),

$$\phi = \phi_1 + h(1 + \frac{ph}{2r_1})(\frac{v_1 + u_1\phi_1}{D}) + \frac{h^2}{h}(\alpha^2 + \frac{1}{L^2})\phi_1 - \frac{h^2}{2}\frac{S_1}{D}$$

$$= \phi_1\left[1 + \frac{hu_1}{D} + \frac{h^2}{2}(\alpha^2 + \frac{1}{L^2}) + \frac{h^2}{2}\frac{p}{r_1}\frac{u_1}{D}\right] + (h + \frac{ph^2}{2r_1})\cdot$$

$$\cdot \frac{v_1}{D} - \frac{h^2}{2}\frac{S_1}{D}$$

$$\text{Now let } u_1 = -\frac{D}{h}\left[1 + \frac{h^2}{2D}\left(\alpha^2 + \frac{1}{L^2}\right) + \lambda\right]$$

$$v_1 = \frac{D}{h}\left[\phi_0 + \frac{h^2 S_1}{2D} + \mu\right] \qquad (2.69)$$

One gets

$$\phi_1\left[\lambda\left(1 + \frac{h}{2}\frac{p}{r_1}\right) + \frac{h}{2}\frac{p}{r_1}\left(1 + \frac{h^2}{2D}\right)\left(\alpha^2 + \frac{1}{L^2}\right)\right]$$

$$= \mu\left[1 + \frac{ph}{2r_1}\right] + \frac{ph}{2r_1}\left[\phi_0 + \frac{h^2 S_1}{2D}\right]$$

Setting both sides to zero gives λ and μ:

$$\lambda = -\frac{\nu}{1+\nu}\left[1 + \frac{h^2}{2D}\left(\alpha^2 + \frac{1}{L^2}\right)\right]$$

$$\mu = -\frac{\nu}{1+\nu}\left[-a_3/a_2 + \frac{h^2 S_1}{2D}\right] \qquad (2.70)$$

$$\nu = \frac{hp}{2r_1}$$

Equations (2.70) contain terms whose values are known which yield u_1 and v_1 (instead of u_0 and v_0) by (2.69). What is done is to set $h = DX = 0.1$ cm in **MEDIPORT**. The integration routine RKS3 automatically selects the largest possible step size consistent with numerical errors involved, and fills up a table of $(u, v, \Delta r)$ triplets

as it goes. Finally the outer boundary condition is applied giving a starting value for ϕ:

$$\phi = \frac{a_4 v - a_6}{a_5 - a_4 u} \tag{2.71}$$

This follows directly from (2.63) and (2.66). The ϕ equation, (2.63), is now integrated back to the core-reflector interface, interpolating for u and v from the values stored on the forward integration. The non-linearity of this equation has been found to require tables of j and v to prevent divergence of u and v if the equations are simply integrated together in the backward direction. Single-precision arithmetic suffices if this scheme is used, whereas otherwise, divergence was observed, even for double-precision arithmetic. References (20) and (21) give additional information about this general method.

Numerous criteria are used to select the integration step size h from:

1. Recommended step $h_R = \frac{0.1}{\sqrt{(\alpha^2 + \frac{1}{L^2})}}$
2. Distance DX to region boundary.
3. $h^* = 0.1\,(u/|\frac{du}{dr}|)\,\frac{DX}{|DX|}$

If $h > DX$, $h = DX$. If $h < DX$, $h = DX/(1 + \left|\frac{DX}{h}\right|$ integer).

Now set $h = h^*$, if $|h^*| < h$. The value h_R is good far from region boundaries and large flux gradients. A smaller interval is used, given by h^*, in regions having large flux gradients.

2.3 DOSIMETRY IN TISSUE

2.3.1 Fast Neutron Dose Rates

Monte Carlo calculations following the history of monoenergetic neutrons incident normally on a 30 cm thick infinite slab of tissue, performed by Snyder and Neufeld[22], give the relationship between neutron flux and total fast neutron dose rate shown in Table 2.2. The effect of multiple collisions is included. All dose calculations are obtained by averaging over an assumed flat flux per unit lethargy within a given neutron energy group. Mathematically, with $D(u)$ the dose rate conversion factor at lethargy u and $\phi(u)$ the flux per unit lethargy, the group i contribution to dose rate is

$$R_i = \int_{u_i}^{u_{i+1}} \phi(u)\, D(u)\, du \simeq \phi(u)\, (u_{i+1} - u_i)\, \hat{D}_i \qquad (2.72)$$

where

$$\hat{D}_i = \int_{u_i}^{u_{i+1}} D(u)\, du \Big/ \int_{u_i}^{u_{i+1}} du \qquad (2.73)$$

Tables 2.3 and 2.4 give energy groups and dose conversion factors that have been used by STAR DATA REDUCTION and MEDIPORT for total fast neutron dose rate measured at the surface of a 30 cm thick infinite slab of tissue.

Total dose rate includes recoils from H, N, C, and O nuclei, gamma rays from H(n, γ)D, and heavy particles from N(n, p)C and N(n, α)B.

Tables 2.3 and 2.4 do not give fast neutron dose rates at depth in tissue. The gamma ray contribution depends on the shape of the tissue, and is calculated separately as described in Section 2.3.3. The heavy particle reactions such as $B^{10}(n, \alpha)Li^{7}$ and $N^{14}(n,p)C^{14}$ depend mainly on the thermal neutron flux distribution, which again depends on the shape of the tissue. Section 2.3.2 gives the method used for this dose contribution. The only other factor left is the first collision dose from the recoil energy of nuclei undergoing elastic scattering neutrons. If A_i is the atomic number of nuclide i, then $\beta_i = \left[(A_i - 1)/(A_i + 1)\right]^2$ is the maximum fraction of the neutron energy remaining after an elastic collision with the nuclide. The maximum fraction of the neutron energy going into recoil is $1 - \beta_i$, and $(1 - \beta_i)/2$ is the average fraction. The differential first collision dose $D_i(E)$ is

$$D_i(E) = \frac{(1-\beta_i)}{2} E \Sigma_{si}(E) = 1.6 \times 10^{-8} \frac{2A_i}{(A_i+1)^2} E \Sigma_{si}(E) \frac{\text{rads}}{\text{n/cm}^2} \qquad (2.74)$$

Here $\Sigma_{si}(E)$ is the macroscopic elastic scattering cross section for nuclide i at neutron energy E in MeV.

Contributions to the first collision dose for H, O, C, and N as a function of neutron energy have been calculated.[23] Two sets of neutron cross sections have been used for MEDIPORT calculations. A uniform lethargy width set was first used which had three groups per energy decade in MeV, starting at 10 MeV. Later, the original Bondarenko groups of non-uniform width have been used. Table 2.5 gives groups and conversion factors for these sets.

TABLE 2.2 Conversion Between Neutron Flux and Dose Rate

E, MeV	10^{-9} Rad per n/cm^2 10^{-2}	Millirad/hr per n/cm^2-sec
Thermal	0.32	0.115
0.0001	0.69	0.28
0.005	0.57	0.205
0.02	0.57	0.205
0.1	1.10	0.396
0.5	2.4	0.86
1.	2.8	1.37
2.5	4.3	1.55
5.	5.8	2.10
7.5	7.1	2.56
10.	7.0	2.52

TABLE 2.3 Dose Conversion Factors for STAR

Group	Energy, MeV	Limits, MeV	Width, MeV	Rad/min per n/cm^2 - sec
1	0.7874	0.1 -1.822	1.722	0.145×10^{-6}
2	3.367	1.822-5.050	3.228	0.283
3	6.733	5.050-8.278	3.228	0.404
4	9.313	8.278-10.00	1.722	0.430

TABLE 2.4 Dose Conversion Factors for MEDIPORT

Group	Limits, MeV	10^{10} x Rad/n/cm^2
1	6.5 - 10.5	70.4
2	4.0 - 6.5	59.3
3	2.5 - 4.0	46.5
4	1.4 - 2.5	41.0
5	0.8 - 1.4	38.3
6	0.4 - 0.8	27.4
7	0.2 - 0.4	17.8
8	0.1 - 0.2	12.8
9	.0465- 0.1	9.5
10	.0215- .0465	7.0
11	.01 - .0215	5.7
12	.00465- .01	5.7

TABLE 2.5 First collision Dose Conversion Factors

Group	Uniform Lethargy Widths Limits, MeV	10^{10} x rad/n/cm^2	Non-uniform Lethargy Widths Limits, MeV	10^{10} x rad/n/cm^2
1	4.64 -10.0	50.3	6.5 -10.5	53.0
2	2.15 - 4.64	37.5	4.0 - 6.5	46.0
3	1.00 - 2.15	27.3	2.5 - 4.0	37.4
4	.464 - 1.00	19.6	1.4 - 2.5	30.0
5	.215 - .464	12.8	0.8 - 1.4	24.2
6	.100 - .215	7.1	0.4 - 0.8	17.8
7	.0465 - .100	3.4	0.2 - 0.4	11.6
8	.0215 - .0465	1.3	0.1 - 0.2	6.7
9	.0100 - .0215	0.9	.0465 - .100	3.4
10	.00465- .0100	0.6	.0215 - .0465	1.3
11	-----	--	.0100 - .0215	0.9
12	-----	--	.00465- .0100	0.6

Group	STAR Limits, MeV	10^{10} xrad/n/cm^2	Rad/min per n/cm^2 - sec
1	0.1 - 1.822	14.1	0.0846 x 10^{-6}
2	1.822 - 5.050	36.8	0.221
3	5.050 - 8.278	49.8	0.299
4	8.278 - 10.00	54.1	0.324

2.3.2 Heavy Particle Dose Rates

Parameters used for the $B^{10}(n, \alpha)\ Li^{7}$ and $N^{14}(n, p)C^{14}$ reactions are:

	$\frac{B^{10}}{3837}$	$\frac{N^{14}}{1.88}$
σ_a(b)		
P (wt. fraction)	50×10^{-6}	0.041
E(MeV)	2.34	0.624
M(AMU)	10.016	14.008

Since the range of the reaction products is of the order of 10 microns in tissue, these reactions produce a very localized dose, R, which can be obtained from

$$R(x, r) = \phi\Sigma_a E = \phi(x)\phi(r)\ \frac{\sigma_a PE}{M} \times 5.79 \times 10^{-7}\ \text{rad/min}$$

Cylindrical coordinates (x, r) refer to depth, x, and radius, r, inside a cylindrical tissue phantom.

2.3.3 Neutron Capture Gamma-Ray Dose Rates

Of most importance is the neutron capture gamma dose-rate along the axis of the phantom. However, to obtain this numerically, radial and angular distributions of neutron flux (and hence capture gamma production rates) within the phantom are required. R. Rydin's[24] results of Figs. 4.1 and 4.2 indicate that the fast flux emergent from the MITR medical beam port is flat to within a few percent, while the thermal flux is asymmetric and varies up to 15%. It is believed to be a good approximation to assume that angular non-uniformities in the thermal flux within the phantom die out within a few centimeters, and that its distribution becomes

$$\phi(x,r,\theta) \; E \; \phi(x)\phi(r) \equiv \phi(x) \left[\cos\left(\frac{\pi}{2}\frac{r}{R'}\right)\right]^{1/4}$$

where $R' = R_o + 0.71\,\lambda_{tr}$ = extrapolated radius, and $\phi(x)$ is known. This variation for $\phi(r)$ reasonably represents the experimental shape. The gamma dose rate off the axis is obtainable just as easily as on the axis.

Account is taken of neutron capture of epithermal and fast neutrons as follows:

$$\text{Total capture rate } R = N \int_0^\infty \sigma_a(E)\phi(E)dE$$

$$= \phi_o \sigma_{ao} + \sum_{j=1}^{NG} \phi_j \sigma_{aj}$$

Assuming $\sigma_a = \sigma_{ao}\sqrt{\frac{E_o}{E}}$ and $\phi_j \sim \frac{1}{E}$ inside the group, then

$$\sigma_{aj} = \frac{\int \sigma_a(E)\phi(E)dE}{\int \phi(E)dE} = \sigma_{ao}\sqrt{E_o}\ \frac{\int \frac{dE}{E^{3/2}}}{\int \frac{dE}{E}}$$

$$= 2\sigma_{ao}\sqrt{E_o}\left[\frac{1}{E_{j+1}} - \frac{1}{E_j}\right] \ln \frac{E_j}{E_{j+1}}$$

$$= \frac{2\sigma_{ao}\sqrt{E_o}}{U\sqrt{E_j}}\left[\frac{E_j}{E_{j+1}} - 1\right]$$

Note that $\sigma_{ao} = \sigma_a(E_o)$, and $E_o = 0.0253$ eV. Using $u_j \equiv \ln \frac{10}{E_j}$, the reaction rate may be written

$$R \simeq N\sigma_{ao}\left\{\phi_o + 1.006 \times 10^{-4} \sum_j \frac{\phi_j}{\Delta U_j}\left[\sqrt{\frac{E_j}{E_{j+1}}} - 1\right] \Big/ \sqrt{E_j}\right\}$$

Hence, one may replace ϕ_o with ϕ, where ϕ is term in

curly brackets in the preceding equation.

It is assumed that both ϕ and ϕ_o vary in the same way radially inside the phantom. Also, it is assumed that the 2200 m/s flux represents all the neutrons with energies less than 0.215 eV (the lower bound of the group fluxes).

A Taylor kernel is used which gives the photon current at $\vec{r}_o$ for a unit source at $\vec{r}$:

$$K(\vec{r}, \vec{r}_o) = \left[Ae^{-(1+\alpha_1)\mu|\vec{r}-\vec{r}_o|} + (1-A)e^{-(1+\alpha_2)\mu|\vec{r}-\vec{r}_o|} \right] 4\pi|\vec{r}-\vec{r}_o|^2$$

where $\vec{r} = (x,r,\theta)$ is the source position, $\vec{r}_o = (x_o, r_o, \theta_o)$ is the observation point position, and $|\vec{r}-\vec{r}_o|^2 = (x-x_o)^2 + r^2 + r_o^2 - 2rr_o \cos(\theta - \theta_o)$.

The gamma-ray dose at $\vec{r}_o$ due to a neutron capturing nuclide of atomic weight M and absorption cross section σ_a which emits n photons of E MeV per capture is:

$$R(\vec{r}_o) = (9.61 \times 10^{-7}\ \mu_a E N\ \sigma_a P n/\rho M) \int_o^{\pi} 2d\theta \int_o^{R_o} \phi(r) r dr \cdot \int_o^{H_o} \phi(x) K(\vec{r}, \vec{r}_o) dx \quad \text{rad/min}$$

where μ_a and μ are photon absorption and total attenuation coefficients in a phantom of density ρ, length H_o and radius R_o. N is Avogadro's number, P is the weight fraction, and A, α_1, and α_2 are tabulated.[25]

The triple integration must be performed numerically. To do this, a special set of subroutines (see Appendix A.1) were coded using the Gaussian quadrature method, as given for double integration by Okazaki and Fowler.[26] These subroutines are:

1. G3: perform outer integration over Θ
2. G24: perform middle integration over r
3. CENTR: perform inner integration over α

Change variable from r to $Y = r/R' = R/RPRIM$, with $\Theta \rightarrow TH$ and $x \rightarrow X$. The integral in Fortran notation is

$$I = \int_{P=o}^{Q=\pi} ANGLE(TH)d(TH) \cdot \int_{A=o}^{B=R_o/R'} G(Y)d(Y) \cdot \int_{C=o}^{D=Ho} F(X,R,TH)d(X)$$

Auxiliary subroutines needed are:

1. ANGLE(TH) computes angular thermal flux distribution. Taking $P = o$, $Q = \pi$, $ANGLE(TH) = 2$ (equivalent to $P = o$, $Q = 2\pi$, $ANGLE(TH) = 1$) one has azimuthal symmetry. This does not mean a double integral will suffice because the kernel $K(\vec{r},\vec{r}_o)$ is a function of x, r, and Θ.

2. $G(Y) = Y(\cos \frac{\pi Y}{2})^{1/4}$, the Y coming from $dV = rdrd\Theta dx$,

since $Y = r/R'$.

3. F(x, R, TH...) computes $K(\vec{r},\vec{r}_o)$ and multiplies by $\phi(x)$ obtained from SPINT.

4. SPINT is a table interpolation subroutine which finds $\phi(x)$ given a ϕ-table at uniform intervals in x, described in Appendix A.1. The main program sets up the $\phi(x)$ table before calling DOSE.

Input parameters NO and NI, which control the order of the Gaussian approximation, for the r and x integrations, may be taken to be 4, 6, or 8. Hence greater accuracy is attainable if required at the expense of additional computer time. The Θ-integration is always performed over (o, π) in the 8-point approximation. Actually, the r and x integrations have been found to be too inaccurate if taken over the full range of the limits. The pole in $K(\vec{r},\vec{r}_o)$ from $\frac{1}{|\vec{r}-\vec{r}_o|^2}$ leads to curve-fitting difficulties if one tries to fit both sides with 4, 6, or 8 points. Doing the r and x integrations in two parts each, with the cutoff point at the pole, has been found to be reasonable. The limits are:

$$\text{r: (A,T), and (T,B), with T} = \begin{cases} 0.25B, & \text{if } r_o=0 \\ r_o/R', & 0 < r_o < R_o \\ 0.75B, & r_o=R_o \end{cases}$$

$$\text{x: (C,Z), and (Z,D), with Z} = \begin{cases} C+0.25(D-C), & \text{if } x_o=C \\ x_o, & \text{if } C<x_o<D \\ C+0.75(D-C), & \text{if } x_o=D \end{cases}$$

In effect, the order of integration becomes

Coordinate	Order
θ	16
r	8, 12, or 16 (NO = 4, 6, or 8)
x	8, 12, or 16 (NI = 4, 6, or 8)

TABLE 2.6 Attenuation Kernel Parameters

Energy MeV	A	$-\alpha_1$	α_2	μ, cm^{-1}	μa, cm^{-1}
.5	23	.136	-.05	.0936	.0320
1.	11	.104	.028	.0683	.0300
1.5	7.85	.087	.074	.0556	.0276
2.	6.4	.076	.092	.0478	.0256
2.5	5.7	.0685	.102	.0423	.0238
3.	5.2	.0627	.108	.0384	.0220
3.5	4.8	.058	.113	.0352	.0213
4.	4.5	.055	.1165	.0329	.0206
4.5	4.2	.0534	.1192	.0308	.0199
5	3.96	.0520	.1215	.0292	.0192
5.5	3.74	.0506	.1228	.0278	.0187
6.	3.55	.0495	.124	.0267	.0182
6.5	3.41	.0480	.1253	.0254	.0178
7.	3.28	.0470	.1264	.0244	.0174
7.5	3.16	.046	.1273	.0237	.0171
8.	3.05	.045	.128	.0233	.0168
8.5	2.95	.0443	.1285	.0227	.0166
9.	2.86	.0436	.129	.0222	.0163
9.5	2.78	.0428	.1295	.0217	.0161
10.	2.70	.042	.13	.0212	.0160

Shown in Table 2.7 are errors in dose-rates relative to the highest order (NI = NO = 8, 16^3 effective points) for three traverses in the phantom for the normal configuration of the M.I.T. Medical Beam.

TABLE 2.7 Accuracy of Gamma Dose Rates

Depth cm	Radius cm	Relative Errors, % 16×4×4 Points	16×8×8 Points	16×12×12 Points
0	0	15.3		
0	2.075	15.8		
0	4.15	12.9		
0	6.225	27.2		
0	8.3	0.8		
0	0			1.28
2.5	0		6.1	1.76
5.0	0		5.6	1.46
7.5	0		3.7	
10	0		2.9	
0	0		6.1	1.76
0	2.075		6.4	1.75
0	4.15		5.4	1.83
0	6.225		4.9	
0	8.3		0.4	
Avg. Error, %		14.4	4.6	1.64

Judging from the trend of error reduction with total points used, the most accurate approximation can be expected to have an error of about $1.64 \times 12^2/16^2 = 0.9\%$. For survey purposes, all cases run have used NI = NO = 6, giving $\simeq 1.6\%$ error.

To save computing time, all gamma rays can be lumped into one effective gamma ray because the tissue phantom is only about a mean free path long. Table 2.8 gives the ratio of total dose-rate from H, Cl, C and B^{10} (50 ppm) to that from H alone for various locations in a phantom 15 cm long and 16.6 cm in diameter. The range of the data is 1.283 ± 0.007 or $\pm 0.55\%$. This error is less than that of the numerical integration, justifying the use of an effective gamma ray to reduce the computing time to one-quarter. What is done is to raise n for H (the principal contributor) from 1.000 to 1.283, and to delete the calculation for Cl, C and B^{10}. The B^{10} contribution is about 5% of the total γ-dose for a uniform distribution of 50×10^{-6} weight fraction B^{10} in the phantom.

TABLE 2.8 Ratio of Total γ-Dose to γ-Dose from H

Depth, cm	Radius, cm	Total γ-Dose/ H γ-Dose
0.0	0.0	1.276
2.5	0.0	1.276
5.0	0.0	1.277
7.5	0.0	1.281
10.0	0.0	1.284
0.0	4.35	1.278
0.0	8.3	1.289
10.0	4.35	1.286
10.0	8.3	1.290

2.4 NEUTRON SCATTERERS

One of the major problems which has contributed to the lack of success of neutron capture therapy is that of delivering a lethal radiation dose to a deep brain tumor without in the process destroying normal tissue above the tumor. When tissue is irradiated by fast neutrons, the neutrons lose their energy primarily by elastic collisions with the atoms composing the tissue. The kinetic energy of the struck atom is dissipated by ionization, excitation and elastic collisions with other atoms. The "fast neutron dose" is largely responsible for damage to normal tissue near the surface. At depths beyond three or four centimeters, the rapid attenuation of fast neutrons in tissue makes the neutron capture gamma ray dose more important.

In a neutron beam such as is available at the M.I.T.R. Medical Beam Port, most of the fast neutron dose comes from neutrons having energies in excess of 0.1 MeV. Significant improvements to neutron dose distribution with depth in tissue could well result if a way were found to selectively deplete the fast neutrons in the beam. As most materials have cross sections which go down as the neutron energy goes up, it is not likely that any material would be capable of "filtering out" fast neutrons by passing a beam through it. However, the probability of a neutron being reflected from an optically thin

slab depends almost linearly on the scattering cross section being small for a small cross section.

Hydrogen has a scattering cross section which varies exceptionally with energy. It is about 20 b for neutron energies less than 1 kev, falling to 11.0 b at 0.1 MeV, and about 1.2b averaged over 6.5 to 10.5 MeV. In addition, the average energy loss per collision is higher for hydrogen than any other element. For these reasons, hydrogenous materials such as lucite, polyethylene, and water would seem to be well suited to use as neutron reflectors, or "scatterers". Computer studies using these materials are reported in Section 5.4.

2.4.1 Geometrical and Angular Considerations

Having decided to place a neutron scatterer in the path of a neutron beam, one must decide a reasonable geometrical arrangement. Figure 2.1 shows the arrangement which has been investigated

Figure 2.1 Geometry of Neutron Scatterer

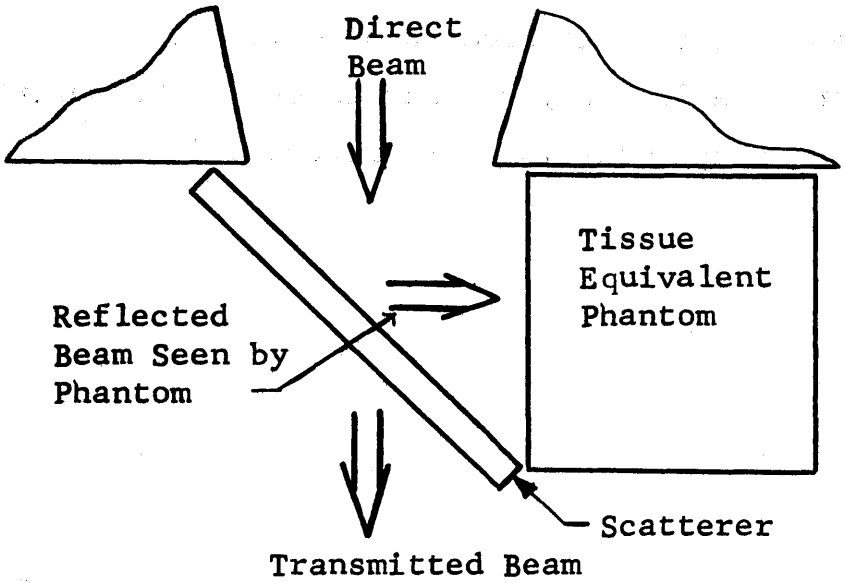

The angular and energy distribution of the direct beam was obtained from the STAR code. Two angular groups were used, the first spanning $60^{o} \leq \theta \leq 90^{o}$, and the second, $0^{o} \leq \theta \leq 60^{o}$. The energy groups are given in Table 2.3. At 45^{o} rotation must be performed on the direct beam in order to give the neutron source as seen be the scatterer. Similarly, the beam reflected from the

scatterer must be rotated to give the neutron source as seen by the phantom. Assuming a flat distribution within each angular group, the relationship between direct and rotated beams is easily obtained. From Figure 2.2 it can be seen that if

S = direct beam flux in angular group ,

S' = flux in rotated angular group ,

then

$$S_1' = \frac{1}{4} S_2, \quad S_2' = \frac{1}{2} S_1 + \frac{3}{4} S_2, \quad S_1 + S_2 - S_1' - S_2' = \frac{1}{2} S_2 \text{ for } 30^\circ$$

$$S_1' = \frac{1}{4} S_2, \quad S_2' = \frac{1}{2} S_1 + \frac{5}{8} S_2, \quad S_1 + S_2 - S_1' - S_2' =$$

$$\frac{1}{8} S_1 + \frac{1}{2} S_2 \text{ for } 45^\circ$$

$$S_1' = \frac{1}{4} S_2, \quad S_2' = \frac{1}{2} S_1 + \frac{1}{2} S_2, \quad S_1 + S_2 - S_1' - S_2' =$$

$$\frac{1}{4} S_1 + \frac{1}{2} S_2 \text{ for } 60^\circ$$

Figure 2.2 45^{o} Rotation of Angular Groups

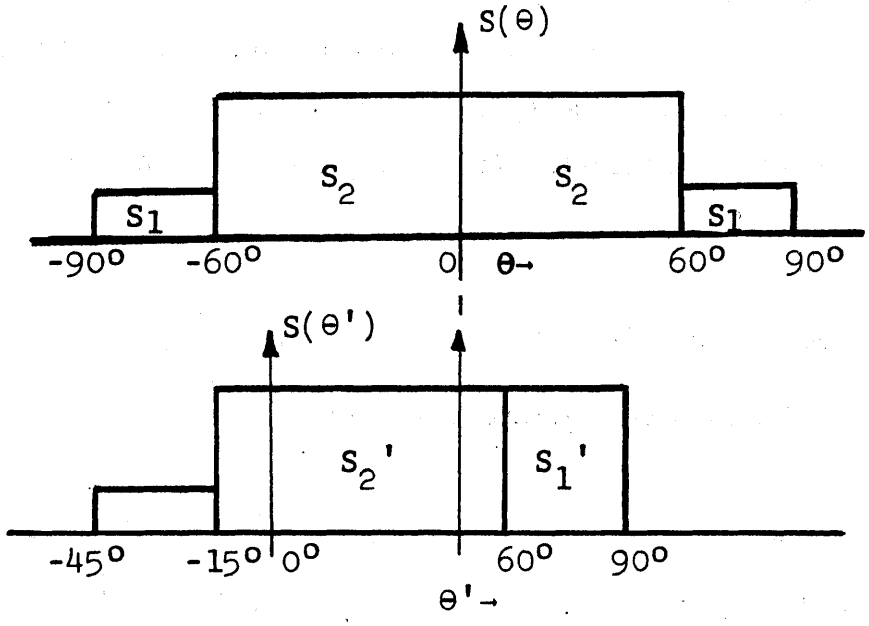

The quantity $S_1 + S_2 - S_1' - S_2'$ is that flux which cannot strike the scatterer. If the phantom is close to the direct beam (as in Figure 2.1) then the direct flux could enter the phantom. Its effect has not been calculated, because it depends on relative sizes and locations of beam portal, scatterer, and phantom. The fast flux in the direct beam predominantly lies rather close to the beam axis. The fast flux becomes more isotropic as the neutron energy decreases, where it becomes less important in terms of fast neutron dose rates.

The scatterer problem has been investigated in a simpler way, using a single angular group, but 25 energy groups from 0.215 ev to 10.5 MeV, via the MEDIPORT code. Total reflection probabilities for a beam of neutrons incident at 45^{o} to slabs were obtained from the TAR(N) code (Section 2.12 and Appendix A.2). No corrections were

applied to account for neutrons reflected away from the scatterer, because absolute overall intensities depend mainly on details of geometrical arrangements.

Section 5.4 discusses calculations obtained for scatterers placed in the M.I.T.R. Medical Facility beam.

CHAPTER III

TEST PROBLEM RESULTS

3.1 MONOENERGETIC NEUTRONS IN A THIN SLAB (ISOTROPIC SCATTERING IN LAB.)

The transport equations describing the fate of neutrons incident on infinite, plane, homogeneous slabs have been solved numerically by the methods given in Chapter II. The computer code written for this purpose is known as TAR(N) (for Transmission, Absorption and Reflection for N collisions), and is described in Appendix A.2. Results have been obtained for uniform beams at a variety of incident angles, as well as for neutron sources with angular distributions proportional to $(\cos\theta)^0$, $(\cos\theta)$, and $(\cos\theta)^2$. The angular leakage flux from an optically thick volume-distributed source having a linear variation of source strength p(x) with distance x into the source volume can be approximated [25] as:

$$\ell(\theta) = \frac{p_o}{4\pi} \lambda_c \cos\theta + \frac{p_1}{4\pi} \lambda_c^2 \cos^2\theta \qquad (3.1)$$

where

$$p(x) = p_o + p_1 x \ (N/cm^3 - sec) \qquad (3.2)$$

and θ and λ_c are the polar angle and mean free path in the source, respectively.

The total leakage is

$$L = \int_0^{\pi/2} e(\theta)\, 2\pi \sin\theta d\theta = \frac{1}{4} P_0 \lambda_c + \frac{1}{6} P_1 \lambda_c^2 \tag{3.3}$$

For two angular groups, with $0 \leq \cos\theta_1 \leq 0.5$, and $.5 \leq \cos\theta_2 \leq 1.0$,

$$L_1 = \frac{1}{16} P_0 \lambda_c + \frac{1}{48} P_1 \lambda_c^2$$

$$L_2 = \frac{3}{16} P_0 \lambda_c + \frac{7}{48} P_1 \lambda_c^2 \tag{3.4}$$

Slabs with optional thicknesses in the range $0.125 \leq \Sigma_t L \leq 5.0$ were investigated, generally for $c = \Sigma_s/\Sigma_t = 1$. Results for $c \neq 1$ may be obtained from these results as described in Section 2.1.3.

3.1.1 Collision History Correlations

One of the first cases considered was that of a slab for which $\Sigma_t L = 0.5$, $c = 0.8$, and the neutron source was either isotropic or a beam at right angles to the slab ($\theta = 0^o$, $\mu = \cos\theta = 1$). The regular variation of transmission and reflection with collision number, k, together with the constant factor of c/2 in Equations (2.27) and (2.28), lead to consideration of two ratios:

$$RT(k) \equiv \frac{2}{c}\, T(k+1)/\, T(k)$$

$$RR(k) \equiv \frac{2}{c}\, R(k+1)/R(k) \qquad (3.5)$$

Figure 3.1 illustrates the smooth convergence of these ratios to an asymptotic value $RT(\infty) = RR(\infty) \simeq 0.8945$. Replotting the difference $RT(k) - RT(\infty)$ in Figure 3.2, a very good exponential behaviour is observed. Some of the scatter is due to errors resulting from obtaining fluxes at only six points.

The basic reason for the trends shown in Figures 3.1 and 3.2 is the smooth variation of flux shape and magnitude with collision number. Several flux generations are plotted in Figure 3.3. Here ϕ_0 is the uncollided flux, and $\phi_{total} = \sum_{k=0}^{\infty} \phi_k$. After many collisions, the flux shape becomes symmetrical, of

approximately cosine shape, but with a faster drop-off near the slab surfaces.

Figures 3.4 and 3.5 give graphical correlations found for a range of slab thicknesses using a neutron source whose angular distribution varied as cos θ. Deviations from straight line behaviour may be the result of insufficient points in the flux calculations, and/or of round off errors inherent with single precision calculations, particularly for the thinnest slab. In any event, the magnitude of $RT(k) - RT(\infty)$ and $RR(\infty) - RR(k)$ is so small as to be negligible with respect to RT(k) or RR(k). The deviations for the thickest slabs are real effects due to the greater change in flux shape in thick slabs during the first few collisions. It was found that the difference between the points and the straight line fit fell off exponentially with collision number. More points would be required in the flux calculations in order to pin down this effect accurately.

Figure 3.6 gives the neutron reflection correlation for a parallel neutron beam incident at 45° to the slab. Deviations from the linear fits tend to be somewhat reduced compared to Figure 3.5.

Probabilities and empirical parameters are given in Figures 3.7 to 3.10 and Tables 3.1 and 3.2, which are required to correlate all the transmission and reflection probabilities for any slab thickness and any collision

number. The relationships fitted are:

$$RT(k;\ \Sigma_t L) \simeq RT(\infty;\ \Sigma_t L) + A(\Sigma_t L)\ \exp(-ka(\Sigma_t L))$$

$$RR(k;\ \Sigma_t L) \simeq RR\ (\infty;\ \Sigma_t L) - B(\Sigma_t L)\ \exp(-kb(\Sigma_t L)) \tag{3.6}$$

The five parameters needed are $RT(\infty;\ \Sigma_t L) = RR(\infty;\ \Sigma_t L)$, A, B, a, and b. First collision reflection and transmission probabilities (R_1 and T_1) can then be put into equations (3.5) for all other R_k and T_k. T_1 and R_1 can be expressed as

$$T_1 = \frac{c}{2} \int_0^{\Sigma_t L} 2E_2(w)E_2\ (\Sigma_t L - w)\ dw$$

$$R_1 = \frac{c}{2} \int_0^{\Sigma_t L} 2\left[E_2(w)\right]^2 dw \tag{3.7}$$

but no reasonable analytical equation can be given for these integrals. Similarly, the variation of $RT(\infty;\ \Sigma_t L)$ with slab thickness cannot be exactly expressed analytically. Figure 11 indicates that

$$RT(\infty;\ \Sigma_t L) \sim 2\left[1 - E_2\ (\tfrac{1}{2}\ \Sigma_t L)\right] \tag{3.8}$$

contains most of its dependence. This equation is exact only at the end points $\Sigma_t L = 0$ or ∞, where flux shape is unimportant. The difference between $RT(\infty)$ and equation (3.8) is caused by differences between real flux shape and assumed flat shape.

Table 3.1 and 3.2 present numerical values used in the MEDIPORT calculation. Note that the input data to MEDIPORT differs by a factor of two in the definitions of $RE(\infty)$, $RR(\infty)$, and the empirical parameters A and B. Denoting MEDIPORT quantities by primes:

$$\begin{aligned} RT'(\infty) &= \frac{1}{2}RT(\infty) \\ RR'(\infty) &= \frac{1}{2}RR(\infty) \\ A' &= \frac{1}{2}A \\ B' &= \frac{1}{2}B \end{aligned} \qquad (3.9)$$

TABLE 3.1 Empirical Parameters and Probabilities for a Cosine Source

Slab Thickness (MFP)	T_1	a	A'	RT'(∞)
0.	0.0000	1.40	0.000	0.0000
.125	.0812	1.25	0.000	.1906
.25	.1192	1.10	0.010	.300
.375	.1380	.985	.035	.386
.5	.1411	.910	.0575	.4468
.75	.1370	.775	.100	.547
1.	.1159	.675	.135	.618
1.25	.0969	.594	.153	.674
1.5	.07867	.535	.205	.7175
2.	.0500	.444	.270	.783
2.5	.03102	.380	.332	.8273
3.	.01880	.331	.390	.859
3.5	.01157	.289	.430	.8841
4.	.00682	.253	.458	.904
4.5	.004094	.222	.475	.9178
5.	.002435	.192	.485	.9288

TABLE 3.2 Empirical Parameters and Probabilities for a 45° Incident Beam

Slab Thickness M.F.P.	R_1	b	B'	RR'(∞)
0.	0.000	1.32	0.000	0.000
.125	0.068	1.20	0.000	.1906
.25	0.1064	1.09	0.015	.300
.375	0.130	0.99	.033	.386
.5	0.149	0.92	.050	.4468
.75	0.170	0.80	.086	.547
1.	0.1793	0.70	.121	.618
1.25	0.185	0.62	.157	.674
1.5	0.1861	0.555	.191	.7175
2.	0.1875	0.45	.253	.783
2.5	0.1881	0.368	.305	.8273
3.	0.1882	0.311	.312	.859
3.5	0.1883	0.266	.310	.8841
4.	0.1883	0.227	.30	.904
4.5	0.1884	0.197	.29	.9178
5.	0.1884	0.171	.28	.9288

The data fits were performed analytically, first evaluating slope parameters a and b, from which the intercepts A and B are easily found. They are not "best" fits, as for example least squares fits in some sense are. That the errors are in fact very small can be seen from a sample calculation of RT(k) given in Table 3.3.

The fitting equation is

$$RT(k) \simeq 1.566 + 0.56 \exp(-.446\ k) \qquad (3.10)$$

TABLE 3.3 Accuracy of Correlation for $\Sigma_t L=2.$, Cosine Source

k	RT	RT(fitted)	RT-RT(fitted)	Relative Error, %
1	1.9278	1.9244	0.0034	0.18
2	1.8042	1.7955	0.0087	0.48
3	1.7117	1.7129	-.0012	-.07
4	1.6574	1.6600	-.0026	-.16
5	1.6242	1.6262	-.0020	-.12
6	1.6033	1.6045	-.0015	-.09
7	1.5899	1.5907	-.0008	-.05
8	1.5814	1.5817	-.0003	-.02
9	1.5759	1.5760	-.0001	-.006
10	1.5723	1.5724	-.0001	-.006

It has been remarked in Section 2.1.4 that the k-th collision flux shapes are assumed to be of the same form for different energy groups, with regard to predicting multigroup downscattered transmission and reflection. The flux shape within a mean free path of the surface is of most importance, due to the E_2 factors in the leakage integrals of Equation (2.27).

The greatest change in flux shape occurs for incident beams at large angles to the slab normal. First, second, and fifth collision fluxes are shown in Figures 3.11, 3.12, and 3.13, for a 45^{o} incident parallel beam. These cases were used to obtain reflection correlations only. It is difficult to estimate how much of a change can be tolerated in Σ_t-values for a neutron transfering to another group as a result of a single collision. A 50% change would seem to be reasonable. As most materials have slowly varying cross sections, errors here should be small.

Hydrogenous materials are most difficult tests of reflection and transmission calculations for numerous reasons. Results for transmission through polyethylene are discussed in Section 3.2.

FIGURE 3.1

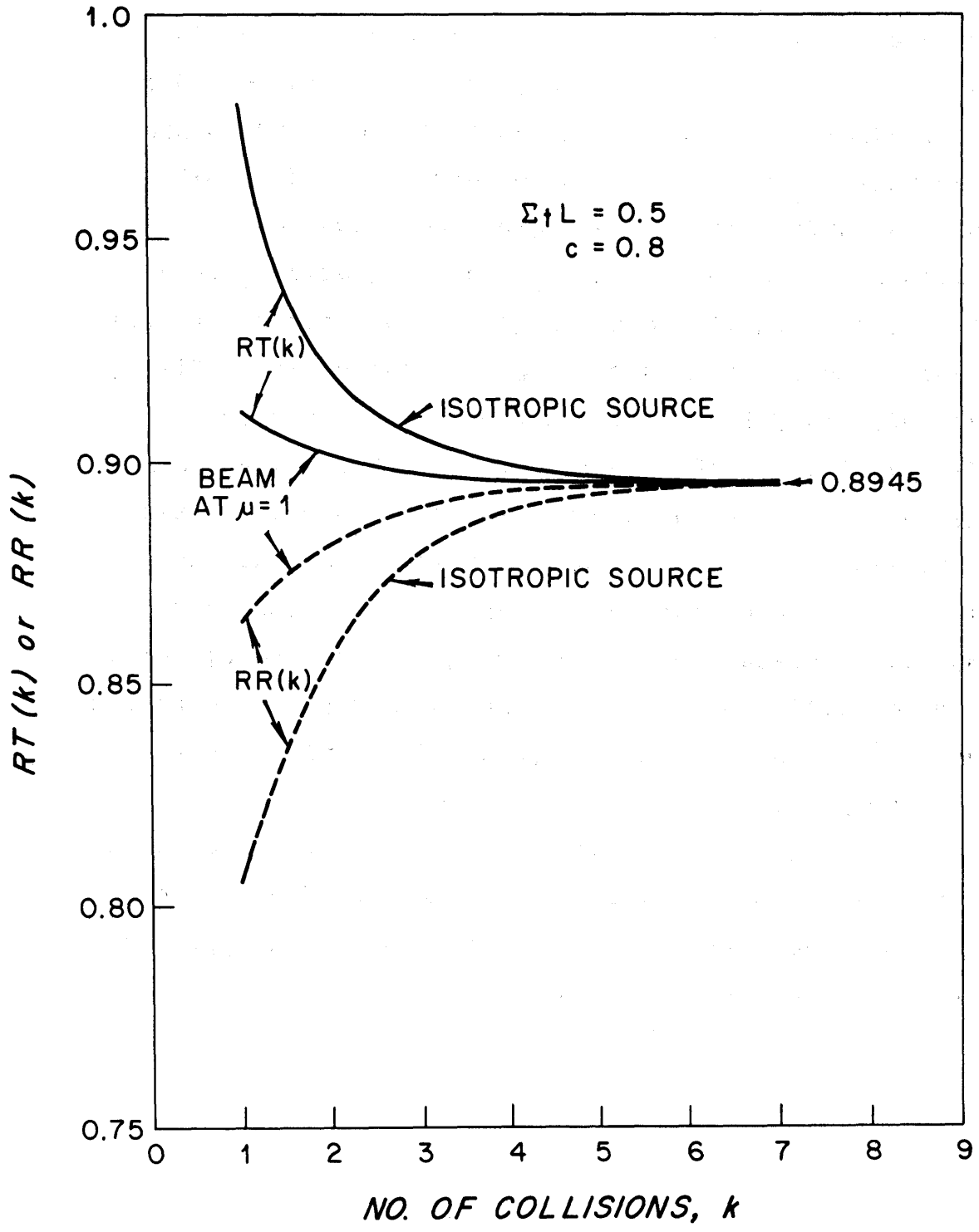
1.0
0.95
0.90
0.85
0.80
0.75
0
1
2
3
4
5
6
7
8
9
$\Sigma_t L = 0.5$
c = 0.8
RT(k)
ISOTROPIC SOURCE
BEAM
AT $\mu = 1$
0.8945
ISOTROPIC SOURCE
RR(k)
RT (k) or RR (k)
NO. OF COLLISIONS, k

FIGURE 3.2

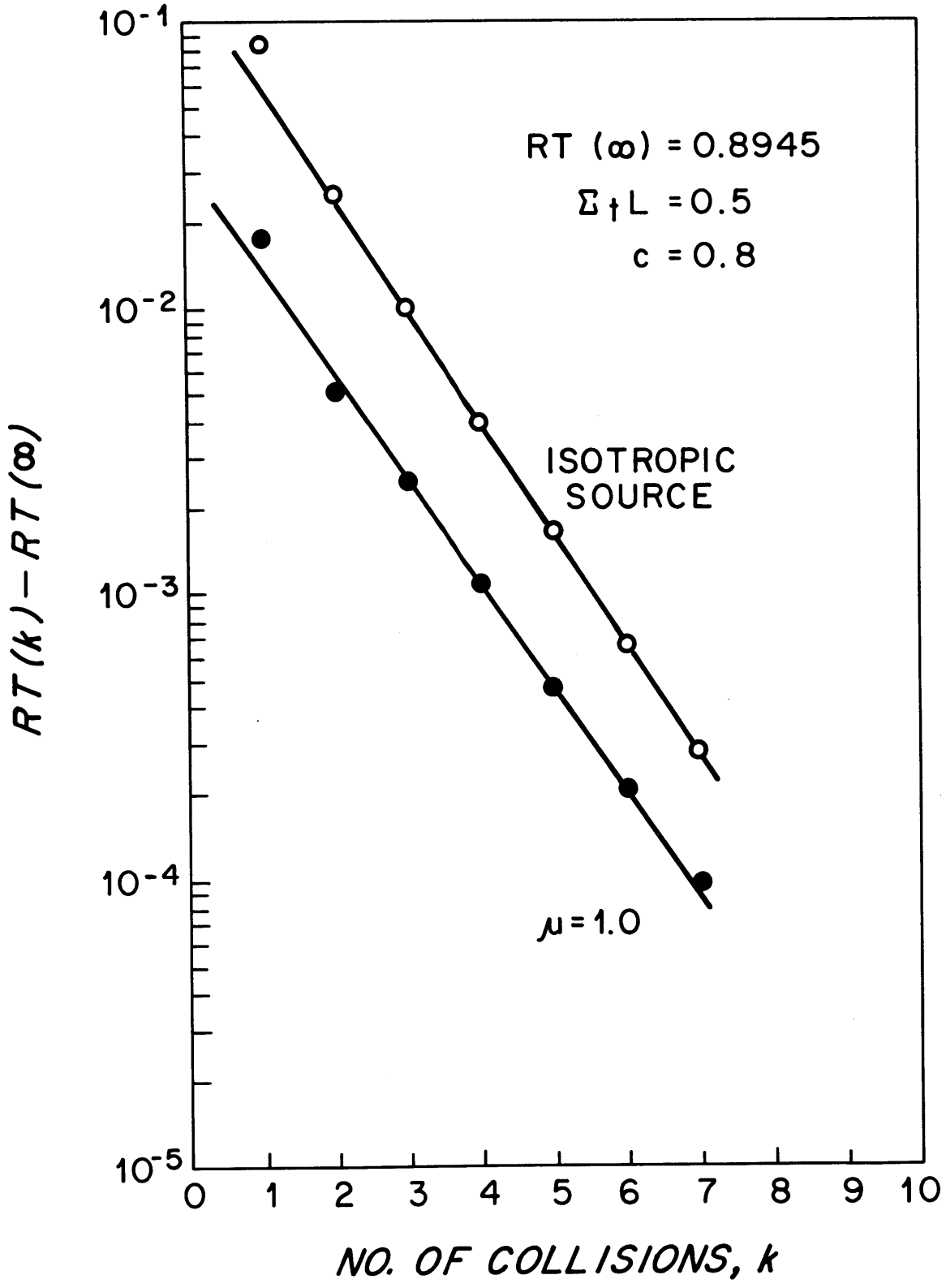
RT (∞) = 0.8945
Σ t L = 0.5
c = 0.8
ISOTROPIC SOURCE
μ = 1.0
RT(k) − RT(∞)
NO. OF COLLISIONS, k
10-1
10-2
10-3
10-4
10-5
0
1
2
3
4
5
6
7
8
9
10

FIGURE 3.3

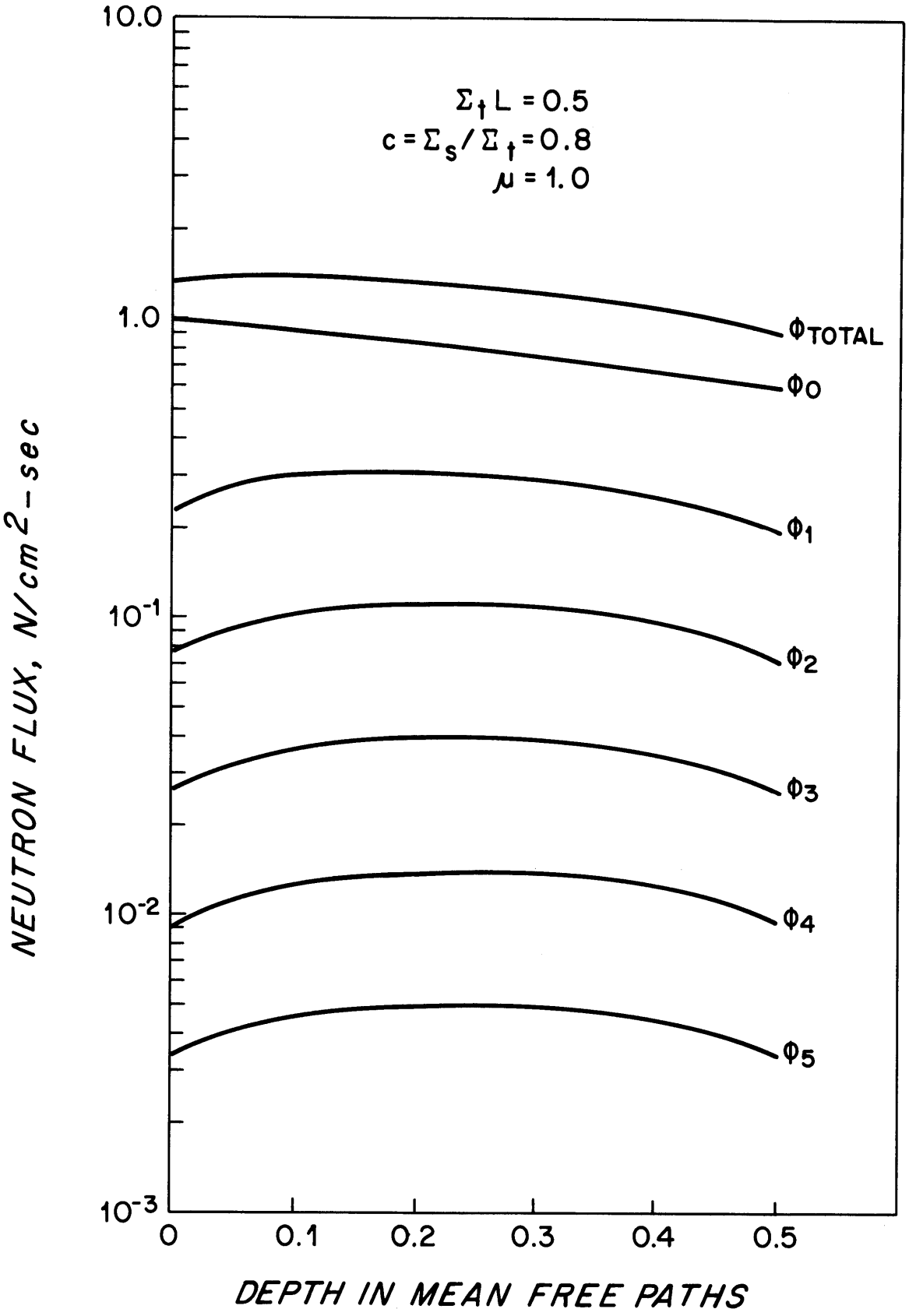
10.0
1.0
10^{-1}
10^{-2}
10^{-3}
$\Sigma_t L = 0.5$
$c = \Sigma_s / \Sigma_t = 0.8$
$\mu = 1.0$
Φ_{TOTAL}
Φ_0
Φ_1
Φ_2
Φ_3
Φ_4
Φ_5
0
0.1
0.2
0.3
0.4
0.5
NEUTRON FLUX, N/cm^2-sec
DEPTH IN MEAN FREE PATHS

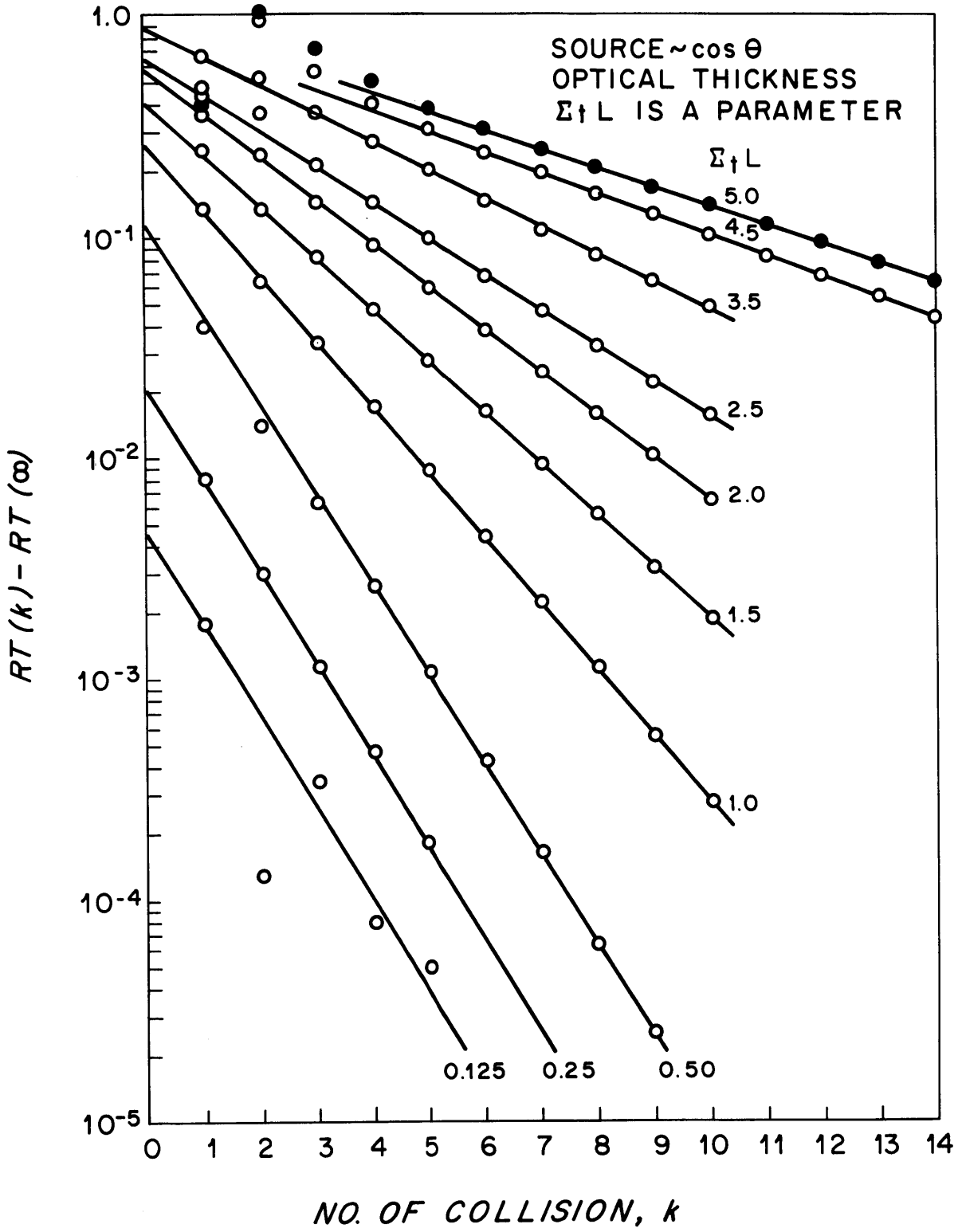
SOURCE ~ cos θ
OPTICAL THICKNESS
Σt L IS A PARAMETER
Σt L
5.0
4.5
3.5
2.5
2.0
1.5
1.0
0.125
0.25
0.50
1.0
10-1
10-2
10-3
10-4
10-5
0 1 2 3 4 5 6 7 8 9 10 11 12 13 14
RT(k) - RT(∞)
NO. OF COLLISION, k

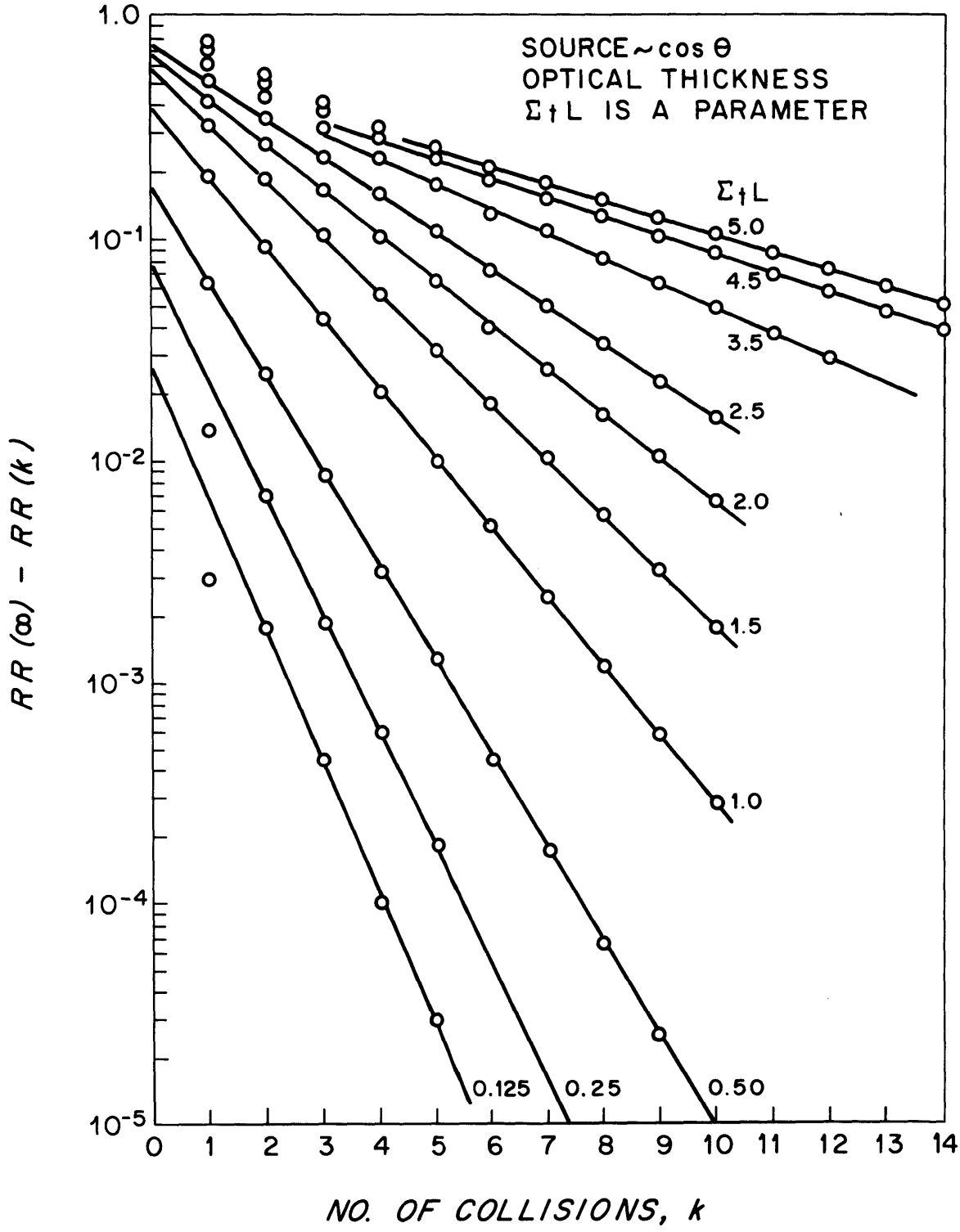
SOURCE ~ cos θ
OPTICAL THICKNESS
Σt L IS A PARAMETER
Σt L
5.0
4.5
3.5
2.5
2.0
1.5
1.0
0.50
0.25
0.125
1.0
10-1
10-2
10-3
10-4
10-5
0 1 2 3 4 5 6 7 8 9 10 11 12 13 14
RR (∞) - RR (k)
NO. OF COLLISIONS, k

FIGURE 3.6

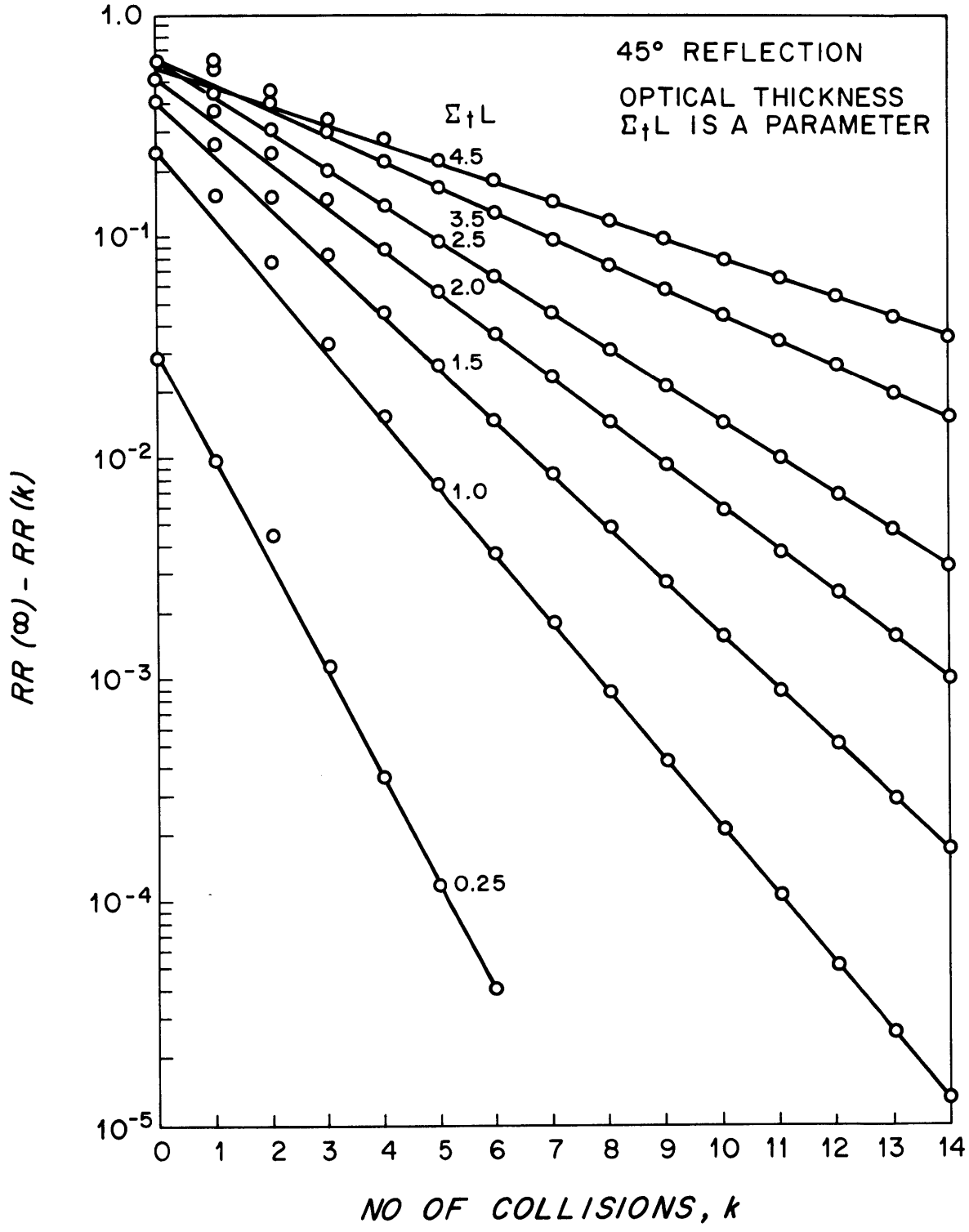
45° REFLECTION
OPTICAL THICKNESS
$\Sigma_t L$ IS A PARAMETER
$\Sigma_t L$
4.5
3.5
2.5
2.0
1.5
1.0
0.25
1.0
10^{-1}
10^{-2}
10^{-3}
10^{-4}
10^{-5}
0 1 2 3 4 5 6 7 8 9 10 11 12 13 14
RR (∞) - RR (k)
NO OF COLLISIONS, k

FIGURE 3.7

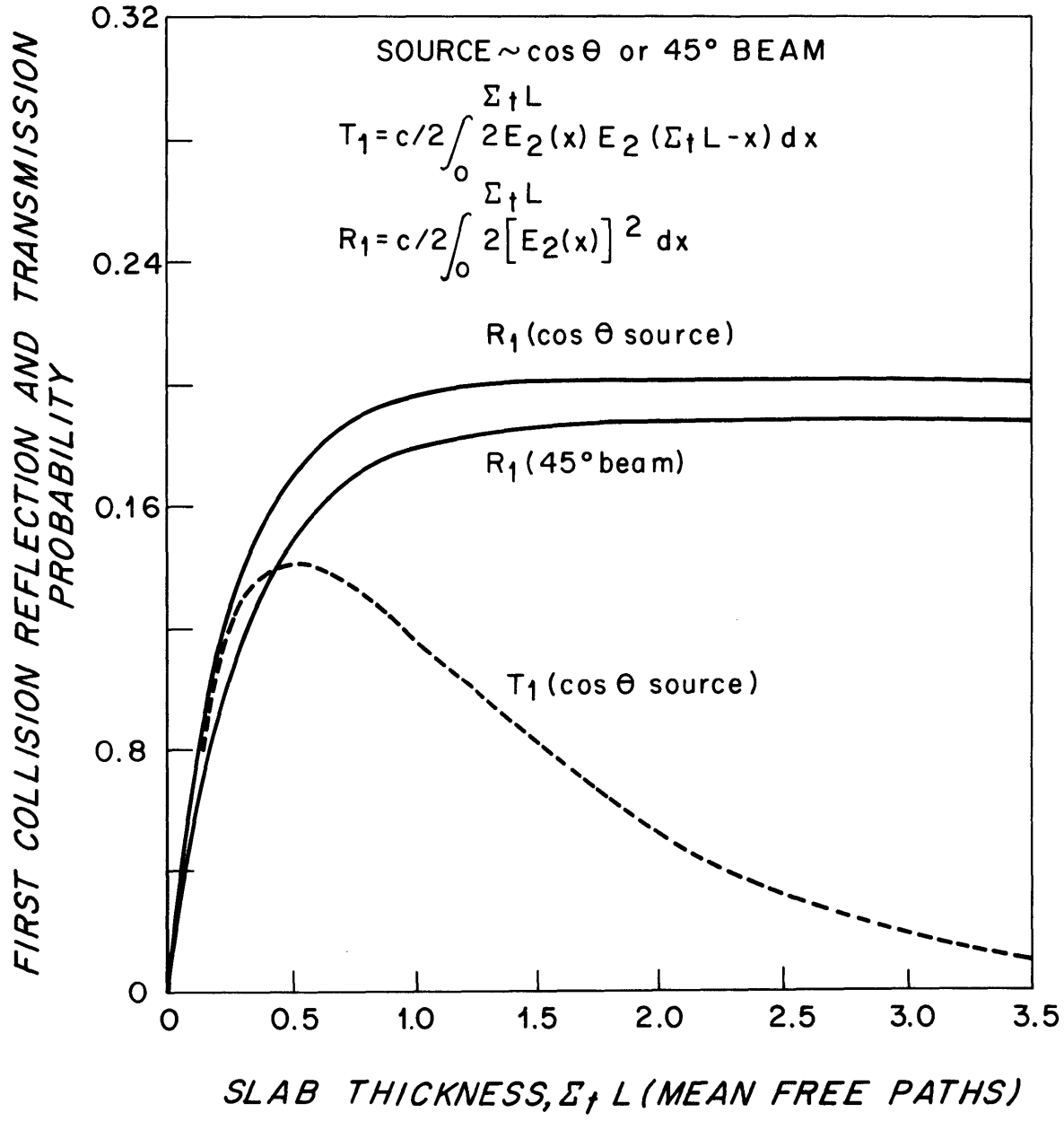
SOURCE ~ cos θ or 45° BEAM
$T_1 = c/2 \int_0^{\Sigma_t L} 2E_2(x)\, E_2(\Sigma_t L - x)\, dx$
$R_1 = c/2 \int_0^{\Sigma_t L} 2\left[E_2(x)\right]^2 dx$
R_1 (cos θ source)
R_1 (45° beam)
T_1 (cos θ source)
FIRST COLLISION REFLECTION AND TRANSMISSION PROBABILITY
0.32
0.24
0.16
0.8
0
0
0.5
1.0
1.5
2.0
2.5
3.0
3.5
SLAB THICKNESS, $\Sigma_t L$ (MEAN FREE PATHS)

FIGURE 3.8

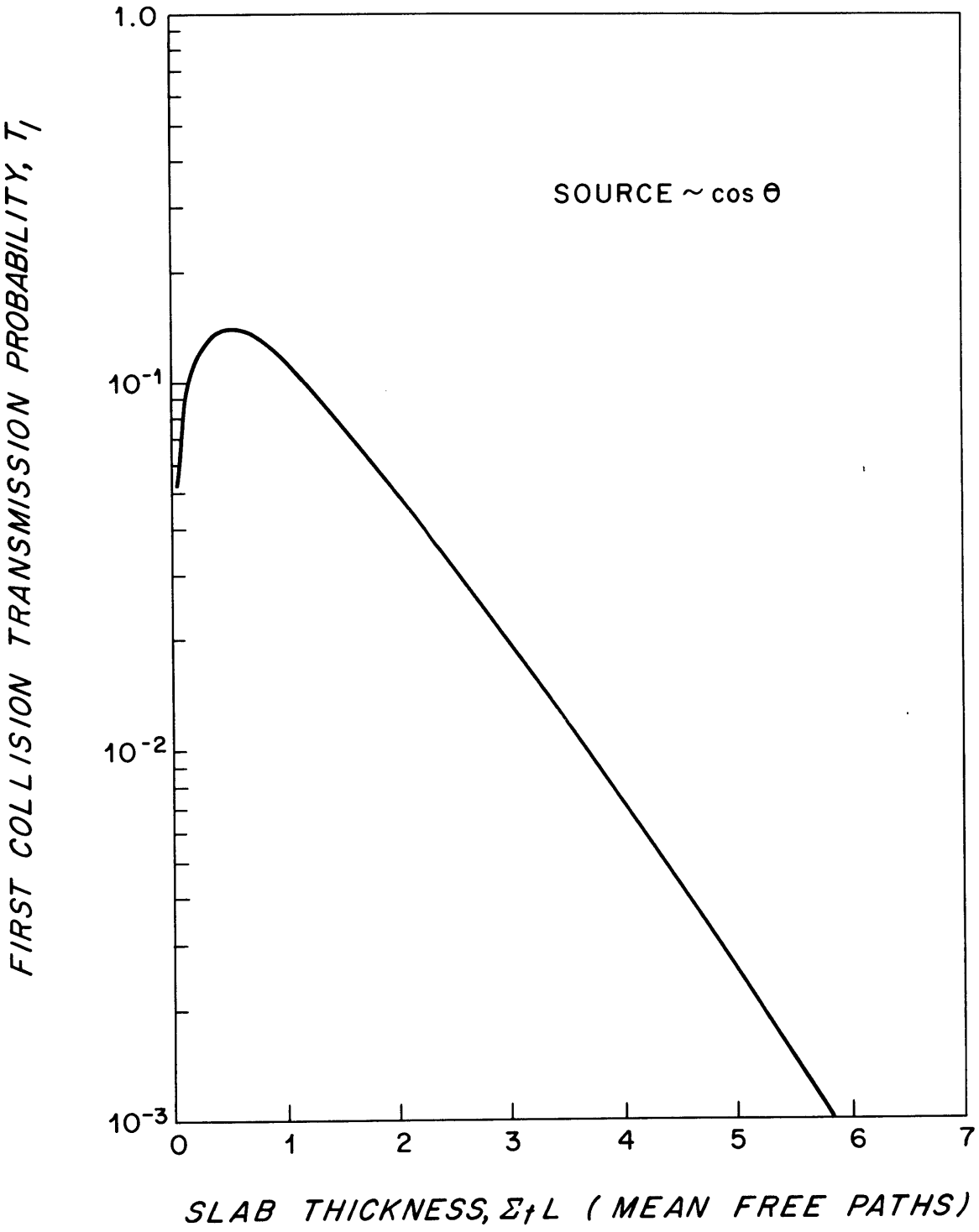
1.0
10^{-1}
10^{-2}
10^{-3}
SOURCE ~ cos θ
0
1
2
3
4
5
6
7
FIRST COLLISION TRANSMISSION PROBABILITY, T_1
SLAB THICKNESS, $\Sigma_t L$ (MEAN FREE PATHS)

FIGURE 3.9

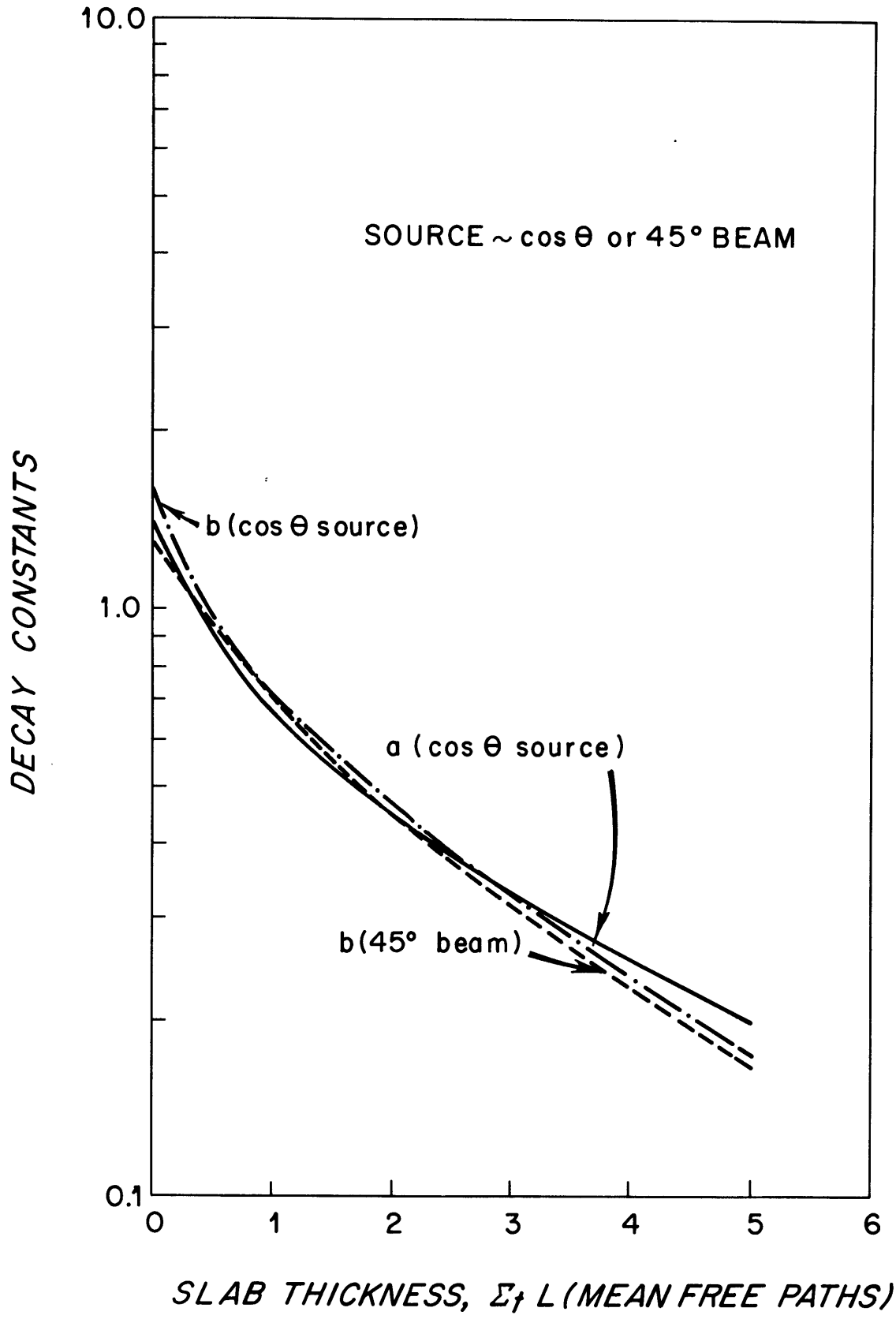
10.0
1.0
0.1
0
1
2
3
4
5
6
SOURCE ~ cos Θ or 45° BEAM
b (cos Θ source)
a (cos Θ source)
b(45° beam)
DECAY CONSTANTS
SLAB THICKNESS, Σt L (MEAN FREE PATHS)

FIGURE 3.10

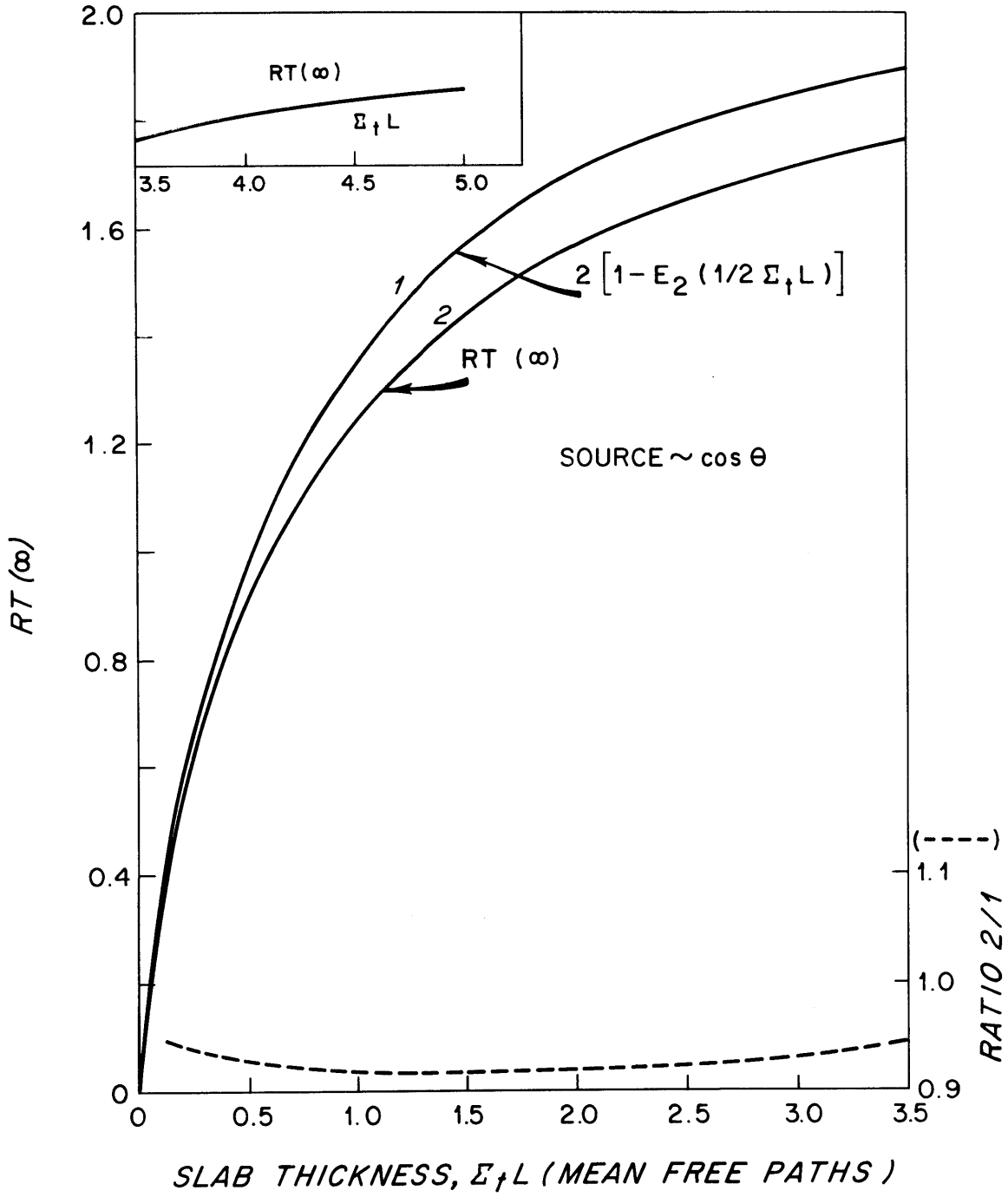
2.0
1.6
1.2
0.8
0.4
0
RT(∞)
$\Sigma_t L$
3.5
4.0
4.5
5.0
1
2
$2\left[1-E_2(1/2\,\Sigma_t L)\right]$
RT (∞)
SOURCE ~ cos θ
RT (∞)
(----)
1.1
1.0
0.9
RATIO 2/1
0
0.5
1.0
1.5
2.0
2.5
3.0
3.5
SLAB THICKNESS, $\Sigma_t L$ (MEAN FREE PATHS)

FIGURE 3.11

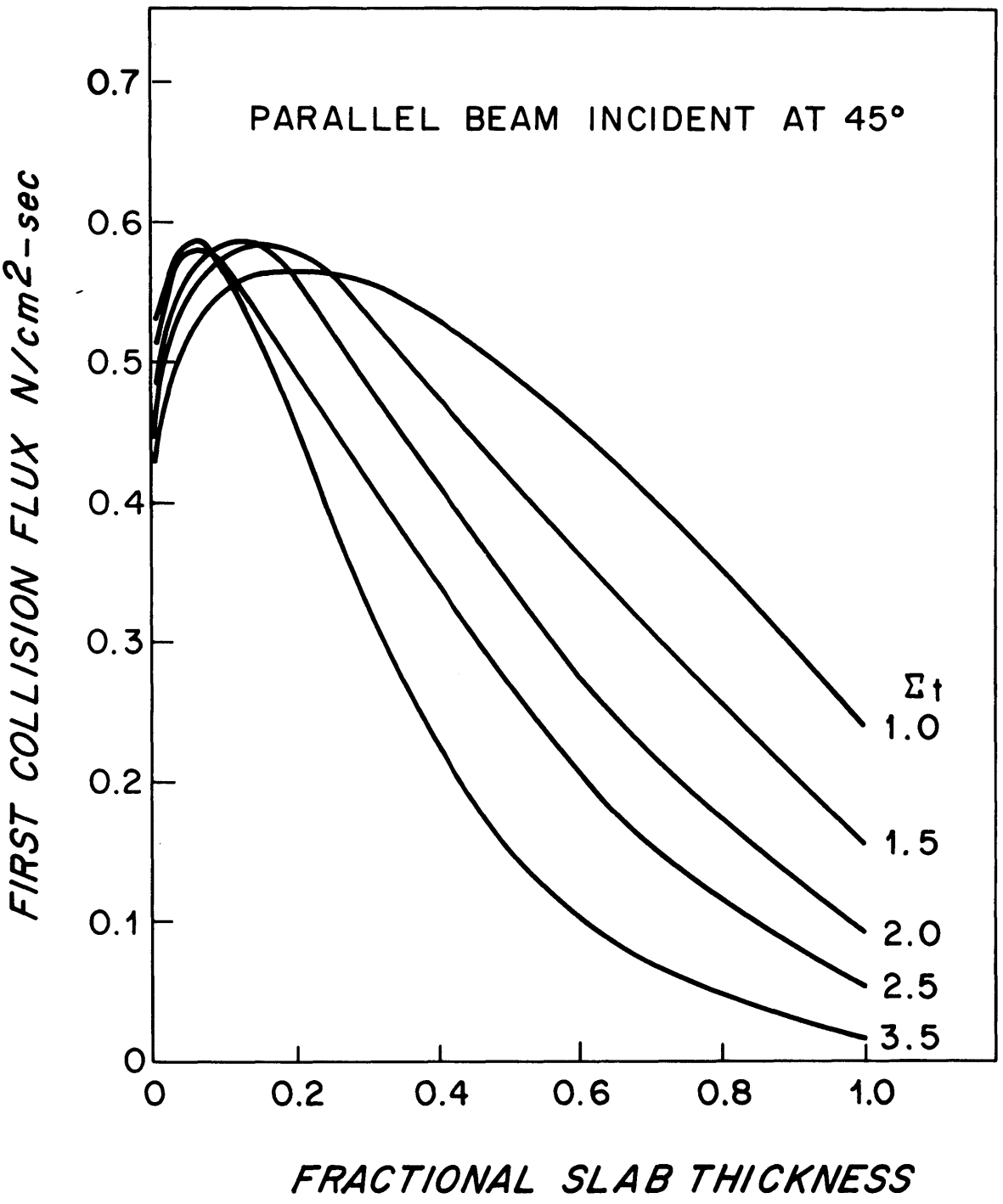
PARALLEL BEAM INCIDENT AT 45°
FIRST COLLISION FLUX N/cm2-sec
FRACTIONAL SLAB THICKNESS
0.7
0.6
0.5
0.4
0.3
0.2
0.1
0
0
0.2
0.4
0.6
0.8
1.0
Σt
1.0
1.5
2.0
2.5
3.5

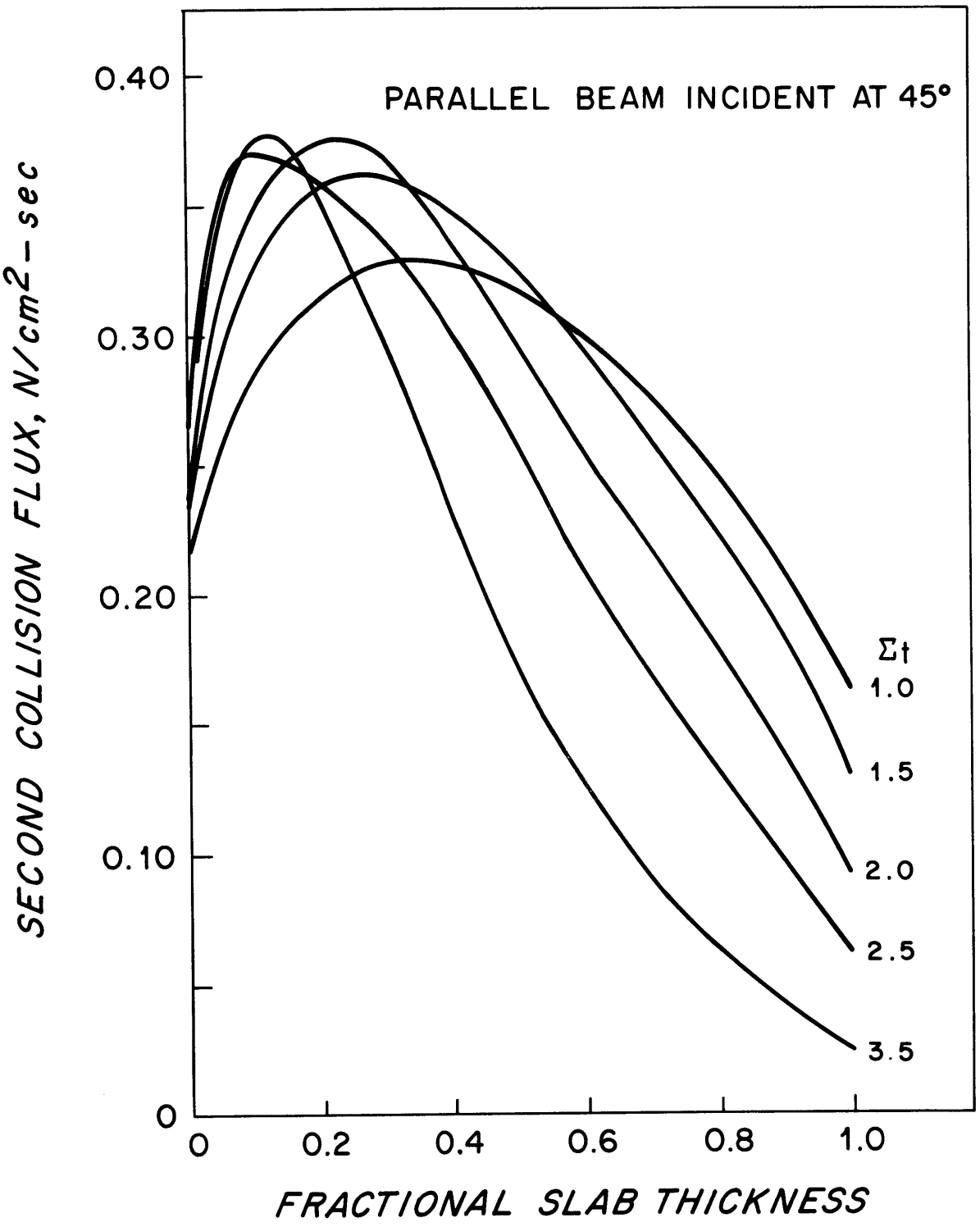
PARALLEL BEAM INCIDENT AT 45°
SECOND COLLISION FLUX, N/cm2-sec
FRACTIONAL SLAB THICKNESS
0.40
0.30
0.20
0.10
0
0
0.2
0.4
0.6
0.8
1.0
Σt
1.0
1.5
2.0
2.5
3.5

FIGURE 3.13

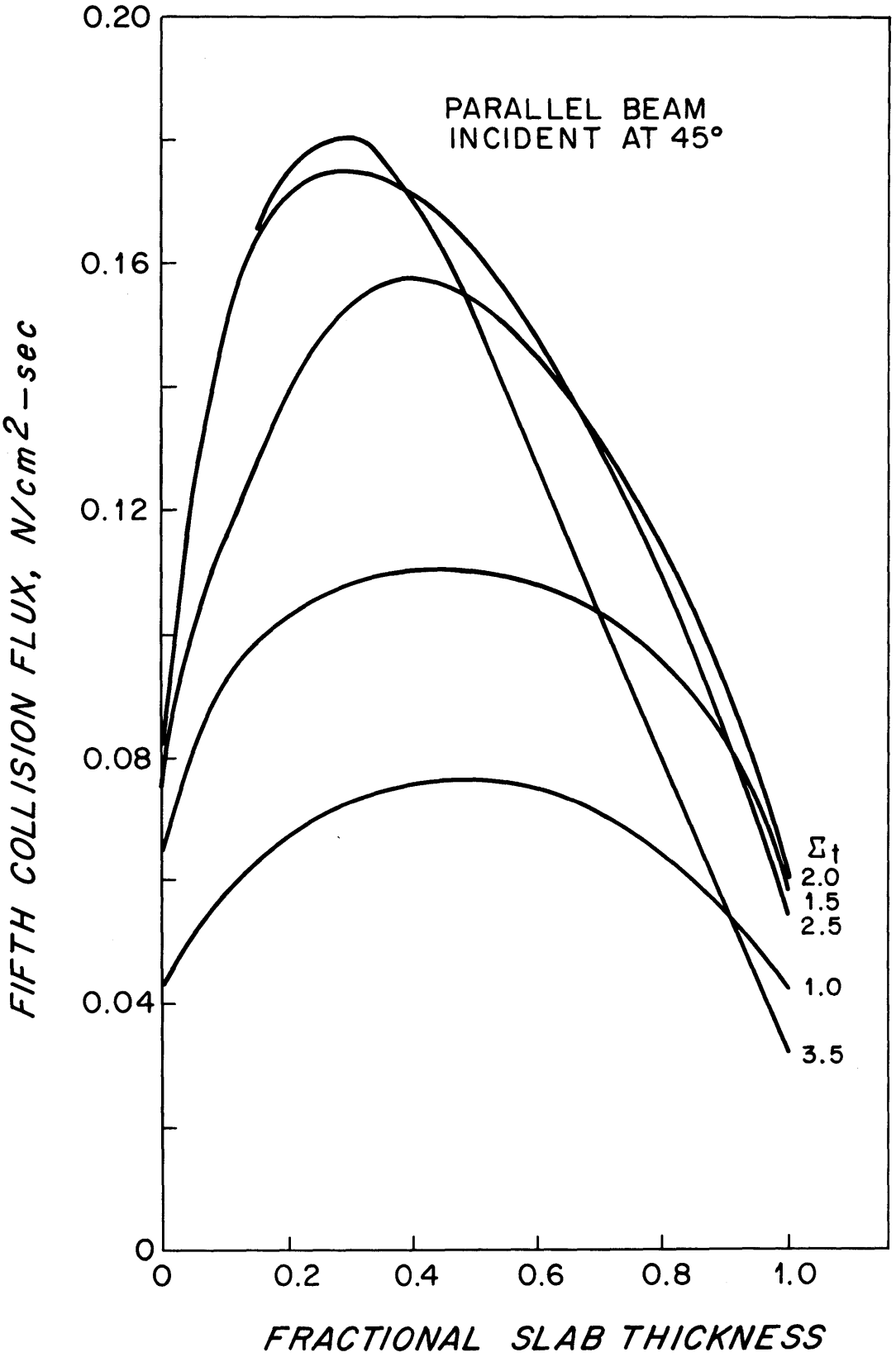
PARALLEL BEAM
INCIDENT AT 45°
0.20
0.16
0.12
0.08
0.04
0
0
0.2
0.4
0.6
0.8
1.0
FIFTH COLLISION FLUX, N/cm2-sec
FRACTIONAL SLAB THICKNESS
Σt
2.0
1.5
2.5
1.0
3.5

3.1.2 Comparison With Markov Matrix Method

The Markov Matrix Method of Eaton and Huddleston[8] has been discussed in Section 2.1.1 with regard to its relationship to methods developed in this work. At this point several comparisons can be made with their calculations.

The first problem to consider is that of a parallel single-velocity neutron beam incident perpendicular to an infinite plane slab for which $\Sigma_t L = 0.5$ and $c = \Sigma_s/\Sigma_t = 0.8$. The exact number of Markov states used is not given, although the comment is made that several values of $s = L/n$ (n = No. of Markov states inside the slab) were used, and results quoted obtained by extrapolating to $s^2 \to 0$. For a similar problem, $s = T/30$ was used indicating about 15 interior points for $\Sigma_t L = 0.5$. The present work used the TAR(N) code, with just three-point Gaussian quadratures to evaluate all integrals in Equations (2.27) and (2.28). Interior fluxes were calculated at six interior points plus both surfaces. Table 3.4 compares numerical results. The agreement is excellent, differing at most by a few digits in the fifth decimal place.

Table 3.4 Markov Matrix Method Versus TAR(N) for $\Sigma_t L=0.5$, $c=0.8$

Quantity	Markov Matrix Method	TAR(N)
T_o	0.60653	0.06053
T_1	0.08383	0.08383
T_2	0.03036	0.03040
T_3	0.01094	0.01093
T_4	0.00393	0.00392
T_5	0.00141	0.00140
$\sum_{k=6}^{\infty} T_k$	0.00078	0.00078
Total Transmission	0.73778	0.73779
R_1	0.09154	0.09155
R_2	0.03137	0.03145
R_3	0.01108	0.01107
R_4	0.00395	0.00394
R_5	0.00141	0.00141
$\sum_{k=6}^{\infty} R_k$	0.00078	0.00078
Total Reflection	0.14013	0.14020
A_1	0.07869	0.07869
A_2	0.02788	0.02788
A_3	0.00996	0.00993
A_4	0.00356	0.00355
A_5	0.00128	0.00127
$\sum_{k=6}^{\infty} A_k$	0.00072	0.00070
Total Absorption	0.12209	0.12202

Total albedos were also obtained for $\Sigma_t L = 1$, $\Sigma_s/\Sigma_t = 0.9$, for a parallel beam incident at $\theta = 40^o$ and 60^o ($\cos\theta = 0.7547$ and 0.5). The results compare as follows:

	Markov Matrix Method	TAR(N)
Total reflection, 40^o	0.3185	0.31863
Total reflection, 60^o	0.3935	0.39355

The Markov Matrix Method results are for 30 sublayers while 3-point Gauss quadratures were used in TAR(N) to find fluxes at just 8 points.

Computing time on the IBM 7094 at the M.I.T. Computation Center required for these TAR(N) results is about 9.6 seconds to obtain the Gauss quadrature weights and abscissas, plus 4.4 seconds for each case having a different source incident angle or angular distribution.

3.1.3 Comparison with the Invariant Imbedding Method

Bellman and Kalaba[27] have applied the Invariant Imbedding Method to the calculation of monoenergetic reflection from plane, infinite slabs. Seven incident angles chosen by Gaussian quadratures are used to obtain differential neutron reflection, from which may be obtained total reflection by summing contributions (Gaussian weighted) at all angles. That is, let

$\rho(\psi, \Theta, x)$ = Specific intensity of reflected radiation in direction Θ per unit area on the face of a slab of thickness x due to a unit intensity beam at angle ψ, the area taken perpendicular to the slab;

$a_j(\psi_j, x)$ = Total reflection due to a unit intensity beam at angle ψ_j incident on a slab of thickness x;

w_i = Gaussian quadrature weight for exit angle Θ_i.

Then:

$$a_j(\psi_j, x) = \int_0^{\pi/2} \rho(\psi_j, \Theta, x) \sin \Theta d\Theta \simeq \sum_{i=1}^{7} w_i \rho(\psi_j, \Theta_i, x) \tag{3.12}$$

Table 3.5 summarizes the comparisons with TAR(N).

TABLE 3.5 Total Albedo for $\Sigma_t L = 1.0$, $\Sigma_s/\Sigma_t = 0.9$

Beam Angle, ψ, Degrees	Cos ψ	Total Albedo Invariant Imbedding	TAR(N)
13.0	0.97455395	0.27159	0.27199
29.4	0.87076559	0.29230	0.29231
45.3	0.70292258	0.33175	0.33179
60.0	0.50000000	0.39365	0.39355
72.7	0.29707742	0.47471	0.47507

The point of the comparisons in this and the previous section is that TAR(N) gets accurate results using many fewer points than are required by the Markov Matrix Method, due to the built-in superiority of Gaussian quadratures for numerical evaluation of integrals. No extrapolations to $s^2 \to 0$ are needed, and the method is applicable to slabs at least five mean free paths thick (the Markov Matrix Method cannot go beyond about one mean free path thickness). While the Invariant Imbedding method is ideal for much thicker slabs, it cannot analyze the fate of neutrons as a function of collision number.

3.1.4 Accuracy of the Calculations

A measure of the numerical accuracy of a given problem can be taken as

$$\text{Error} = \Delta = \left| 1 - \sum_{k=o}^{\infty} (T_k + R_k + A_k) \right| = \left| 1 - T - R - A \right| \tag{3.13}$$

The error depends upon both the average point spacing in mean free paths, and the distribution of points. It has been observed that results tend to be much poorer if the points at which fluxes are calculated are not evenly distributed. Their distribution is fixed by the order of the quadrature formula and the slab thickness. Figure 3.14 illustrates the variation of Δ with average point spacing. It can be seen that Δ varies by a factor of as much as 10^3 depending on distribution. Several cases had $\Delta < 10^{-4}$ for average point spacings between 0.1 and 0.3 mean free paths. Round-off errors will not likely be important except for $\Delta < 10^{-5}$. The upper bound shown in Figure 3.14 indicates the maximum error likely to be found for a given average point spacing.

FIGURE 3.14

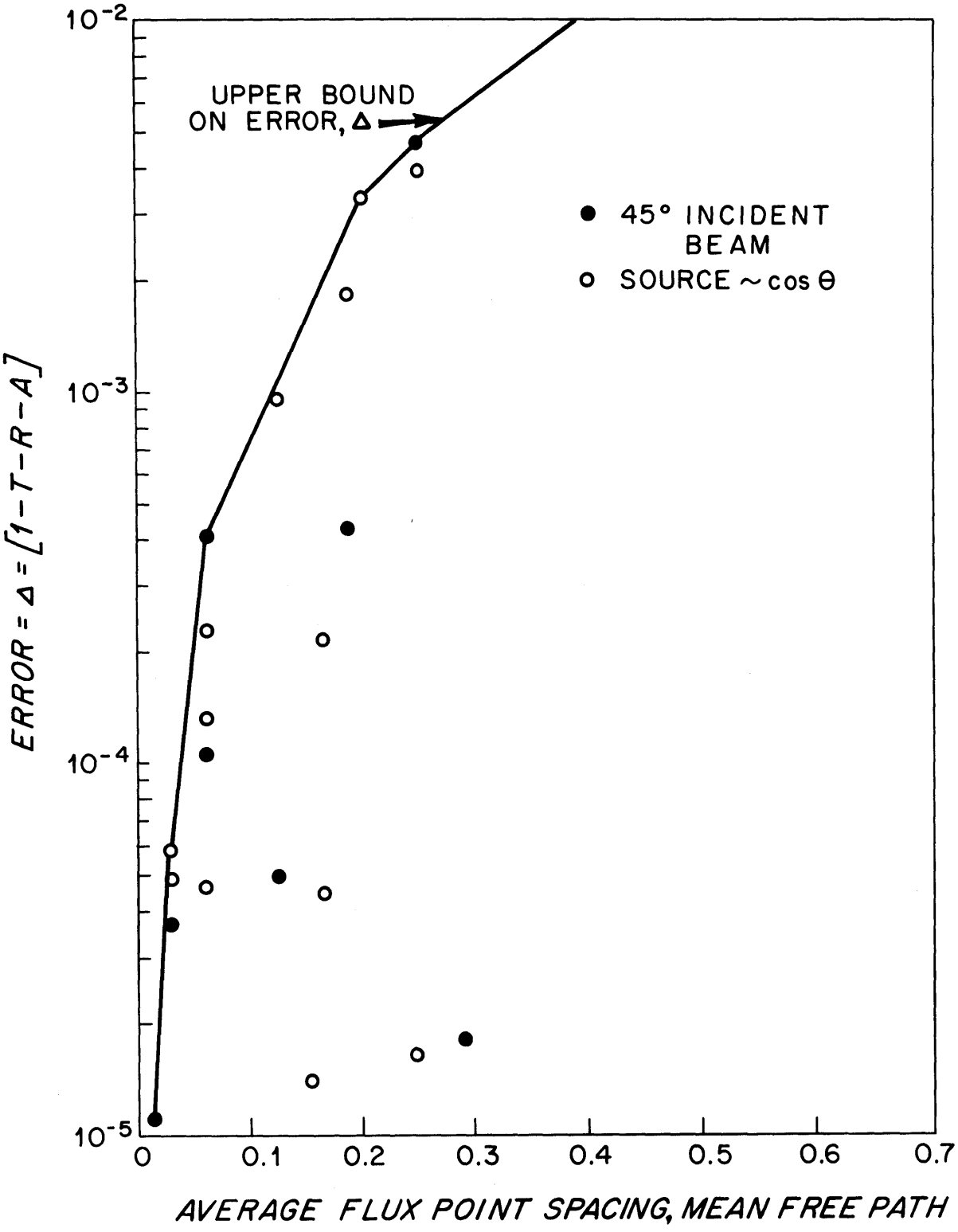
10^{-2}
10^{-3}
10^{-4}
10^{-5}
UPPER BOUND
ON ERROR, Δ
45° INCIDENT
BEAM
SOURCE ~ cos θ
ERROR = Δ = [1 − T − R − A]
0
0.1
0.2
0.3
0.4
0.5
0.6
0.7
AVERAGE FLUX POINT SPACING, MEAN FREE PATH

3.2 TRANSMISSION OF FISSION NEUTRONS BY POLYETHYLENE

Reference results for total fast neutron dose transmitted through a polyethylene slab have been obtained in three ways. Monte Carlo calculations by Allen et al[28] give a dose transmission factor of 0.0014 for 30.5 cm of polyethylene of ρ = 0.97 density. For comparison with other results at ρ = 0.907, this thickness can be scaled by the density ratio 0.97/0.907 to give 32.6 cm. Invariant Imbedding results for 32.6 cm of ρ = 0.907 polyethylene have been obtained by Mathews[17] and by the author using the STAR code. Mathews used two angular groups and four and five energy groups over 0.1 to 10.0 MeV to obtain factors of 0.0018 and 0.0015, respectively. The author used two angular groups and four energy energy groups over 0.1 to 10.0 MeV to obtain a fast neutron dose transmission factor of 0.0026. The neutron cross sections used in all the STAR calculations came from the Goldstein[29] set. However, the energy points selected by Mathews are unknown, and are not likely to be the same as used by the author. This must be the reason for the four-energy-group results not agreeing closely.

The MEDIPORT code was used to calculate the transmission matrix $\underline{T}$ for a 5 cm thick slab of polyethylene, using the transmission probability method as described in Chapter II. Then the transmission matrix for two

5 cm thick slabs was obtained from Equation (2.6):

$$\underline{T} = \underline{T}_2 \left(\underline{T}_1 + \underline{R}_1^* \underline{R}_2 \underline{T}_1 + (\underline{R}_1^* \underline{R}_2)^2 \underline{T}_1 + \ldots\right) \qquad (2.6)$$

which simplifies somewhat as $\underline{T}_1 = \underline{T}_2$, $\underline{R}_1^* \underline{R}_2 = \underline{R}_1^2 = \underline{R}_1 \underline{R}_2$:

$$\underline{T} = \underline{T}_1 \left(\underline{T}_1 + \underline{R}_1^2 + \underline{R}_1^4 \underline{T}_1 + \ldots\right) \qquad (3.14)$$

Neutron cross sections were taken from the Bondarenko[16] set. Eight groups spanned 0.1 to 10.5 MeV. Transport corrections were applied for scattering collisions leaving a neutron in the same energy group, but not for transfering to another group. This is equivalent to assuming isotropic scattering between groups - not a good assumption for hydrogenous materials. However, none of the materials in the beam ports of the M.I.T.R. or the Brookhaven M.R.R. contain hydrogen. For the purposes intended for MEDIPORT, the additional complication of transport-correcting group transfers was not deemed necessary.

The transmission matrix T for 10 cm of polyethylene was obtained in three orders of approximation.

$$\underline{T} \simeq \underline{T}^{(0)} + \underline{T}^{(1)} + \underline{T}^{(2)}; \qquad (3.15)$$

$$\underline{T}^{(0)} = \underline{T}_1 \underline{T}_2,$$
$$\underline{T}^{(1} = \underline{T}_1 \underline{R}_1^{\,2} \underline{T}_2, \qquad (3.16)$$
$$\underline{T}^{(2)} = \underline{T}_1 \underline{R}_1^{\,4} \underline{T}_2.$$

Table 3.6 gives the transmitted fluxes given by the individual terms of $\underline{T}$. The fast neutron dose transmission factor at 10 cm thickness changed from 0.0552 to 0.0558, up to about 1%, by including fluxes coming from $\underline{T}^{(1)}$ and $\underline{T}^{(2)}$. It is apparent that multiple reflections at the interface between the slabs are not important in terms of transmitted fast neutron dose. This makes physical sense in that most of these scattering collisions take place with hydrogen, which seriously degrades the neutron energy at each collision. Table 3.6 bears this out. The fluxes from $\underline{T}^{(1)}$ and $\underline{T}^{(2)}$ are greatly depleted in the highest energy groups, and are largest in the lowest energy groups.

TABLE 3.6 Contributions to Fluxes Transmitted by 10 cm Polyethylene

Group Range, MeV	Flux per Unit Lethargy, 10^{-5} n/cm^2-sec		
	$\underline{T}^{(0)}$	$\underline{T}^{(1)}$	$\underline{T}^{(2)}$
6.5 - 10.5	382	0.062	0.00001
4.0 - 6.5	1460	1.35	0.0010
2.5 - 4.0	2070	7.06	0.016
1.4 - 2.5	2100	14.6	0.059
0.8 - 1.4	1460	20.7	0.141
0.4 - 0.8	1010	22.8	0.235
0.2 - 0.4	752	22.5	0.296
0.1 - 0.2	572	20.0	0.298

The flux and dose transmitted through k slabs of polyethylene each 5 cm thick have been obtained using the zeroth approximation to the transmission matrix:

$$\underline{T}^{(0)} \text{ (k slabs)} \simeq \underline{T}_1^{k}. \qquad (3.17)$$

The results are shown in Figure 3.15. The error of this approximation is believed to be very small, a few percent at most. The reason is that the highest five energy groups contribute about 85% and 95% of the dose transmitted through 10 cm and 30 cm respectively. Hence pile-up of multiply-reflected neutrons in the lowest energy groups will have little effect on transmitted dose. Better agreement with the Monte Carlo result can be expected if transport corrections are applied to group transfer cross sections. Even so, the present result is very little worse than the 4-group STAR calculation, as compared to the Monte Carlo dose transmission factor through 32.6 cm of polyethylene.

The IBM - 7094 computer time used by MEDIPORT was about 0.06 minute for eight energy groups. STAR used 1.37 minutes for a four group calculation not counting 2.44 minutes required to generate input with CSDP on the same computer. In view of the speed of the MEDIPORT calculations, the accuracy attained looks very encouraging.

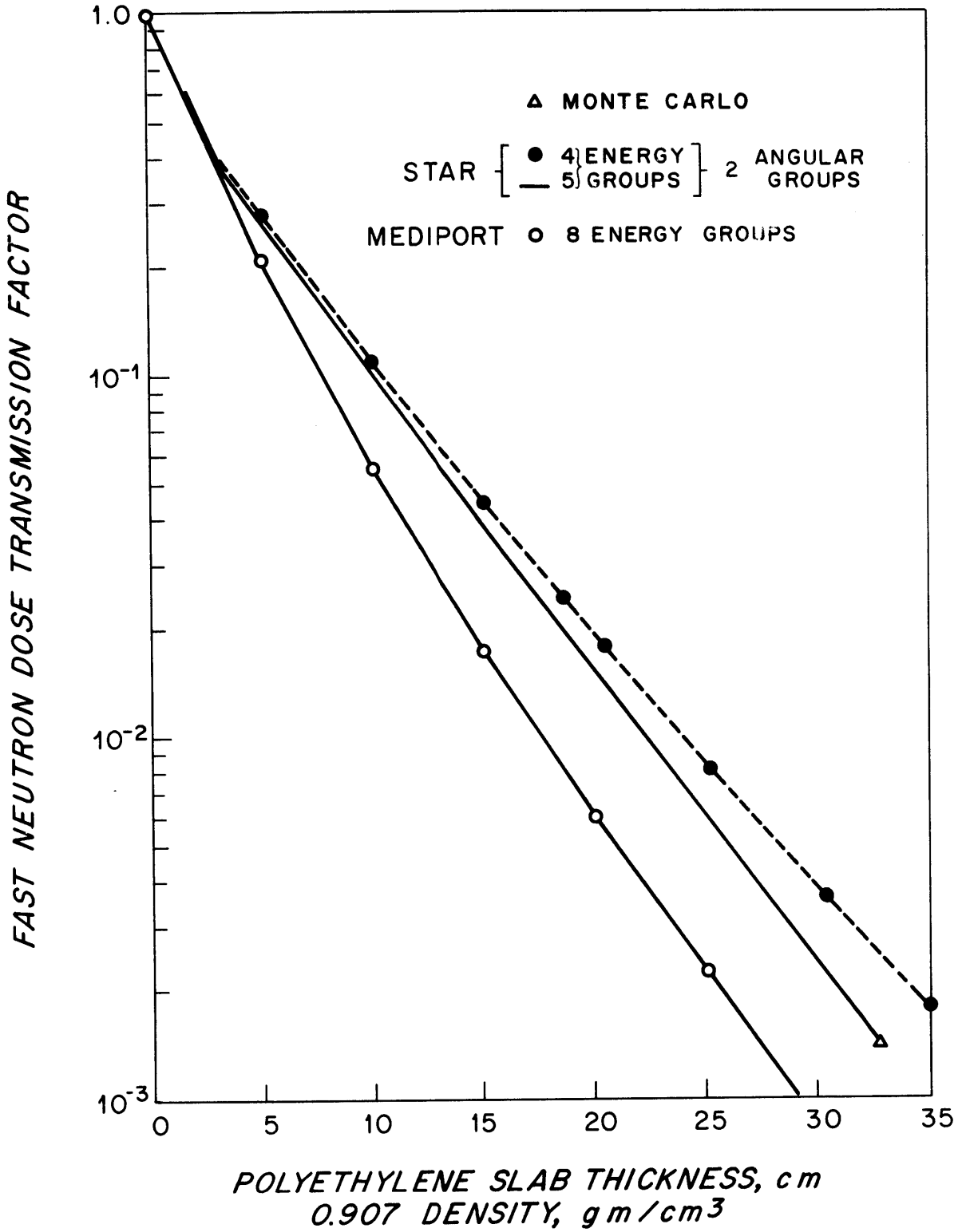
1.0
10^{-1}
10^{-2}
10^{-3}
0
5
10
15
20
25
30
35
△ MONTE CARLO
STAR { ● 4 } ENERGY GROUPS, — 5 } ENERGY GROUPS } 2 ANGULAR GROUPS
MEDIPORT ○ 8 ENERGY GROUPS
FAST NEUTRON DOSE TRANSMISSION FACTOR
POLYETHYLENE SLAB THICKNESS, cm
0.907 DENSITY, gm/cm3

3.3 TRANSMISSION OF FISSION NEUTRONS BY D_2O

The M.I.T.R. Medical Beam Port contains 53.34 cm of D_2O, while as much as 18.0 cm of D_2O may be used in the treatment ports at the Brookhaven M.R.R. Heavy water is also an excellent moderator, which makes its contribution to fast neutron attenuation a major portion of the total attenuation through these beam facilities. In view of this, calculations have been performed for an idealized D_2O shielding problem in order to assess the accuracy of the methods used by MEDIPORT.

Neutrons from an isotropic fission source are incident upon a plane, infinite slab of D_2O. The slab thickness is variable up to 40 cm. The shielding effectiveness of the slab is to be given in terms of the total fast neutron dose transmitted through the slab as measured at the surface of a 30 cm thick infinite slab of tissue (see Section 2.3).

Neutron cross sections for oxygen, used by STAR and MEDIPORT, and for deuterium used by MEDIPORT, have the same sources and corrections as given in Section 3.2 for the polyethylene problem. For STAR, deuterium angular cross sections $\sigma(\theta)$ barns/steradian were picked off from the curves given in BNL-400,[30] and converted to Legendre polynomial form with LPF (Appendix A.3). Table 3.7 gives the coefficients $F_\ell(E)$ of the expansion in Legendre polynomials $P_\ell(\cos\theta)$:

$$\sigma(\theta) = \frac{\sigma_s(E)}{4\pi}\left[1 + \sum_{\ell=1}^{7}(2\ell + 1)\, F_\ell\,(E)\, P_\ell(\cos\theta)\right] \quad (3.18)$$

Also shown are the total elastic scattering cross sections $\sigma_s(E)$ derived from the angular cross sections, and the corresponding values taken from BNL-325.[31] It is believed that the BNL-325 values for $\sigma_s(E)$ are more accurate. They were used in preparing input for STAR.

A large gap exists in experimental angular cross section data between 5.5 and 14.1 MeV. Upon plotting the first few $F_\ell(E)$, one finds a reasonable variation with neutron energy E from which values at intermediate energies may be linearly interpolated. These values are also given in Table 3.7.

TABLE 3.7 Angular Scattering Cross Section for Deuterium (.100(-5)=.100x10^{-5})

E,MeV	BNL-325/Derived	$F_1(E)$	$F_2(E)$	$F_3(E)$	$F_4(E)$	$F_5(E)$	$F_6(E)$
0.100	3.35/3.34	-.494(-1)	.530(-2)	.187(-3)	-.778(-4)	.530(-3)	-.107(-7)
0.200	3.3/3.23	-.142	.123(-1)	.535(-3)	-.942(-4)	.434(-3)	-.128(-3)
0.500	3.2/3.01	-.278	.788(-1)	-.382(-1)	.151(-1)	-.425(-2)	.844(-3)
0.750	3.07/2.75	-.189	.294(-1)	-.132(-2)	-.190(-2)	-.687(-3)	.242(-3)
1.000	2.95/2.86	-.257	.117	-.430(-1)	.181(-1)	-.752(-2)	.305(-2)
1.95	2.60/2.52	-.139	.159	-.576(-1)	.280(-1)	-.126(-1)	.556(-2)
2.45	2.40/2.39	.151(-2)	.171	-.334(-1)	.131(-1)	-.458(-2)	-.111(-2)
3.27	2.12/2.13	.419(-1)	.186	-.463(-1)	.141(-1)	-.108(-2)	-.247(-2)
4.50	1.772/1.57±.2	..169	.221	-.487(-1)	.122(-1)	-.153(-2)	.134(-2)
5.50	1.55/1.63±.2	.232	.223	-.359(-1)	.863(-2)	-.851(-3)	.712(-3)
5.98	1.45	.243	.222	-.373(-1)	.105(-1)		
7.32	1.232	.264	.220	-.430(-1)	.160(-1)		
8.09	1.126	.270	.218	-.460(-1)	.187(-1)		
8.94	1.031	.275	.216	-.494(-1)	.22(-1)		
9.89	0.936	.279	.214	-.532(-1)	.257(-1)		
10.93	0.852	.280	.212	-.576(-1)	.297(-1)		
14.10		.278	.208	-.703(-1)	.425(-1)	.238(-1)	.113(-1)

The MEDIPORT code was used to calculate the transmission matrix $\underline{T}$ for a 10 cm thick slab of D_2O, using the transmission probability method described in Chapter II. Then the transmission matrix for two 10 cm thick D_2O slabs was obtained in zeroth and first approximation in the same way as for polyethylene (Section 3.2).

Table 3.8 gives the fluxes transmitted through two 10 cm thick slabs using these approximations. The first approximation contribution to dose attenuation through 20 cm of D_2O amounts to only a 1.9% increase over the zeroth order term. As with polyethylene, the multiply-reflected neutrons have lost much of their energy. Relatively more reflected neutrons "pile up" in the lower energy groups because D_2O is not as good a moderator as polyethylene.

Figure 3.16 gives the fast neutron dose attenuation factor through D_2O given by the zeroth zpproximation to the transmission matrix, and compares this with Invariant Imbedding results from program STAR.

TABLE 3.8 Contributions to Fluxes Transmitted by 20 cm D_2O

Group Range, MeV	Flux per Unit Lethargy, 10^{-5} n/cm^2-sec	
	$\underline{T}^{(0)}$	$\underline{T}^{(0)}$
6.5 - 10.5	144	0.133
4.0 - 6.5	562	2.35
2.5 - 4.0	786	7.24
1.4 - 2.5	706	10.5
0.8 - 1.4	533	12.9
0.4 - 0.8	585	20.1
0.2 - 0.4	594	30.0
0.1 - 0.2	596	46.0

FIGURE 3.16

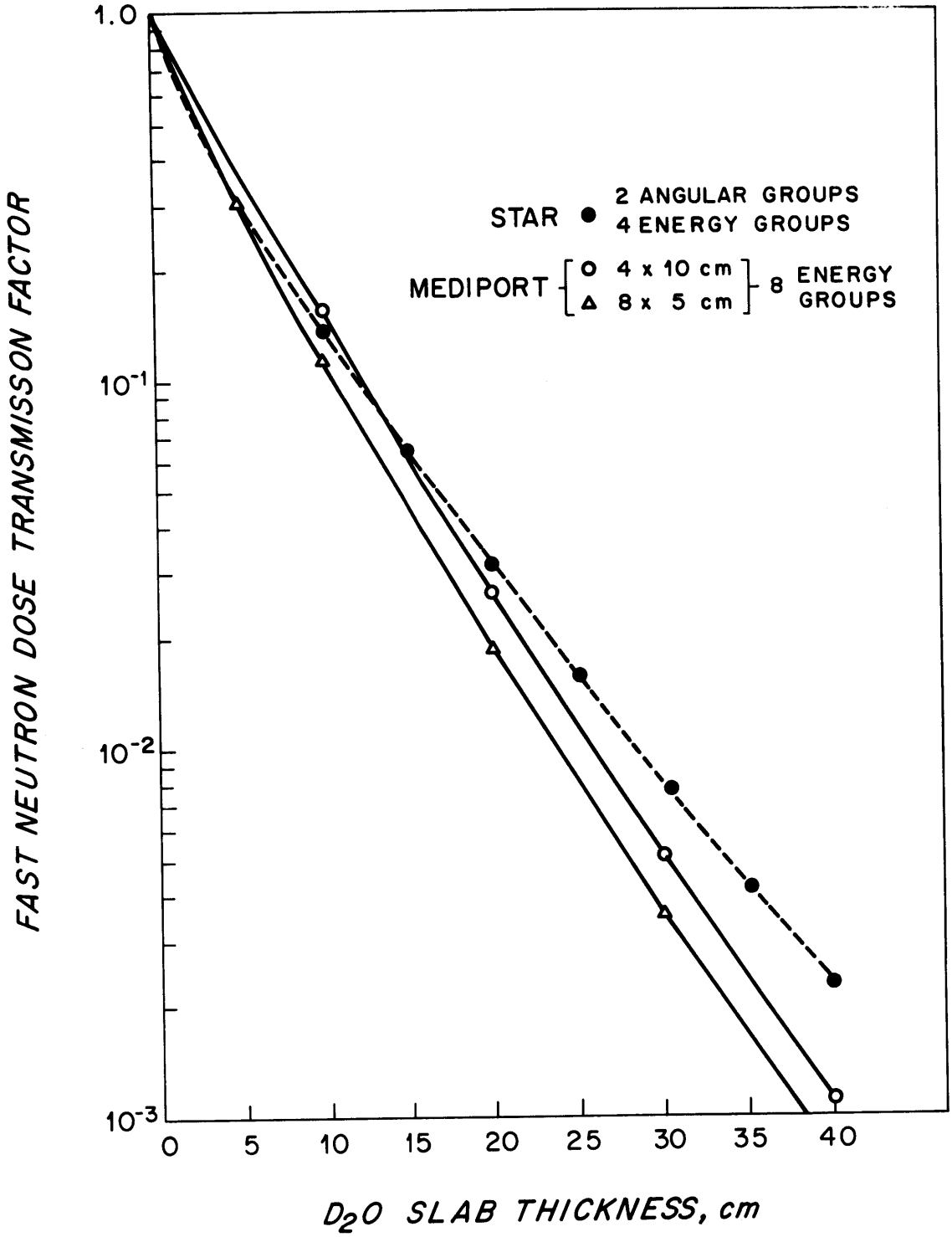
1.0
10^{-1}
10^{-2}
10^{-3}
0
5
10
15
20
25
30
35
40
FAST NEUTRON DOSE TRANSMISSON FACTOR
D_2O SLAB THICKNESS, cm
STAR ● 2 ANGULAR GROUPS 4 ENERGY GROUPS
MEDIPORT ○ 4 x 10 cm △ 8 x 5 cm 8 ENERGY GROUPS

CHAPTER IV

COMPARISON WITH EXPERIMENT AT THE BROOKHAVEN MEDICAL RESEARCH REACTOR

4.1 THE MRR MEDICAL FACILITY

The Medical Research Reactor[32] is a heterogeneous, tank-type reactor designed exclusively for medical and biological studies. It is water cooled and moderated, with a graphite reflector. Seventeen plate-type fuel elements with an active length of 23 5/8" fit inside a 23 1/2 inch I.D. reactor vessel. Power levels up to 5 MW are available. Two shielded rooms at opposite sides of the core are equipped with special treatment ports and shutters. A broad beam experimental area located at the end of a thermal column is used for whole-body irradiation studies. Three 4-inch horizontal thimbles traverse the core.

The treatment ports have provision for changing the thickness and type of materials in the neutron flight path, in order to adjust relative strengths of fast, epithermal, and thermal neutrons, and gamma rays. Drainable D_2O tanks permit adjusting the D_2O moderator thickness from 0 to 18 cm. At all times there is a minimum of 21.6 cm of graphite and 34.3 cm of bismuth between the core and the point of irradiation.

"Epithermal" beams can be produced by filtering out the thermal neutrons with a cadmium or lithium filter.

4.2 EXPERIMENTAL MEASUREMENTS

A rather extensive survey of the production and use of epithermal neutrons for neutron capture therapy has been reported by Fairchild.[33] His experiments consisted mainly in measuring (by Au and Na foil activation) thermal neutron flux along the axis of a cylindrical, tissue-equivalent phantom. The phantom was 16.6 cm dia., 23 cm high, with 0.5 cm thick polyethylene walls. It was suspended directly in front of the beam port, with the cylindrical axis on the beam port axis.

The relationship used for obtaining the thermal neutron flux was $\phi_{th} = \phi_{bare} - 1.02\ \phi_{Cd\ cov.}$, where the 1.02 factor corrects for resonance absorption in the 0.76 mm thick cadmium covers.

Epithermal neutron flux per energy decade was derived from cadmium ratio data as follows:

$$\frac{\phi_{th}}{\phi \text{ per energy decade}} \simeq \left(\frac{Rcd}{1.02} - 1\right) \int_{0.5\ ev}^{\infty} \sigma_a(E)\,dE/E \Big] / (2.3\ \sigma_a(th) \qquad (4.1)$$

Rcd = bare foil activation / 0.76 mm Cd-covered foil activation.

Threshold detectors S^{32}, U^{238}, Np^{237}, and Pu^{239} were used to measure integrated fast flux above 3, 1.5, 0.6 and 0.01 MeV, respectively. Fast neutron dose for tissue in air was obtained from the threshold detector activations with the formula (US NBS 1957):

$$\text{Dose} = \left[0.63\ (\phi_{Pu} - \phi_{Np}) + 2.23\ (\phi_{Np} - \phi_{U}) + 3.07(\phi_{U} - \phi_{s}) + 4.04\ \phi_{s}\right] \times 10^{-7} \quad \text{ERGS/GM}, \tag{4.2}$$

assuming a 1/E neutron energy distribution.

4.3 COMPUTER SIMULATION

The reactor core can be approximately replaced by an infinite, plane source of angular distribution and strength given by Equations (3.1) and 3.3). To obtain p_o, p_1, and λ, the core was homogenized as an equivalent cylinder, 24.4 cm radius by 60.0 cm height. Assuming 3.1×10^{16} fission/sec. per Mw, and $\nu = 2.43$ fast neutrons/ fission, then at a power of 5 Mw the average source strength of fission neutrons in the core is

$$\bar{q} = \frac{3.10 \times 10^{16} \text{ fiss/sec/Mw} \times 2.43 \text{ fast neut./fiss} \times 5 \text{ Mw}}{\pi(24.4)^2\ 60.0 \text{ cm}^3} \tag{4.3}$$

$$= 3.35 \times 10^{12} \text{ n/cm}^3\text{-sec.}$$

and

$q_{max} = 1.68\bar{q} = 5.63 \times 10^{12}$ n/cm^3-sec (1.68 is measured peak/ avg. flux ratio).

Assuming that the fast neutron source follows the thermal neutron flux, which is 7×10^{13} at $r = 0$, and 5.40×10^{13} at $r = 31.8$ cm, then the radial buckling, B^2, is approximately given by

$$\phi(r) \sim \phi_{max} \cos Br \tag{4.4}$$

$$B = \cos^{-1} (5.40 \times 10^{13}/7.0 \times 10^{13})/31.8 = 0.0210 \text{ cm}^{-1} \tag{4.5}$$

$$p_o = \frac{5.63 \times 10^{12}}{4} \times \cos(.0210 \times 24.4) \times 0.68 =$$

$$8.31 \times 10^{11} \text{ n/cm}^3\text{-sec} \qquad (4.6)$$

$$p_1 = \frac{4}{6}(.0210) \tan(.0210 \times 24.4) p_o = 0.065 \times 10^{11} \text{n/cm}^4\text{-sec}$$

The neutron flight path from the reactor core edge to the phantom passes through numerous cylindrical layers of materials. Some grouping together of layers can be made in order to simplify the calculations. Negligible error is incurred (an example is discussed in Chapter V) The regions are:

Table 4.1 MRR Geometry, all 18.0 cm D_2O in place

Actual		Simplified	
Material	Thickness, cm.	Material	Thickness, cm.
C	21.37	C	21.37
Air	2.54	Bi	19.05
Bi	19.05	Air	6.54
Air	4.0	D_2O	18.0
D_2O	12.0	Air	20.4
Air	6.4	Bi	10.5
D_2O	6.0	Air	48.0
Air	14.4		
Bi	7.5		
Air	48.0		
Bi	3.0		

Multigroup core cross sections and mean free paths $\lambda = 1/\Sigma_t$ were obtained using homogenized atom densities and volume fractions of

N_{U-235}	= 0.00172	f_{U-235}	= 0.036
N_{Al}	= 0.00523	f_{Al}	= 0.087
N_{H2O}	= 0.00709	f_{H2O}	= 0.212
N_C	= 0.0557	f_C	= 0.665
			1.000

Basic cross section data come from the Bondarenko[16] set. The macroscopic thermal neutron absorption and scattering cross sections for tissue-equivalent fluid were calculated as $\Sigma_a = 0.023$ cm^{-1} and $\Sigma_s = 3.06$ cm^{-1} for the following composition:

Element	Weight Fraction, %
O	70.9
C	15.6
H	9.73
N	3.54
Cl	0.15
Na	0.10

Schermer and Brownell[34] have measured total cross sections for tissue, from 0.01 to 1 ev. They find

Σ_t (tissue) $\simeq 1.1 \times \Sigma_t(H_2O)$. That is, Σ_t(tissue at 0.0253 ev) $\simeq 3.45$ cm. However, the diffusion coefficient D and the diffusion length L have not been measured for tissue. In order to obtain D and L from neutron cross sections, the average cosine of the scattering angle $\bar{\mu}_o$ is needed. The equations are:

$$\frac{1}{L^2} = 3\,\Sigma_t\,\Sigma_a(1-\bar{\mu}_o)\left(1 - \frac{\Sigma a}{\Sigma_t}\left[4/5 - \bar{\mu}_o/(1-\bar{\mu}_o)\right]\right) \quad (4.7)$$

$$D = \Sigma_a L^2$$

The structural details of atoms in tissue determine $\bar{\mu}_o$, which has not been measured. Hence a reasonable solution adopted was to use the diffusion parameters for pure water - D=0.17 cm and L = 2.76 cm - because Σ_a(tissue) is within 4% of Σ_a(water) and Σ_s(tissue) is within about 10% of Σ_s(water).

The computed fast neutron spectrum in the Reference Case (18 cm D_2O in place) was normalized to match the fast neutron dose rate of 182 rad/min given by Equation (4.2). The lateral leakage of thermal neutrons diffusing through the many regions from the core to the phantom was adjusted to match the measured thermal neutron flux at the surface of the phantom. This flux is $\phi_o = 4.06 \times 10^{11}$ n/cm^2-sec. Section 2.2 discusses the lateral leakage leakage parameter α^2.

Figure 4.1 indicates the effect of D_2O removal on the relative thermal neutron flux in the phantom (fluxes are normalized to ϕ_o). The measured fluxes have relaxation lengths which are quite close to those of the computed curves. In general, the measured fluxes attenuate slightly slower than predicted. This may be due to epithermal and fast neutrons penetrating the cadmium-wrapped sides of the phantom. Fairchild found that the relaxation length of thermal neutrons in a phantom totally wrapped in 1.5 mm of cadmium dropped from 6.7 cm to 4.7 cm when an additional 7.6 cm of lithiated paraffin was added at the sides and end of the phantom. The experimental results shown in Figure 4.1 were obtained using 1.5 mm cadmium on the sides and end of the phantom, with the front surface bare. Due to the relatively large thermal neutron flux penetrating the bare front surface of the phantom, the effect of epithermal and fast neutrons entering the sides of the phantom would not be expected to be very large.

But for the cases using lithium filters placed on the front surface of the phantom, very few thermal neutrons get into the phantom. The shape of the thermal neutron flux curve is then determined mainly by the epithermal and fast neutrons which thermalize inside the phantom. A significant contribution is made by neutrons penetrating the sides of the phantom.

Figure 4.2 compares predicted and measured relative thermal neutron fluxes in the phantom for the reference case and for filters of 2 mm Li (7.52 atom % Li^6), 1 mm Li (95.6 atom % Li^6), and 3 mm Li(95.6 atom % Li^6). The deviation from exponential behaviour at depths greater than about 4 cm is caused by neutrons penetrating the sides of the phantom. The predicted fluxes for 1 and 3 mm Li (95.6 atom % Li^6) are somewhat low near the front surface of the phantom. Part of this discrepancy is due to using exactly 1 and 3 mm of Li, whereas in fact these dimensions turned out to be nominal only. The lithium sheets used in the experiments averaged about 10% thinner than nominal rating.

An idea of the magnitude of the thermal neutron flux created by epithermal and fast neutrons penetrating the sides of the phantom can be obtained from the difference between the computed and measured flux. This difference is also shown in Figure 4.2, for the 3 mm Li^6 filter cases. It turns out to be very large, greater at most depths than the thermal neutron flux generated by neutrons entering the face of the phantom.

The effect of D_2O removal on fast neutron dose

rate in tissue at the front surface of the phantom is shown in Figure 4.3, relative to the dose rate with all 18 cm D_2O removed. The agreement between simulation and experiment is excellent. Section 2.1.5 discusses the approximations involved in the simplified calculation of neutron spectra used for these results. Experience with the latest spectrum calculation used by MEDIPORT indicates that the simplified spectra were slightly over-attenuated. Somewhat better agreement with dose attenuation for 18 cm D_2O may be possible using the latest neutron spectrum calculation.

In conclusion, these studies indicated that the methods used in MEDIPORT gave reasonable results as to the effect of changes from a reference condition. Considering the differences between the experimental measurements and "clean" calculations, overall agreement between simulation and experiment was quite satisfactory.

FIGURE 4.1

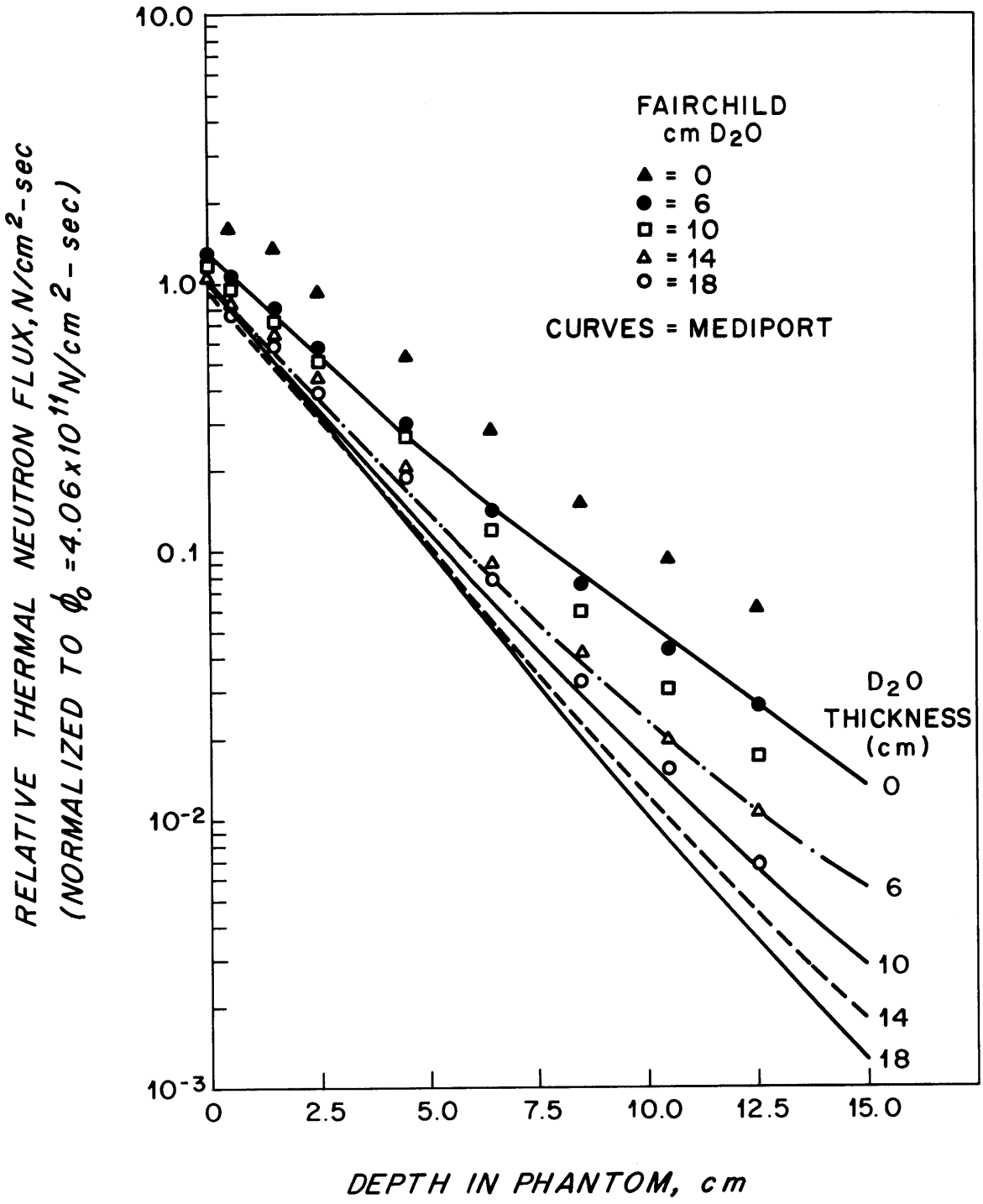
FAIRCHILD
cm D_2O
▲ = 0
● = 6
□ = 10
△ = 14
○ = 18
CURVES = MEDIPORT
D_2O THICKNESS (cm)
0
6
10
14
18
10.0
1.0
0.1
10^{-2}
10^{-3}
0
2.5
5.0
7.5
10.0
12.5
15.0
RELATIVE THERMAL NEUTRON FLUX, N/cm^2-sec
(NORMALIZED TO $\phi_0 = 4.06 \times 10^{11} N/cm^2$-sec)
DEPTH IN PHANTOM, cm

FIGURE 4.2

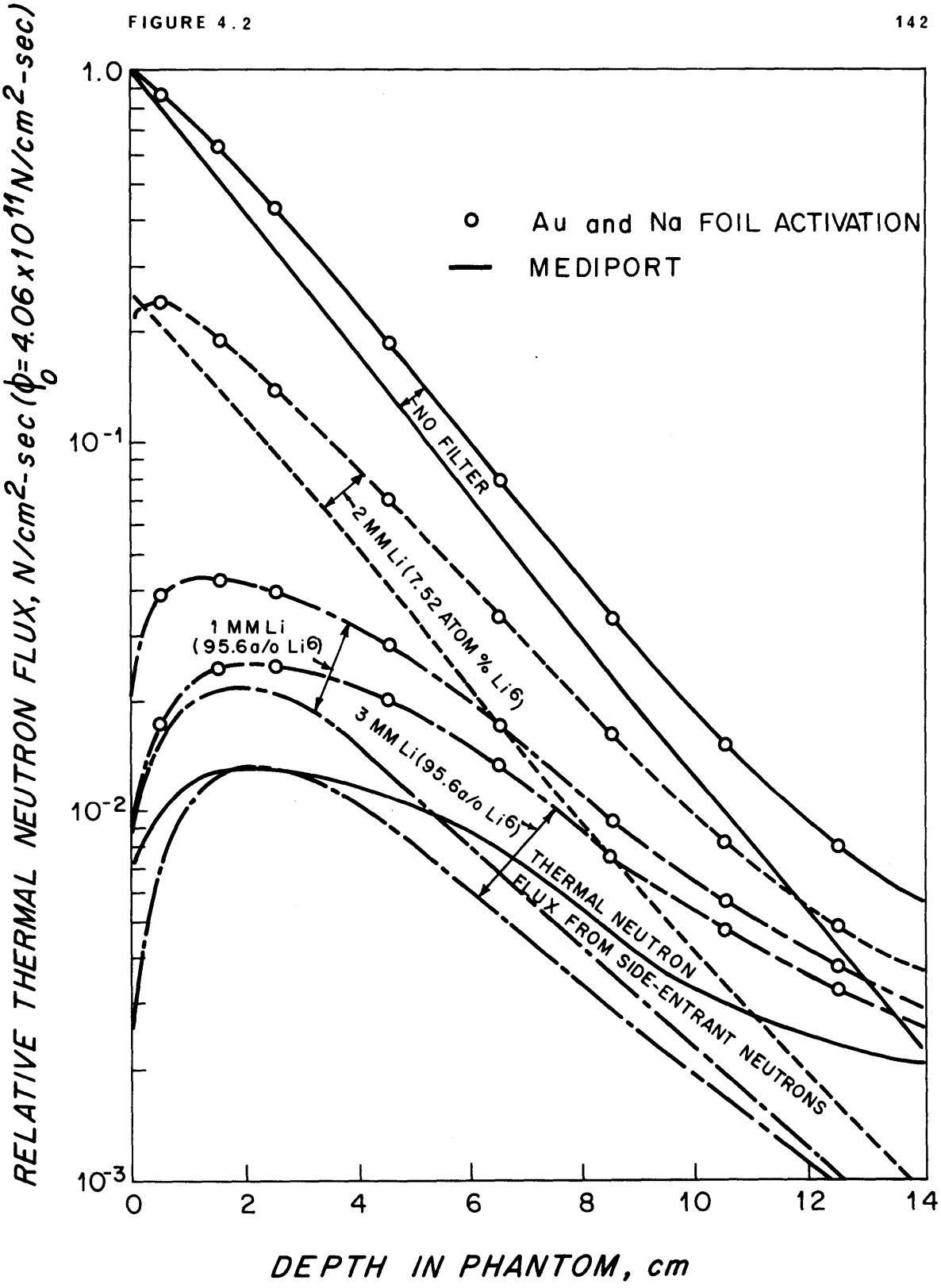
RELATIVE THERMAL NEUTRON FLUX, N/cm²-sec (ϕ_o= 4.06 x 10¹¹ N/cm²-sec)
1.0
10^{-1}
10^{-2}
10^{-3}
0
2
4
6
8
10
12
14
DEPTH IN PHANTOM, cm
o Au and Na FOIL ACTIVATION
— MEDIPORT
NO FILTER
2 MM Li (7.52 ATOM % Li6)
1 MM Li (95.6a/o Li6)
3 MM Li (95.6a/o Li6)
THERMAL NEUTRON FLUX FROM SIDE-ENTRANT NEUTRONS

FIGURE 4.3

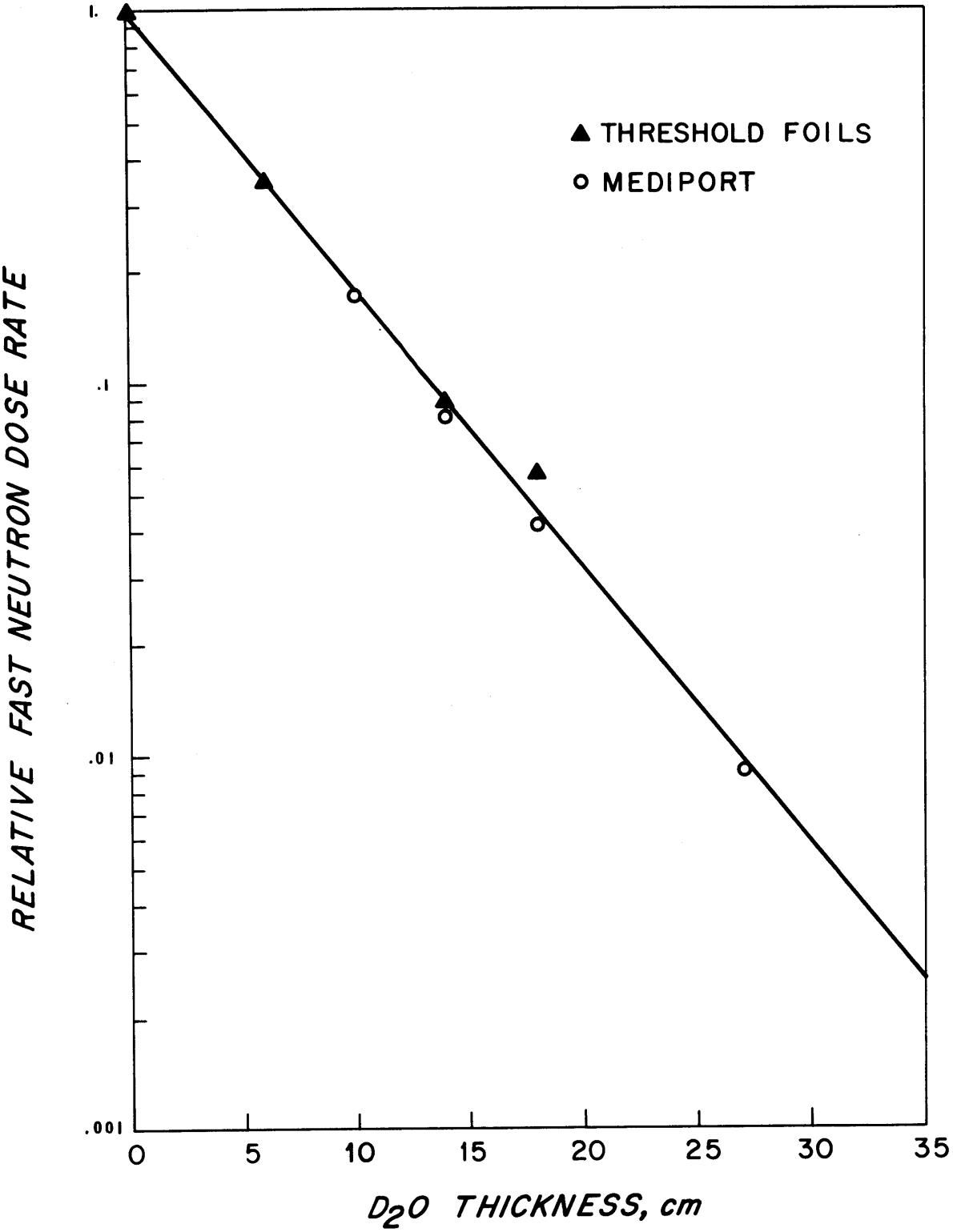
RELATIVE FAST NEUTRON DOSE RATE
1.
.1
.01
.001
0
5
10
15
20
25
30
35
D2O THICKNESS, cm
▲ THRESHOLD FOILS
o MEDIPORT

CHAPTER V

RESULTS FOR THE M.I.T.R. MEDICAL FACILITY

5.1 INTRODUCTION

The M.I.T.R. Medical Beam Port is shown in Figure 5.1. A brief description of the entire Medical Facility shown in Figure 1.1 has been given in Section 1.1. Neutrons emerging from the portal have traversed slabs of heavy water, bismuth, and aluminum, plus a few air gaps. The dimensions and composition of these regions are given in Table 5.1 starting at the core-reflector interface (i.e., at the bottom of the fuel). Also given are simplified structures obtained by grouping nearby layers together. An example will be given later in this chapter to confirm that the error resulting from regrouping layers is only a few percent. In slab geometry, the air gaps may be omitted in epithermal and fast neutron transmission calculations. The gaps must be accounted for in thermal neutron flux calculations, due to the lateral loss of thermal neutrons absorbed by the beam port walls.

5.2 COMPUTER SIMULATION

The reactor core can be approximately replaced by an infinite plane source with strength and angular distribution given by Equations (3.1) and (3.3). The equivalent homogenized core is a cylinder with radius and height of 41.9 cm and 60.0 cm, respectively. Assuming 3.10×10^{16} fission/sec per Mw, and $\nu = 2.43$ fast neutrons/fission, then at a power of 5 Mw the average source strength of fission neutrons in the core is

$$\bar{q} = \frac{3.10 \times 10^{16} \text{ fiss./sec/Mw} \times 2.43 \text{ fast neut./fiss.} \times 5\text{Mw}}{\pi(41.9)^2\, 60} \qquad (5.1)$$

$$= 1.136 \times 10^{12} \text{ fast neutrons/cm}^3 \text{ - sec}$$

The radial and axial flux distributions in the core are given by Mathews[35]. Averaging the Cu and Co foil activation data for each fuel ring gives a radial average to maximum flux ratio of 0.966. The axial average to maximum flux ratio is 0.899 assuming a cosine axial flux distribution and using the measured axial buckling of 0.000710 cm^{-2}. The maximum fast neutron

source strength is then

$$q_{max} = \bar{q}/(0.966 \times 0.899) = 1.308 \times 10^{12} \text{ fast neut./cm}^3\text{-sec} \qquad (5.2)$$

The magnitude of q at the core-reflector interface (30 cm below the axial midplane of the core) is

$$q_{30} = q_{max} \cos \left[B_{axial}(30)\right] = 0.912 \times 10^{12} \text{fast neutrons/cm}^3\text{-sec} \tag{5.3}$$

The neutron source for the Medical Beam is very wide at the core-reflector interface. Because of this, the effective source strength is radially averaged:

$$p_o = 0.966\ (0.912)10^{12} = 0.880 \times 10^{12} \text{ fast neutrons/cm}^3\text{-sec} \tag{5.4}$$

and

$$p_1 = (B \tan [30B]\ )p_o = 0.0241 \times 10^{12} \text{ fast neutrons/cm}^3\text{-sec} \tag{5.5}$$

The volume fractions of core materials are:[34]

$$f_{D_2O} = 0.9085$$

$$f_{Al} = 0.0880$$

$$f_U = \frac{0.0035}{1.0000}$$

Combining these volume fractions with group-averaged neutron cross sections gives

$$\lambda(E) = 1/\Sigma_t(E) = \left[f_{D_2O}\,\Sigma_t(D_2O) + f_{Al}\,\Sigma_t(Al) + f_U\,\Sigma_t(U)\right]^{-1}$$

The neutron source in each energy group and angular group is given by Equations (3.1) and (3.4) except for a multiplicative factor X_k which is the fraction of fission spectrum neutrons emitted within the group. For example, the four energy group, two angular group neutron source used with STAR is:

Energy Group, k	Boundaries MeV	X_k	$L_1(k)$ 10^{10}n/cm^2-sec	$L_2(k)$ 10^{10}n/cm^2-sec
1	0.1 - 1.822	0.5654	9.15	28.4
2	1.822- 5.05	0.3701	10.37	32.9
3	5.05 - 8.278	0.04469	2.010	6.55
4	8.278-10.0	0.003579	0.1930	0.639

TABLE 5.1 Medical Beam Port Geometry for Shutters Open

Actual Geometry		Simplified for MEDIPORT		Simplified for STAR	
Material	Thickness (cm)	Material	Thickness (cm)	Material	Thickness
D_2O	33.02	D_2O	34.29	D_2O	34.29
Al	0.317	Bi	11.43	Bi	11.43
Bi	3.17	D_2O	19.05	D_2O	19.05
Al	0.317	Al	1.588	Al	1.588
D_2O	1.27	Void	144.7	Bi	16.82
Al	0.317	Bi	16.82		
Bi	3.17				
Al	0.317				
D_2O	1.27				
Al	0.317				
Bi	3.17				
Al	0.317				
D_2O	17.78				
Al	0.953				
Void	11.60				
Al	0.317				
Void	98.5				
Al	0.317				
Void	34.6				
Bi	3.33				
Bi	13.49				

MEDIPORT spectrum calculations were obtained using the neutron cross section set tabulated by Bondarenko. It consists of a thermal group plus 25 epithermal and fast neutron groups from 0.215 ev to 10.5 MeV. The groups have uniform lethargy widths up to 0.1 MeV (3 per energy decade). For simplicity, uniform lethargy width cross sections from 0.1 MeV to 10 MeV at three per decade were derived from the given group cross sections using flux-weighting to preserve the total reaction rate. The intra-group flux per unit lethargy $\phi(u)$ was assumed to be a constant below 2.15 MeV, and a fission spectrum at higher energies. The "overlap" or fraction of the new group flux coming from each old group flux is:

Fraction of old group k in new group j =

$$\int_{\xi}^{\zeta} \phi(u)\, du \Big/ \int_{u_j}^{u_{j+1}} \phi(u)\, du \qquad (5.6)$$

where

$\xi = u_k$ if $u_j < u_k < u_{j+1}$; $\zeta = u_{k+1}$, if $u_j < u_{k+1} < u_{j+1}$

$= u_j$ if $u_k < u_j < u_{k+1}$; $= u_{j+1}$, if $u_k < u_{j+1} < u_{k+1}$

$= u_{k+1}$, otherwise. $= u_{k+1}$, otherwise.

The conversion to uniform lethargy group cross sections $\hat{\sigma}$ is:

$$\hat{\sigma}_1 = 0.232\ \sigma_1 + 0.768\ \sigma_2$$

$$\hat{\sigma}_2 = 0.122\ \sigma_2 + 0.636\ \sigma_3 + 0.242\ \sigma_4$$

$$\hat{\sigma}_3 = 0.556\ \sigma_4 + 0.444\ \sigma_5$$

$$\hat{\sigma}_4 = 0.288\ \sigma_5 + 0.712\ \sigma_6 \qquad (5.8)$$

$$\hat{\sigma}_5 = 0.193\ \sigma_6 + 0.807\ \sigma_7$$

$$\hat{\sigma}_6 = 0.0964\ \sigma_7 + 0.9036\ \sigma_8$$

More recent results have used the non-uniform groups as given by Bondarenko.

Neutron cross sections used by STAR have come from two sources. Data for H, C, and O came from a tabulation by Goldstein[29]. Angular elastic scattering cross sections for D, Al, and Bi were taken from the curves in BNL-400[30] and fitted to eight-term Legendre polynomial expansions using LPF(Appendix A.3) Equation (3.18) gives the expansion formula. Table 3.7 lists the coefficients in the expansion of the angular scattering cross section for deuterium. The total scattering cross section given in BNL-325 [31] for D, Al and Bi was used rather than the values derived from the integral of the angular cross sections. Total and inela tic scattering cross sections were taken from BNL-325 also. For Al and Bi, the energy spectrum of

inelastically scattered neutrons was also required at discrete energies E_i. In Mathews'[17] notation:

$g_{in'i}$ (E_k, E_m) = the probability that an inelastically scattered neutron with incident energy E_k is left with exit energy E_m. (5.9)

The normalization on g_{in} is:

$$\int_0^\infty g_{in',i}\ (E_k, E_m)dE_m = 1 \qquad (5.10)$$

The Bondarenko cross section set gives the inelastic scattering cross section $\sigma_{in}(k \rightarrow m)$ for scattering from group k to group m and the total inelastic scattering cross section σ_{in}. The relationship to the g-function is

$$\int_{\text{group}} \phi\ (E_k)\ dE_k \quad \int_{\text{group m}} g_{in,i}(E_k, E_m)\ dE_m = \sigma_{in}\ (k \rightarrow m)/\sigma_{in} \qquad (5.11)$$

A reasonable approximation to the g-function was obtained by graphical differentiation of a smooth curve passing through the ratios $\sigma_{in}(k \rightarrow m)/\sigma_{in}$. The normalization condition

$$\int_{0.10\text{MeV}}^{10\text{MeV}} g_{in,i}\ (E_k, E_m)\ dE_m = 1 \qquad (5.12)$$

was satisfied automatically by modifying the CSDP code (Appendix A.5). Equation (5.12) implies σ_{in} is the total inelastic cross section for a neutron with energy E_k going to E_m, for $E_m > 0.10$ MeV.

5.3 EPITHERMAL NEUTRON BEAMS

A reduction in thickness of moderating material in the beam flight path is the simplest method by which the beam intensity in the epithermal region can be increased. Similarly, filtering out a large proportion of the thermal neutrons by means of a thin layer of Li^6 or Cd is a simple device to raise the average neutron energy, and hence the penetrating power of the beam. These two effects have been examined by two series of five cases (without, and with, a $\frac{1}{2}$ mm thick layer of Li^6 preceding the phantom), for 0, 5, 10, 15, and 19.04 cm of D_2O removed out of the total of 53.34 cm presently in the M.I.T.R. Medical Beam flight path. The phantom is a tissue-equivalent cylinder of 16.6 cm diameter by 15 cm long. From Figures 5.1 and 5.2 it can be seen that removing D_2O yields relatively large increases in thermal neutron flux at depths greater than 2 cm for modest changes in incident flux. Adding a $\frac{1}{2}$ mm thick Li^6 filter lowers markedly the incident thermal neutron flux, and greatly improves the penetrating power and depth distribution of the beam at the cost of a small reduction in thermal neutron flux at moderate depths.

Figs. 5.3 and 5.4 compare the same cases in terms of the ratio of therapeutic dose from B^{10} (weight fraction 50×10^{-6}) to total background dose from fast neutrons, capture gamma rays, and protons from

$N^{14}(n,p)C^{14}$. From this point of view, removing D_2O is not as beneficial as it appears to be from Figs. 5.1 and 5.2 since the fast neutron dose component of the background dose increases very rapidly. However, the Li^6 filter yields a very flat dose ratio curve over a wide range of depths, in contrast to the rapid fall-off of the existing beam (Case 1). Should it be possible to raise the B^{10} concentration in tumor tissue above a weight fraction of 50×10^{-6}, the filter arrangement looks very promising.

Dose ratios given in Figures 5.2 and 5.4 are somewhat pessimistic. The first collision dose for Case 1 was calculated to be 92.7 rad/min at the surface of the phantom. Gamma rays contribute 41.8 rad/min and 34.0 rad/min come from $N^{14}(n,p)C^{14}$ reactions, for a total background dose rate of 168.5 rad/min. Calculations using STAR will be discussed later in this chapter which indicate a smaller first collision dose rate. In addition, a revised first collision dose calculation gives reduced dose rates. However, relative results for the various cases will not be affected by a change in total background dose rate.

First collision dose rates were calculated similarly to the method given in Section 2.3.1. The only difference was in the calculation of the average energy loss per collision. The method used assumed that all neutrons in group $j(u_j \leq u \leq u_{j+1})$ had an energy corresponding

to a lethargy $\bar{u}_j = \frac{1}{2}(u_j + u_{j+1})$. That is, $\bar{E}_j = 10 \exp(-\bar{u}_j)$. Then assuming the average lethargy loss per scattering collision to be constant for all groups, and given by ξ, then the average energy after collision is $E_j' = 10 \exp(-\bar{u}_j + \xi)$. The average energy lost becomes $E_j - E_j' = \bar{E}_j [1 - \exp(-\xi)]$. The main difficulties with this method are that ξ depends on energy in most materials (except hydrogen), and that the neutron groups are too wide for this averaging to be accurate.

FIGURE 5.1

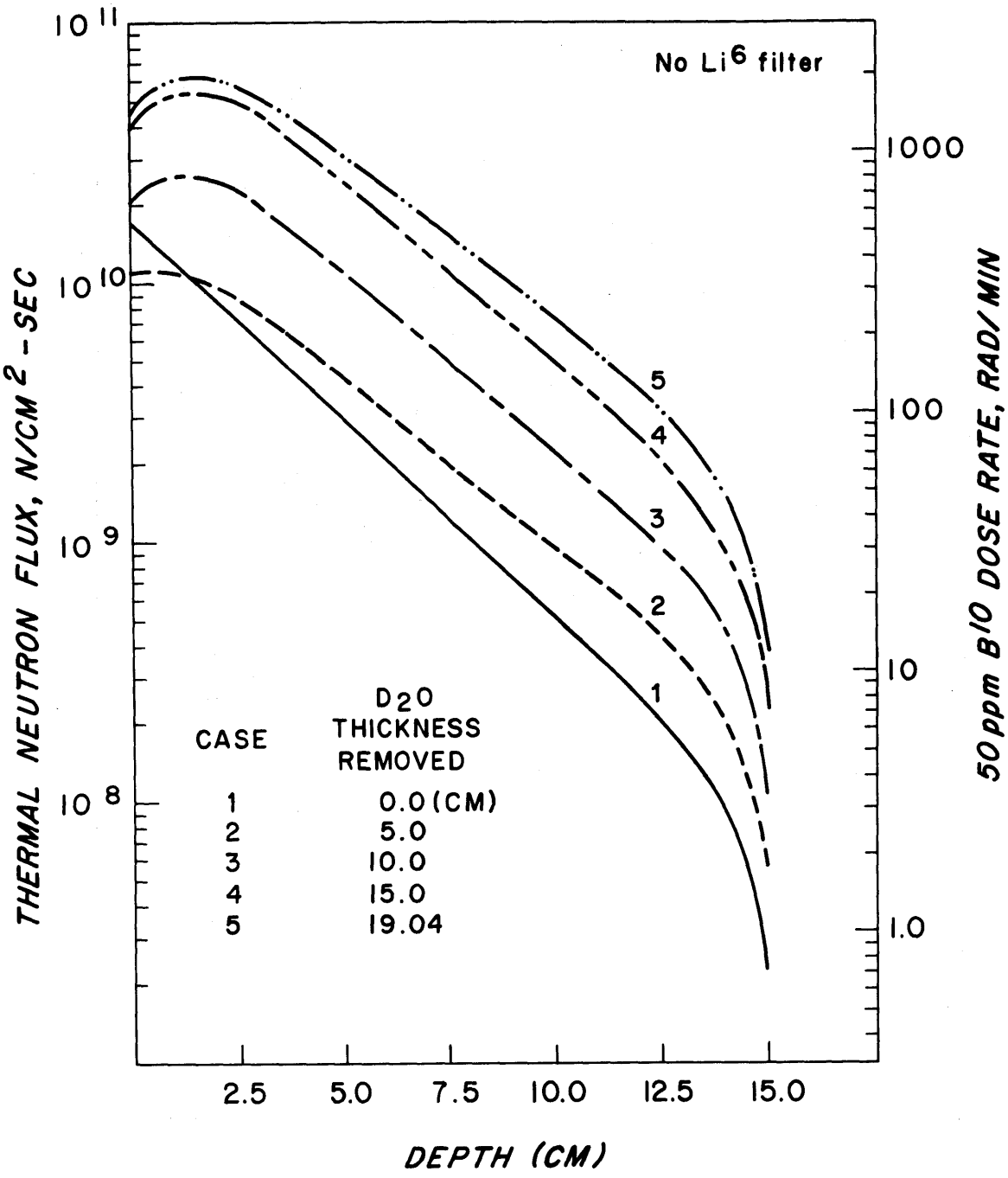
No Li6 filter
THERMAL NEUTRON FLUX, N/CM2-SEC
50 ppm B10 DOSE RATE, RAD/MIN
DEPTH (CM)
CASE
D2O THICKNESS REMOVED
1 0.0 (CM)
2 5.0
3 10.0
4 15.0
5 19.04

FIGURE 5.2

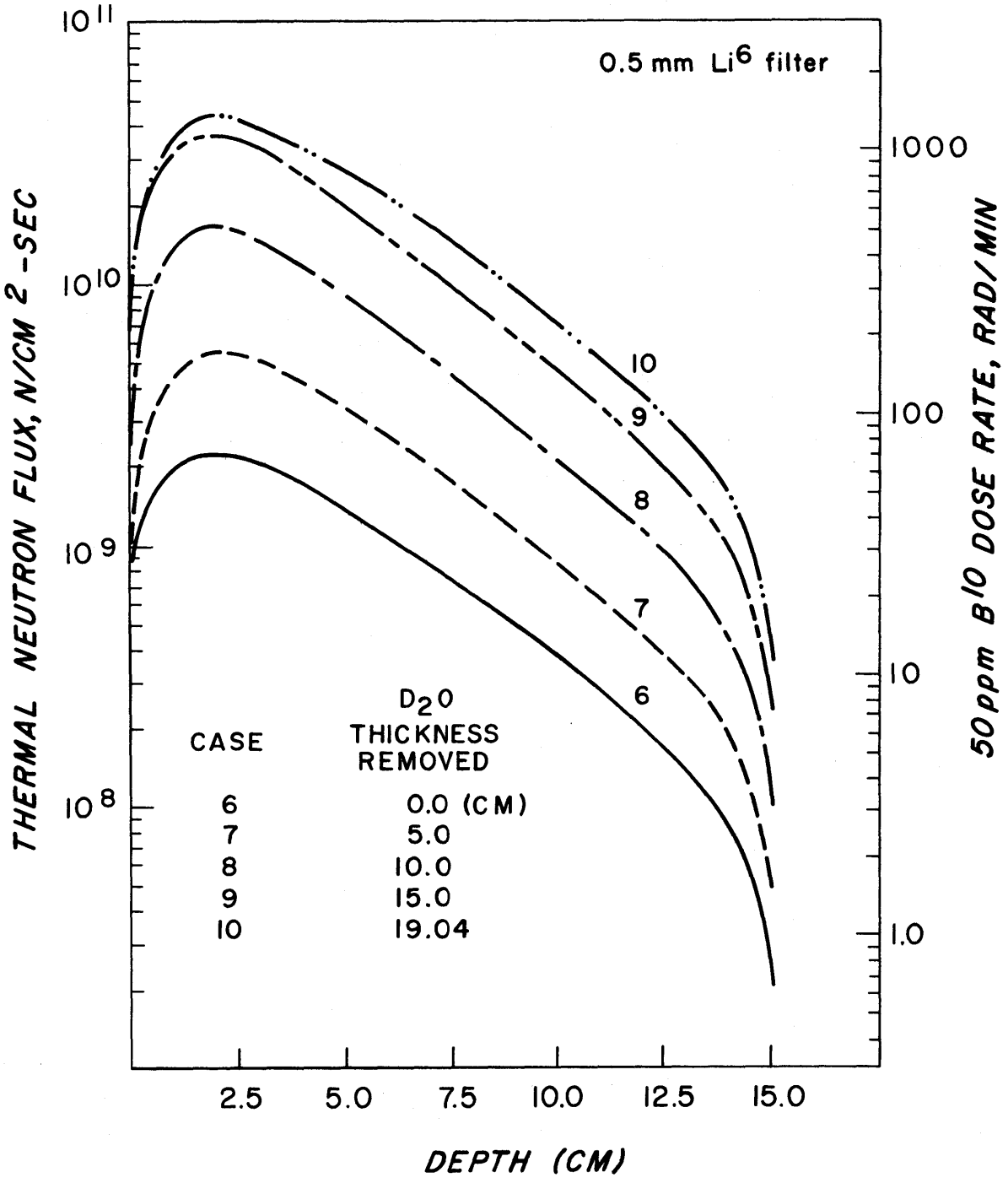
0.5 mm Li6 filter
THERMAL NEUTRON FLUX, N/CM 2 -SEC
50 ppm B10 DOSE RATE, RAD/MIN
DEPTH (CM)
10 11
10 10
10 9
10 8
1000
100
10
1.0
2.5
5.0
7.5
10.0
12.5
15.0
10
9
8
7
6
D2O THICKNESS REMOVED
CASE
6 0.0 (CM)
7 5.0
8 10.0
9 15.0
10 19.04

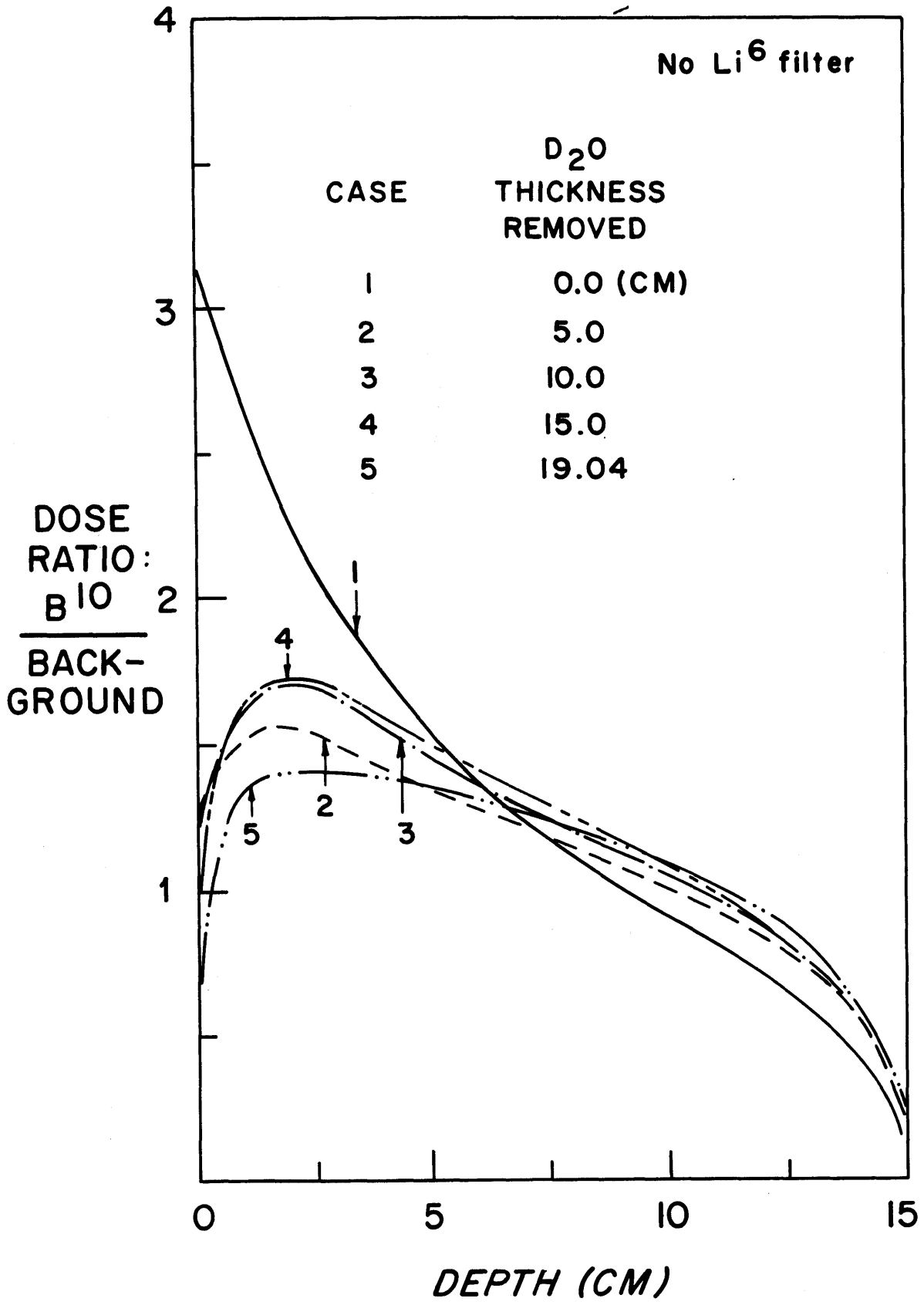
No Li6 filter
D2O
CASE THICKNESS REMOVED
1 0.0 (CM)
2 5.0
3 10.0
4 15.0
5 19.04
DOSE RATIO: B10 / BACK-GROUND
DEPTH (CM)
0
5
10
15
1
2
3
4

FIGURE 5.4

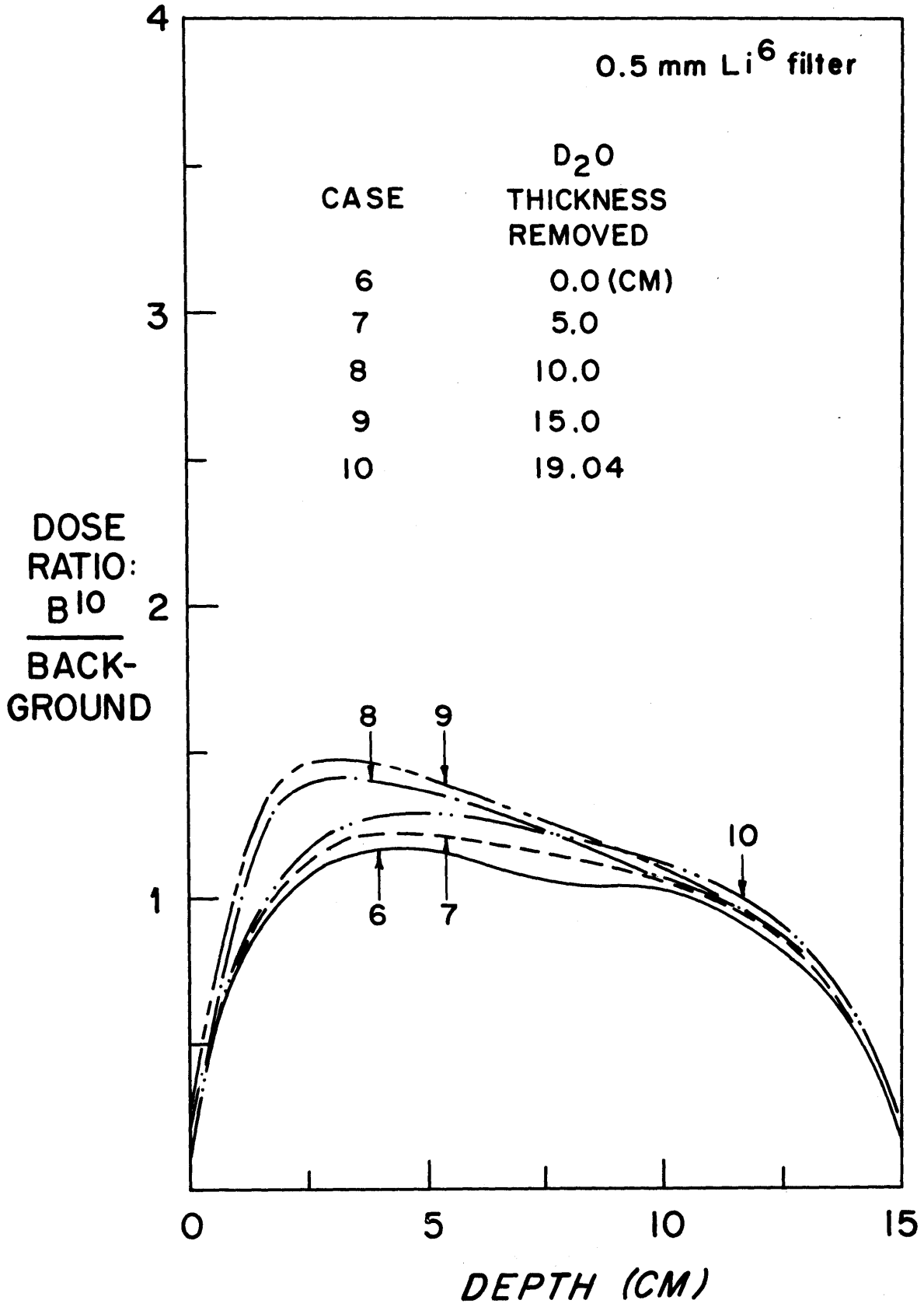
0.5 mm Li6 filter
D2O
CASE
THICKNESS REMOVED
6 0.0 (CM)
7 5.0
8 10.0
9 15.0
10 19.04
DOSE RATIO: B10 / BACK-GROUND
4
3
2
1
0
5
10
15
DEPTH (CM)
8
9
10
6
7

5.4 THE USE OF NEUTRON FILTERS

Some of the cases included in this section are similar to those reported in Section 5.3. The differences are mainly due to improvements in the calculational methods. First collision dose rates are calculated as described in Section 2.3.1. Inelastic scattering processes are accounted for in an improved manner, but the entire spectrum calculation is somewhat simpler than the method ultimately developed (Section 2.1). The radial variation of neutron flux in the phantom is assumed to be flatter than a cosine distribution because experimental measurements have shown this. A reasonable approximation is the following:

$$\phi(r) = \phi_o \left[\cos \left(\frac{\pi}{2} \frac{r}{R'} \right) \right]^{1/4} \qquad (5.13)$$

R' is the extrapolated radius (8.6 cm) and r is the radial coordinate. The neutron spectrum was normalized to the measured[24] flux per unit energy of 3.88 $\times 10^{12}$ n/cm^2 - sec - MeV at 4.90 ev and 5 Mw. The measurement was derived from the cadmium ratio for gold foils.

The cases listed in Table 5.2 cover a wide variation in beam port materials. Neutron "filters" of Li, Li^6, Cr,V, Al, and C are included. Case 10 is included for completeness. It represents the effect

of replacing all hydrogen in tissue with deuterium.

It can be seen from Figure 5.5 that the thermal neutron flux down the axis of the Medical Beam varies considerably in magnitude. The rapid drop at about 62 cm from the core followed by a nearly flat flux out to over 200 cm results from matching boundary conditions on flux and current at the interface between a thin aluminum slab and a large air gap.

Results obtained for epithermal beams created by removing D_2O and by absorbing the thermal neutron flux incident on the phantom with various lithium filters are shown in Figures 5.6 to 5.9. The ratio of tumor dose/maximum normal tissue dose is for a boron-10 weight fraction of 50×10^{-6} in a differential volume at any depth (weight fractions above 60×10^{-6} are lethal in humans). Invariably, the maximum normal tissue dose occurs at the surface of the phantom.

Figure 5.10 is for 5.0 cm D_2O removed to increase the proportion of epithermal neutrons in the beam. Neutron filters of Al and C replace the D_2O removed in order to keep down the fast neutron dose rate. However, the thermal neutron flux and boron capture dose rate decrease faster than the fast neutron dose rate, resulting in a decrease in beam effectiveness.

TABLE 5.2 M.I.T.R. CASES STUDIED

Case Number	Description
1	Normal beam
2	Normal beam plus 2 mm Li filter
3	Normal beam plus 1 mm Li^6 filter
4	Normal beam plus 3 mm Li^6 filter
5	2.5 cm D_2O removed
6	5.0 cm D_2O removed
6a	5.0 cm D_2O removed plus 0.5 mm Li^6 filter
6b	5.0 cm D_2O replaced by 5.0 cm Al+1 mm Li^6 filter
6c	5.0 cm D_2O replaced by 5.0 cm void + 1 mm Li^6 filter
6d	5.0 cm D_2O replaced by 5.0 cm C + 1 mm Li^6 filter
7	10.0 cm D_2O removed
8	5.0 cm D_2O removed plus 5.0 cm Cr filter
9	5.0 cm D_2O removed plus 5.0 cm V filter
10	Normal beam plus D_2O tissue-equivalent phantom

The same effect is shown in Figure 5.11 for Cr and V filters. These materials have scattering cross sections which peak in the region from 2 to 50 kev. Increased scattering in this region of the neutron spectrum tends to diminish the total fast neutron dose rate, but the rather large thermal neutron absorption cross sections ($\sigma_a(V) = 5.0b$, $\sigma_a(Cr)=3.16b$) reduce the boron capture dose rate at a much faster rate. No other isotopes have scattering cross sections which have broad peaks in the kev region.

It if were possible to replace all hydrogen in tissue with deuterium, then much more favorable conditions would exist for neutron capture therapy. Figure 5.12 compares this hypothetical situation (Case 10) with the corresponding result for hydrogenous tissue. The improvement is considerable. Benefits arise from a much reduced first collision dose rate, better penetration of the beam, and considerably reduced neutron capture gamma ray dose rate.

The best configuration out of all these possibilities is still the normal beam as it exists at the M.I.T.R. (Case 1). The background dose rate from gamma rays, $N^{14}(n,p)C^{14}$, and recoils as a function of depth in tissue are given in Figure 5.13. Gamma rays from the reactor core and from neutron capture in the walls of the beam port contribute about 25 rad/min at the surface of the phantom (at 5 Mw). This effect is not included in any of the results because both the magnitude and

distribution of these gamma rays inside the phantom are not well known. However, the dose rate from these gamma rays may be important in some cases.

Figure 5.14 shows the first collision dose rate at the surface of the phantom as a function of the thickness of D_2O removed from the lower portion of the reflector of the M.I.T.R. (Case 1). Cases 6b, 6d, 8 and 9 study replacement of D_2O by an equal thickness of Al, C, Cr, and V, respectively. None of these materials is as good as D_2O in moderating fast neutrons, but their effects on epithermal neutrons and thermal neutrons are also of great importance. Figure 5.14 gives a simple correlation of relative effectiveness of these materials in moderating fast neutrons. The net worth of these filters for neutron capture therapy is best shown in Figures 5.8 to 5.11.

The relative fast neutron dose rate at the portal as a function of D_2O and Bi thickness removed is shown in Figure 5.15. It can be seen that the latest neutron spectrum calculation in MEDIPORT as described in Chapter II gives relative fast neutron dose rates which agree with STAR results to within a few percent. The new spectrum calculations significantly improves the accuracy of the MEDIPORT results.

FIGURE 5.5

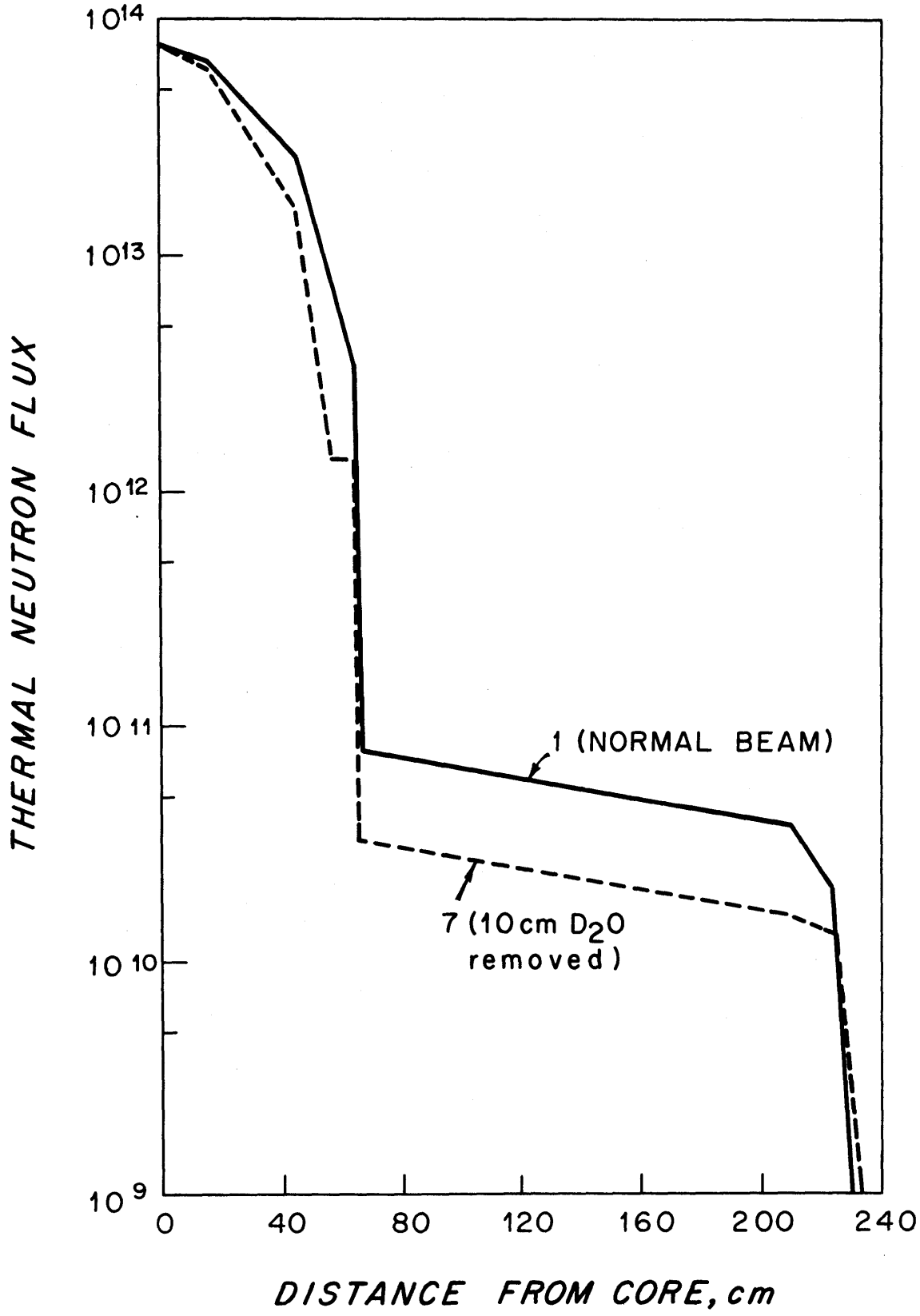
THERMAL NEUTRON FLUX
10^14
10^13
10^12
10^11
10^10
10^9
0
40
80
120
160
200
240
DISTANCE FROM CORE, cm
1 (NORMAL BEAM)
7 (10cm D2O removed)

FIGURE 5.6

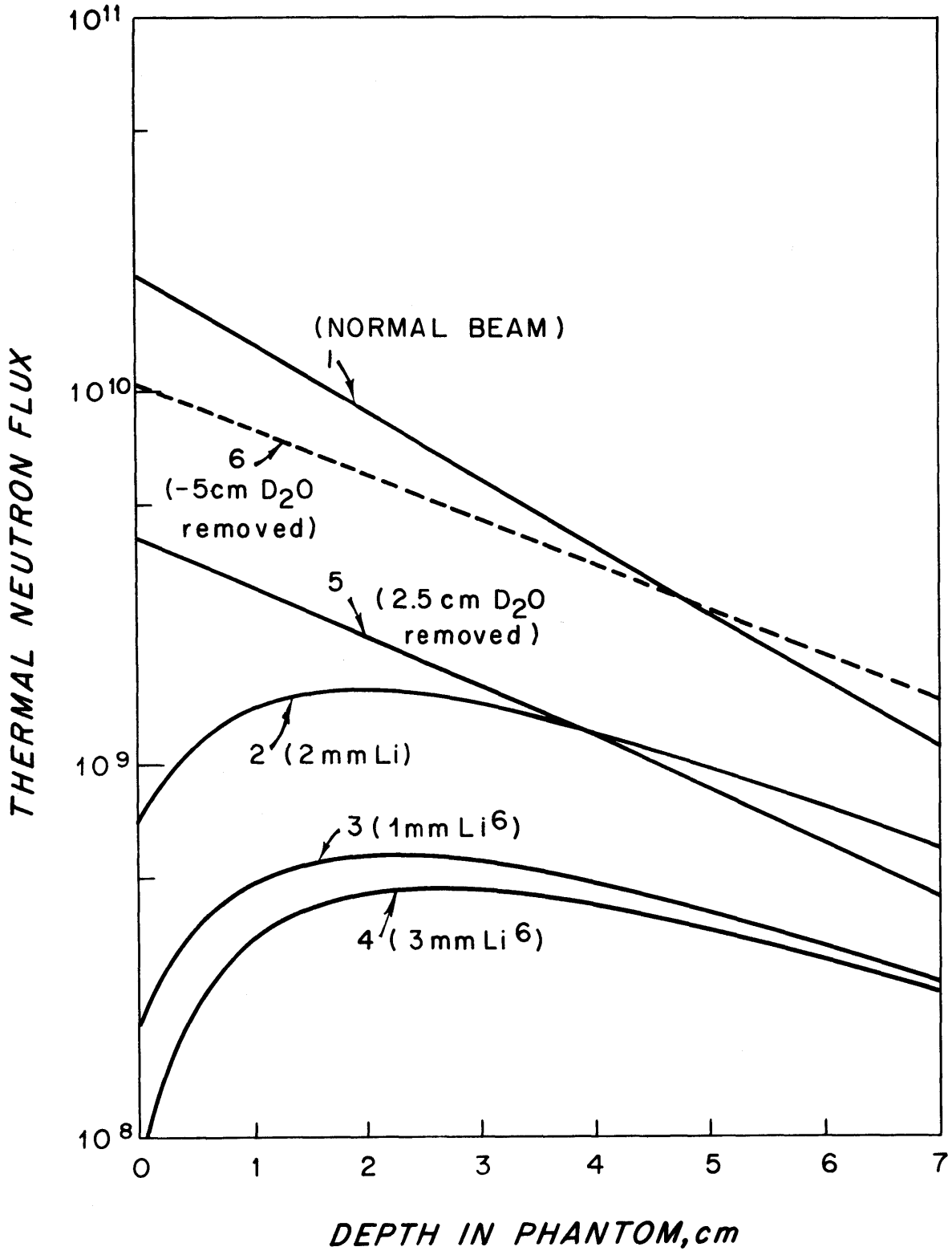
THERMAL NEUTRON FLUX
10^{11}
10^{10}
10^{9}
10^{8}
(NORMAL BEAM)
1
6
(-5cm D_2O removed)
5
(2.5 cm D_2O removed)
2 (2mm Li)
3 (1mm Li^6)
4 (3mm Li^6)
0
1
2
3
4
5
6
7
DEPTH IN PHANTOM, cm

FIGURE 5.7

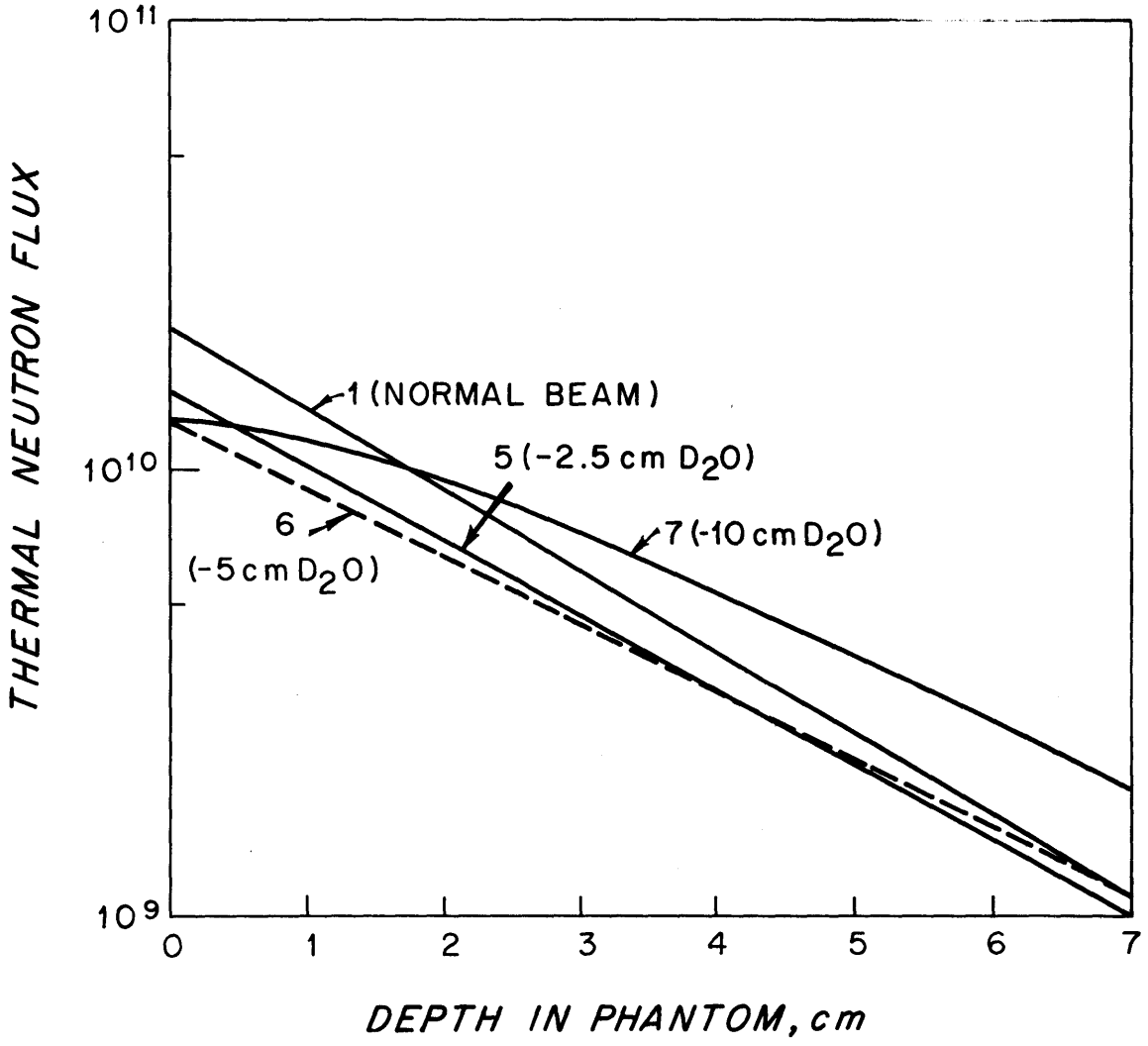
THERMAL NEUTRON FLUX
10^{11}
10^{10}
10^{9}
1 (NORMAL BEAM)
5 (-2.5 cm D_2O)
6
(-5 cm D_2O)
7 (-10 cm D_2O)
0
1
2
3
4
5
6
7
DEPTH IN PHANTOM, cm

FIGURE 5.8

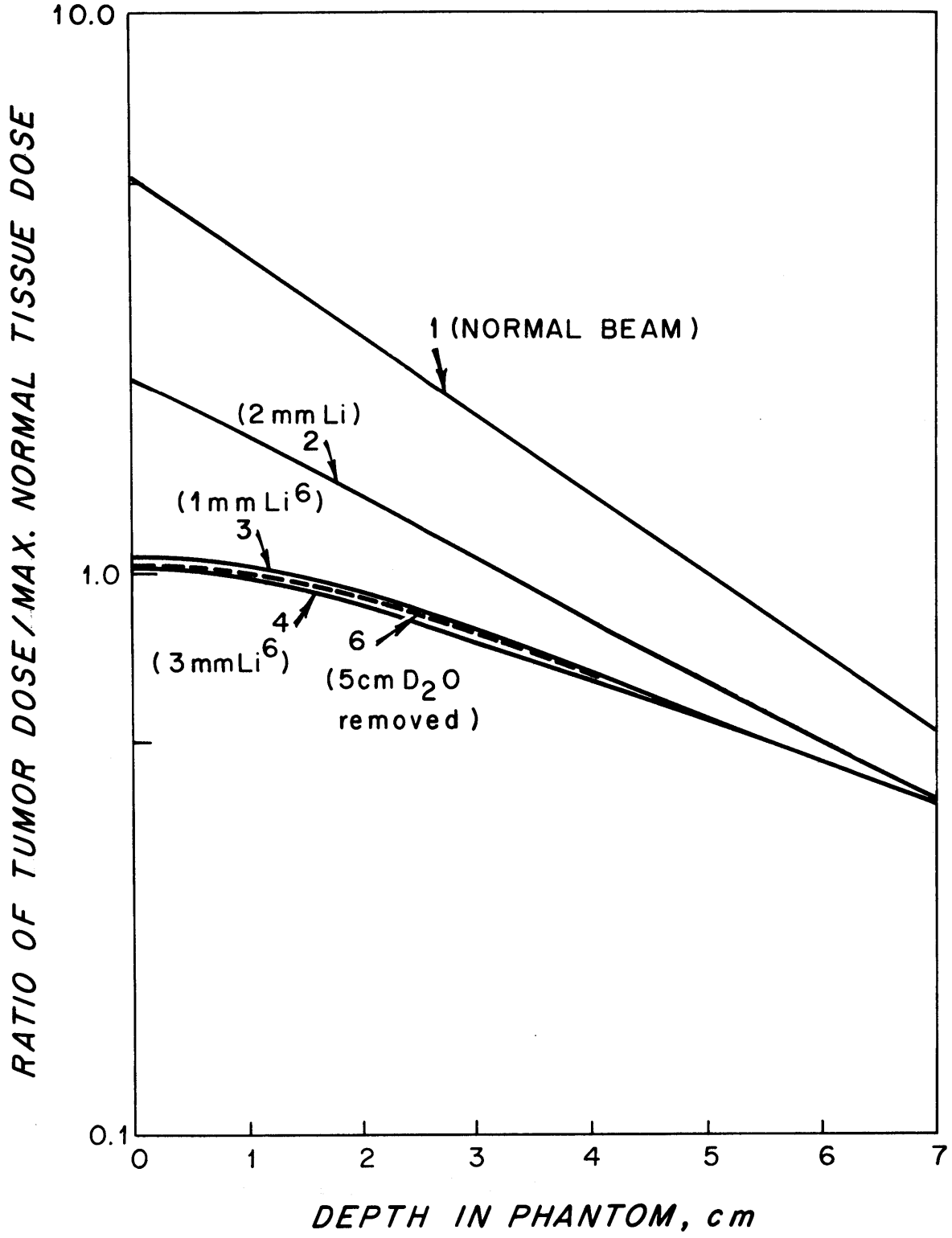
10.0
1.0
0.1
RATIO OF TUMOR DOSE/MAX. NORMAL TISSUE DOSE
1 (NORMAL BEAM)
(2 mm Li)
2
(1 mm Li6)
3
4
(3 mm Li6)
6
(5cm D2O
removed)
0
1
2
3
4
5
6
7
DEPTH IN PHANTOM, cm

FIGURE 5.9

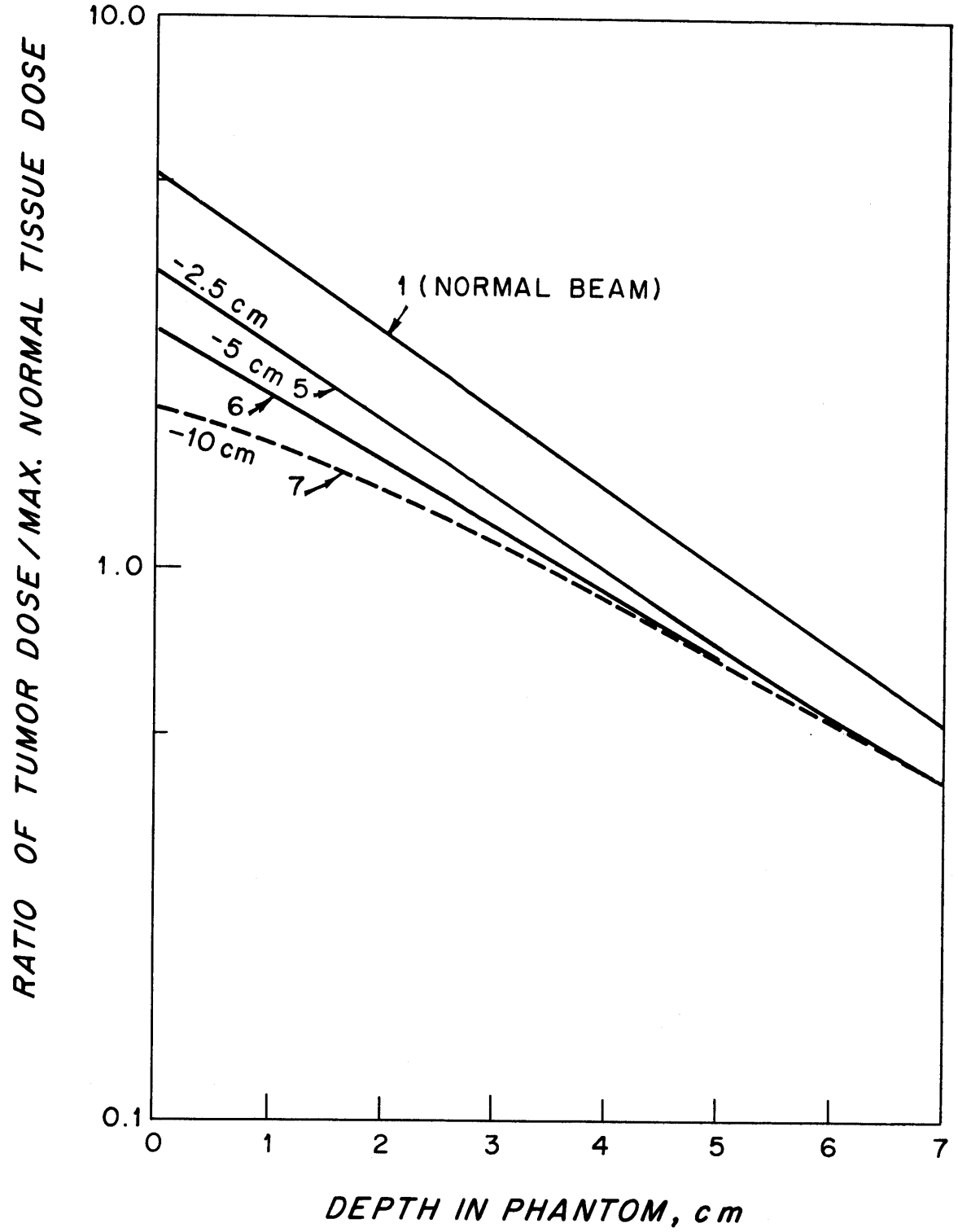
10.0
1.0
0.1
0
1
2
3
4
5
6
7
1 (NORMAL BEAM)
-2.5 cm
-5 cm
5
6
-10 cm
7
RATIO OF TUMOR DOSE/MAX. NORMAL TISSUE DOSE
DEPTH IN PHANTOM, cm

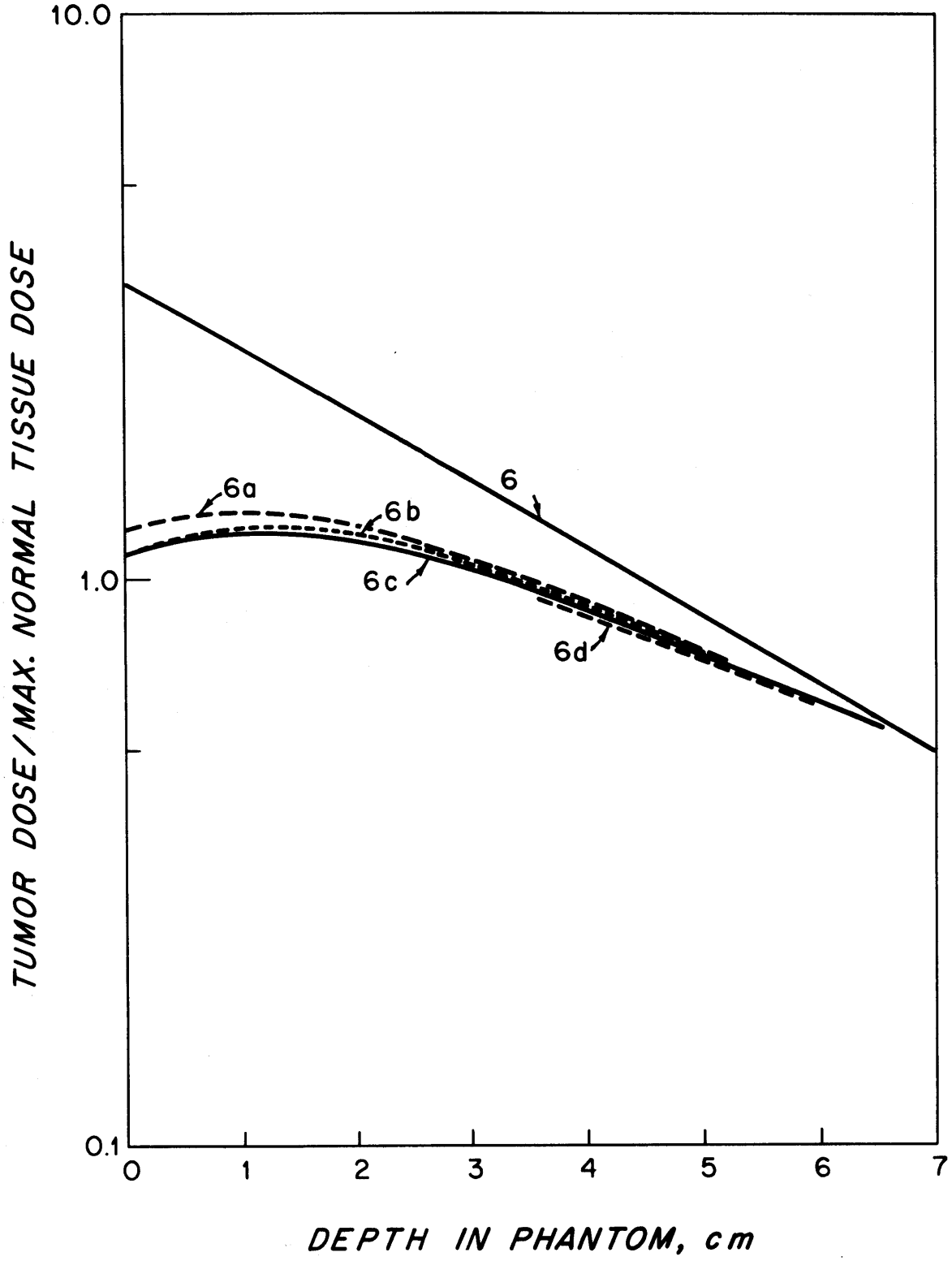
10.0
1.0
0.1
TUMOR DOSE/MAX. NORMAL TISSUE DOSE
6
6a
6b
6c
6d
0
1
2
3
4
5
6
7
DEPTH IN PHANTOM, cm

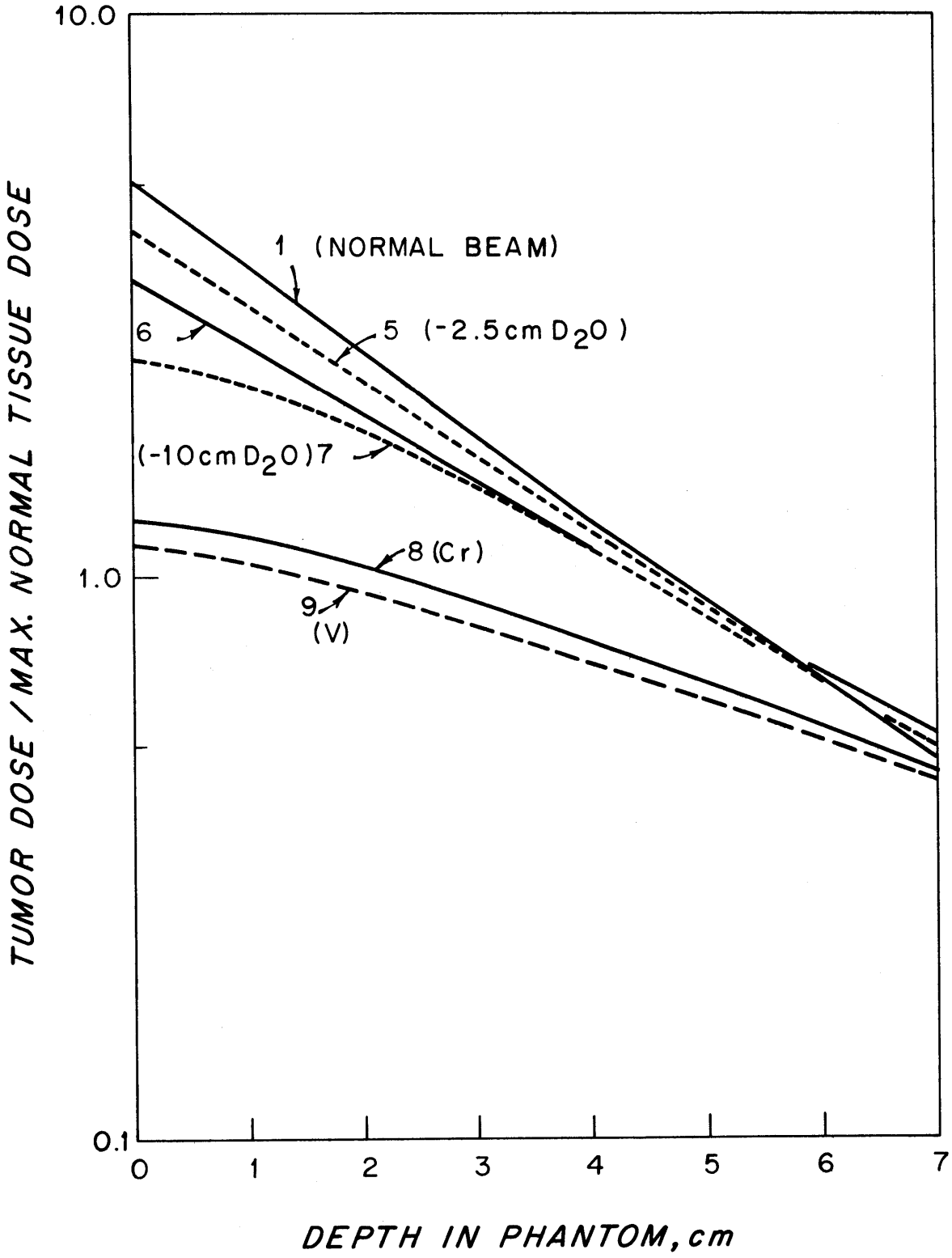
10.0
1.0
0.1
0
1
2
3
4
5
6
7
1 (NORMAL BEAM)
5 (-2.5cm D2O)
6
(-10cm D2O)7
8 (Cr)
9
(V)
TUMOR DOSE / MAX. NORMAL TISSUE DOSE
DEPTH IN PHANTOM, cm

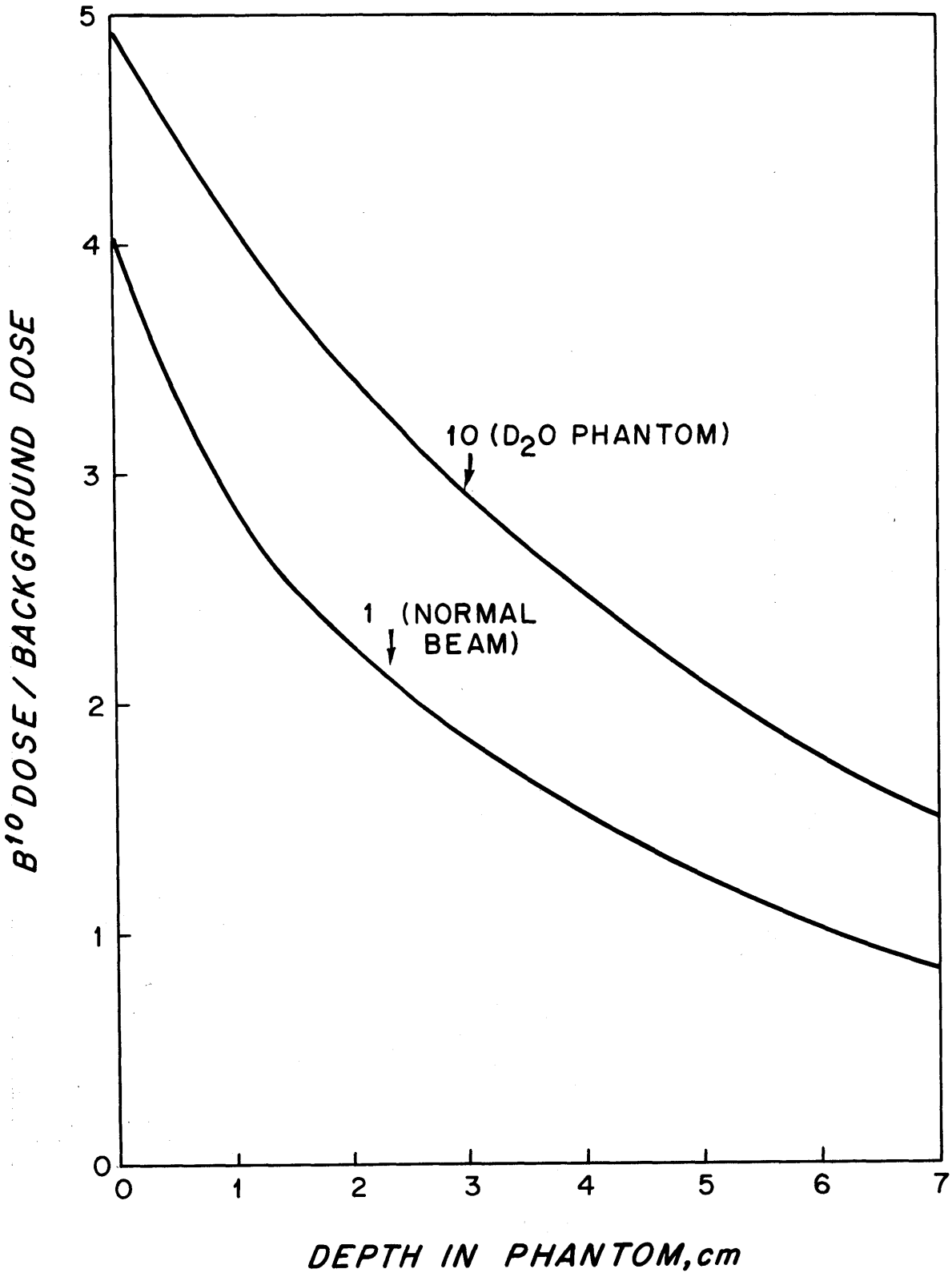
5
4
3
2
1
0
0
1
2
3
4
5
6
7
10 (D_2O PHANTOM)
1 (NORMAL BEAM)
B^{10} DOSE / BACKGROUND DOSE
DEPTH IN PHANTOM, cm

FIGURE 5.13

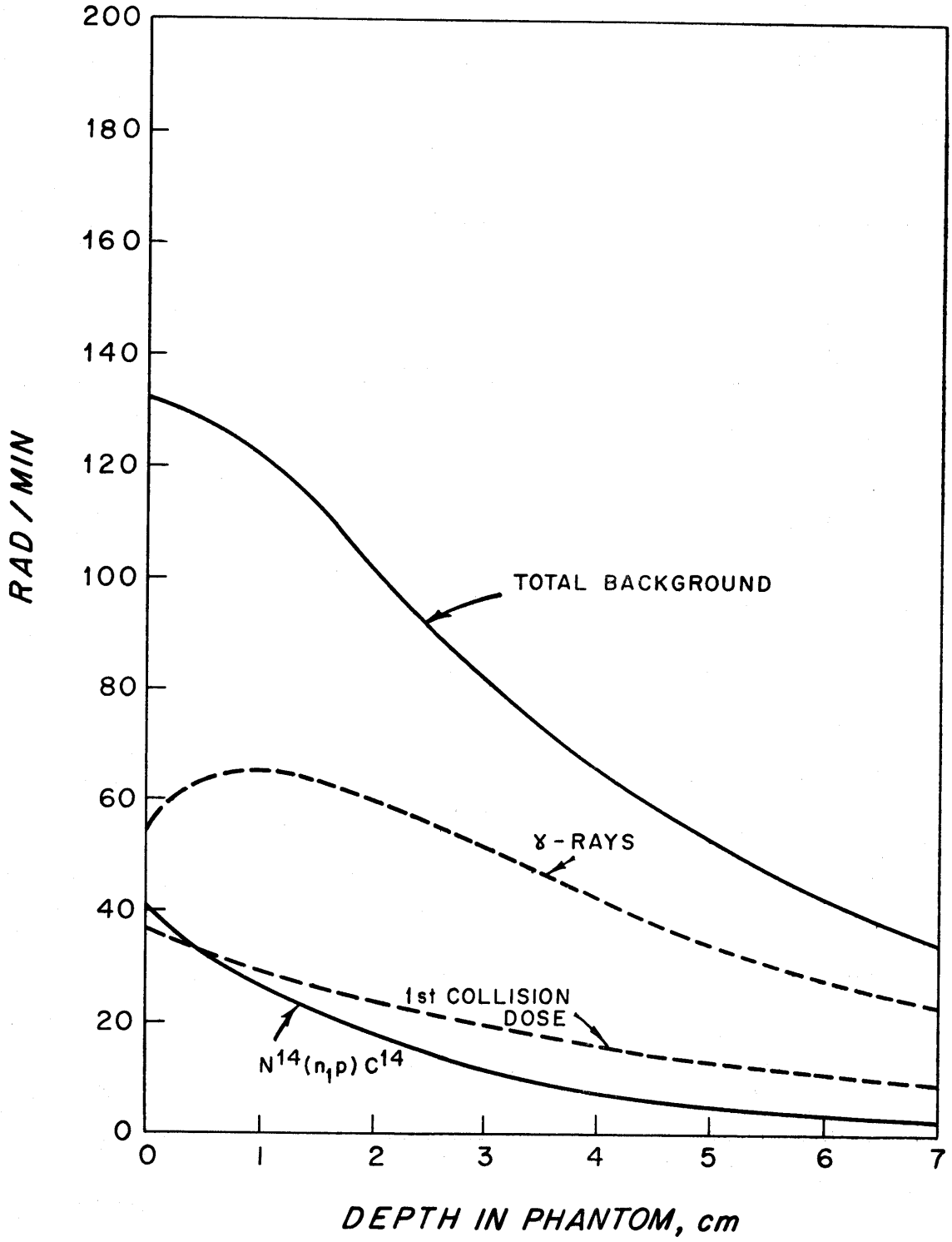
200
180
160
140
120
100
80
60
40
20
0
RAD / MIN
TOTAL BACKGROUND
γ - RAYS
1st COLLISION DOSE
N14(n1p) C14
0
1
2
3
4
5
6
7
DEPTH IN PHANTOM, cm

FIGURE 5.14

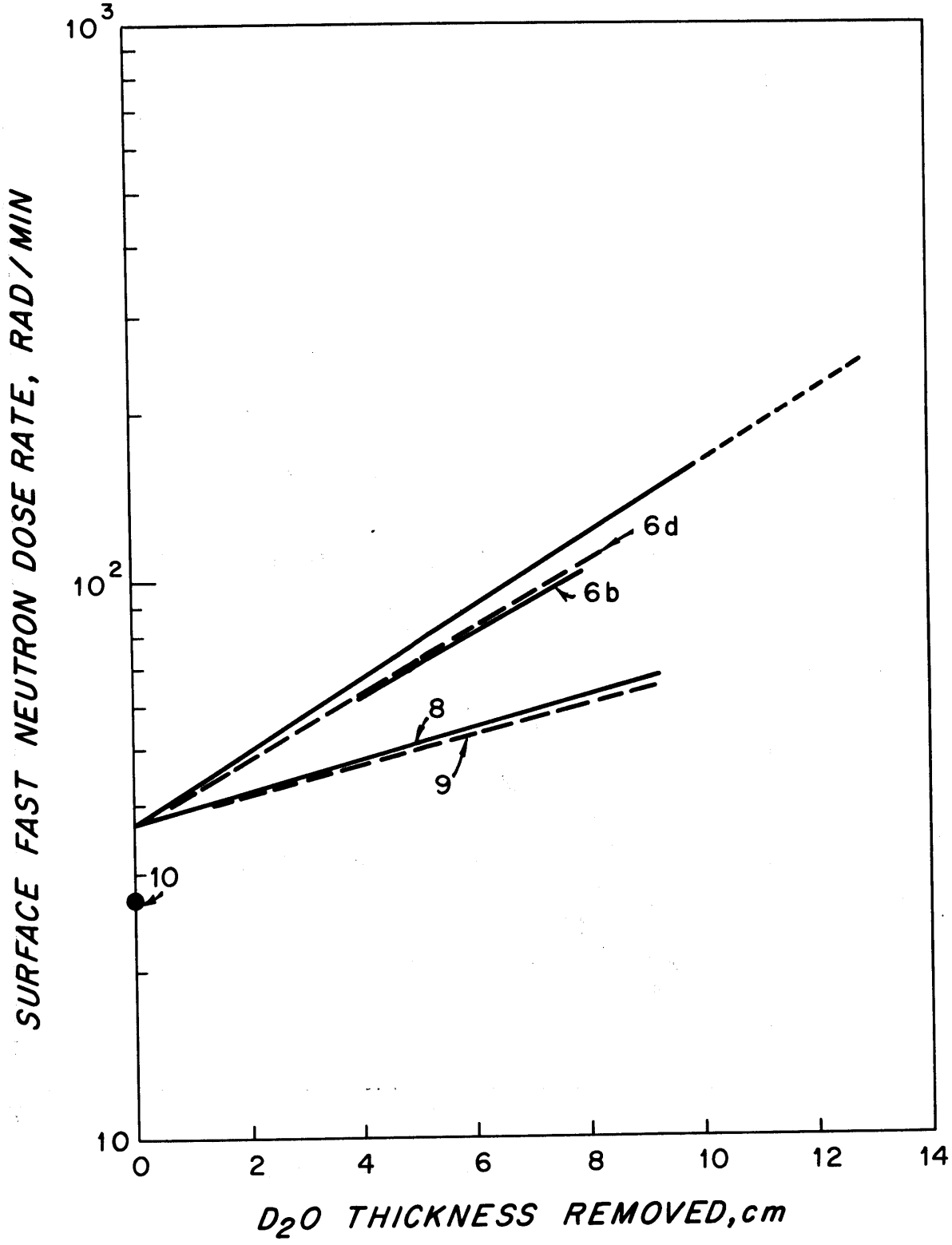
SURFACE FAST NEUTRON DOSE RATE, RAD/MIN
10^3
10^2
10
0
2
4
6
8
10
12
14
D_2O THICKNESS REMOVED, cm
6d
6b
8
9
10

FIGURE 5.15

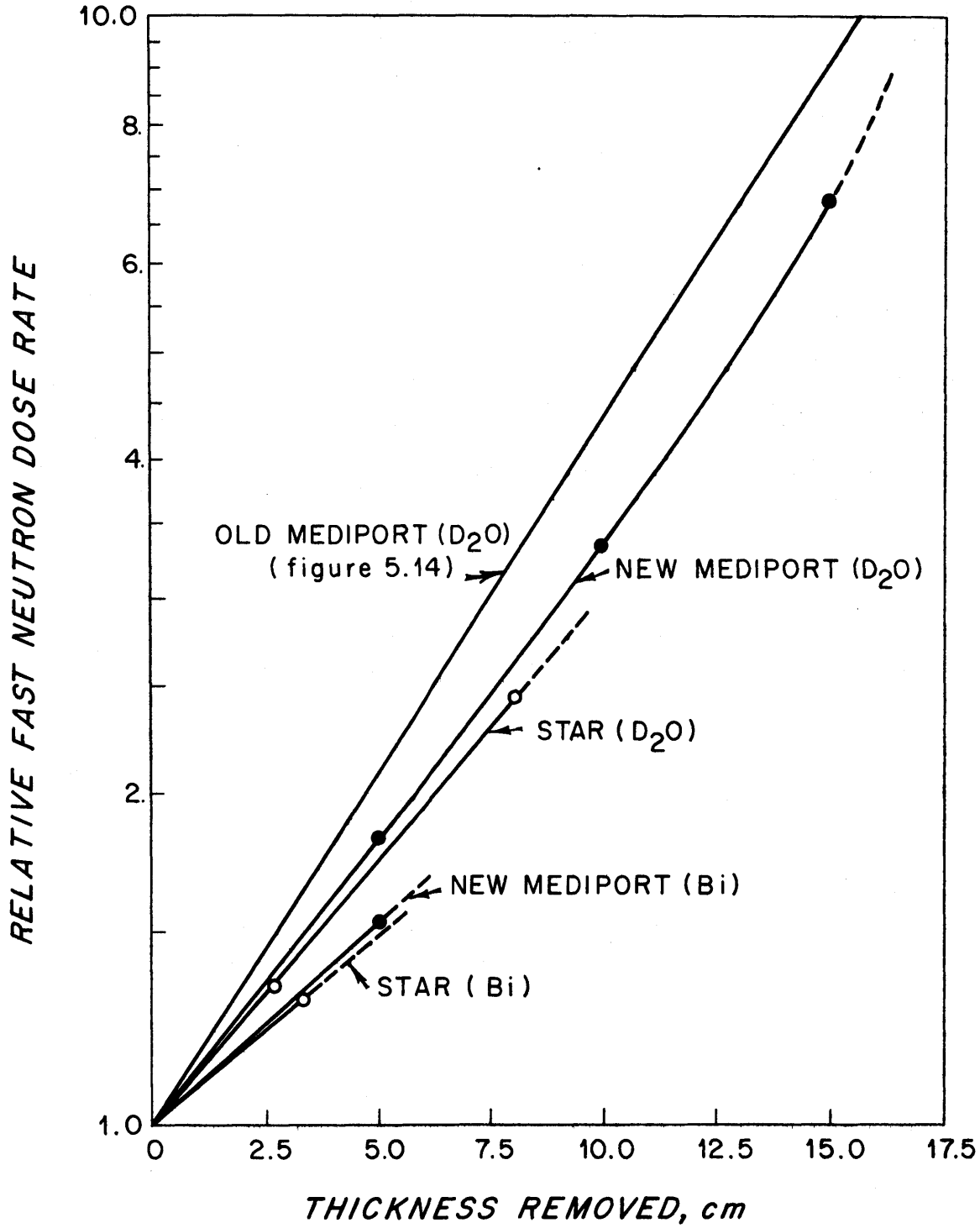
10.0
8.
6.
4.
2.
1.0
0
2.5
5.0
7.5
10.0
12.5
15.0
17.5
RELATIVE FAST NEUTRON DOSE RATE
THICKNESS REMOVED, cm
OLD MEDIPORT (D_2O)
(figure 5.14)
NEW MEDIPORT (D_2O)
STAR (D_2O)
NEW MEDIPORT (Bi)
STAR (Bi)

5.5 THE USE OF SCATTERED NEUTRONS

Introductory justification for the use of scattered neutrons has been given in Section 2.4. Now results are to be presented for a range of neutron scatterers made in various thicknesses from lucite, polyethylene, and water. Computer studies with STAR are primarily for accurate fast neutron spectra from 0.1 to 10.0 MeV, but also serve as "benchmark" calculations to normalize MEDIPORT results. The MEDIPORT code handles the entire neutron spectrum from thermal to 10.5 MeV. Accurate results are obtained with MEDIPORT for variations from a reference or benchmark condition whose normalization has been established by more accurate methods. The calculations are also compared with experimental results whenever possible.

Many of the MEDIPORT results given in previous sections were obtained with a simplified geometrical simulation. The total thickness of materials in the neutron beam flight path was conserved, but some combining and re-ordering of thin layers of material was utilized to speed the calculations. Justification for this procedure comes from a pair of STAR calculations for neutron transmission through the M.I.T.R. Medical Beam Port. One calculation included all materials and thicknesses exactly as they exist in the Medical Beam, while the other simplified the geometry. Table 5.1 gives the materials and thicknesses used for each

calculation. The results for a unit, isotropic fission spectrum source are as follows:

TABLE 5.3 Neutron Spectra Through Exact and Simplified Geometry

Neutron Group	Differential Flux, n/cm^2-sec-MeV		Flux Ratio: Exact/Simplified
	Exact	Simplified	
1	8.625×10^{-6}	8.149×10^{-6}	1.057
2	1.562×10^{-6}	1.495×10^{-6}	1.070
3	8.123×10^{-7}	7.490×10^{-7}	1.085
4	1.521×10^{-7}	1.440×10^{-7}	1.057

The total fast neutron dose ratio is 1.06. The flux ratios indicate that the spectrum has mainly been shifted about six percent, with quite small deviations for each group from the average behaviour. The differences between the two results are well within the uncertainties in normalization of the neutron source at the core-reflector interface.

The transmission matrix obtained in exact geometry by STAR for neutron transmission through the Medical Beam, combined with the neutron source in each energy and angular group, gives the neutron spectrum at the portal. Section 5.2 gives the neutron source, and Appendix A.4 describes the STAR DATA REDUCTION code which performs the necessary calculations. Tables 5.4 and 5.5 summarize the results.

TABLE 5.4 Angular Fast Neutron Spectrum at Portal

	Differential Flux, 10^7 n/cm^2-sec/MeV/unit μ			
Energy Group	1	2	3	4
Angular Group 1	2.882	0.3572	0.1090	0.01991
Angular Group 2	4.679	0.7432	0.5033	0.1226

TABLE 5.5 Scalar Flux and Dose at Portal

Group	Scalar Flux 10^7n/cm^2 -sec/MeV	Flux per unit lethargy 10^7n/cm^2 -sec/unit leth.	1st. Coll Dose Ratio, Rad/Min	Total Fast Neutron Dose Rate Rad/Min
1	3.781	2.977	5.51	9.44
2	0.5502	1.852	3.93	5.03
3	0.3061	2.061	2.96	3.99
4	0.07123	0.6634	0.40	0.527
			11.80 Total	19.00

The first collision dose rate at the surface of tissue placed at the portal is 11.80 rad/min.

All STAR calculations for phantoms placed in the Medical Beam have been obtained using the angular flux given in Table 5.4 as the neutron source. Figure 5.16 shows the Table 5.4 results as integral flux above energy E(MeV) emerging through the portal. The MEDIPORT result is normalized to give the same fast neutron dose rate as predicted by STAR. Also shown are the foil activation data points obtained by Rydin[24]

(from Fig. 4.15), scaled to 5 Mw. Other than at about 1 to 2 MeV, the measured and predicted curves do not agree very well. The two computed integral flux curves agree very well in shape, indicating that perhaps the measured integral fluxes have rather large errors other than the statistical errors shown by the bars.

The entire spectrum above thermal energies is shown in Figure 5.17. Rydin's spectrum above 3 MeV lies below his threshold foil data points, which in turn are rather below the curves obtained from STAR and MEDIPORT. Also, an arbitrary "bump" at 1 MeV was added by Rydin which does not show up in the computed spectra. The first collision dose rate at the surface of the tissue phantom from Rydin's spectrum is 32.0 rad/min at 5 Mw. This compares with 11.80 rad/min for the STAR result, which is a factor of 2.7 smaller. Experiments by Drs. Reddy and Ayyangar (Physics Res. Lab., M.G.H.) are in progress to resolve this discrepancy. Preliminary results tend to confirm the STAR calculation of first collision dose rate.

STAR calculations of transmission matrices have been made for infinite slab phantoms 3, 6, 9, 12 and 15 cm thick composed of tissue, lucite, polyethylene, and light water. Using the known angle-dependent and energy-dependent flux at the portal as the source incident on the phantoms, calculations have been made

giving the transmitted flux per unit lethargy and total fast neutron dose rate at the surface of a 30 cm thick infinite slab of tissue. The recoil (or 1st collision) dose rate has been obtained also for tissue. Table 5.6 presents the transmitted neutron flux and Table 5.7 gives the 1st collision dose rate. Table 5.8 gives the total fast neutron dose rate transmitted through these phantoms as measured at the surface of a 30 cm thick infinite slab of tissue. Figure 5.18 shows the dose rate distributions from Tables 5.7 and 5.8. It can be seen that phantoms of lucite, tissue, and H_2O are very nearly identical with regard to transmitted fast neutron dose rate. The atom number densities used are:

Material	N_H	N_C	N_O (10^{24} atoms/cm^3)
Tissue	.0592	.00673	.02635
Lucite	.0418	.0418	.01046
Polyethylene	.0768	.0392	---
Water	.0670	---	.0335

Neutron cross sections for tissue do not include the contributions from N, Cl or other trace elements as they will not appreciably influence fast neutron transmission.

FIGURE 5.16

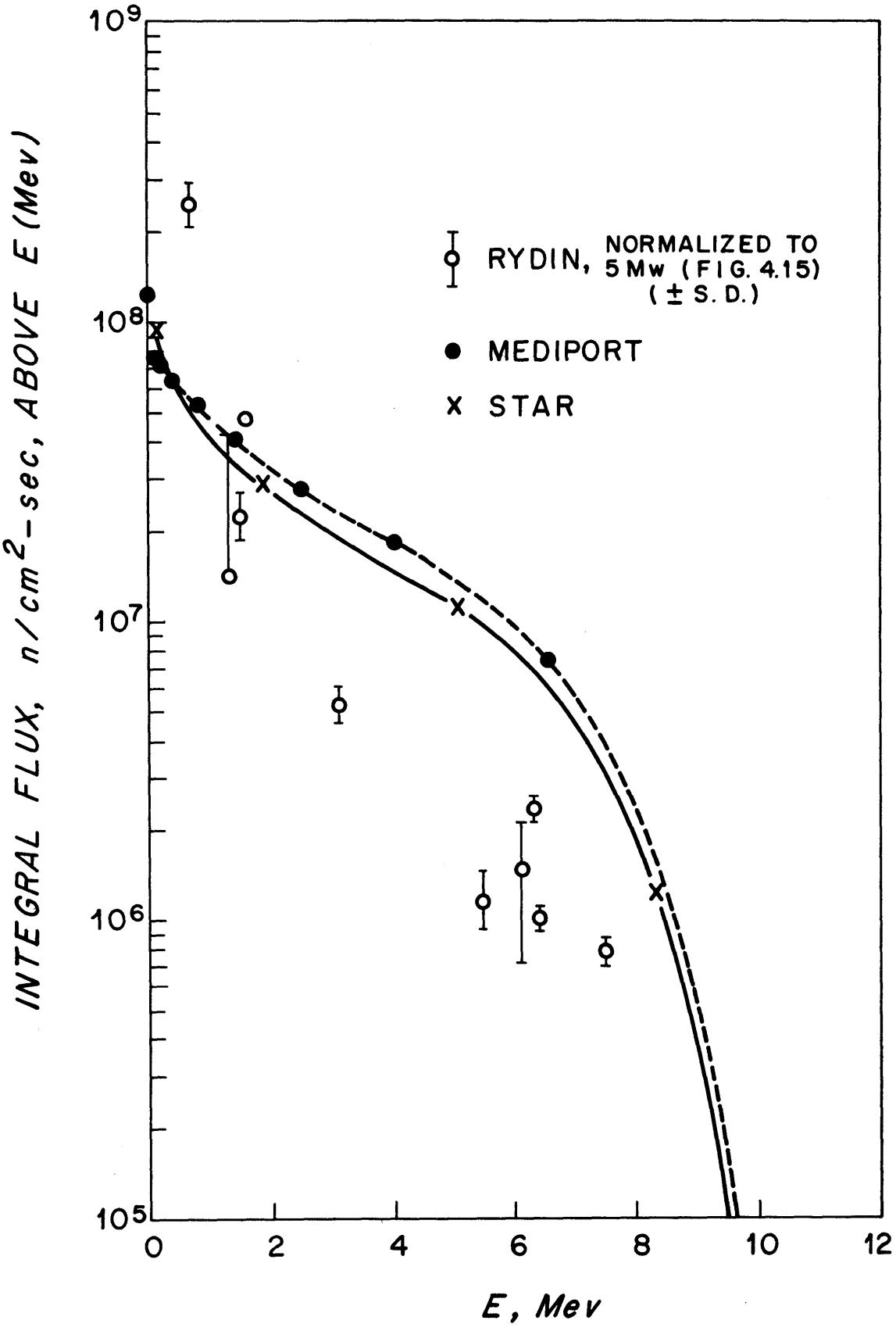
INTEGRAL FLUX, n/cm²-sec, ABOVE E (Mev)
10⁹
10⁸
10⁷
10⁶
10⁵
0
2
4
6
8
10
12
E, Mev
RYDIN, NORMALIZED TO 5 Mw (FIG. 4.15) (± S.D.)
MEDIPORT
STAR

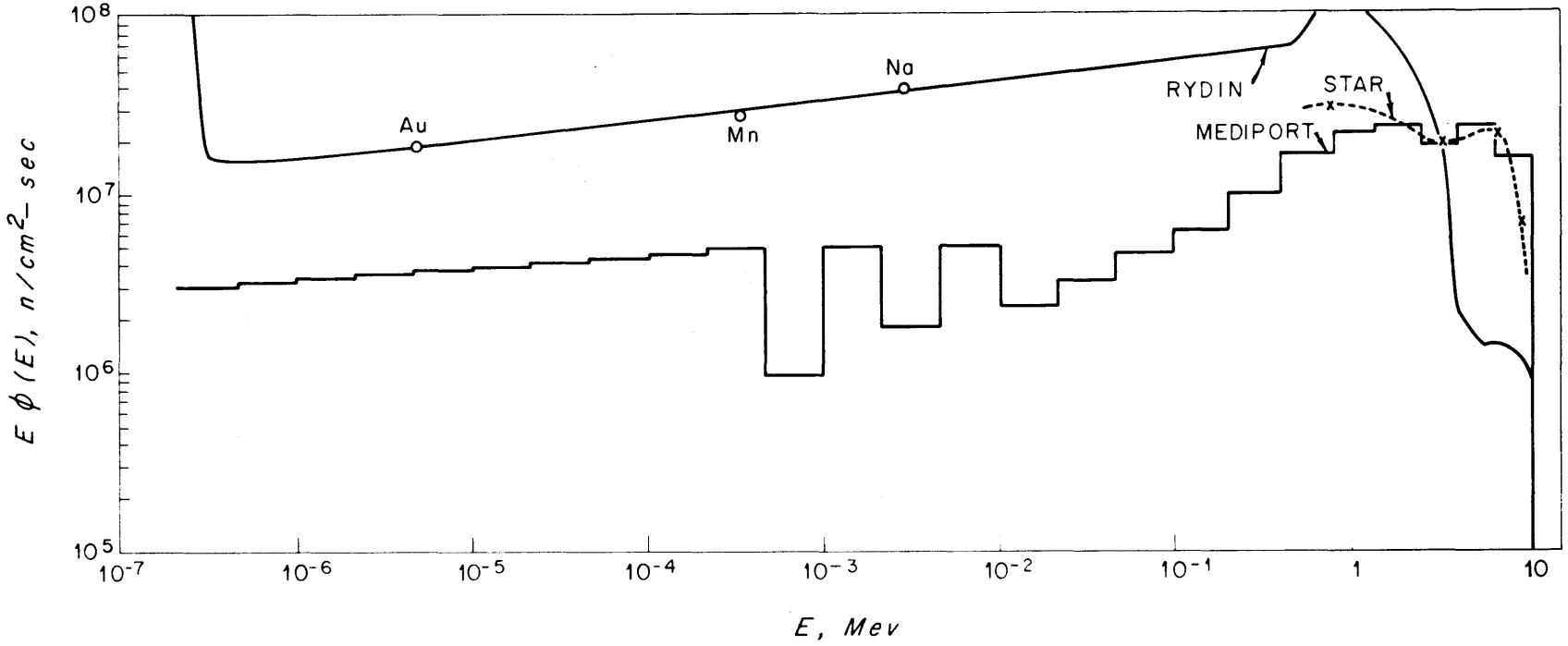
10^8
10^7
10^6
10^5
$E\,\phi(E)$, n/cm^2_sec
Au
Mn
Na
RYDIN
STAR
MEDIPORT
10^{-7}
10^{-6}
10^{-5}
10^{-4}
10^{-3}
10^{-2}
10^{-1}
1
10
E, Mev

FIGURE 5.17

FIGURE 5.18

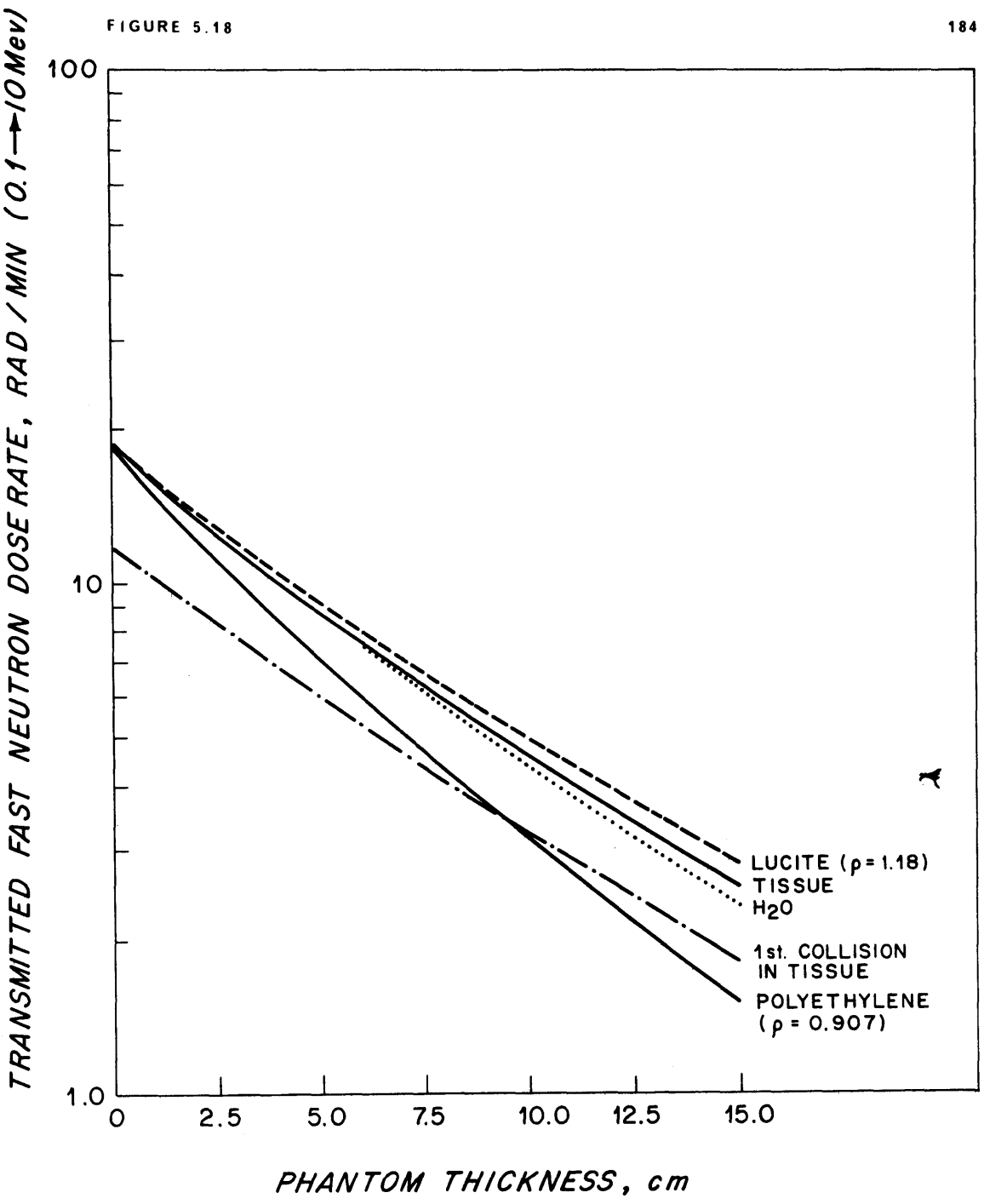
TRANSMITTED FAST NEUTRON DOSE RATE, RAD / MIN (0.1→10 Mev)
100
10
1.0
0
2.5
5.0
7.5
10.0
12.5
15.0
PHANTOM THICKNESS, cm
LUCITE (ρ = 1.18)
TISSUE
H2O
1st. COLLISION IN TISSUE
POLYETHYLENE (ρ = 0.907)

TABLE 5.6 Fast Neutron Spectra in Various Phantoms

Transmitted flux per unit lethargy
(n/cm^2-sec/unit leth.)

u_k	2.5416	1.0886	0.3956	0.0712
E_k, MeV	0.7874	3.367	6.733	9.313
Depth cm		Tissue		
0	.2977 E8	.1852 E8	.2061 E8	.6634 E7
3	.1486 E8	.1183 E8	.1587 E8	.4489 E7
6	.8570 E7	.8149 E7	.1220 E8	.3156 E7
9	.5138 E7	.5715 E7	.9358 E7	.2254 E7
12	.3177 E7	.4045 E7	.7171 E7	.1620 E7
15	.2021 E7	.2884 E7	.5490 E7	.1167 E7
		Lucite		
3	.1574 E8	.1198 E8	.1626 E8	.4326 E7
6	.9636 E7	.8315 E7	.1269 E8	.2944 E7
9	.6112 E7	.5857 E7	.9827 E7	.2035 E7
12	.3958 E7	.4158 E7	.7587 E7	.1415 E7
15	.2605 E7	.2970 E7	.5849 E7	.9859 E6
		Light Water		
3	.1585 E8	.1148 E8	.1468 E8	.4780 E7
6	.9644 E7	.7699 E7	.1055 E8	.3515 E7
9	.6051 E7	.5242 E7	.7592 E7	.2594 E7
12	.3867 E7	.3595 E7	.5467 E7	.1919 E7
15	.2506 E7	.2478 E7	.3938 E7	.1421 E7
		Polyethylene		
3	.1309 E8	.1005 E8	.1454 E8	.3828 E7
6	.6714 E7	.6069 E7	.1025 E8	.2351 E7
9	.3597 E7	.3758 E7	.7217 E7	.1471 E7
12	.1999 E7	.2364 E7	.5073 E7	.9249 E6
15	.1151 E7	.1509 E7	.3562 E7	.5823 E6

TABLE 5.7 First Collision Dose at Depth in Tissue

	Contribution to First Collision Dose Rate in Tissue Rad/Min.				Total Dose Rate Rad/Min
E_{max}, MeV	1.822	5.05	8.278	10.00	
E_{min}, MeV	0.10	1.822	5.05	8.278	
Depth, cm					
0	5.51	3.93	2.96	0.40	11.80
3	2.75	2.51	2.28	0.27	7.81
6	1.585	1.73	1.75	0.19	5.26
9	0.95	1.21	1.34	0.14	3.64
12	0.588	.858	1.030	0.097	2.573
15	0.374	.612	.789	0.070	1.845

TABLE 5.8 Neutron Energy Dependence of Fast Neutron Dose Rate Transmitted by Infinite Slabs of Tissue, Lucite, H_2O and Polyethylene

	Contribution to Fast Neutron Dose Rate Rad/Min				Total Dose Rate
E_{max}, MeV	1.822	5.05	8.278	10.0	Rad/Min
E_{min}, MeV	0.10	1.822	5.05	8.278	
Depth, cm		Tissue			
0	9.440	5.026	3.992	0.527	18.99
3	4.712	3.210	3.073	0.357	11.35
6	2.718	2.211	2.363	0.251	7.542
9	1.629	1.551	1.813	0.179	5.172
12	1.007	1.098	1.389	0.129	3.622
15	0.641	0.783	1.063	0.093	2.579
		Lucite			
3	4.991	3.251	3.150	0.344	11.74
6	3.056	2.256	2.457	0.234	8.003
9	1.938	1.589	1.903	0.162	5.592
12	1.255	1.128	1.470	0.113	3.966
15	0.826	0.806	1.133	0.078	2.843
		Light Water			
3	5.028	3.115	2.844	0.381	11.37
6	3.058	2.089	2.043	0.279	7.470
9	1.919	1.422	1.470	0.206	5.018
12	1.226	0.975	1.059	0.153	3.413
15	0.795	0.672	0.763	0.113	2.343
		Polyethylene			
3	4.151	2.726	2.816	0.304	9.997
6	2.129	1.647	1.986	0.187	5.949
9	1.141	1.020	1.398	0.117	3.675
12	0.634	0.642	0.983	0.074	2.332
15	0.365	0.409	0.690	0.046	1.511

TABLE 5.9 Flux and Dose in Tissue: 45° Lucite Scatterers
(.100 E6 = .100 x 10^6)

Depth in Tissue Phantom, cm	$\phi(u)$, n/cm^2-sec/unit lethargy Dose Contribution, Rad/Min				1st Collision Dose Rate Rad/Min
	0.25 cm Lucite				
0	.1097 E7	.2695 E6	.1189 E6	.2893 E4	
	.203	.0572	.0171	.0002	0.278
3	.7020 E6	.1995 E6	.9673 E5	.2140 E4	
	.1300	.0423	.0140	.0001	.1864
6	.3737 E6	.1359 E6	.7550 E5	.1559 E4	
	.0691	.0288	.0109	.0001	.1089
9	.2022 E6	.9105 E5	.5798 E5	.1129 E4	
	.0374	.0193	.0084	.0001	.0652
12	.1112 E6	.6100 E5	.4423 E5	.8155 E3	
	.0206	.0129	.0064	.0000	.0399
15	.6213 E5	.4102 E5	.3366 E5	.5887 E3	
	.0115	.0087	.0049	.0000	.0251
	0.50 cm Lucite				
0	.1984 E7	.5061 E6	.2261 E6	.5216 E4	
	.367	.117	.0326	.0003	.517
3	.1260 E7	.3735 E6	.1836 E6	.3858 E4	
	.233	.0782	.0265	.0002	.338
6	.6721 E6	.2544 E6	.1432 E6	.2810 E4	
	.1244	.0540	.0206	.0002	.1992
9	.3646 E6	.1705 E6	.1100 E6	.2035 E4	
	.0675	.0361	.0159	.0001	.1196
12	.2010 E6	.1143 E6	.8388 E5	.1470 E4	
	.0372	.0242	.0121	.0001	.0736
15	.1126 E6	.7689 E5	.6383 E5	.1061 E4	
	.0208	.0163	.0092	.0001	.0464
Lethargy, u	2.5416	1.0886	.3956	.0712	

TABLE 5.9 (Cont.)

0.75 cm Lucite

0	.2720 E7	.7151 E6	.3230 E6	.7084 E4	
	.503	.1516	.0465	.0004	.702
3	.1716 E7	.5263 E6	.2619 E6	.5240 E4	
	.318	.1116	.0378	.0003	.468
6	.9161 E6	.3583 E6	.2042 E6	.3816 E4	
	.169	.0759	.0294	.0002	.275
9	.4979 E6	.2402 E6	.1567 E6	.2763 E4	
	.0905	.0508	.0226	.0002	.1641
12	.2751 E6	.1611 E6	.1195 E6	.1996 E4	
	.0509	.0342	.0172	.0001	.1024
15	.1546 E6	.1084 E6	.9093 E5	.1441 E4	
	.0286	.0230	.0131	.0001	.0648

1.00 cm Lucite

0	.3342 E7	.9006 E6	.4107 E6	.8588 E4	
	.618	.191	.0591	.0005	.869
3	.2094 E7	.6610 E6	.3325 E6	.6351 E4	
	.388	.140	.0479	.0004	.576
6	.1120 E7	.4499 E6	.2591 E6	.4625 E4	
	.207	.0954	.0373	.0003	.340
9	.6095 E6	.3017 E6	.1988 E6	.3349 E4	
	.113	.0640	.0286	.0002	.206
12	.3374 E6	.2024 E6	.1516 E6	.2420 E4	
	.0624	.0429	.0218	.0001	.1272
15	.1900 E6	.1362 E6	.1153 E6	.1746 E4	
	.0352	.0289	.0166	.0001	.0808
	2.5416	1.0886	.3956	.0712	

TABLE 5.9 (Cont.)

1.25 cm Lucite

0	.3875 E7	.1066 E7	.4904 E6	.9801 E4	
	.717	.226	.0707	.0006	1.014
3	.2415 E7	.7804 E6	.3964 E6	.7247 E4	
	.447	.166	.0570	.0004	.670
6	.1292 E7	.5310 E6	.3087 E6	.5277 E4	
	.239	.113	.0445	.0003	.397
9	.7045 E6	.3561 E6	.2368 E6	.3821 E4	
	.130	.0755	.0341	.0002	.240
12	.3906 E6	.2389 E6	.1806 E6	.2761 E4	
	.0723	.0507	.0260	.0002	.149
15	.2204 E6	.1609 E6	.1374 E6	.1993 E4	
	.0408	.0341	.0198	.0001	.0948

1.50 cm Lucite

0	.4339 E7	.1214 E7	.5630 E6	.1078 E5	
	.802	.258	.0812	.0006	1.142
3	.2690 E7	.8868 E6	.4543 E6	.7970 E4	
	.498	.188	.0655	.0005	.752
6	.1441 E7	.6032 E6	.3536 E6	.5804 E4	
	.267	.128	.0509	.0004	.446
9	.7865 E6	.4046 E6	.2712 E6	.4202 E4	
	.145	.0858	.0392	.0003	.270
12	.4367 E6	.2715 E6	.2068 E6	.3036 E4	
	.0809	.0575	.0298	.0002	.168
15	.2468 E6	.1829 E6	.1573 E6	.2191 E4	
	.0457	.0388	.0227	.0001	.1073
	2.5416	1.0886	.3956	.0712	

TABLE 5.9 (Cont.)

3.00 cm Lucite

0	.6223 E7	.1849 E7	.8856 E6	.1378 E5	
	1.152	.392	.128	.0008	1.673
3	.3781 E7	.1333 E7	.7088 E6	.1018 E5	
	.699	.283	.102	.0006	1.085
6	.2032 E7	.9054 E6	.5500 E6	.7412 E4	
	.376	.192	.0792	.0005	.648
9	.1114 E7	.6076 E6	.4213 E6	.5366 E4	
	.206	.129	.0606	.0003	.396
12	.6214 E6	.4082 E6	.3211 E6	.3877 E4	
	.1148	.0865	.0463	.0002	.248
15	.3531 E6	.2754 E6	.2442 E6	.2798 E4	
	.0653	.0583	.0352	.0002	.1590

6.00 cm Lucite

0	.7871 E7	.2457 E7	.1214 E7	.1493 E5	
	1.457	.521	.175	.0009	2.154
3	.4722 E7	.1745 E7	.9598 E6	.1103 E5	
	.874	.370	.1383	.0007	1.383
6	.2543 E7	.1182 E7	.7415 E6	.8027 E4	
	.470	.251	.1067	.0005	.828
9	.1398 E7	.7938 E6	.5670 E6	.5811 E4	
	.269	.168	.0817	.0003	.519
12	.7827 E6	.5337 E6	.4318 E6	.4197 E4	
	.145	.113	.0622	.0003	.321
15	.4465 E6	.3605 E6	.3283 E6	.3030 E4	
	.0837	.0763	.0473	.0002	.208
	2.5416	1.0886	.3956	.0712	

TABLE 5.10 Flux in Tissue: 45^{o} H_2O Scatterers
(.100 E6 = .100 x 10^6)

0.25 cm H_2O

0	.1074 E7	.2036 E6	.8042 E5	.9863 E4
3	.6866 E6	.1528 E6	.6645. E5	.7185 E4
6	.3621 E6	.1042 E6	.5224 E5	.5203 E4
9	.1937 E6	.6968 E5	.4029 E5	.3759 E4
12	.1050 E6	.4658 E5	.3084 E5	.2713 E4
15	.5775 E5	.3124 E5	.2353 E5	.1958 E4

0.50 cm H_2O

0	.1930 E7	.3766 E6	.1501 E6	.1837 E5
3	.1223 E7	.2817 E6	.1238 E6	.1337 E5
6	.6455 E6	.1920 E6	.9728 E5	.9677 E4
9	.3458 E6	.1284 E6	.7501 E5	.6991 E4
12	.1879 E6	.8587 E5	.5741 E5	.5046 E4
15	.1035 E6	.5762 E5	.4381 E5	.3641 E4
	2.5416	1.0886	.3956	.0712

TABLE 5.10 (Cont.)

0.75 cm H_2O

0	.2633 E7	.5246 E6	.2108 E6	.2572 E5
3	.1653 E7	.3912 E6	.1736 E6	.1870 E5
6	.8732 E6	.2664 E6	.1363 E6	.1353 E5
9	.4684 E6	.1783 E6	.1051 E6	.9776 E4
12	.2548 E6	.1192 E6	.8040 E5	.7056 E4
15	.1406 E6	.8002 E5	.6135 E5	.5091 E4

1.00 cm H_2O

0	.3221 E7	.6521 E6	.2638 E6	.3209 E5
3	.2006 E7	.4847 E6	.2168 E6	.2332 E5
6	.1060 E7	.3300 E6	.1702 E6	.1687 E5
9	.5693 E6	.2208 E6	.1312 E6	.1218 E5
12	.3100 E6	.1477 E6	.1004 E6	.8792 E4
15	.1713 E6	.9917 E5	.7657 E5	.6344 E4
	2.5416	1.0886	.3956	.0712

TABLE 5.10 **(Cont.)**

1.25 cm H_2O

0	.3722 E7	.7625 E6	.3103 E6	.3762 E5
3	.2301 E7	.5650 E6	.2546 E6	.2731 E5
6	.1217 E7	.3846 E6	.1997 E6	.1975 E5
9	.6540 E6	.2574 E6	.1539 E6	.1426 E5
12	.3565 E6	.1722 E6	.1177 E6	.1029 E5
15	.1972 E6	.1156 E6	.8984 E5	.7428 E4

1.50 cm H_2O

0	.4157 E7	.8588 E6	.3513 E6	.4244 E5
3	.2554 E7	.6345 E6	.2878 E6	.3079 E5
6	.1351 E7	.4317 E6	.2256 E6	.2226 E5
9	.7265 E6	.2889 E6	.1738 E6	.1607 E5
12	.3962 E6	.1933 E6	.1330 E6	.1160 E5
15	.2194 E6	.1298 E6	.1014 E6	.8369 E4
	2.5416	1.0886	.3956	.0712

TABLE 5.10 (Cont.)

3.00 cm H_2O

0	.5908 E7	.1240 E7	.5168 E6	.6109 E5
3	.3544 E7	.9029 E6	.4197 E6	.4413 E5
6	.1876 E7	.6129 E6	.3280 E6	.3185 E5
9	.1010 E7	.4102 E6	.2524 E6	.2298 E5
12	.5516 E6	.2746 E6	.1930 E6	.1658 E5
15	.3058 E6	.1846 E6	.1472 E6	.1196 E5

6.00 cm H_2O

0	.7392 E7	.1556 E7	.6555 E6	.7466 E5
3	.4369 E7	.1115 E7	.5262 E6	.5359 E5
6	.2312 E7	.7544 E6	.4095 E6	.3859 E5
9	.1244 E7	.5047 E6	.3146 E6	.2782 E5
12	.6797 E6	.3380 E6	.2404 E6	.2007 E5
15	.3769 E6	.2273 E6	.1833 E6	.1447 E5
	2.5416	1.0886	.3956	.0712

TABLE 5.11 Flux in Tissue: 45° Polyethylene Scatterers
(.100 E6 = .100 x 10^6)

0.25 cm Polyethylene

0	.1168 E7	.2539 E6	.1093 E6	.2051 E4
3	.7511 E6	.1890 E6	.8913 E5	.1518 E4
6	.3979 E6	.1288 E6	.6962 E5	.1106 E4
9	.2140 E6	.8626 E5	.5347 E5	.8012 E3
12	.1168 E6	.5774 E5	.4079 E5	.5789 E3
15	.6475 E5	.3879 E5	.3104 E5	.4179 E3

0.50 cm Polyethylene

0	.2046 E7	.4638 E6	.2038 E6	.3578 E4
3	.1301 E7	.3440 E6	.1659 E6	.2650 E4
6	.6906 E6	.2344 E6	.1295 E6	.1931 E4
9	.3724 E6	.1570 E6	.9939 E5	.1398 E4
12	.2039 E6	.1052 E6	.7582 E5	.1010 E4
15	.1134 E6	.7072 E5	.5769 E5	.7292 E3
	2.5416	1.0886	.3956	.0712

TABLE 5.11 (Cont.)

0.75 cm Polyethylene

0	.2731 E7	.6389 E6	.2859 E6	.4716 E4
3	.1720 E7	.4723 E6	.2322 E6	.3492 E4
6	.9142 E6	.3217 E6	.1811 E6	.2544 E4
9	.4939 E6	.2157 E6	.1390 E6	.1843 E4
12	.2711 E6	.1445 E6	.1060 E6	.1331 E4
15	.1511 E6	.9724 E5	.8066 E5	.9610 E3

1.00 cm Polyethylene

0	.3282 E7	.7864 E6	.3575 E6	.5563 E4
3	.2050 E7	.5794 E6	.2898 E6	.4120 E4
6	.1091 E7	.3946 E6	.2259 E6	.3002 E4
9	.5901 E6	.2646 E6	.1733 E6	.2174 E4
12	.3244 E6	.1774 E6	.1322 E6	.1571 E4
15	.1813 E6	.1194 E6	.1005 E6	.1134 E4
	2.5416	1.0886	.3956	.0712

TABLE 5.11 (Cont.)

1.25 cm Polyethylene

0	.3735 E7	.9114 E6	.4201 E6	.6195 E4
3	.2316 E7	.6695 E6	.3399 E6	.4587 E4
6	.1233 E7	.4559 E6	.2648 E6	.3342 E4
9	.6682 E6	.3058 E6	.2031 E6	.2420 E4
12	.3679 E6	.2051 E6	.1549 E6	.1749 E4
15	.2059 E6	.1382 E6	.1178 E6	.1262 E4

1.50 cm Polyethylene

0	.4116 E7	.1018 E7	.4752 E6	.6665 E4
3	.2537 E7	.7460 E6	.3838 E6	.4935 E4
6	.1352 E7	.5078 E6	.2988 E6	.3596 E4
9	.7331 E6	.3407 E6	.2291 E6	.2604 E4
12	.4041 E6	.2286 E6	.1747 E6	.1882 E4
15	.2265 E6	.1541 E6	.1329 E6	.1358 E4
	2.5416	1.0886	.3956	.0712

TABLE 5.11 (Cont.)

3.00 cm Polyethylene

0	.5522 E7	.1421 E7	.6969 E6	.7804 E4
3	.3334 E7	.1027 E7	.5577 E6	.5779 E4
6	.1780 E7	.6982 E6	.4327 E6	.4210 E4
9	.9679 E6	.4689 E6	.3314 E6	.3049 E4
12	.5353 E6	.3152 E6	.2525 E6	.2203 E4
15	.3011 E6	.2128 E6	.1920 E6	.1590 E4

6.00 cm Polyethylene

0	.6466 E7	.1721 E7	.8814 E6	.8031 E4
3	.3866 E7	.1228 E7	.6971 E6	.5947 E4
6	.2067 E7	.8335 E6	.5385 E6	.4333 E4
9	.1126 E7	.5602 E6	.4118 E6	.3138 E4
12	.6240 E6	.3771 E6	.3136 E6	.2267 E4
15	.3520 E6	.2550 E6	.2384 E6	.1637 E4
u	2.5416	1.0886	.3956	.0712

The STAR code has been used to obtain the reflection matrix for infinite slabs of lucite, H_2O, and polyethylene having thicknesses of 0.25, 0.50, 0.75, 1.00, 1.25, 1.50, 3.00, and 6.00 cm. The STAR DATA REDUCTION (SDR) code rotated by 45^o the angular fast neutron spectrum at the portal (Table 5.4) using the method given in Section 2.4.1. This rotation gave the source as seen by the scatterer. Succeeding operations by SDR computed the flux reflected from the scatterer, then rotated the reflected flux by 45^o to give the source incident on an infinite slab tissue phantom, followed by a calculation of flux transmitted by the tissue phantom. Tables 5.9, 5.10 and 5.11 give the results of these manipulations for lucite, H_2O, and polyethylene scatterers, respectively. The fast neutron flux and dose rate down the axis of a cylindrical phantom comparable in size to a human head should agree quite well with the infinite slab calculations. One would expect lateral leakage to diminish the flux near the edge of the phantom, and to decrease the deeply penetrating flux even on the axis.

It is of interest to examine some of the data in Table 5.9 in terms of the effect of a lucite scatterer on both fast and thermal neutrons. For thermal neutrons $\Sigma_s/\Sigma_t = 1.831/1.845 = 0.9924$, very nearly unity. The total reflection, R, for a beam incident at 45^o on a slab for which $\Sigma_s/\Sigma_t = 1.0$ has been obtained from TAR(N). It is given in Table 5.12. Assuming that the thermal neutrons can be treated as a

beam incident at 45° one can obtain the probability of reflection as a function of lucite thickness from plotting R (Table 5.12). This calculation is given in Table 5.13, together with the ratio of first collision dose at the surface of a tissue phantom using reflected neutrons to using the direct beam. The advantage factor given is the ratio of thermal neutron reflection probability to the first collision dose ratio. For example, a 1.0 cm thick lucite scatterer has an advantage factor of 7.9. This means that whereas the first collision dose rate has fallen to 0.0736 of that for the direct beam, the thermal neutron flux (and B^{10} dose rate) has only dropped to 0.579, which is 7.9 times higher. Geometrical attenuation between the portal and the phantom has not been accounted for in these calculations. In general, one would expect little reduction in fast neutron flux because it is strongly peaked in the forward direction (Table 5.4). A greater reduction can be expected for thermal neutrons, which will depend somewhat on the scatterer thickness. With no reflecting, material near the portal, Rydin has measured the thermal neutron flux to be 7.10×10^9 n/cm^2-sec at 5 Mw and 2.5 inches below the portal. With a phantom in place, the reflection from the phantom increases the thermal flux at the portal by a factor of 2.5 to 3.0. A 1 cm thick lucite scatterer at 45° will also increase the thermal neutron flux about 0.58 times as much as for the optically thick phantom. Shielding will be required nearby, which will also reflect some neutrons. The estimation of all these effects is not very reliable.

Experiments are being set up by Drs. Reddy and Ayyangar (M.G.H.) to measure thermal neutron flux and fast neutron dose rates in a phantom irradiated by neutrons reflected from lucite. The theoretical advantages in using scattered neutrons are most encouraging. Reduced fluxes and dose rates are inherent to this method. The increased irradiation time required for the same dose could be a disadvantage.

TABLE 5.12 Perfectly Reflecting Slab: 45^{o} Incident Beam

Slab Thickness, $\Sigma_t L$	Total Reflection Probability, R
Mean Free Paths	
0.00	0.000
.25	.151
.50	.263
.75	.348
1.00	.420
1.50	.523
2.00	.600
2.50	.651
3.50	.724
4.50	.760

TABLE 5.13 Lucite Scatterer: Reflection Probabilities

Thickness, cm	1st Coll. Dose Ratio: Reflected/Direct	Thermal Neutron Reflection Prob.	Advantage Factor
0.00	0.0000	0.000	--
0.25	0.0235	0.248	10.6
0.50	0.0438	0.400	9.1
0.75	0.0595	0.505	8.5
1.00	0.0736	0.579	7.9
1.25	0.0859	0.635	7.4
1.50	0.0967	0.675	7.0
3.00	0.1417	~0.79	5.6
6.00	0.1826	~0.94	~3.8

Final calculations have been made with MEDIPORT of the flux and dose distributions inside a tissue cylinder irradiated by neutrons from the direct beam at the M.I.T.R. (Table 5.14), and irradiated by neutrons scattered from an 0.5 cm thick lucite slab mounted at 45^{o} to the direct beam (Table 5.15). The surface first collision dose rates obtained with STAR have been used to normalize the neutron spectra computed by MEDIPORT. The thermal neutron flux incident on the tissue phantom was assumed to be 2.0×10^{10} and 3.0×10^{9} n/cm^2-sec, respectively. These fluxes are conservative compared to experiment. Tables 5.14 and 5.15 are reproduced directly from the MEDIPORT printout. Radius and depth are in cm, and dose rates are in units of 0.1 and 0.01 rad/min, respectively. The quantity labelled "ratio" in the key is the ratio of B^{10} dose to total background dose, multiplied by 1000. The dose rates shown are for a B^{10} weight fraction of 50×10^{-6} and are calculated assuming no perturbation to the thermal neutron flux by B^{10} capture. In a patient irradiation the fluxes and dose rates would be reduced near the tumor. "Fast" is the recoil dose rate from fast neutrons, "Heavy" is heavy particle dose rate from $N^{14}(n,p)C^{14}$, "Gamma" is the dose rate from gamma rays produced by neutron capture in tissue (principally in H, C, Cl, and B^{10}). "Total" is the sum of "Fast", "Heavy", and "Gamma". The quantity labelled "B-10" is the local heavy particle dose rate from $B^{10}(n,\alpha)Li^{7}$.

Out of all the cases discussed in this chapter dealing with epithermal beams, D_2O removal, neutron filters, and combinations of these changes, the optimum configuration

is the one with the most D_2O in the neutron flight path. In other words, the configuration as it exists at the M.I.T.R. Medical Facility is best in the sense that it produces the largest ratio of B^{10} dose to tumor/maximum normal tissue dose. However, even the normal beam cannot provide a tumor/max. normal tissue dose ration in excess of unity at depths greater than 4.5 cm.

Additional optimization is possible by extending the number of variables to include neutron scatterers. Table 5.13 has shown that the best scatterer is one of zero thickness - but dose rates vanish too. A compromise between reasonable dose rates and diminishing effectiveness of the scatterer is required. Such an example is given in Table 5.15 for an 0.5 cm thick lucite scatterer. It can be seen that the fast neutron dose contribution to the total background dose at the surface is cut from about 13% with the direct beam (Table 5.15) to 3.4% using scattered neutrons. At depth greater than 2 cm about 80% of the background dose to normal tissue comes from thermal neutron capture gamma rays. An "epithermal" beam produced by absorbing thermal neutrons at the surface of the phantom, combined with the scatterer, would produce a lower normal tissue dose rate at the surface as well as shift the gamma ray dose peak to a greater depth. In this way it may be possible to improve on the dose ratio of B^{10}/max. normal tissue.

TABLE 5.14 FLUX AND DOSE RATES IN PHANTOM, DIRECT BEAM, MITR

KEY TO TABLE
THERMAL FLUX(N/CM2-SEC)
FAST HEAVY
GAMMA TOTAL
RATIO B-10

DEPTH, CM	RADIUS, CM				
	0.	2.075	4.150	6.225	8.300
0.	.199E 11	.195E 11	.184E 11	.160E 11	.963E 10
	135 396	135 389	135 365	135 319	135 191
	509 1040	497 1021	448 949	359 813	199 525
	4968 5167	4967 5072	5025 4769	5116 4160	4759 2499
1.	.126E 11	.124E 11	.116E 11	.102E 11	.610E 10
	97 251	97 246	97 231	97 202	97 121
	606 954	585 928	533 861	435 734	232 450
	3430 3273	3463 3214	3509 3022	3591 2636	3517 1583
2.	.798E 10	.784E 10	.737E 10	.643E 10	.386E 10
	71 159	71 156	71 147	71 128	71 77
	547 777	529 756	481 699	390 589	217 365
	2666 2072	2690 2034	2735 1912	2831 1668	2745 1002
3.	.506E 10	.497E 10	.467E 10	.407E 10	.245E 10
	54 101	54 99	54 93	54 81	54 49
	458 613	445 598	403 550	326 461	190 293
	2140 1312	2155 1289	2203 1212	2292 1057	2167 635
4.	.320E 10	.314E 10	.296E 10	.258E 10	.155E 10
	42 64	42 63	42 59	42 51	42 31
	374 480	363 468	329 430	266 359	163 236
	1731 831	1743 816	1783 767	1863 669	1703 402
5.	.203E 10	.199E 10	.187E 10	.163E 10	.980E 09
	34 40	34 40	34 37	34 32	34 19
	300 375	292 366	264 335	214 281	137 191
	1402 526	1409 516	1447 485	1505 423	1329 254
6.	.128E 10	.126E 10	.119E 10	.103E 10	.621E 09
	28 26	28 25	28 24	28 21	28 12
	240 294	234 286	211 263	173 221	116 156
	1132 333	1143 327	1171 308	1212 268	1032 161
7.	.812E 09	.798E 09	.750E 09	.654E 09	.393E 09
	23 16	23 16	23 15	23 13	23 8
	192 231	187 225	169 207	140 175	97 128
	913 211	919 207	942 195	971 170	796 102

DOSE IN UNITS OF 0.10 RAD/MIN.
B-10 WEIGHT FRACTION 50.0 PARTS PER MILLION

TABLE 5.15 FLUX AND DOSE RATES IN PHANTOM, 0.5 CM LUCITE SCATTERER AT 45 DEGREES

KEY TO TABLE
THERMAL FLUX(N/CM2-SEC)
FAST HEAVY
GAMMA TOTAL
RATIO B-10

DEPTH, CM	RADIUS, CM				
	0.	2.075	4.150	6.225	8.300
0.	.299E 10	.293E 10	.276E 10	.240E 10	.144E 10
	47 594	47 583	47 548	47 478	47 287
	764 1405	746 1376	673 1268	539 1064	298 633
	5516 7750	5529 7609	5641 7154	5864 6240	5922 3749
1.	.189E 10	.186E 10	.175E 10	.152E 10	.915E 09
	29 376	29 369	29 347	29 303	29 182
	909 1315	877 1276	800 1176	653 985	348 559
	3734 4911	3778 4821	3854 4533	4014 3954	4250 2376
2.	.120E 10	.118E 10	.111E 10	.964E 09	.579E 09
	19 238	19 234	19 220	19 192	19 115
	820 1077	794 1046	721 960	586 796	325 459
	2885 3108	2917 3052	2989 2870	3144 2503	3276 1504
3.	.759E 09	.745E 09	.701E 09	.611E 09	.367E 09
	13 151	13 148	13 139	13 121	13 73
	688 851	668 829	605 757	489 624	285 371
	2313 1969	2332 1934	2401 1818	2541 1586	2568 953
4.	.481E 09	.472E 09	.444E 09	.387E 09	.233E 09
	9 96	9 94	9 88	9 77	9 46
	560 665	545 648	493 590	399 485	244 299
	1875 1247	1890 1225	1952 1152	2070 1004	2016 603
5.	.304E 09	.299E 09	.281E 09	.245E 09	.147E 09
	7 60	7 59	7 56	7 49	7 29
	451 518	438 504	396 459	322 377	206 242
	1523 789	1537 775	1586 728	1684 635	1578 382
6.	.193E 09	.189E 09	.178E 09	.155E 09	.932E 08
	5 38	5 38	5 35	5 31	5 19
	360 404	350 393	317 358	259 295	174 197
	1237 500	1249 491	1290 462	1366 403	1228 242
7.	.122E 09	.120E 09	.113E 09	.982E 08	.590E 08
	4 24	4 24	4 22	4 20	4 12
	288 316	280 308	254 280	210 233	146 162
	999 316	1009 311	1042 292	1094 255	944 153

DOSE IN UNITS OF 0.01 RAD/MIN.
B-10 WEIGHT FRACTION 50.0 PARTS PER MILLION

5.6 THE USE OF A REFLECTING ANNULUS

In all of the cases considered previously, the thermal neutron flux inside a tissue-equivalent cylindrical phantom falls off asymptotically with depth at distances beyond a few centimeters from the surface. In some cases, the thermal neutron flux incident at the surface completely overwhelms the thermal neutron flux produced by epithermal neutrons slowing down. For these cases the thermal neutron flux behaves asymptotically right from the surface as

$$\phi(x) \sim \phi_o \exp\left[-\left(\frac{1}{L^2} + \left(\frac{2.405}{R'}\right)^2\right)^{1/2} x\right] \qquad (5.14)$$

where R' is the extrapolated radius of the phantom (8.6 cm).

It is of considerable interest to examine the effect of varying R' to reduce lateral leakage and to increase the thermal neutron flux and boron capture dose rate at large depths. Table 5.16 gives the relative thermal neutron flux down the axis of a tissue-equivalent phantom cylinder 8.3 cm in radius surrounded by an annulus of material with the same thermal neutron diffusion coefficient D and diffusion length L as assumed for tissue ($D = 0.170$ cm, $L = 2.76$ cm). It is assumed that the flux varies with depth, x, as in Equation (5.14). Defining the ratio of flux with the annulus to flux without the

annulus as the thermal neutron flux enhancement factor, one obtains the results given in Table 5.17. Even a 5 cm thick annulus gives a sizeable enhancement factor of 1.31 to 1.46 at depths from 5 to 7 cm. One can combine this result with the normal beam parameters given in Table 5.14. It can be shown that the depth at which the tumor dose is the same as the maximum normal tissue dose increases from about 4.5 cm to about 5.5 cm. The ultimate depth is 6.2 cm, using an effectively infinite reflecting annulus. If instead a reflected neutron beam is used such as given in Table 5.15, the corresponding depths increase from 4.8 cm to 6.0 cm and 6.5 cm respectively. Another benefit is a flatter radial distribution of thermal neutron flux and boron capture dose.

Theoretically, the reflecting annulus offers very worthwhile improvements in dose distribution. The capture gamma ray dose from the annulus should be as small as possible. Neutron absorption in the reflector should probably be as small as possible, although one can also visualize an "epithermal" neutron reflector. Heavy water, with or without a thermal neutron absorber such as Li^6, would be an excellent choice. A lucite vessel with thin walls could be used to contain the D_2O. Reactor-grade graphite is another possibility.

The use of a reflecting annulus would also be beneficial for irradiations using "epithermal" beams. It is reasonable to expect improvements in thermal neutron flux at depth of the same order of magnitude as presented in Table 5.17.

TABLE 5.16 Relative Thermal Neutron Flux in Phantom with Reflecting Annulus (Phantom Radius 8.3 cm).

Depth in Phantom, cm	Annulus Thickness, cm. 0	5	10	15	∞
0	1.000	1.000	1.000	1.000	1.000
1	.633	.669	.681	.687	.697
2	.401	.447	.464	.472	.485
3	.254	.299	.316	.324	.338
4	.1607	.1999	.2153	.2226	.2355
5	.1017	.1337	.1467	.1529	.1640
6	.0644	.0894	.0999	.1049	.1143
7	.0408	.0598	.0681	.0721	.0796

TABLE 5.17 Thermal Neutron Flux Enhancement in Phantom with Reflecting Annulus (Phantom Radius 8.3 cm).

Depth in Phantom, cm.	Annulus Thickness, cm. 5	10	15	∞
0	1.000	1.000	1.000	1.000
1	1.056	1.076	1.085	1.100
2	1.115	1.157	1.177	1.211
3	1.178	1.245	1.277	1.332
4	1.244	1.340	1.385	1.465
5	1.314	1.441	1.503	1.612
6	1.387	1.551	1.630	1.774
7	1.465	1.668	1.768	1.952

CHAPTER VI

CONCLUSIONS AND RECOMMENDATIONS FOR FUTURE WORK

6.1 COMPUTATIONAL METHODS

A new numerical solution has been obtained for the problem of neutron transport in finite-thickness slabs with isotropic scattering in the laboratory system. The method uses Gaussian quadratures to numerically evaluate neutron transport integrals containing the exponential integral functions as weighting functions. It has been shown that low-order quadratures yield neutron transmission, absorption, and reflection probabilities with accuracy comparable to results obtained at greater cost in computing time by the Markov Matrix and Invariant Imbedding methods. The Gaussian quadrature method developed in this work has several advantages over the Markov Matrix Method:

1. Many fewer flux-points required (fewer machine operations);
2. Applicable to thicker slabs;
3. No extrapolations of sub-slab thickness to zero.

The Invariant Imbedding Method is ideal for much thicker slabs, but it cannot analyze the neutron collision histories. It is very accurate, but rather costly in computer time, which restricts its application to few-group calculations.

Collision history correlations have been devised analytically and empirically, guided by physical insight, which express in simple analytical form the probability of neutron transmission, reflection and absorption as a function of slab thickness and collision number. Using only five parameters it is possible to predict the fate of neutrons incident on an infinite slab of arbitrary thickness (less than about five mean free paths) having arbitrary macroscopic neutron absorption and scattering cross sections.

Multigroup transfer matrices and neutron spectra can be calculated by combining the collision history correlations with single-collision group-to-group transition probabilities. The transfer matrix for two adjacent slabs is easily found to as high an order of approximation as necessary. It has been shown that the lowest order approximation given by the product of the individual transfer matrices is quite accurate for fast neutron dose attenuation calculations through polyethylene and D_2O. Some examples of multiply-reflected fluxes have been calculated to illustrate their unimportance compared to the directly transmitted flux. Excellent results have been obtained for the effects on neutron spectra of changes in complicated neutron shields, compared with experimental results and more accurate and costly theoretical calculations.

Thermal neutron flux distributions down the axis of a beam port facility and inside a tissue phantom have been calculated by numerical integration of a set of three

coupled, non-linear, first-order differential equations equivalent to the diffusion equation. This method has been employed because its automatic adjustment of step-size in the numerical integration frees the user from specifying anything other than neutron cross sections, region boundaries, and two-point boundary conditions. It also relates easily to the slowing-down source of thermal neutrons given by the neutron spectrum calculations and gives a flux distribution inside a tissue phantom from which dosimetry calculations are readily obtained. Methods have been devised to calculate radiation dose rates in tissue from recoil nuclei struck by fast neutrons, and from heavy particles and gamma rays emitted as a result of neutron capture.

The resulting computer code, MEDIPORT, performs all flux and dosimetry calculations required to survey the effects of changes to multiple-slab shields on neutron beam characteristics for use in neutron capture therapy. The computational methods used in MEDIPORT have been shown to give results sufficiently accurate to be extremely useful for comparisons with experiment, for surveys of modifications to existing beam facilities too difficult to perform experimentally, to suggest new experiments, and to optimize a neutron beam for maximum usefulness for neutron capture therapy. A typical ten region shield problem plus a tissue phantom takes about three minutes on an IBM-7094 to obtain a 25-group epithermal and fast neutron spectrum, thermal neutron flux, and all dosimetry

calculations. Half of this time is consumed by the gamma ray dose rate calculation at forty locations inside the phantom, and about a quarter of the time each by the calculations of neutron spectra and thermal neutron flux. Such economy of computer time is highly advantageous to extensive parametric surveys.

Future work is recommended to improve and develop the neutron spectrum calculation. The first step would be to write the TAR(N) code in FORTRAN-IV, using double precision arithmetic throughout. The Gaussian quadratures method has no fundamental restriction on the maximum slab thickness which can be solved. However, numerical accuracy greater than single precision (eight decimals) is needed for thicknesses in excess of five mean free paths. More accurate fits to the ratios RT(k) and RR(k) of Equation (3.6) could be obtained by adding another term with a different decay constant, as follows:

$$RT(k) \simeq RT(\infty)\left|\Sigma_t L + A(\Sigma_t L)\exp\left(-ka(\Sigma_t L)\right) + D(\Sigma_t L)\exp(-kd(\Sigma_t L)\right)$$

Preliminary calculations indicate that equations of this form would significantly increase the accuracy of the empirical correlations for small k and large $\Sigma_t L$.

Empirical correlations such as these may have wider application. For example, Monte Carlo calculations of neutron penetration through slabs follow neutrons, collision by collision, generating the probability of transmission as a function of collision number. The effects

of neutrons suffering many collisions could be accurately extrapolated using collision history correlations.

It would not be too difficult to transport-correct the group-transfer cross sections $\sigma(i \rightarrow j)$. If $\mu(i \rightarrow j)$ is the average cosine of the scattering angle, the transport corrected group-transfer cross section is $\sigma(i \rightarrow j) \left[1 - \mu(i \rightarrow j)\right]$. The remainder, $\sigma(i \rightarrow j)\, \mu(i \rightarrow j)$, represents small-angle scattering which is best treated like the uncollided flux. A development of this type would be of particular value for neutron transmission through D_2O and hydrogeneous materials, because $\mu(i \rightarrow j)$ is fairly large.

6.2 RESULTS

The primary goal of this work has been to develop fast accurate computational methods for simulating production and use of neutron beams for neutron capture therapy, and to apply these methods to an optimization of the M.I.T.R. Medical Beam Facility. A secondary result of this work has been additional light thrown on a fundamental problem in neutron transport theory: the fate of neutrons incident on a finite-thickness, infinite slab or series of slabs. Numerous results of transmission, absorption, and reflection probabilities have been tabulated and compared to results obtained by the Markov Matrix and Invariant Imbedding methods. These results speak for themselves, and need not be tabulated again. Excellent agreement has been obtained in all comparisons.

Computer simulation of neutron capture therapy experiments at the Brookhaven M.R.R. has verified the ability of MEDIPORT to predict the effect of D_2O removal on fluxes and dose rates in a tissue phantom. Predicted thermal neutron flux distributions in the phantom when bombarded by neutrons "filtered" by lithium tend to be low, compared with experiment. However, rather large fluxes penetrated the sides of the phantom in the actual experiments, which accounts for much of the differences. Also, the thickness of lithium assumed in the calculations was significantly greater than actually used.

Optimization of the M.I.T.R. Medical Facility for neutron capture therapy has been performed in three

stages. The first stage is characterized by irradiating tissue with neutrons coming directly from the portal. "Epithermal" neutron beams have been studied because their increased penetration into tissue offered the possibility of better depth-dose distribution in tissue. The "epithermal" beams produced by removing D_2O and/or by adding lithium to absorb thermal neutrons do give considerable improvements in penetration of thermal neutrons, and in addition have low surface thermal fluxes. This latter feature is desirable to minimize damage to normal tissue above the tumor. Unfortunately, the recoil dose rate from fast neutrons increases very rapidly with D_2O removal. The magnitude of the thermal neutron flux at tumor depths also falls significantly when a lithium filter is used, making the recoil dose rate from fast neutrons the most important component of background radiation. The result is that losses caused by increased background radiation from fast neutrons exceed gains from better penetration or distribution of thermal neutrons. The important parameter here is the depth at which a tumor can be given the same dose as the maximum received by normal tissue. The normal beam (all D_2O in place) without a filter is able to reach a tumor at greater depth in normal tissue than any of the "epithermal" beams produced by D_2O removal or lithium filters.

Another series of calculations was performed incorporating several refinements to the calculational

methods. Other filter materials besides Li and Li^6 studies were: Cr, V, Al, and C. The motivation was to control the recoil dose rate from fast neutrons by replacing D_2O with these materials. Invariably, the thermal neutron flux and boron capture dose rate decreased faster than the recoil dose rate. The conclusion is that D_2O is the best material to use to moderate fast neutrons. Consequently the existing configuration of shielding in the Medical Beam is the optimum of the cases studied. The trends certainly show that even more D_2O would produce a better beam. It is recommended that provision be made to insert known thicknesses of D_2O into the light water shutter.

The second stage in the optimization consisted in studying the use of neutron beams scattered from hydrogeneous materials, to selectively attenuate fast neutrons in the scattered beam. Lucite, polyethylene, and water were investigated. No other materials exhibit as large a reduction in scattering cross section with increasing neutron energy in the region above 0.01 MeV. Lucite was selected for additional calculations because of its convenient physical properties for experimental use. The neutron reflecting properties of polyethylene, water and lucite are rather similar. In all cases, the scattering slab was assumed to be at 45^o to the direct beam from the portal, and the phantom was irradiated by neutrons deflected on the average through 90^o.

Studies of the effect of slab thickness show an optimum for a zero-thickness slab - but the dose rates also go to zero. A compromise is required between neutron reflecting characteristics and irradiation times (dose rates). Fortunately, reasonable dose rates are obtainable without much loss in efficiency of the scatterer. Results have been given for an 0.5 cm thick lucite scatterer which show a factor of about four in diminishing the fraction of background radiation dose at the tissue surface coming from fast neutrons. The fractions are 13% and 3.4%, respectively. Experimental verification of the predictions for lucite scatterers is recommended.

The effectiveness of the lucite scatterer in selectively removing fast neutrons is sufficiently good that little further improvements are possible without recourse to other techniques, or combinations of techniques. Another parameter, stage three in the optimization, investigates a new approach. A reflecting annulus surrounding the phantom would reduce lateral leakage of neutrons, and would significantly increase the axial thermal neutron penetration. The optimum annulus thickness is that thickness for which it becomes an effectively infinite reflector. Calculations have shown that even a 5 cm thick annulus of tissue-equivalent material leads to 31% and 46% increases in thermal neutron flux at depths of 5 and

7 cm. The depth at which the tumor dose equals the maximum normal tissue dose increases from 4.5 cm to 5.5 cm (normal beam), and from 4.8 cm to 6.0 cm (0.5 cm lucite scatterer).

The material and exact details of the reflecting annulus have not been investigated because an experimental study is required and recommended. A lucite-walled vessel containing D_2O would be a good choice because of the excellent thermal neutron penetration and negligible capture gamma ray dose rate. Similarly, reactor-grade graphite could be used. In effect a "bath" of thermal neutrons could be obtained having a relatively flat axial and radial distribution inside the phantom. A broad source, rather than a well-collimated source, would probably give best results. Experimental checks on the performance of a reflecting annulus are recommended because they promise large gains in depth at which tumors can be fatally irradiated without destroying normal tissue, and because it would be fairly easily performed.

It seems possible that D_2O addition or removal could be combined with a neutron scatterer to control fast neutron dose and a lithium filter to produce a better thermal flux shape axially in tissue. Studies of this type could be done on the computer with MEDIPORT.

Extensive surveys of neutron beam characteristics for use in neutron capture therapy have been performed by computer simulation. Many promising ideas have emerged, of which all but a few failed to fulfill expectations. In this regard, what not to do experimentally is as important as what to do. It is confidently expected that experimental studies of the use of a reflecting annulus around a tissue phantom and of a neutron beam reflected from a thin layer of lucite will give new hope for the ultimate success of neutron capture therapy.

APPENDIX A

COMPUTER CODES

A.1 MEDIPORT

The purpose of the MEDIPORT code is to combine in a unit all calculations necessary to simulate patient irradiations for neutron capture therapy. For convenience in development it is partitioned into a main program plus about twenty subroutines. It is written largely in FORTRAN-II for the Fortran Monitor System as used by the IBM-7094 computer at the M.I.T. Computation Center. The code is machine-independent in that any digital computer with 32K memory and a FORTRAN-II compiler could be used. Input/output magnetic tape unit numbers would have to be changed to conform to the requirements of another computer system. The only other possible change would be in some FAP-coded mathematical subroutines from the Share Library.

Restrictions on the size of problem are:

1. $\leq$ 26 energy groups above thermal energies; 1 thermal group.
2. $\leq$ 11 regions. Each region may be subdivided into arbitrarily many sub-regions all of the same thickness, the total number of sub-groups not greater than 100. More regions can be handled by several cases, back-to-back.

Succeeding calculations use output of previous cases and continue on.

3. No up-scatter from a lower energy group to a higher energy group.
4. Down scatter from a given group to a maximum of 10 lower energy groups.
5. Thermal neutron flux must be found in less than 500 integration steps.
6. $\leq$ 5 neutron-capture gamma sources in tissue phantom.
7. $\leq$ 5 neutron-capture heavy particle sources in tissue phantom.
8. $\leq$ 24 uniformly spaced points axially in tissue phantom at which dose rates are to be calculated.
9. $\leq$ 10 uniformly spaced points radially in tissue phantom at which dose rates are to be calculated.

The next Section, A.1.1, gives a description of input data used by MEDIPORT. The entire code except the Share Library Subroutines is listed in Section A.1.2. Numerous comments have been added to clarify the code. Sample input for two fairly complicated problems is given in Section A.1.3. The first problem is a 26-group calculation of neutron reflection from a scatterer composed of an 0.5 cm thick lucite slab at 45^{o}, followed by a calculation of flux and dose rates inside a cylindrical phantom bombarded by the reflected beam. The

result of this problem is given in Table 5.15. First collision transmission probabilities have been arbitrarily increased by 10%, in order to correct approximately for anisotropic group transfer cross sections. Little change in neutron spectrum occurs above 0.1 MeV, but a somewhat larger epithermal flux is obtained which agrees better with experimental measurements by Rydin.

The second problem attenuates a fission source through 10 cm of D_2O, followed by double reflection at the interface between two 10 cm thick D_2O slabs, and finally transmission through 30 cm of D_2O from the interface (i.e., a total of 40 cm D_2O). The result of this problem is given in Table 3.3.2. The first problem uses a special version of the SINT subroutine to read the neutron source from data cards, while the second problem uses the normal SINT subroutine together with SPECT and GAS4 to compute the fission neutron source strength in each energy group. Also given are 26 group cross sections for Al and Bi.

Special subroutines for three-dimensional numerical integration by Gaussian quadratures and for numerical interpolation are described in Sections A.1.4 and A.1.5, respectively.

A.1.1 INPUT DATA FOR MEDIPORT

Set 1. Cross Section Library

Card 1: Format (212,6x,11A6,A4)

1. NNEW = number of cross section sets in library. If NNEW = 0, it is assumed that the library and Set 2 are in memory already.
2. IQ = number of abscissas in tables of parameters T_1, $a(\Sigma_t L)$, $RT'(\infty)$, $A'(\Sigma_t L)$. Required only if NNEW > 0. ≤ IQ 25.
3. Alphanumeric title for tables, in columns 11-80.

Card 2: Format (I5,4E10.3,I2)

1. NENG = 1 + number of energy groups above the thermal group.
2. p_0 = neutron source strength, fast neutrons/cm^3-sec.
3. p_1 = derivative of neutron source strength, fast neutrons/cm^4-sec, inward (toward the source), at the surface.
4. CN = atom number density inside the distributed volume source, atoms/cm^3.
5. ZTAC = control parameter. If ≥ 0, call SINT subroutine for new neutron source. If < 0, use last flux of previous case as source.
6. NVAL = source angular distribution parameter. $S(\theta) \sim (\cos\theta)^{NVAL-1}$. Uncollided transmission $\sim E_{NVAL}(\Sigma_t x)$. Must be consistent with Set 2.

Card 3: Format (8E10.3)

J. E(J) = upper bound of energy group J, MeV.
J = 1...NENG. Highest energy group is J = 1. E(J) must decrease monatonically with increasing J. Use more cards if NENG > 8.

For each of NNEW cross section sets, the following is required:

Card 1: Format (I5, 5x, A5, F10.5, I5, 2F10.5)

1. NCODE = identification number of this set ($\leq$ 11). The code assumes that cross sections for the volume source have NCODE = 1.
2. AMAT = Alphanumeric label for the set, e.g., D20, POLY.
3. BARMU = $\bar{\mu}_0$, the average cosine of the thermal neutron scattering angle in the laboratory system.
4. NDS = number of downscatter transfer cross sections of form $\sigma(i \rightarrow i + j)$; $0 \leq j \leq$ NDS.
5. SAT = microscopic thermal neutron absorption cross section (b).
6. SST = microscopic thermal neutron scattering cross section (b).

For each energy group J($1 \leq J$ NENG ≤ -1), the following is required:

Card 1: Format (6F10.5)

1. σ_{tr} = transport cross section for group J(b).
2. $\sigma_{tr}(J \rightarrow J)$ = single-collision cross section for

remaining in group J (b).

⋮

6. $\sigma(J \rightarrow J + 4)$

Card 2:

1. $\sigma(J \rightarrow J + 5)$

⋮

6. $\sigma(J \rightarrow J + 10)$ = single-collision cross section for transfer from group J to group J + 10.

Set 2. Collision History Correlation Tables

At each abscissa, arbitrarily spaced, the following is required:

Card 1: Format (8E10.3)

1. XPL = abscissa, $\Sigma_t L$.
2. T_1 = first collision transmission probability (or R_1 for reflection).
3. $a(\Sigma_t L)$ = correlation decay constant (or $b(\Sigma_t L)$ for reflection).

Set 3. Case Data

Card 1: Format (I2, 8x, 11A6, A4)

1. NREG = number of regions ($\leq$ 11). If zero, job terminates.
2. ITITLE = alphanumeric title for the case, in columns 11-80.

For each region, the following is required:

Format (2I5, 7F10.5)

1. NNCODE = identification number of library cross section set.

2. INT = number of sub-regions in this region. $1 \leq$ INT. Purpose is to provide sub-slabs with optional thickness less than the maximum tabulated in Set 2, and to provide a reasonable thickness to linearly approximate the slowing-down source of thermal neutrons.
3. A = atomic weight, AMU.
4. RHO = density, gm/cm^3.
5. T = region thickness, cm. Sub-region thickness is T/INT.
6. Spare
7. Spare
8. Spare
9. ALP2= α^2 = lateral buckling, cm^{-2}. Taken to be $(2.405/R')^2$ for phantom having extrapolated radius R'.

Card NREG + 1: Format (7(A5, 5x), F7.3, I3)

1. ALPH(1) = abbbb
2. ALPH(2) = babbb
3. ALPH(3) = bbabb
4. ALPH(4) = bbbab
5. ALPH(5) = bbbba
6. ALPH(6) = cbbbb
7. ALPH(7) = bbbbb
8. ϵ = tolerance in calculation of transfer matrix, $\underline{T}$ (Section 2.1.4). Normally, set ϵ = 0.0001.
9. NCOLL = maximum number of collisions allowed to find $\underline{T}$ (Section 2.1.4). Normally, set NCOLL = 40.

Symbols a and c denote any desired alphanumeric characters; a is used to mark a data point, while c forms the grid marks on a computer plot of log(Ø(u)) vs u. A blank is denoted by b. Symbols a and c have usually been "+" and "·" respectively.

Card NREG + 2: Format (F3.0, 7E11.4)

1. p = 0, 1, or 2 to denote slab, cylindrical, or spherical geometry.
2. XO = axial location of front surface of first region, cm. In slab geometry, XO is arbitrary. In cylindrical and shperical geometry, XO must be the radius of the front surface of the first region.
3. AA(1)
4. AA(2)
5. AA(3)

   Thermal neutron flux boundary condition parameters at x = XO:

   $AA(1)D\frac{d\phi}{dx} + AA(2)\phi + AA(3) = 0$ at x = XO.

6. AA(4)
7. AA(5)
8. AA(6)

   $AA(4)D\frac{d\phi}{dx} + AA(5)\phi + AA(6) = 0$ at outer face of last region.

Card NREG + 3: Format (9F4.1, I4, 5F8.3)

1. DIG(1) = output control parameter. If > 0, get Σ_{tr} for each region and energy group.
2. DIG(2) = output control parameter. If > 0, output PHI1, the uncollided flux transmission probability for each energy group and region.
3. DIG(3) = spare
4. DIG(4) = output control parameter. If > 0, subroutine GRAPH is called to print out plot of

log(Ø(u)) versus u, for flux transmitted through each region.

5. DIG(5) = slowing-down source control parameter. If DIG(5) = 0, a flat slowing-down source distribution of thermal neutrons is assumed within a sub-region. If ≠ 0, then a linear approximation is used if the next sub-region is in the same region. If not, a flat approximation applies.
6. DIG(6) = sequence switch. If ≤ 0, subroutine DOSE is called to perform all dose rate calculations. Omit DOSE call if > 0.
7. DIG(7) = scatterer switch. If > 0, the second-last region is assumed to be a scatterer, and the last a phantom. If NREG = 1, then the only region in the problem is the scatterer. As currently coded, the treatment of a scatterer requires three successive cases:
   1. preceding shield - transmission tables;
   2. scatterer - reflection tables;
   3. phantom - transmission tables.

Cases 2. and 3. are one-region problems, with input of Sets 1 and 2 required to change to reflection tables and beck again. Section A.1.3 lists input for a problem of this type. The output of case 1 is the source used by 2, and similarly for case 3. If both reflection and transmission tables were loaded at the same time, DIG(7) could be used to handle a scatterer in one case. This modification would be fairly simple to incorporate into

MEDIPORT. As it is, the result is obtained using a few more input cards.

8. DIG(8) = output control parameter for intermediate values of x, dx, u, du/dx, v, dv/dx, ϕ, and $d\phi/dx$. Print if > 0.
9. DIG(9) = output control parameter. If > 0, print the transfer matrix TFN(J,K) for transfer from input group J to output group K (J is row number, K is column number). Below the diagonal appears the highest power of the F-matrix used to obtain TFN ($\underline{T}$, in Chapter II), in reverse order for both rows and columns.
10. ITHRM = sequence switch. If > 0, delete calculation of thermal neutron flux. This is useful for fast neutron dose transmission problems and for scatterer problems.
11. Spare
12. Spare
13. Spare
14. Spare
15. ATTEN1 = fraction of uncollided flux that is to be added to collided flux for scatterer region only. If a scatterer problem, i.e., DIG(7) > 0, ATTEN1 = 0 may be used as no uncollided flux is reflected from the scatterer. ATTEN1 is automatically set to unity regardless of its input value, if DIG(7) $\leq$ 0.

The following set is only required if the special SINT subroutine is used to read the multigroup neutron source from data cards.

Set 4. Multigroup Neutron Source

Card 1: Format (5E15.8)

1. S(1) = forward-directed neutron source strength in group 1, n/cm^2-sec
2. S(2)
3. S(3)
4. S(4)
5. S(5)

Cards 2, 3,...: As Card 1, with enough cards to contain NENG source strengths. Set S(NENG) = 0.

The following sets are required only if DIG(6) $\leq$ 0.

Case 5: Case Data for DOSE

Card 1: Format (I1)

1. IGAM $\leq$ 0, omit all dose input, but perform dosimetry calculations. $>$ 0, read all DOSE input and perform dosimetry calculations. After the first case, succeeding cases using the same DOSE data need not re-read it.

Card 2: Format (4I5)

1. II = number of neutron capture gamma-emitting nuclides. II $\leq$ 5.
2. MX = number of points down cylindrical axis, MX $\leq$ 24.

3. MR = number of points across radius of cylinder. MR ≤ 10.

4. JJ = number of neutron capture heavy particle emitting nuclides. JJ ≤ 5.

Card 3: Format (10A5)

J. ISO(J) E alphanumeric label for J-th neutron capture gamma-emitting nuclide. 1 ≤ J ≤ II.

J+5. ISO(J+5) = alphanumeric label for J-th heavy particle emitting nuclide. 1 ≤ J ≤ JJ.

Set 6. Gamma source data. Format (5F16.8). Five cards, each containing II words.

Card 1:

J. σ_{aJ} = (n,γ) cross section of J-th γ-emitter, barns.

Card 2:

J. P_J = weight fraction of element J in cylinder.

Card 3:

J. A_J = atomic weight of J-th γ-emitter, MeV.

Card 4:

J. E_J = characteristic γ-ray energy of γ-emitter J, MeV.

Card 5:

J. n_J = number of γ-rays emitted by J per neutron capture.

Set 7 Heavy particle (H.P.) source data. Format (5F16.8). Four cards, each containing JJ words. By H.P. is meant p, D, T, He, Li, etc.

Card 1:

J. $\sigma_a(J+5)$ = (n, H.P.) cross section of J-th H.P. emitter, barns.

Card 2:

J. P(J+5) = weight fraction of J-th H.P. emitter.

Card 3:

J. A(J+5) = atomic weight of J-th H.P. emitter.

Card 4:

J. E(J+5) = characteristic energy release (Q value in physics per (n, H.P.) reaction, for J-th H.P. emitter.

Set 8 Gamma-ray attenuation tables. Five tables, Format (8F10.5), each preceded by a marker card in the following sequence.

1. AA(I) = build-up factor in attenuation kernel $K(\vec{r},\vec{r}_o)$.
2. ALF1(I) = build-up factor in attenuation kernel $K(\vec{r},\vec{r}_o)$.
3. ALF2(I) = build-up factor in attenuation kernel $K(\vec{r},\vec{r}_o)$.
4. GMU(I) = total γ-attenuation coefficient.
5. GMUA(I) = γ-ray energy absorption coefficient.

These tables are functions of γ-ray energy; entries must be uniformly spaced in energy. The maximum number of entries per table is 25. Each table is preceded by a marker card, containing in Format (2F10.5, I5) the following:

1. Energy of first tabular entry, MeV (XOA, XOALFI, XOALF2, XOGMU, or XOGMUA).
2. Energy interval between all entries, MeV, (HA, HALFI, HALF2, HGMU, or HGMUA).
3. Number of tabular entries (≤25), (NA, NALFI, NALF2, NGMU, or NGMUA).

Set 9

Card 1:

1. NI = order of Gaussian quadrature numerical integration for radial co-ordinate. NI = 4, 6, or 8.
2. NO = order of Gaussian quadrature numerical integration for axial co-ordinate. NO = 4,6, or 8.
3. NX = unused parameter.
4. RZERO = radius of cylinder, cm.
5. R' = extrapolated radius of cylinder, cm (for thermal neutron flux distribution of Form ϕ = $\phi\ (x)\left[\cos\left(\frac{\pi r}{2RPRIM}\right)\right]^{1/4}$.
6. RHO = density of material composing cylinder, gm/cm^3.
7. HH = axial length of cylinder, cm.
8. GC = conversion factor to give dose in desired units. If GC = 9.613×10^{-7}, get dose in rad/min.

Card 2

1. DX = axial dose mesh spacing, cm.
2. DY = radial dose mesh spacing, cm.

Set 10 First collision dose table, containing (NENG-1) group-averaged values of 10^{10} x dose (rad)/neutron, in Format (8F10.5).

A.1.2 LISTING OF MEDIPORT

```
C        MEDIPORT JULY 1967 MIT VERSION        A P OLSON
       DIMENSION AMAT(11),A(11),RHO(11),T(11),E(26),EN(11),ETA(11),BSIGA(
      111,26),ESIGA(11,26),BSIGS(11,26),ESIGS(11,26),TEMPA(11,26),TEMPS(1
      21,26),THETA(11,26),PHI1(11,26),PHI2(11,26),
      3PHI(80),      F(27,26),    THETAN(11),TEMP(26),S(26),FISS(26),
      4FLUX(11,26),XI(11),DU(26), PLOT( 51,21), ALPH(7),U(26),GEOM(11),
      5DIG(9),ITYPE(12),NCODE(11),ITITLE(12),NNCODE(11),INT(11),NVECT(11)
      6,Q(100),QQ(100),QQQ(100),PSI(100),FLUXU(11,26),AREG(11),Y(3),DY(3)
      7,DD(100),ALP1(11),ALP2(11),AA(6),ATABL(3),RTABL(3),WORK(33),DDD(10
      8),BARMU(11),W(1500),SNN(12,25,11)
       DIMENSION NDS(11),XPL(25),TTAB(25),ATAB(25),RTINF(25),CAPA(25),
      1TFN(27,26),SAT(11),SST(11),FF(11,26),SAVE(26)
       COMMON AMAT,A,RHO,T,E,EN,ETA,BSIGA,ESIGA,BSIGS,ESIGS,TEMPA,TEMPS,
      1THETA,PHI1,PHI2,PHI,F,THETAN,TEMP,S,FISS,FLUX,XI,DU, PLOT, ALPH,
      2U,GEOM,DIG,ITYPE,NCODE,ITITLE,NNCODE,INT,NVECT,Q,QQ,QQQ,PSI,FLUXU,
      3AREG,Y,DY,DD,ALP1,ALP2,AA,ATABLE,RTABL,WORK,DDD,BARMU,D,P,SIGMA,
      4S1,X,XX,SLOPE,XMAX,NTRY,M,IFVD,IBKP,IERR,DX,DDX,W,L,IQ,NTH,XS,DXS,
      5NDS,XPL,TTAB,ATAB,RTINF,CAPA,TFN,SAT,SST,NG,SNN
F      TAINT
C  AMAT=MATERIAL IDENTIFICATION
C  A=ATOMIC WEIGHT,RHO=DENSITY IN GM/CM3,NREG=NO. OF REGIONS
C  NENG=NO.OF ENERGIES,T=THICKNESS OF MATERIALS IN CM,E=ENERGY
 1000 READ INPUT TAPE 4,400,NNEW,  IQ,(ITYPE(I),I=1,12)
  400 FORMAT(    2I2,6X,11A6,A4)
  499 FORMAT(1HO,2I2,6X,11A6,A4)
      WRITE OUTPUT TAPE 2,9991
      WRITE OUTPUT TAPE 2,499,NNEW,  IQ,(ITYPE(I),I=1,12)
      IF( NNEW)401,401,402
  402 READ INPUT TAPE 4,450,          NENG,PO,P1,CN,ZTAC,NVAL
      WRITE OUTPUT TAPE 2,9994
      READ INPUT TAPE 4,403,(E(J),J=1,NENG)
      WRITE OUTPUT TAPE 2,9995
      NONEW=NNEW
      NTAB=IQ
 9995 FORMAT(51H NENG     PO          P1          CN          ZTAC NVAL)
  403 FORMAT(8E10.3)
 9991 FORMAT(1H1)
 9994 FORMAT(1H4)
      WRITE OUTPUT TAPE 2,450,          NENG,PO,P1,CN,ZTAC,NVAL
  450 FORMAT(I5,4E10.3,I2)
      NG=NENG-1
      DO 404 J=1,NG
      U(J)=LOGF(10./E(J))
  404 DU(J)=LOGF(E(J)/E(J+1))
      DO 405 N=1,NONEW
      READ INPUT TAPE 4,406,NCODE(N),AMAT(N),BARMU(N),NDS(N),SAT(N),SST(
     1N)
  406 FORMAT(I5,5X,A5,F10.5,I5,2F10.5)
      WRITE OUTPUT TAPE 2,406,NCODE(N),AMAT(N),BARMU(N),NDS(N),SAT(N),
     1SST(N)
      READ INPUT TAPE 4,498,((SNN(M,K,N),M=1,12),K=1,NG)
  498 FORMAT(6F10.5)
  405 CONTINUE
      DO 250 N=1,NONEW
      WRITE OUTPUT TAPE 2,251,AMAT(N),((SNN(M,K,N),M=1,12),K=1,NG)
  250 CONTINUE
  251 FORMAT(1HO,A5,/,(1H ,12F10.5))
      DO 240 K=1,NTAB
      READ INPUT TAPE 4,403, XPL(K),TTAB(K),ATAB(K),RTINF(K),CAPA(K)
```

```
      WRITE OUTPUT TAPE 2,403, XPL(K),TTAB(K),ATAB(K),RTINF(K),CAPA(K)
  240 CONTINUE
  401 READ INPUT TAPE 4,400,NREG,IQ,(ITITLE(I),I=1,12)
C     IQ IS AN UNUSED DUMMY
      IF( NREG)1001,1001,1002
 1001 CALL EXIT
 1002 WRITE OUTPUT TAPE 2,9991
      WRITE OUTPUT TAPE 2,499,NREG,IQ,(ITITLE(I),I=1,12)
      DO 407 I=1,NREG
  407 READ INPUT TAPE 4,408,NNCODE(I),INT(I),A(I),RHO(I),T(I),ETA(I),
     1THETAN(I),GEOM(I),ALP2(I)
  488 FORMAT(1H0,2I5,7F10.5)
  408 FORMAT(2I5,7F10.5)
      WRITE OUTPUT TAPE 2,417
  417 FORMAT(80H NNCODE INT  A(I)      RHO(I)      T(I)      ETA(I)   THETA
     1N(I)  GEOM(I)    ALP2(I))
      DO 416 I=1,NREG
  416 WRITE OUTPUT TAPE 2,488,NNCODE(I),INT(I),A(I),RHO(I),T(I),ETA(I),
     1THETAN(I),GEOM(I),ALP2(I)
      DO 470 I=1,NREG
      DO 410 N=1,NONEW
      IF(NCODE(N)-NNCODE(I))410,409,410
  410 CONTINUE
  409 NVECT(I)=N
  470 AREG(I)=AMAT(N)
      READ INPUT TAPE 4,204,( ALPH(I),I=1,7),CRIT,NCOLL
  204 FORMAT(7(A5,5X),F7.3,I3)
      READ INPUT TAPE 4,290,P,X0,(AA(I),I=1,6)
  290 FORMAT(F3.0,7E11.4)
      READ INPUT TAPE 4,2002,(DIG(I),I=1,9),ITHRM,CAPR,CAPD,CAPL,CAPTH,
     1  ATTEN1
 2002 FORMAT(9F4.1,I4,5F8.3)
      WRITE OUTPUT TAPE 2,2040,( ALPH(I),I=1,7),CRIT,NCOLL
 2040 FORMAT(1H0,8H ALPH(I),/,7(A5,5X),F7.3,I3)
      WRITE OUTPUT TAPE 2,291,P,X0,(AA(I),I=1,6)
  291 FORMAT(1H0,8H P    X0,25X,5HAA(I),/,F3.0, 7E11.4)
      WRITE OUTPUT TAPE 2,2003
 2003 FORMAT(1H0,13H CONTROL CARD)
      WRITE OUTPUT TAPE 2,2002,(DIG(I),I=1,9),ITHRM,CAPR,CAPD,CAPL,
     1  CAPTH,ATTEN1
C
C     ITHRM GREATER THAN ZERO DELETES THERMAL FLUX CALCULATION
C  CALCULATE N AND XI FOR EACH MATERIAL
      WRITE OUTPUT TAPE 2,33
   33 FORMAT(1H0,54H  MATERIAL        N           XI          1/L**2
     1 D)
      IF(DIG(7))1555,1555,1557
 1555 ATTEN1=1.
 1557 DO 1 I=1,NREG
      XI(I)=ETA(I)
      EN(I)=0.6025*RHO(I)/A(I)
      IF(XI(I))1,777,1
  777 XI(I)=1.-((((A(I)-1.)**2.)/(2.*A(I)))*LOGF((A(I)+1.)/(A(I)-1.)))
    1 CONTINUE
      X=0.
      Z=EXN(NVAL,X)
C       TEMPS CONTAINS OPTICAL PATH FOR GROUP J PRECEDING REGION I
      DO 2 J=1,NG
      TEMPS(1,J)=0.
      S(J)=Z
    2 CONTINUE
```

```
C
      DO 351 I=1,NREG
      N=NVECT(I)
      C=INT(I)
      X=T(I)/C
      DO 35 J=1,NG
      BSIGA(I,J)=EN(I)*SNN(1,J,N)
C         BSIGA IS TOTAL MACRO X-SECTION
      FLUXU(I,J)=0.
      XX=BSIGA(I,J)*X
      Z=XX+TEMPS(I,J)
      EX2=EXN(NVAL,Z)
      FLUX(I,J)=EX2/S(J)
      FLUXU(I,J)=XX
      IF(I-NREG)3,4,4
    3 Z=TEMPS(I,J)+C*XX
      TEMPS(I+1,J)=Z
      S(J)=EXN(NVAL,Z)
    4 PHI1(I,J)=1.-FLUX(I,J)
      PLOT(J,I)=EX2
      IF(THETAN(I))363,336,363
  363 THETA(I,J)=THETAN(I)/(E(J)**(0.5))
      GO TO 35
  336 THETA(I,J)=200./((A(I)**(1./3.))*(E(J)**(0.5)))
   35 CONTINUE
      J=NENG
      BSIGA(I,J)=EN(I)*SAT(N)
      Z=EN(I)*(SAT(N)+SST(N))
      XX=BARMU(N)
      ALP1(I)=3.*Z*BSIGA(I,J)*(1.-XX)*(1.-BSIGA(I,J)*(0.8-XX/(1.-XX))/Z)
      DDD(I)=BSIGA(I,J)/ALP1(I)
      WRITE OUTPUT TAPE 2,31,AREG(I),EN(I),XI(I),ALP1(I),DDD(I)
   31 FORMAT(1HO,3X,A5,4X,4E12.5)
  351 CONTINUE
      IF(DIG(1))3001,3001,3000
 3000 WRITE OUTPUT TAPE 2,36,(AREG(I),I=1,NREG)
   36 FORMAT(1H1,21HCAPITAL SIGMA (TOTAL),     //,9H MATERIAL,11(6XA5))
      WRITE OUTPUT TAPE 2,360
      DO 38 J=1,NENG
      WRITE OUTPUT TAPE 2,41,E(J),(BSIGA(I,J),I=1,NREG)
   38 CONTINUE
  360 FORMAT(1H ,6HENERGY)
 3001 X=1.
      WRITE OUTPUT TAPE 2,1103
 1103 FORMAT(1H4,55H     E(J)          U(J)       DU(J)          S(J)    LAM
     1BDA)
      IF(ZTAC)1150,790,790
  790 CALL SINT(NENG,E,   S,X)
C       ZTAC LESS 0 ALLOWS USING LAST FLUX OF A PREVIOUS CASE AS SOURCE
      IF(ZTAC)1150,1120,1121
 1150 DO 1151 J=1,NG
      S(J)=SAVE(J)
 1151 CONTINUE
      S(NENG)=0.
      GO TO 1121
 1120 X=0.
      DO 1100 J=1,NG
      S(J)=X+S(J)
 1100 X=S(J)
 1121 DO 1102 J=1,NG
      IF(ZTAC)1102,1122,1102
```

```
C       XX=CORE MEAN FREE PATH (CM)
 1122 XX=1./(SNN(1,J,1)*CN)
      S(J)=S(J)*P0*XX*(1.+P1*XX/P0)
 1102 WRITE OUTPUT TAPE 2,1104,E(J), U(J),DU(J),S(J),XX
 1104 FORMAT(5E12.4)
      S(NENG)=0.
C
C  CALCULATE FRACTION REMAINING AFTER ABS. AND SCATT.
      DO 47 J=1,NG
      DO 49 I=1,NREG
      N=NVECT(I)
      IF(THETA(I,J)-90.)51,53,53
   51 C=90./THETA(I,J)
      GO TO 55
   53 C=1.
C  C=NO. OF COLLISIONS REQUIRED TO LOSE A NEUTRON BY SCATTER
C  PL=PROBABILITY OF LOSING A NEUTRON BY SCATTER
   55 PL=PLCALC(I,J,N,GEOM,SNN)
      PHI2(I,J)=PHI1(I,J)*PL
      FLUX(I,J)=FLUX(I,J)*PL
      TEMPA(I,J)=PL
   49 CONTINUE
   47 CONTINUE
      IF(DIG(2))3003,3003,3002
 3002 WRITE OUTPUT TAPE 2,39,(AREG(I),I=1,NREG)
   39 FORMAT(1H1,10H PHI1(I,J),//9H MATERIAL,
     1/,7H ENERGY,11(6XA5))
      DO 37 J=1,NG
   37 WRITE OUTPUT TAPE 2,41,E(J),(PHI1(I,J),I=1,NREG)
   41 FORMAT(1H ,E10.3,11E11.3)
      WRITE OUTPUT TAPE 2,45,(AREG(I),I=1,NREG)
   45 FORMAT(1HO,10H PHI2(I,J),//,9H MATERIAL,
     1/,7H ENERGY,11(6XA5))
      DO 58 J=1,NG
      WRITE OUTPUT TAPE 2,41,E(J),(PHI2(I,J),I=1,NREG)
   58 CONTINUE
      WRITE OUTPUT TAPE 2,272,(AREG(I),I=1,NREG)
  272 FORMAT(1H1,25H NON-INTERACTING FRACTION,//,9H MATERIAL,/,7H ENERGY
     1,11(6XA5))
      DO 271 J=1,NG
      PHI1(1,J)=S(J)
      WRITE OUTPUT TAPE 2,41,E(J),(FLUX(I,J),I=1,NREG)
  271 CONTINUE
      WRITE OUTPUT TAPE 2,9994
      DO 7 J=1,NG
      WRITE OUTPUT TAPE 2,41,E(J),(TEMPS(I,J),I=1,NREG)
      WRITE OUTPUT TAPE 2,41,U(J),(PLOT(J   ,I),I=1,NREG)
    7 CONTINUE
C
 3003 Z=X0
      NN=0
      NMAX=0
      DO 430 I=1,NREG
      ATTEN2=1.
      IN=NVECT(I)
      CALL FCALC(SNN,NENG,IN,F,NDS)
      CALL SCALC(NENG,CRIT,I,TAINT,NCOLL)
      TI=INT(I)
      TI=T(I)/TI
      II=INT(I)
      IF(DIG(6))1523,1523,1520
```

```
C      OMIT IF NO PHANTOM IE DIG(6) GRTR 0.
 1523 IF(I-NREG)1520,1521,1521
 1521 IF(NMAX)1522,1522,1520
 1522 NMAX=NN
      PPRIM=P
C      NMAX IS VALUE OF NN FOR LAST REGION BEFORE PHANTOM
C      WE WANT P=0. FOR PHANTOM REGARDLESS
 1520 IF(DIG(7))1550,1550,1551
 1551 IF(NREG-I-1)1552,1552,1550
 1552 ATTEN2=ATTEN1
 1550 DO 431 N=1,II
      PPP=1.
      PP=1.
      IF(P-1.)1514,1513,1512
 1512 PP=PP*Z/(Z+TI)
      PPP=PPP*(Z+TI)/(Z+0.5*TI)
 1513 PP=PP*Z/(Z+TI)
      PPP=PPP*(Z+TI)/(Z+0.5*TI)
 1514 DO 432 J=1,NENG
      ATTEN=1.
      IF(DIG(7))1566,1566,1565
 1565 IF(NREG-I-1)1566,1567,1566
 1567 ATTEN=1.+(CAPR/CAPD)**2.
      ATTEN=LOGF(ATTEN)*0.5
 1566 ATTEN=ATTEN*PP
      ATTEN2=ATTEN2*PP
      PHIO=PHI2(I,J)*S(J)*ATTEN
      DO 432 K=J,NENG
      F(J,K)=TFN(J,K)*PHIO
  432 CONTINUE
      DO 14 K=1,NENG
C         THIS FLUX UNDERGOES NO INTERACTIONS TRAVERSING  THE REGION
      X=0.
      DO 15 J=1,K
   15 X=X+F(J,K)
      S(K)=FLUX(I,K)*S(K)*ATTEN2 + X
      PHI1(N+1,K)=S(K)
      SAVE(K)=S(K)
C       PHI1 STORES SPECTRUM FOR FAST NEUTRON DOSE CALCULATION
      TEMP(K)    =S(K)/DU(K)
      FF(I,K)=TEMP(K)
   14 CONTINUE
C  NOW FOR SOME FLUX OUTPUTS
      WRITE OUTPUT TAPE 2,104,I,( S(J)      ,J=1,NG)
      WRITE OUTPUT TAPE 2,104,I,(TEMP(J)    ,J=1,NG)
  104 FORMAT(1HO,I2,2X,(12E10.3))
      NN=NN+1
      Q(NN)=S(NENG)*PPP/TI
      QQQ(NN)=DDD(I)*(ALP1(I)+ALP2(I))
      DD(NN)=DDD(I)
      Z=Z+TI
      QQ(NN)=Z
C      UPDATE VALUES IF INT(I) GRTR 1
      IF(II-1)431,431,5
    5 DO 6 J=1,NG
      TEMPS(I,J)=TEMPS(I,J)+FLUXU(I,J)
      XX=TEMPS(I,J)+FLUXU(I,J)
      X=EXN(NVAL,XX)
      C=X/PLOT(J,I)
      FLUX(I,J)=TEMPA(I,J)*C
      PHI2(I,J)=TEMPA(I,J)*(1.-C)
```

```
      PLOT(J,I)=X
    6 CONTINUE
      ATTEN2=1.
      IF(DIG(7))431,431,1651
 1651 IF(NREG-I-1)1652,1652,431
 1652 ATTEN2=ATTEN1
  431 CONTINUE
  430 CONTINUE
C     NOW DO WE WANT TO CALC. THERMAL FLUX
      IF(ITHRM)700,700,701
  700 WRITE OUTPUT TAPE 2,433,(QQ(N),Q(N),N=1,NN)
  433 FORMAT(1H1,40H AXIAL POSITION   THERMAL SOURCE DENSITY,/,
     1(F12.3,10X,E11.4))
      XS=XO
      DO 850 I=1,NREG
  850 XS=XS+T(I)
      GSO=XS-T(NREG)
      NGS=79
      HGS=T(NREG)/79.
      NTH=80
      DXS=T(NREG)/79.
      CALL THERM(XO,NREG,NMAX,NN,PPRIM)
      WRITE OUTPUT TAPE 2,699,(QQ(N),PSI(N),N=1,NN)
  699 FORMAT(1H4,26H  DISTANCE    THERMAL FLUX,/,(2E12.4))
  701 DO 860 I=1,NREG
      DO 861 J=1,NG
      FLUXU(I,J)=FF(I,J)
  861 CONTINUE
  860 CONTINUE
      IF(DIG(4))3010,3010,3006
C  BEGIN PLOT OF SPECTRUM
 3006 CALL GRAPH(NREG,NG)
 3010 I=NREG
      NNREG=INT(NREG)+1
      XXI=XI(NREG)
      II=INT(NREG)+1
      DO 870 I=1, II
      WRITE OUTPUT TAPE 2,104,I,(PHI1(I,J),J=1,NG)
  870 CONTINUE
      IF(DIG(6))3600,3600,1000
C       OMIT DOSE CALL IF DIG(6) GRTR THAN 0.
 3600 CALL DOSE(PHI,NGS,HGS,GSO,PHI1,NNREG,XXI,S,DU,NG,PHI2,TEMPA,TEMPS,
     1FLUX,F,TFN)
C     NGS=NO. INTERVALS, GSO=STARTING VALUE OF X, HGS=INTERVAL
C     PHI CONTAINS TABLE OF THERMAL FLUXES AT EQUAL INTERVALS IN X,
C     FOR LAST REGION
      GO TO 1000
      END
*     LABEL
*     SUBROUTINE DOSE      A P OLSON
      SUBROUTINE DOSE(GSX,NGS,HGS,GSO,PHI1,NNREG,XI,S,DU,NG,SP1,SP2,SP3,
     1SP4,R,RR)
      DIMENSION GSX(80),PHI1(11,26),GG(10,5),AA(25),ALF1(25),ALF2(25),
     1  R(27,26),AH(18),GMU(25),GMUA(25),S(26),DU(26),RR(27,26),
     2GH(5,5),TF(25,10),SP1(11,26),SP2(11,26),SP3(11,26),SP4(11,26),ISO(
     310),MASK(60),PSI(20),FAST(20),W(26)
C       CALCULATION OF GAMMA RADIATION DOSE INSIDE A CYLINDER SUBJECT TO
C     A SPACE-DEPENDENT VOLUME-DISTRIBUTED SOURCE OF GAMMA RAYS, FOR
C     AS MANY AS 5 DISCRETE RADIOISOTOPES.  ALSO CALCULATION OF FAST
C     NEUTRON DOSE DOWN AXIS OF CYLINDER(X AXIS).
C     GSX CONTAINS THERMAL FLUX TABLE, FOR NGS INTERVALS OF WIDTH HGS
```

```
C      AND STARTING VALUE GSO.  PHI1 CONTAINS FAST FLUX WITHIN LAST REGION.
F      F,G,ANGLE
       READ INPUT TAPE 4,142,IGAM
           WRITE OUTPUT TAPE 2,108,IGAM
  142 FORMAT(I1)
  108 FORMAT(1H1,6H IGAM=,I1)
       IF(IGAM)141,141,140
  140 READ INPUT TAPE 4,119,II,MX,MR,JJ
       READ INPUT TAPE 4,129,ISO
  129 FORMAT(10A5)
       DO 1 J=1,5
    1 READ INPUT TAPE 4,137,(GG(J,I),I=1,II)
       DO 19 J=1,4
   19 READ INPUT TAPE 4,137,(GH(J,I),I=1,JJ)
  137 FORMAT(5F16.8)
  100 FORMAT(8F10.5)
  119 FORMAT(4I5)
       CALL DATA(   XOA,    HA,    NA,    AA)
       CALL DATA(XCALF1, HALF1, NALF1,  ALF1)
       CALL DATA(XCALF2, HALF2, NALF2,  ALF2)
       CALL DATA(XCGMU , HGMU , NGMU ,  GMU )
       CALL DATA(XCGMUA, HGMUA, NGMUA,  GMUA)
       READ INPUT TAPE 4,102,NI,NO,NX,RZERO,RPRIM,  RHO,HH,GC
       READ INPUT TAPE 4,100,DX,DY
       READ INPUT TAPE 4,100,(W(J),J=1,NG)
  102 FORMAT(3I5,5X,4F10.5,E12.4)
       AH( 1)=.86113631
       AH( 2)=.33998104
       AH( 3)=.34785485
       AH( 4)=.65214515
       AH( 5)=.93246951
       AH( 6)=.66120939
       AH( 7)=.23861919
       AH( 8)=.17132449
       AH( 9)=.36076157
       AH(10)=.46791393
       AH(11)=.96028986
       AH(12)=.79666648
       AH(13)=.52553241
       AH(14)=.18343464
       AH(15)=.10122854
       AH(16)=.22238103
       AH(17)=.31370665
       AH(18)=.36268378
       WRITE OUTPUT TAPE 2,110,II,MX,MR,JJ
       WRITE OUTPUT TAPE 2,130,ISO
  130 FORMAT(1HO,10A5)
  109 FORMAT(1HO,5F16.8)
  110 FORMAT(24H NO. GAMMA PRODUCERS=II=,I2,4H MX=,I2,4H MR=,I2,4H JJ=,I
      12)
       WRITE OUTPUT TAPE 2,107,NI,NO,NX,RZERO,RPRIM,RHO  ,HH,GC
  107 FORMAT(66H   NI   NO   NX       RZERO     RPRIM       RHO       HH
      1        GC,/,3I5,5X,4F10.5,E12.4)
       WRITE OUTPUT TAPE 2,133,DX,DY
  133 FORMAT(4H DX=,F10.5,4H DY=,F10.5)
       WRITE OUTPUT TAPE 2,160,(W(J),J=1,NG)
  160 FORMAT(1HO,5H W(J),/,(10F10.5))
  141 XX=GSO-DX
       DO 12 J=1,MX
       XX=XX+DX
       YY=-DY
```

```
      DO 13 K=1,MR
      YY=YY+DY
C     STORE THERMAL FLUX IN TF(J,K), FOR OBSERVATION POINT (XX,YY)
      TF(J,K)=SPINT(XX,GSX,NGS,GSO,HGS)*(COSF(1.570796*YY/RPRIM)**0.25)
C     NOTE REVERSED INDICES IN SP ARRAYS
   13 CONTINUE
   12 CONTINUE
C     CALC. OF FAST NEUTRON DOSE DOWN BEAM AXIS
      A=60.E-10
      WRITE OUTPUT TAPE 2,117
  117 FORMAT(1H4,33H FAST NEUTRON DOSE DOWN BEAM AXIS,/,20H     X
     1RAD/MIN,8X,9HFAST FLUX)
      X=GSO
      XX=NGS
      YY=NNREG-1
C      AS NNREG=INT(NREG)+1
      H=XX*HGS/YY
      DO 9 I=1,NNREG
      FUDGE=0.
      XX=0.
      SUM=0.
      SUMU=0.
      DO 10 J=1,NG
      YY=1.006E-4*(EXPF(0.5*DU(J)) -1.)/DU(J)
      PSI1=SQRTF(10.)*EXPF(-SUMU/2.)
      FUDGE=FUDGE+PHI1(I,J)*YY/PSI1
      XX=XX+PHI1(I,J)
      SUMU=SUMU+DU(J)
   10 SUM=SUM+PHI1(I,J)*W(J)
      SUM=SUM*A
      FAST(I)=LOGF(SUM)
      PSI(I)=LOGF(YY*FUDGE)
      WRITE OUTPUT TAPE 2,116,X,SUM,XX
      X=X+H
    9 CONTINUE
      WRITE OUTPUT TAPE 2,149,(PSI(I),I=1,NNREG)
  149 FORMAT(1H4,7H PSI(I),(10E12.4))
      IF(NNREG-1)21,21,22
   21 H=H/2.
      NNREG=3
      FAST(3)=FAST(2)
      FAST(2)=0.5*(FAST(1)+FAST(2))
      PSI(3)=PSI(2)
      PSI(2)=0.5*(PSI(1)+PSI(2))
   22 L=NNREG-1
C       L=NO. OF INTERVALS IN LAST SLAB, INT(NREG), FUDGED TO 2 OR MORE
      XX=GSO-DX
C      FAST FLUX FALLS OFF EXPONENTIALLY   TAKING LOGS GIVES BETTER
C         INTERPOLATION
      DO 23 J=1,MX
      XX=XX+DX
      YY=EXPF(SPINT(XX,FAST,  L,GSO,H))
      DO 24 K=1,MR
      RR(J,K)=YY
   24 SP3(K,J)=YY
      WRITE OUTPUT TAPE 2,200,(SP3(K,J),K=1,MR)
   23 CONTINUE
      XX=GSO-HGS
      L=NGS+1
      M=NNREG-1
      DO 42 K=1,L
```

```
      XX=XX+HGS
      YY=EXPF(SPINT(XX,PSI,  M,GSO,H))
      GSX(K)=GSX(K) + YY
   42 CONTINUE
      WRITE OUTPUT TAPE 2,200,(GSX(K),K=1,L)
  200 FORMAT(1H4,(    10E12.4))
      N1=NALF1-1
      N2=NALF2-1
      N3=NA-1
      N4=NGMU-1
      N5=NGMUA-1
      A=0.
      B=RZERO/RPRIM
      P=0.
      Q=3.1415927
      C=NGS
      D=C*HGS+GSO
      C=GSO
      DO 3 J=1,MX
      DO 3 K=1,MR
      SP2(K,J)=0.
    3 SP1(K,J)=0.
C     SP1 CONTAINS TOTAL GAMMA DOSE RATE
      DO 4 I=1,II
      XX=GSO-DX
      E=GG(4,I)
      GG(6,I)=SPINT(E, GMU,N4, XOGMU, HGMU)
      GG(7,I)=SPINT(E,GMUA,N5,XOGMUA,HGMUA)
      GG(8,I)=SPINT(E,ALF1,N1,XOALF1,HALF1)
      GG(9,I)=SPINT(E,ALF2,N2,XOALF2,HALF2)
      GG(10,I)=SPINT(E,AA,N3,XOA,HA)
      WRITE OUTPUT TAPE 2,109,(GG(J,I),J=6,10)
      V6=GG(6,I)
      V7=GG(7,I)
      V8=GG(8,I)
      V9=GG(9,I)
      V10=GG(10,I)
      GGC=GC*V7*E/RHO
      CK=0.6024*GG(1,I)*GG(2,I)*GG(5,I)/GG(3,I)
      GK=GGC*CK
      DO 5 J=1,MX
      XX=XX+DX
      IF(XX-D)35,36,36
   36 Z=0.75*(D-C) + C
      GO TO 37
   35 Z=XX
      IF(XX-C)38,38,37
   38 Z=0.25*(D-C) + C
   37 YY=-DY
      DO 6 K=1,MR
      YY=YY+DY
      IF(YY-RZERO)33,34,34
   34 T=0.75*B
      GO TO 32
   33 T=YY/RPRIM
      IF(T)31,31,32
   31 T=0.25*B
   32      R1=GK*G3(A,T,C,Z,F,G,NI,NO,AH,V6,V7,V8,V9,V10,GSX,NGS,HGS,GSO,
     1XX,YY,ANGLE,P,Q,RPRIM)
           R2=GK*G3(T,B,C,Z,F,G,NI,NO,AH,V6,V7,V8,V9,V10,GSX,NGS,HGS,GSO,
     1XX,YY,ANGLE,P,Q,RPRIM)
```

```
      R3=GK*G3(A,T,Z,D,F,G,NI,NO,AH,V6,V7,V8,V9,V10,GSX,NGS,HGS,GSO,
     1XX,YY,ANGLE,P,Q,RPRIM)
      R4=GK*G3(T,B,Z,D,F,G,NI,NO,AH,V6,V7,V8,V9,V10,GSX,NGS,HGS,GSO,
     1XX,YY,ANGLE,P,Q,RPRIM)
      R(J,K)=R1+R2+R3+R4
      RR(J,K)=RR(J,K)+R(J,K)
      SP1(K,J)=SP1(K,J)+R(J,K)
      WRITE OUTPUT TAPE 2,134,XX,YY,R1,R2,R3,R4
  134 FORMAT(1H ,2F10.5,4E12.3)
    6 CONTINUE
    5 CONTINUE
      WRITE OUTPUT TAPE 2,131,ISO(I)
  131 FORMAT(1H1,16H GAMMA DOSE FOR ,A5)
      DO 7 J=1,MX
    7 WRITE OUTPUT TAPE 2,114,(R(J,K),K=1,MR)
  114 FORMAT(1H0,10E12.4)
    4 CONTINUE
      WRITE OUTPUT TAPE 2,132
      DO 2 J=1,10
    2 WRITE OUTPUT TAPE 2,109,(GG(J,I),I=1,II)
C     CALCULATION OF HEAVY PARTICLE DOSE
      DO 11 J=1,JJ
      GH(5,J)=       (GH(1,J)*GH(2,J)*GH(4,J)/GH(3,J))*5.79E-7
   11 CONTINUE
      WRITE OUTPUT TAPE 2,132
  132 FORMAT(1H4)
      DO 20 J=1,4
   20 WRITE OUTPUT TAPE 2,109,(GH(J,I),I=1,JJ)
      DO 14 L=1,JJ
      WRITE OUTPUT TAPE 2,120,ISO(L+5)
  120 FORMAT(1H1,25H HEAVY PARTICLE DOSE FOR ,A5)
      XX=-DX+GSO
      DO 15 J=1,MX
      XX=XX+DX
      FUDGE=SPINT(XX,GSX,NGS,GSO,HGS)
      YY=-DY
      DO 16 K=1,MR
      YY=YY+DY
      R(J,K)=GH(5,L)*FUDGE*(COSF(1.570796*YY/RPRIM)**0.25)
      IF(L-1)41,41,40
   41 SP4(K,J)=R(J,K)
      GO TO 16
C        SAVE DOSE FROM FIRST HEAVY PARTICLE EMITTER  EG B-10
C          AND LEAVE IT OUT OF THE TOTAL FOR BACKGROUND DOSE
   40 SP2(K,J)=SP2(K,J)+R(J,K)
      RR(J,K)=RR(J,K)+R(J,K)
   16 CONTINUE
      WRITE OUTPUT TAPE 2,114,(R(J,K),K=1,MR)
   15 CONTINUE
   14 CONTINUE
C     MAKE R-VALUE TABLE FOR OUTPUT TABLE
      YY=-DY
      DO 25 K=1,MR
      YY=YY+DY
      GSX(K)=YY
   25 CONTINUE
      FUDGE=0.
      DO 26 J=1,MX
      DO 26 K=1,MR
      IF(RR(J,K)-FUDGE)26,26,27
   27 FUDGE=RR(J,K)
```

```
   26 CONTINUE
      FUDGE=LOGF(FUDGE)/LOGF(10.)
      I=FUDGE-4.
      FUDGE=I
      FUDGE=10.**FUDGE
      DO 28 J=1,MX
      DO 28 K=1,MR
      I=RR(J,K)/FUDGE+0.5
      RR(J,K)=I
      I=SP1(K,J)/FUDGE+0.5
      SP1(K,J)=I
      I=SP2(K,J)/FUDGE+0.5
      SP2(K,J)=I
      I=SP3(K,J)/FUDGE+0.5
      SP3(K,J)=I
      I=SP4(K,J)/FUDGE+0.5
      SP4(K,J)=I
   28 CONTINUE
      WRITE OUTPUT TAPE 2,124,ISO(6),(GSX(K),K=1,MR)
  124 FORMAT(1H1,13H KEY TO TABLE,27X,13HSUMMARY TABLE,/,24H THERMAL FLU
     1X(N/CM2-SEC),/,13H FAST   HEAVY,/,13H GAMMA  TOTAL,/,8H RATIO  ,A5
     2,//,6H DEPTH,14X,13H R-COORDINATE,/,10X,(10(F10.3,2X)))
      XX=-DX
      DO 29 J=1,MX
      XX=XX+DX
      DO 30 K=1,MR
      MASK(K)=SP3(K,J)
      MASK(K+10)=SP2(K,J)
      MASK(K+20)=SP1(K,J)
      MASK(K+30)=RR(J,K)
      MASK(K+40)=1000.*SP4(K,J)/RR(J,K)
      MASK(K+50)=SP4(K,J)
   30 CONTINUE
      WRITE OUTPUT TAPE 2,125,XX,(TF(J,K),K=1,MR)
      WRITE OUTPUT TAPE 2,126,(MASK(K),MASK(K+10),   K=1,MR)
      WRITE OUTPUT TAPE 2,126,(MASK(K+20),MASK(K+30),K=1,MR)
      WRITE OUTPUT TAPE 2,126,(MASK(K+40),MASK(K+50),K=1,MR)
      WRITE OUTPUT TAPE 2,127
   29 CONTINUE
      WRITE OUTPUT TAPE 2,128,FUDGE
      FUDGE=GH(2,1)*1E6
      WRITE OUTPUT TAPE 2,136,ISO(6),FUDGE
  116 FORMAT(1H ,F10.5,2E14.4)
  125 FORMAT(1H ,F8.3,2X,(10(E10.3,2X)))
  126 FORMAT(1H ,10X,(10(2I5,2X)))
  127 FORMAT(1H0)
  128 FORMAT(1H0,17H DOSE IN UNITS OF,F10.5,8H RAD/MIN)
  136 FORMAT(1H0,A5,12H WT FRACTION,F8.2,4H PPM)
      RETURN
      END
*     SUBROUTINE DERIV
      SUBROUTINE DERIV
      DIMENSION AMAT(11),A(11),RHO(11),T(11),E(26),EN(11),ETA(11),BSIGA(
     111,26),ESIGA(11,26),BSIGS(11,26),ESIGS(11,26),TEMPA(11,26),TEMPS(1
     21,26),THETA(11,26),PHI1(11,26),PHI2(11,26),
     3PHI(80),      F(27,26),   THETAN(11),TEMP(26),S(26),FISS(26),
     4FLUX(11,26),XI(11),DU(26), PLOT( 51,21), ALPH(7),U(26),GEOM(11),
     5DIG(9),ITYPE(12),NCODE(11),ITITLE(12),NNCODE(11),INT(11),NVECT(11)
     6,Q(100),QQ(100),QQQ(100),PSI(100),FLUXU(11,26),AREG(11),Y(3),DY(3)
     7,DD(100),ALP1(11),ALP2(11),AA(6),ATABL(3),RTABL(3),WORK(33),DDD(10
     8),BARMU(11),W(1500),SNN(12,25,11)
```

```
      DIMENSION NDS(11),XPL(25),TTAB(25),ATAB(25),RTINF(25),CAPA(25),
     1TFN(27,26),SAT(11),SST(11)
      COMMON AMAT,A,RHO,T,E,EN,ETA,BSIGA,ESIGA,BSIGS,ESIGS,TEMPA,TEMPS,
     1THETA,PHI1,PHI2,PHI,F,THETAN,TEMP,S,FISS,FLUX,XI,DU, PLOT, ALPH,
     2U,GEOM,DIG,ITYPE,NCODE,ITITLE,NNCODE,INT,NVECT,Q,QQ,QQQ,PSI,FLUXU,
     3AREG,Y,DY,DD,ALP1,ALP2,AA,ATABLE,RTABL,WORK,DDD,BARMU,D,P,SIGMA,
     4S1,X,XX,SLOPE,XMAX,NTRY,M,IFVD,IBKP,IERR,DX,DDX,W,L,IQ,NTH,XS,DXS,
     5NDS,XPL,TTAB,ATAB,RTINF,CAPA,TFN,SAT,SST,NG,SNN
      DY(1)=(Y(1)**2.)/D-SIGMA-P*Y(1)/X
      DY(2)=Y(1)*Y(2)/D+S1+(X-0.5*(XMAX+XX))*SLOPE-P*Y(2)/X
      DY(3)=-(Y(2)+Y(1)*Y(3))/D
      RETURN
      END
*     LABEL
*     SUBROUTINE CNTRL(NTRY)
      SUBROUTINE CNTRL(NTRY)
      DIMENSION AMAT(11),A(11),RHO(11),T(11),E(26),EN(11),ETA(11),BSIGA(
     111,26),ESIGA(11,26),BSIGS(11,26),ESIGS(11,26),TEMPA(11,26),TEMPS(1
     21,26),THETA(11,26),PHI1(11,26),PHI2(11,26),
     3PHI(80),      F(27,26),   THETAN(11),TEMP(26),S(26),FISS(26),
     4FLUX(11,26),XI(11),DU(26), PLOT( 51,21), ALPH(7),U(26),GEOM(11),
     5DIG(9),ITYPE(12),NCODE(11),ITITLE(12),NNCODE(11),INT(11),NVECT(11)
     6,Q(100),QQ(100),QQQ(100),PSI(100),FLUXU(11,26),AREG(11),Y(3),DY(3)
     7,DD(100),ALP1(11),ALP2(11),AA(6),ATABL(3),RTABL(3),WORK(33),DDD(10
     8),BARMU(11),W(1500),SNN(12,25,11)
      DIMENSION NDS(11),XPL(25),TTAB(25),ATAB(25),RTINF(25),CAPA(25),
     1TFN(27,26),SAT(11),SST(11)
      COMMON AMAT,A,RHO,T,E,EN,ETA,BSIGA,ESIGA,BSIGS,ESIGS,TEMPA,TEMPS,
     1THETA,PHI1,PHI2,PHI,F,THETAN,TEMP,S,FISS,FLUX,XI,DU, PLOT, ALPH,
     2U,GEOM,DIG,ITYPE,NCODE,ITITLE,NNCODE,INT,NVECT,Q,QQ,QQQ,PSI,FLUXU,
     3AREG,Y,DY,DD,ALP1,ALP2,AA,ATABLE,RTABL,WORK,DDD,BARMU,D,P,SIGMA,
     4S1,X,XX,SLOPE,XMAX,NTRY,M,IFVD,IBKP,IERR,DX,DDX,W,L,IQ,NTH,XS,DXS,
     5NDS,XPL,TTAB,ATAB,RTINF,CAPA,TFN,SAT,SST,NG,SNN
      IF(M-2)3,6,7
    6 YDY=Y(1)/DY(1)
      DLTA1=0.15*ABSF(YDY)
      IF(DLTA1-.0010)18,18,19
   18 DLTA1=1.
   19 DLTA2=XMAX-X
      DLTA2=ABSF(DLTA2)
      DLTA3=ABSF(DDX)
      DLTA1=MIN1F(DLTA1,DLTA2,DLTA3)
      DX=SIGNF(DLTA1,DX)
      W(L)=Y(1)
      W(L+1)=DX
      W(L+2)=Y(2)
      W(L+3)=Y(1)
      L=L+3
      GO TO 8
    7 IF(IQ)9,9,10
   10 IQ=0
      GO TO 8
    9 L=L-3
      Y(1)=W(L+3)
      Y(2)=W(L+5)
      DX=-W(L+1)
      NTRY=4
      IQ=1
      GO TO 2
    8 IF(DIG(8))80,80,81
   81 WRITE OUTPUT TAPE 2,20,X,DX,(Y(I),DY(I),I=1,M)
```

```
   20 FORMAT(1H ,8E13.5)
   80 IF(M-2)12,12,16
   16 IF(NTH)12,12,11
   11 PHI(1)=Y(3)
      IF(X-XS)13,13,14
   13 PHI(NTH)=Y(3)+((XS-X)/(XP-X))*(PHIP-Y(3))
      WRITE OUTPUT TAPE 2,1,XS,PHI(NTH)
    1 FORMAT(1H ,F12.5,E15.4)
      NTH=NTH-1
      XS=XS-DXS
      GO TO 16
   14 PHIP=Y(3)
      XP=X
   12 W1=XMAX-X
      IF(DDX)4,3,5
    4 W1=-W1
    5 IF(W1-.0001)3,3,2
    3 NTRY=2
    2 RETURN
      END
*     LABEL
      FUNCTION PLCALC(I,J,N,GEOM,SNN)
      DIMENSION GEOM(11),SNN(12,25,11)
      PLCALC=1.-GEOM(I)
      RETURN
      END
*     LABEL
*     SUBROUTINE SINT(NENG,E,FLUX,PHIMIT)
      SUBROUTINE SINT(NENG,E,FLUX,PHIMIT)
F     SPECT
      DIMENSION  E(26),FLUX(26)
      M=8
      N=NENG-1
      FLUX(NENG)=0.
      DO 1 I=1,N
      IF(E(I)-.001)2,2,3
C      ASSUMES NO FISSION NEUTRONS BELOW .001 MEV
    2 FLUX(I)=0.
      GO TO 1
    3 A= E(I+1)
      C= E(I)
      B=(A+C)*0.5
C      GAS4 USES 4TH ORDER GAUSSIAN FIT OVER 2 SUB-INTERVALS PER GROUP
      F1=GAS4(SPECT,A,B)
      F2=GAS4(SPECT,B,C)
      FLUX(I)=PHIMIT*(F1+F2)
    1 CONTINUE
      WRITE OUTPUT TAPE 2,4,(E(I),FLUX(I),I=1,N)
    4 FORMAT(1H1,7H ENERGY,5X,15HSOURCE STRENGTH,/,(F7.3,F14.8))
      RETURN
      END
*     SUBROUTINE DATA
      SUBROUTINE DATA(X,H,N,A)
      DIMENSION A(25)
      READ INPUT TAPE 4,3,X,H,N
      READ INPUT TAPE 4,4,(A(I),I=1,N)
      WRITE OUTPUT TAPE 2,5,X,H,N,(A(I),I=1,N)
      RETURN
    3 FORMAT(2F10.5,I5)
    4 FORMAT(8F10.5)
    5 FORMAT(1HO,2F10.5,I5/(8F10.5))
```

```
      END
*     LABEL
      FUNCTION SPECT(X)
      Y=SQRTF(2.29*X)
      SPECT=0.4527*EXPF(-X/0.965)*TANHF(Y)/SQRTF(1.-(TANHF(Y))**2.)
      RETURN
      END
*     LABEL
      FUNCTION SPINT(X,A,N,XO,H)
      DIMENSION A(80)
C     4-TH DIFFERENCE=FOURF(J)
C     2-ND DIFFERENCE=TWOF(J)
C     MODIFIED EVERETT FORMULA INTERPOLATION, WITH ERROR PROPORTIONAL
C           TO FOURF(J)
      XX=X-XO
      M=XX/H
      M=M+1
      T=MODF(XX,H)/H
      I1=1
      I2=2
      I3=3
      IF(M-2)4,3,6
    6 IF(M-N+1)2,3,5
    3 D4=0.
      D41=0.
      GO TO 8
    2 D4=FOUR(A,M-2)
      D41=FOUR(A,M-1)
    8 D2=TWO(A,M-1)
      D21=TWO(A,M)
      TB=1.-T
      G=0.184
      C=1./6.
      FX=TB*(A(M)+C*(TB*TB-1.)*(D2-G*D4))+T*(A(M+1)+C*(T*T-1.)*(D21-
     1  G*D41))
      SPINT=FX
      RETURN
    5 I1=N-1
      I2=N
      I3=N+1
      B=M-N+1
      T=T+B
      GO TO 7
    4 B=M-1
      T=T+B
    7 FX=0.5*(T-2.)*(T-1.)*A(I1)-T*(T-2.)*A(I2)+0.5*T*(T-1.)*A(I3)
      SPINT=FX
      RETURN
      END
*     LABEL
      FUNCTION FOUR(A,I)
      DIMENSION A(80)
      FOUR=A(I)-4.*(A(I+1)+A(I+3))+6.*A(I+2)+A(I+4)
      RETURN
      END
*     LABEL
      FUNCTION TWO(A,I)
      DIMENSION A(80)
      TWO=A(I)-2.*A(I+1)+A(I+2)
      RETURN
      END
```

```
*       LABEL
        FUNCTION G3(A,B,C,D,F,G,NI,NO,AH,V6,V7,V8,V9,V10,GSX,NGS,HGS,GSO,X
       1X,YY,ANGLE,P,Q,RPRIM)
        DIMENSION AH(18),GSX(80)
F       F,G,ANGLE
        SUM=0.
        AVG=(Q+P)/2.
        DIF=(Q-P)/2.
        J=10
        K=14
        DO 4 I=1,4
        L=I+J
        TH=AVG+AH(L)*DIF
        F1=ANGLE(TH)*G24(A,B,C,D,F,G,NI,NO,AH,V6,V7,V8,V9,V10,GSX,NGS,HGS,
       1GSO,XX,YY,TH,RPRIM)
        TH=AVG-AH(L)*DIF
        F2=ANGLE(TH)*G24(A,B,C,D,F,G,NI,NO,AH,V6,V7,V8,V9,V10,GSX,NGS,HGS,
       1GSO,XX,YY,TH,RPRIM)
        M=I+K
    4   SUM=SUM+AH(M)*(F1+F2)
        G3=SUM*DIF*RPRIM*RPRIM
        RETURN
        END
*       LABEL
        FUNCTION G24(A,B,C,D,F,G,NI,NO,AH,V6,V7,V8,V9,V10,GSX,NGS,HGS,GSO,
       1XX,YY,TH,RPRIM)
        DIMENSION AH(18),GSX(80)
F       F
        SUM=0.
        N1=NO+1
        N2=NO/2
        AVG=(B+A)/2.
        DIF=(B-A)/2.
        J=0
        IF(NO-6)1,2,3
    2   J=4
        GO TO 1
    3   J=10
    1   K=J+N2
        DO 4 I=1,N2
        L=I+J
        Y=AVG+AH(L)*DIF
        R=Y*RPRIM
        F1=G(Y)*CENTR(F,C,D,NI,R,AH,V6,V7,V8,V9,V10,GSX,NGS,HGS,GSO,XX,YY,
       1TH)
        Y=AVG-AH(L)*DIF
        R=Y*RPRIM
        F2=G(Y)*CENTR(F,C,D,NI,R,AH,V6,V7,V8,V9,V10,GSX,NGS,HGS,GSO,XX,YY,
       1TH)
        M=I+K
    4   SUM=SUM+AH(M)*(F1+F2)
        G24=SUM*DIF
        RETURN
        END
*       LABEL
        FUNCTION CENTR(F,C,D,NI,R,AH,V6,V7,V8,V9,V10,GSX,NGS,HGS,GSO,XX,
       1YY,TH)
        DIMENSION AH(18),GSX(80)
        SUM=0.
        N1=NI+1
        N2=NI/2
```

```
      AVG=(D+C)/2.
      DIF=(D-C)/2.
      J=0
      IF(NI-6)1,2,3
    2 J=4
      GO TO 1
    3 J=10
    1 K=J+N2
      DO 4 I=1,N2
      L=I+J
      X=AVG+AH(L)*DIF
      F1=F(X,R,V6,V7,V8,V9,V10,GSX,NGS,HGS,GSO,XX,YY,TH)
      X=AVG-AH(L)*DIF
      F2=F(X,R,V6,V7,V8,V9,V10,GSX,NGS,HGS,GSO,XX,YY,TH)
      M=I+K
    4 SUM=SUM+AH(M)*(F1+F2)
      CENTR=SUM*DIF
      RETURN
      END
*     LABEL
      FUNCTION F(X,R,GMU,V7,AL1,AL2,A,GSX,NGS,HGS,GSO,XX,YY,TH)
      DIMENSION GSX(80)
      EL2=(X-XX)**2.+R*R+YY*YY-2.*R*YY*COSF(TH)
      EL=SQRTF(EL2)
      S=SPINT(X,GSX,NGS,GSO,HGS)
      F=S*(A*EXPF(-(1.-AL1)*GMU*EL) + (1.-A)*EXPF(-(1.+AL2)*GMU*EL))/(
     1   EL2*12.566371)
      RETURN
      END
*     LABEL
      FUNCTION G(Y)
      G=Y*(COSF(1.570796*Y)**0.25)
      RETURN
      END
*     LABEL
      FUNCTION ANGLE(TH)
C     THERE IS NO ANGULAR DEPENDENCE IN THIS
      ANGLE=2.
      RETURN
      END
*     LABEL
*     SUBROUTINE SCALC
      SUBROUTINE SCALC(NENG,CRIT,I,TAINT,NCOLL)
      DIMENSION AMAT(11),A(11),RHO(11),T(11),E(26),EN(11),ETA(11),BSIGA(
     111,26),ESIGA(11,26),BSIGS(11,26),ESIGS(11,26),TEMPA(11,26),TEMPS(1
     21,26),THETA(11,26),PHI1(11,26),PHI2(11,26),
     3PHI(80),      F(27,26),   THETAN(11),TEMP(26),S(26),FISS(26),
     4FLUX(11,26),XI(11),DU(26), PLOT( 51,21), ALPH(7),U(26),GEOM(11),
     5DIG(9),ITYPE(12),NCODE(11),ITITLE(12),NNCODE(11),INT(11),NVECT(11)
     6,Q(100),QQ(100),QQQ(100),PSI(100),FLUXU(11,26),AREG(11),Y(3),DY(3)
     7,DD(100),ALP1(11),ALP2(11),AA(6),ATABL(3),RTABL(3),WORK(33),DDD(10
     8),BARMU(11),W(1500),SNN(12,25,11)
      DIMENSION NDS(11),XPL(25),TTAB(25),ATAB(25),RTINF(25),CAPA(25),
     1TFN(27,26),SAT(11),SST(11)
      COMMON AMAT,A,RHO,T,E,EN,ETA,BSIGA,ESIGA,BSIGS,ESIGS,TEMPA,TEMPS,
     1THETA,PHI1,PHI2,PHI,F,THETAN,TEMP,S,FISS,FLUX,XI,DU, PLOT, ALPH,
     2U,GEOM,DIG,ITYPE,NCODE,ITITLE,NNCODE,INT,NVECT,Q,QQ,QQQ,PSI,FLUXU,
     3AREG,Y,DY,DD,ALP1,ALP2,AA,ATABLE,RTABL,WORK,DDD,BARMU,D,P,SIGMA,
     4S1,X,XX,SLOPE,XMAX,NTRY,M,IFVD,IBKP,IERR,DX,DDX,W,L,IQ,NTH,XS,DXS,
     5NDS,XPL,TTAB,ATAB,RTINF,CAPA,TFN,SAT,SST,NG,SNN
      NTAB=16
```

```
      M=NENG+1
      L=0
      DO 30 J=1,NG
      TEMP(J)=0.
      JJ=NENG+2-J
      DO 30 K=J,NENG
      KK=M-K
      TFN(J,K)=0.
      TFN(JJ,KK)=F(J,K)
   30 CONTINUE
   20 L=L+1
      ITEST=0
C     NOW GET TRANSMISSION PROBABILITIES FOR ALL GROUPS
C     FISS(J) CONTAINS PREVIOUS TRANSMISSIONS, IF L GRTR 1, FOR C=1.
C     FLUXU CONTAINS THICKNESS IN MFP
      IQ=4
      DMON=0.
      DO 1 J=1,NG
      IF(L-1)2,2,5
    2 X=FLUXU(I,J)
      CALL TAINT(XPL,TTAB,X,XX,NTAB,IQ,NERR,DMON,ATAB,XS,RTINF,XMAX,
     1  CAPA,DXS)
    4 FISS(J)=XX
      PLOT(J+26,1)=XMAX
      PLOT(J+26,2)=DXS
      PLOT(J+26,3)=XS
      WRITE OUTPUT TAPE 2,19,X,XX,XMAX,DXS,XS
      GO TO 1
    5 S1=L
      FISS(J)=(PLOT(J+26,1)+PLOT(J+26,2)*EXPF(-PLOT(J+26,3)*S1))*FISS(J)
    1 CONTINUE
C
      DO 7 J=1,NG
      JJ=NENG+2-J
      XX=FISS(J)
      DO 8 K=J,NENG
      KK=M-K
      TFN(J,K)=TFN(JJ,KK)*XX + TFN(J,K)
    8 CONTINUE
      R=TFN(J,J)
      IF(R)9,7,9
    9 R=(TEMP(J)-R)/R
      R=ABSF(R)-CRIT
      TEMP(J)=TFN(J,J)
      IF(R)7,7,10
   10 ITEST=1
    7 CONTINUE
      IF(ITEST)11,11,12
   11 WRITE OUTPUT TAPE 2,100,L,I,R
  100 FORMAT(1H ,I3,27H COLLISIONS USED FOR REGION,I3,3H R=,E10.3)
      IF(DIG(9))16,16,17
   17 WRITE OUTPUT TAPE 2,25
   25 FORMAT(1H1,9H TFN(J,K))
      DO 18 J=1,M
      WRITE OUTPUT TAPE 2,19,(TFN(J,K),K=1,NENG)
   18 CONTINUE
   19 FORMAT(1HO,(13F9.6))
   16 RETURN
   12 IF(L-NCOLL)13,11,11
C     NOW RAISE F ANOTHER POWER, FOR NEXT COLLISION
   13 DO 14 J=1,NG
```

```
      JJ=NENG+2-J
      DO 14 K=J,NENG
      KK=M-K
      F(JJ,KK)=0.
      DO 14 MM=J,K
      JK=M-MM
      F(JJ,KK)=F(JJ,KK)+TFN(JJ,JK)*F(MM,K)
   14 CONTINUE
      DO 15 J=1,NENG
      JJ=NENG+2-J
      DO 15 K=J,NENG
      KK=M-K
      TFN(JJ,KK)=F(JJ,KK)
   15 CONTINUE
      GO TO 20
      END
      SUBROUTINE FCALC(SNN,NENG,IN,F,NDS)
      DIMENSION SNN(12,25,11),F(27,26),NDS(11)
      DO 1 J=1,NENG
      IF(J-NENG)9,2,2
    9 IF(SNN(1,J,IN))2,2,4
    2 DO 3 K=1,NENG
      F(J,K)=0.
    3 CONTINUE
      GO TO 1
    4 X=1./SNN(1,J,IN)
      DO 5 K=1,NENG
      L=K-J
      IF(L)6,7,7
    6 F(J,K)=0.
      GO TO 5
    7 IF(NDS(IN)-L)6,8,8
    8 F(J,K)=X*SNN(L+2,J,IN)
    5 CONTINUE
    1 CONTINUE
   10 RETURN
      END
*     LABEL
*     SUBROUTINE SINT
      SUBROUTINE SINT(NENG,E,FLUX,PHIMIT)
      DIMENSION E(26),FLUX(26)
      READ INPUT TAPE 4,1,(FLUX(I),I=1,NENG)
    1 FORMAT(5E15.8)
      WRITE OUTPUT TAPE 2,4,(E(I),FLUX(I),I=1,NENG)
    4 FORMAT(F10.3,E15.8)
      RETURN
      END
*     SUBROUTINE THERM
      SUBROUTINE THERM(XO,NREG,NMAX,NN,PPRIM)
      DIMENSION AMAT(11),A(11),RHO(11),T(11),E(26),EN(11),ETA(11),BSIGA(
     111,26),ESIGA(11,26),BSIGS(11,26),ESIGS(11,26),TEMPA(11,26),TEMPS(1
     21,26),THETA(11,26),PHI1(11,26),PHI2(11,26),
     3PHI(80),      F(27,26),   THETAN(11),TEMP(26),S(26),FISS(26),
     4FLUX(11,26),XI(11),DU(26), PLOT( 51,21), ALPH(7),U(26),GEOM(11),
     5DIG(9),ITYPE(12),NCODE(11),ITITLE(12),NNCODE(11),INT(11),NVECT(11)
     6,Q(100),QQ(100),QQQ(100),PSI(100),FLUXU(11,26),AREG(11),Y(3),DY(3)
     7,DD(100),ALP1(11),ALP2(11),AA(6),ATABL(3),RTABL(3),WORK(33),DDD(10
     8),BARMU(11),W(1500),SNN(12,25,11)
      DIMENSION NDS(11),XPL(25),TTAB(25),ATAB(25),RTINF(25),CAPA(25),
     1TFN(27,26),SAT(11),SST(11)
      COMMON AMAT,A,RHO,T,E,EN,ETA,BSIGA,ESIGA,BSIGS,ESIGS,TEMPA,TEMPS,
```

```
     1THETA,PHI1,PHI2,PHI,F,THETAN,TEMP,S,FISS,FLUX,XI,DU, PLOT, ALPH,
     2U,GEOM,DIG,ITYPE,NCODE,ITITLE,NNCODE,INT,NVECT,Q,QQ,QQQ,PSI,FLUXU,
     3AREG,Y,DY,DD,ALP1,ALP2,AA,ATABLE,RTABL,WORK,DDD,BARMU,D,P,SIGMA,
     4S1,X,XX,SLOPE,XMAX,NTRY,M,IFVD,IBKP,IERR,DX,DDX,W,L,IQ,NTH,XS,DXS,
     5NDS,XPL,TTAB,ATAB,RTINF,CAPA,TFN,SAT,SST,NG,SNN
F      DERIV,CNTRL
       Y(3)=0.
       DY(3)=0.
       X=X0
       IQ=0
       DX=QQ(1)-X0
       NO=1
       IF(AA(1))600,602,600
  600  Y(1)=AA(2)/AA(1)
       Y(2)=AA(3)/AA(1)
       NO=0
  602  IFVD=1
       M=2
       L=1
       IBKP=0
       NNN=1
       IF(DIG(7))1553,1553,1554
 1554  NNN=NN-INT(NREG)+1
       N1=NREG-1
       DO 1 I=1,N1
       X=X+T(I)
       PSI(I)=0.
    1  CONTINUE
 1553  DO 603 N=NNN,NN
       IF(DIG(6))1530,1530,1531
 1530  IF(N-NMAX)1531,1531,1533
 1533  P=0.
 1531  SIGMA=QQQ(N)
       DX=QQ(N)-X
       DDX=DX
       XMAX=QQ(N)
       XX=X
       D=DD(N)
       IF(NN-N)605,605,604
  605  SLOPE=0.
       N1=NN
       GO TO 606
  604  SLOPE=2.*(Q(N+1)-Q(N))/(QQ(N+1)-XX)
       N1=N+1
       IF(D-DD(N+1))686,606,686
  686  SLOPE=0.
  606  IF(DIG(5))640,641,640
  641  SLOPE=0.
  640  S1=Q(N)
       H=0.1/SQRTF(SIGMA/D)
C      H IS RECOMMENDED SUB-INTERVAL
       IF(DX-H)688,688,662
  662  KK=1.+DX/H
       H=KK
       DX=DX/H
       DDX=DX
  688  IF(NO)663,663,685
  685  NO=0
       DX=0.01
       SS=S1+(X-0.5*(XMAX+XX))*SLOPE
       FLAM=0.5*DX*P/X
```

```
      FLAM=-FLAM/(1.+FLAM)
      FMU=FLAM*(-AA(3)/AA(2)+0.5*DX*SS*DX/D)
      FFLAM=FLAM*(1.+0.5*DX*DX*QQQ(1)/D)
      Y(1)=-D/DX-0.5*DX*QQQ(1)-D*FFLAM/DX
      Y(2)=-D*AA(3)/(AA(2)*DX)+0.5*DX*SS+D*FMU/DX
C     D GRTR 5. MEANS IT MUST BE AN AIR GAP.  PP=GAP ATTENUATION FACTOR
  663 IF(D-1000.)651,650,650
  650 PP=1.
      IF(P-1.)654,653,652
  652 PP=PP*XMAX/X
  653 PP=PP*XMAX/X
  654 Y(1)=Y(1)/PP
      Y(2)=Y(2)/PP
      DY(3)=DY(3)*PP*DD(N)/DD(N1)
      X=XMAX
  651 CALL RKS3(DERIV,CNTRL,Y,DY,ATABL,RTABL,WORK,X,DX,M,IFVD,IBKP,NTRY,
     1IERR)
  603 CONTINUE
      PSI(NN)=(AA(4)*Y(2)-AA(6))/(AA(5)-AA(4)*Y(1))
      Y(3)=PSI(NN)
      M=3
      L=L-3
      DO 607 I=NNN,NN
      N=NN+NNN-I
      IF(DIG(6))1540,1540,1541
 1540 IF(N-NMAX)1542,1542,1541
 1542 P=PPRIM
 1541 J=N-1
      N1=J
      IF(J-NNN)612,611,611
  611 DX=QQ(J)-X
      GO TO 610
  612 DX=X0-X
      N1=NNN
  610 SIGMA=QQQ(N)
      XMAX=X+DX
      XX=X
      DDX=DX
      D=DD(N)
      IF(NN-N)608,608,609
  608 SLOPE=0.
      GO TO 613
  609 SLOPE=2.*(Q(N)-Q(N+1))/(XMAX-QQ(N+1))
      IF(D-DD(N+1))687,613,687
  687 SLOPE=0.
  613 IF(DIG(5))680,681,680
  681 SLOPE=0.
  680 S1=Q(N)
      IF(D-1000.)655,656,656
  656 PP=1.
      IF(P-1.)659,658,657
  657 PP=PP*XMAX/X
  658 PP=PP*XMAX/X
  659 Y(1)=Y(1)/PP
      Y(2)=Y(2)/PP
      DY(3)=DY(3)*PP*DD(N)/DD(N1)
      X=XMAX
  655 H=0.1/SQRTF(SIGMA/D)
      IF(-DX-H)665,665,664
  664 KK=1.-DX/H
      H=KK
```

```
      DX=DX/H
      DDX=DX
  665 CALL RKS3(DERIV,CNTRL,Y,DY,ATABL,RTABL,WORK,X,DX,M,IFVD,IBKP,NTRY,
     1IERR)
      IF(J)607,607,661
  661 PSI(J)=Y(3)
  607 CONTINUE
      RETURN
      END
*     LABEL
*     SUBROUTINE GRAPH
      SUBROUTINE GRAPH(NREG,NG)
      DIMENSION AMAT(11),A(11),RHO(11),T(11),E(26),EN(11),ETA(11),BSIGA(
     111,26),ESIGA(11,26),BSIGS(11,26),ESIGS(11,26),TEMPA(11,26),TEMPS(1
     21,26),THETA(11,26),PHI1(11,26),PHI2(11,26),
     3PHI(80),      F(27,26),   THETAN(11),TEMP(26),S(26),FISS(26),
     4FLUX(11,26),XI(11),DU(26), PLOT( 51,21), ALPH(7),U(26),GEOM(11),
     5DIG(9),ITYPE(12),NCODE(11),ITITLE(12),NNCODE(11),INT(11),NVECT(11)
     6,Q(100),QQ(100),QQQ(100),PSI(100),FLUXU(11,26),AREG(11),Y(3),DY(3)
     7,DD(100),ALP1(11),ALP2(11),AA(6),ATABL(3),RTABL(3),WORK(33),DDD(10
     8),BARMU(11),W(1500),SNN(12,25,11)
      DIMENSION NDS(11),XPL(25),TTAB(25),ATAB(25),RTINF(25),CAPA(25),
     1TFN(27,26),SAT(11),SST(11)
      COMMON AMAT,A,RHO,T,E,EN,ETA,BSIGA,ESIGA,BSIGS,ESIGS,TEMPA,TEMPS,
     1THETA,PHI1,PHI2,PHI,F,THETAN,TEMP,S,FISS,FLUX,XI,DU, PLOT, ALPH,
     2U,GEOM,DIG,ITYPE,NCODE,ITITLE,NNCODE,INT,NVECT,Q,QQ,QQQ,PSI,FLUXU,
     3AREG,Y,DY,DC,ALP1,ALP2,AA,ATABLE,RTABL,WORK,DDD,BARMU,D,P,SIGMA,
     4S1,X,XX,SLOPE,XMAX,NTRY,M,IFVD,IBKP,IERR,DX,DDX,W,L,IQ,NTH,XS,DXS,
     5NDS,XPL,TTAB,ATAB,RTINF,CAPA,TFN,SAT,SST,NG,SNN
      DO 200 L=3,50
      DO 200 M=1,21
  200  PLOT(L,M)= ALPH(7)
      DO 207 L=1,41,10
      DO 207 M=1,21
       PLOT(L,M)= ALPH(6)
       PLOT(L+1,M)= ALPH(6)
       PLOT(L+4,M)= ALPH(6)
  207  PLOT(L+7,M)= ALPH(6)
      DO 208 M=1,21
  208  PLOT( 51,M)= ALPH(6)
      XX=0.
      DO 1 J=1,NG
      IF(XX-FLUXU(1,J))2,1,1
    2 XX=FLUXU(1,J)
    1  CONTINUE
      IF(XX)3,3,4
    4 XX=LOGF(XX)/LOGF(10.)+1.
      IQ=XX
      DO 3333 N=1,NREG
      DO 201 J=1,NG
      UPRM=20.-DU(J)
      X=IQ
      X=-X+LOGF(FLUXU(N,J))/LOGF(10.)+10.
      NC=UPRM+1.1
      CC=NC
      MC=5.*(UPRM+1.1-CC)
      MC=MC+1
      NR=10.*(X+0.05)
      NR= 51-NR
      IF(NR)201,201,209
  209 IF(NR- 51)210,210,201
```

```
  210 IF(NC)201,201,211
  211 IF(NC-21)212,212,201
  212 PLOT(NR,NC)=ALPH(MC)
  201 CONTINUE
 3333 CONTINUE
      X=IQ
      X=10.**X
      WRITE OUTPUT TAPE 2,205
  205 FORMAT(1H1,16X,4(1H*,10X,1H*,11X),1H*,12H PHI(U) VS U)
      DO 222  K=1,41,10
      WRITE OUTPUT TAPE 2,223,X,( PLOT(K,M),M=1,21)
  223 FORMAT(1H ,E8.2,21A5)
      DO 224 LL=1,9
      L=LL+K
      WRITE OUTPUT TAPE 2,225,( PLOT(L,M),M=1,21)
  224 CONTINUE
  225 FORMAT(1H ,8X,21A5)
      X=X/10.
  222 CONTINUE
      WRITE OUTPUT TAPE 2,223,X,( PLOT(  51,M),M=1,21)
      WRITE OUTPUT TAPE 2,220
  220 FORMAT(1H ,7X,102H20                              15
     1  10                          5                          0,/,9H LETHAR
     2GY)
    3 RETURN
      END
                ENC OF FILE
```

Subroutine EXN, listed on page 286, is also used by MEDIPORT.

A.1.3 SAMPLE PROBLEMS FOR MEDIPORT

```
*      DATA
 116          BONDARENKO GROUP X-SECTIONS    TRANSPORT APPROX.
   26                                  1.000E+00 2
 1.050E+01 6.500E 00 4.000E 00 2.500E 00 1.400E 00 0.800E 00 0.400E 00 0
                                                                .200E 00
 0.100E 00 0.465E-01 0.215E-01 0.100E-01 0.465E-02 0.215E-02 0.100E-02 0
                                                                .465E-03
 0.215E-03 0.100E-03 0.465E-04 0.215E-04 0.100E-04 0.465E-05 0.215E-05 0
                                                                .100E-05
 0.465E-06 0.215E-06
    6     LUC                 10     .01     10.
   2.36        .455       .814       .315       .388       .158
    .092       .029       .016       .009       .004       .003
   3.06        .967      1.150       .375       .255       .156
    .078       .034       .018       .008       .004       .003
   4.17       1.594      1.597       .418       .279       .139
    .070       .037       .018       .009       .004       .002
   4.56       1.725      1.530       .650       .325       .163
    .087       .040       .019       .009       .004       .003
   6.75       2.767      2.428       .779       .389       .209
    .097       .045       .021       .010       .004       .004
   8.58        3.59      2.924      1.033       .553       .257
    .119       .055       .026       .012       .006       .004
  11.20        4.24      4.059      1.572       .732       .338
    .157       .073       .034       .016       .007       .004
  13.98        3.85      5.394      1.984       .919       .427
    .199       .092       .043       .020       .009       .008
  17.34        5.49      6.299       2.43      1.128       .524
    .243       .113       .052       .024       .011       .010
  18.55        5.84      7.294      2.882      1.338       .621
    .288       .134       .062       .029       .013       .011
  20.16        6.12      8.028      3.212      1.491       .692
    .321       .149       .069       .032       .015       .013
  20.77        6.19       8.33       3.35      1.556       .722
    .335       .156       .072       .033       .016       .013
  21.2         6.24       8.49       3.42      1.588       .737
    .342       .159       .074       .034       .016       .014
  21.4         6.27       8.60      3.472      1.612       .748
    .347       .161       .075       .035       .016       .014
  21.4         6.30       8.64      3.489       1.62       .752
    .349       .162       .075       .035       .016       .014
  21.5         6.30       8.68      3.506      1.628       .756
    .351       .163       .076       .035       .016       .014
  21.5         6.30       8.68      3.506      1.628       .756
    .351       .163       .076       .035       .030        .
  21.6         6.31       8.71      3.524      1.636       .759
    .352       .164       .076       .066        .          .
  21.6         6.31       8.71      3.524      1.636       .759
    .352       .164       .142        .          .          .
  21.6         6.31       8.71      3.524      1.636       .759
    .352       .306        .          .          .          .
  21.6         6.31       8.71      3.524      1.636       .759
    .658        .          .          .          .          .
  21.6         6.31       8.71      3.524      1.636      1.417
    .          .          .          .          .          .
  21.6         6.31       8.71      3.524      3.053       .
    .          .          .          .          .          .
  21.7         6.31       8.71      6.577       .          .
    .          .          .          .          .          .
```

```
  21.7        6.31      15.29         .           .           .
    .           .         .           .           .           .
 0.000E 00 0.000E 00 1.320E 00 0.000E 00 0.000E 00
 0.125E 00 0.068E 00 1.200E 00 1.906E-01  .   E
 0.250E 00 1.064E-01 1.090E 00 0.300E 00-0.015E 00
 0.375E 00 0.130E 00 0.990E 00 0.386E 00-0.033E 00
 0.500E 00 0.149E 00 0.920E 00 4.468E-01-0.050E 00
 0.750E 00 0.170E 00 0.800E 00 0.547E 00-0.086E 00
 1.000E 00 1.793E-01  .700E 00 0.618E 00-0.121E 00
 1.250E 00 0.185E 00 0.620E 00 0.674E 00- .157E 00
 1.500E 00 1.861E-01 0.555E 00 7.175E-01- .191
 2.000E 00 1.875E-01 0.450E 00 0.783E 00- .253E 00
 2.500E 00 1.881E-01 0.368E 00 8.273E-01- .305E 00
 3.000E 00 1.882E-01  .311E 00 0.859E 00-0.312E 00
 3.500E 00 1.883E-01 0.266E 00 8.841E-01-0.310E 00
 4.000E 00 1.883E-01  .227E    0.904E 00-0.300E 00
 4.500E 00 1.884E-01  .197E 00 9.178E-01- .290E 00
 5.000E 00 1.884E-01  .171E 00 9.288E-01- .280E 00
 1          LUCITE SCATTERER
    6    1   1.          .0695    0.50       1.
+           +           +           +           +      .
                                                                .0001 50
0  +0.0000E+00+           -0.1000E 01 0.1000E 11 0.2130E 01 0.1000E 01
 1.  1.  1.  0.  1.  1.  1.  1.  1.    1
 0.184      E 08  .280      E 08  .219      E 08  .335      E 08 0.303      E
                                                                  08
 0.281      E 08 0.169      E 08 0.106      E 08 0.867      E 07 0.618      E
                                                                  07
 0.438      E 07 0.980      E 07 0.336      E 07 0.967      E 07 0.181      E
                                                                  07
 0.937      E 07 0.855      E 07 0.813      E 07 0.775      E 07 0.738      E
                                                                  07
 0.706      E 07 0.675      E 07 0.643      E 07 0.606      E 07 0.568      E
                                                                  07
 0.000      E 00
 116         BONDARENKO GROUP X-SECTIONS    TRANSPORT APPROX.
   26                                  -1.000E+00 2
 1.050E+01 6.500E 00 4.000E 00 2.500E 00 1.400E 00 0.800E 00 0.400E 00 0
                                                                .200E 00
 0.100E 00 0.465E-01 0.215E-01 0.100E-01 0.465E-02 0.215E-02 0.100E-02 0
                                                                .465E-03
 0.215E-03 0.100E-03 0.465E-04 0.215E-04 0.100E-04 0.465E-05 0.215E-05 0
                                                                .100E-05
 0.465E-06 0.215E-06
    5      TISS      .324      10      .376     48.7
   1.64        .23        .552        .257        .221        .124
    .081       .038       .016        .009        .004        .003
   2.24        .52        .741        .375        .211        .138
    .069       .034       .018        .008        .004        .003
   2.78        .77       1.036        .418        .279        .139
    .070       .037       .018        .009        .004        .002
   3.49        .92       1.173        .650        .325        .163
    .087       .040       .019        .009        .004        .003
   5.50       1.92       2.018        .779        .389        .209
    .097       .045       .021        .010        .004        .004
   6.97       2.41       2.487       1.033        .553        .257
    .119       .055       .026        .012        .006        .004
   8.54       2.22       3.39        1.572        .732        .338
    .157       .073       .034        .016        .007        .004
  11.         2.45       4.65        1.984        .919        .427
    .199       .092       .043        .020        .009        .008
```

```
  13.2        3.07        5.59        2.43        1.128       .524
    .243       .113        .052        .024        .011       .010
  15.3        3.36        6.57        2.882       1.338       .621
    .288       .134        .062        .029        .013       .011
  15.9        3.58        7.28        3.212       1.491       .692
    .321       .149        .069        .032        .015       .013
  17.5        3.66        7.58        3.35        1.556       .722
    .335       .156        .072        .033        .016       .013
  17.9        3.72        7.74        3.42        1.588       .737
    .342       .159        .074        .034        .016       .014
  18.1        3.75        7.85        3.472       1.612       .748
    .347       .161        .075        .035        .016       .014
  18.1        3.78        7.89        3.489       1.62        .752
    .349       .162        .075        .035        .016       .014
  18.2        3.78        7.93        3.506       1.628       .756
    .351       .163        .076        .035        .016       .014
  18.2        3.78        7.93        3.506       1.628       .756
    .351       .163        .076        .035        .030        .
  18.3        3.79        7.96        3.524       1.636       .759
    .352       .164        .076        .066        .           .
  18.3        3.79        7.96        3.524       1.636       .759
    .352       .164        .142        .           .           .
  18.3        3.79        7.96        3.524       1.636       .759
    .352       .306        .           .           .           .
  18.3        3.79        7.96        3.524       1.636       .759
    .658       .           .           .           .           .
  18.3        3.79        7.96        3.524       1.636      1.417
    .           .           .           .           .          .
  18.3        3.79        7.96        3.524       3.053       .
    .           .           .           .           .          .
  18.5        3.79        7.96        6.577       .           .
    .           .           .           .           .          .
  18.5        3.79       14.54        .           .           .
    .           .           .           .           .          .
 0.000E 00 0.000E 00 1.400E 00 0.000E 00 0.000E 00
 0.125E 00 8.820E-02 1.250E 00 1.906E-01  .   E
 0.250E 00 1.310E-01 1.100E 00 0.300E 00 0.010E 00
 0.375E 00 0.152E 00 0.985E 00 0.386E 00 0.035E 00
 0.500E 00 1.550E-01 0.910E 00 4.468E-01 0.575E-01
 0.750E 00 0.147E 00 0.775E 00 0.547E 00 0.100E 00
 1.000E 00 1.276E-01 0.675E 00 0.618E 00 0.135E 00
 1.250E 00 0.106E 00 0.594E 00 0.674E 00 0.153E 00
 1.500E 00 8.660E-02 0.535E 00 7.175E-01 0.205E 00
 2.000E 00 0.055E 00 0.444E 00 0.783E 00 0.270E 00
 2.500E 00 3.410E-02 0.380E 00 8.273E-01 0.332E 00
 3.000E 00 0.207E-01 0.331E 00 0.859E 00 0.390E 00
 3.500E 00 1.276E-02 0.289E 00 8.841E-01 0.430E 00
 4.000E 00 0.750E-02 0.253E 00 0.904E 00 0.458E 00
 4.500E 00 4.500E-03 0.222E 00 9.178E-01 0.475E 00
 5.000E 00 2.670E-03 0.192E 00 9.288E-01 0.485E 00
 1          TISSUE PHANTOM   MITR  45 DEGREE SCATTERER
    5    5   1.          .0982   15.         1.
                                                          .0783
+          +          +          +          +     .
                                                         .0001 50
0  +0.0000E+0+0.0000E 00-0.1000E 01 0.3000E 10 0.2130E 01 0.1000E 01
 1.  1.  1.  0.  1.  0.  0.  1.  1.
1
    1    8    5    2
ALL                        B-10 N-14
       .330           31.6                .0032       3837.
```

```
      .099              .0013              .134              .000050
     1.008            35.457            12.011            10.016
     2.23              8.57              4.95               .48
     1.283             1.                1.                 .936
  3837.                1.88
      .000050           .041
    10.016            14.008
     2.34              .624
  0.5       0.5       20
 23.       11.        7.85      6.4       5.7       5.2       4.8
                                                                4.5
  4.2       3.96      3.74      3.55      3.41      3.28      3.16
                                                               3.05
  2.95      2.86      2.78      2.70
  0.5       0.5       20
   .136      .104      .087      .076      .0685     .0627     .058
                                                              .055
   .0534     .0520     .0506     .0495     .0480     .0470     .0460
                                                             .0450
-  .05       .028      .074      .092      .102       .08      .113
                                                             .1165
   .1192     .1215     .1228     .1240     .1253     .1264     .1273
                                                            .1280
   .1285     .129      .1295     .13
  0.5       0.5       20
   .0936     .0683     .0556     .0478     .0423     .0384     .0352
                                                            .0329
   .0308     .0292     .0278     .0267     .0254     .0244     .0237
                                                           .0233
   .0227     .0222     .0217     .0212
  0.5       0.5       20
   .0320     .0300     .0276     .0256     .0238     .0220     .0213
                                                           .0206
   .0199     .0192     .0187     .0182     .0178     .0174     .0171
                                                          .0168
   .0166     .0163     .0161     .0160
   6    6    1         8.3       8.6       1.        15.       9.6126E-07
  1.         2.075
 53.0      46.0      37.4      30.0      24.2      17.8      11.6
                                                              6.7
  3.4       1.3       0.9       0.6       0.

  0.

  0.

116        BONDARENKO GROUP X-SECTIONS    TRANSPORT APPROX.
  26                                1.000E+00 2
1.050E+01 6.500E 00 4.000E 00 2.500E 00 1.400E 00 0.800E 00 0.400E 00 0
                                                                .200E 00
0.100E 00 0.465E-01 0.215E-01 0.100E-01 0.465E-02 0.215E-02 0.100E-02 0
                                                                .465E-03
0.215E-03 0.100E-03 0.465E-04 0.215E-04 0.100E-04 0.465E-05 0.215E-05 0
                                                                .100E-05
0.465E-06 0.215E-06
   5     TISS     .324     10     .376     48.7
  1.64       .23       .552      .257      .221      .124
   .081      .038      .016      .009      .004      .003
  2.24       .52       .741      .375      .211      .138
   .069      .034      .018      .008      .004      .003
  2.78       .77      1.036      .418      .279      .139
```

.070	.037	.018	.009	.004	.002
3.49	.92	1.173	.650	.325	.163
.087	.040	.019	.009	.004	.003
5.50	1.92	2.018	.779	.389	.209
.097	.045	.021	.010	.004	.004
6.97	2.41	2.487	1.033	.553	.257
.119	.055	.026	.012	.006	.004
8.54	2.22	3.39	1.572	.732	.338
.157	.073	.034	.016	.007	.004
11.	2.45	4.65	1.984	.919	.427
.199	.092	.043	.020	.009	.008
13.2	3.07	5.59	2.43	1.128	.524
.243	.113	.052	.024	.011	.010
15.3	3.36	6.57	2.882	1.338	.621
.288	.134	.062	.029	.013	.011
15.9	3.58	7.28	3.212	1.491	.692
.321	.149	.069	.032	.015	.013
17.5	3.66	7.58	3.35	1.556	.722
.335	.156	.072	.033	.016	.013
17.9	3.72	7.74	3.42	1.588	.737
.342	.159	.074	.034	.016	.014
18.1	3.75	7.85	3.472	1.612	.748
.347	.161	.075	.035	.016	.014
18.1	3.78	7.89	3.489	1.62	.752
.349	.162	.075	.035	.016	.014
18.2	3.78	7.93	3.506	1.628	.756
.351	.163	.076	.035	.016	.014
18.2	3.78	7.93	3.506	1.628	.756
.351	.163	.076	.035	.030	.
18.3	3.79	7.96	3.524	1.636	.759
.352	.164	.076	.066	.	.
18.3	3.79	7.96	3.524	1.636	.759
.352	.164	.142	.	.	.
18.3	3.79	7.96	3.524	1.636	.759
.352	.306	.	.	.	.
18.3	3.79	7.96	3.524	1.636	.759
.658	.	.	.	.	.
18.3	3.79	7.96	3.524	1.636	1.417
.	.	.	.	.	.
18.3	3.79	7.96	3.524	3.053	.
.	.	.	.	.	.
18.5	3.79	7.96	6.577	.	.
.	.	.	.	.	.
18.5	3.79	14.54	.	.	.
.	.	.	.	.	.

0.000E 00	0.000E 00	1.400E 00	0.000E 00	0.000E 00
0.125E 00	8.820E-02	1.250E 00	1.906E-01	. E
0.250E 00	1.310E-01	1.100E 00	0.300E 00	0.010E 00
0.375E 00	0.152E 00	0.985E 00	0.386E 00	0.035E 00
0.500E 00	1.550E-01	0.910E 00	4.468E-01	0.575E-01
0.750E 00	0.147E 00	0.775E 00	0.547E 00	0.100E 00
1.000E 00	1.276E-01	0.675E 00	0.618E 00	0.135E 00
1.250E 00	0.106E 00	0.594E 00	0.674E 00	0.153E 00
1.500E 00	8.660E-02	0.535E 00	7.175E-01	0.205E 00
2.000E 00	0.055E 00	0.444E 00	0.783E 00	0.270E 00
2.500E 00	3.410E-02	0.380E 00	8.273E-01	0.332E 00
3.000E 00	0.207E-01	0.331E 00	0.859E 00	0.390E 00
3.500E 00	1.276E-02	0.289E 00	8.841E-01	0.430E 00
4.000E 00	0.750E-02	0.253E 00	0.904E 00	0.458E 00
4.500E 00	4.500E-03	0.222E 00	9.178E-01	0.475E 00
5.000E 00	2.670E-03	0.192E 00	9.288E-01	0.485E 00

```
 1        MITR SIMPLIFIED GEOMETRY   25 GROUPS
    5     5   1.            .0982   15.         1.

 +          +          +          +          +      .                  .0783

0  +0.0000E+00+0.0000E 00-0.1000E 01 0.2000E 11 0.2130E 01 0.1000E 01 .0001 50
 1.  1.  1.  0.  1.  0.  0.  1.  1.
  .737       E  7 1.12      E  7  .875     E  7 1.337     E  7 1.212    E
                                                                  7
 1.122       E  7  .675     E  7  .422     E  7  .347     E  7  .247    E
                                                                  7
  .175       E 07  .392     E 07 1.344     E 06  .387     E 07  .725    E
                                                                  6
  .375       E 07  .342     E 07  .325     E 07  .310     E 07  .295    E
                                                                  7
  .282       E 07  .270     E 07  .257     E 07  .242     E 07  .227    E
                                                                  7
  .          E
1
   1    8    5    2
ALL                         B-10 N-14
         .330            31.6                 .0032      3837.
         .099              .0013              .134           .000050
        1.008            35.457             12.011          10.016
        2.23              8.57               4.95             .48
        1.283             1.                 1.               .936
     3837.                1.88
         .000050           .041
       10.016            14.008
        2.34               .624
   0.5          0.5       20
  23.           11.       7.85       6.4        5.7        5.2        4.8
                                                                       4.5
   4.2          3.96      3.74       3.55       3.41       3.28       3.16
                                                                       3.05
   2.95         2.86      2.78       2.70
   0.5          0.5       20
    .136         .104      .087       .076       .0685      .0627      .058
                                                                       .055
    .0534        .0520     .0506      .0495      .0480      .0470      .0460
                                                                       .0450
 -  .05          .028      .074       .092       .102       .08        .113
                                                                       .1165
    .1192        .1215     .1228      .1240      .1253      .1264      .1273
                                                                       .1280
    .1285        .129      .1295      .13
   0.5          0.5       20
    .0936        .0683     .0556      .0478      .0423      .0384      .0352
                                                                       .0329
    .0308        .0292     .0278      .0267      .0254      .0244      .0237
                                                                       .0233
    .0227        .0222     .0217      .0212
   0.5          0.5       20
    .0320        .0300     .0276      .0256      .0238      .0220      .0213
                                                                       .0206
    .0199        .0192     .0187      .0182      .0178      .0174      .0171
                                                                       .0168
    .0166        .0163     .0161      .0160
   6     6      1          8.3        8.6        1.         15.        9.6126E-07
  1.            2.075
 53.0          46.0       37.4       30.0       24.2       17.8       11.6
```

```
                                                                    6.7
   3.4        1.3        0.9        0.6        0.
   0.
   0.
 116         BONDARENKO GROUP X-SECTIONS    TRANSPORT APPROX.    T-TABLES
    9                                  1.000E+00 2
 1.050E+01 6.500E 00 4.000E 00 2.500E 00 1.400E 00 0.800E 00 0.400E 00 0
                                                                  .200E 00
 0.100E 00
    1      D2O      0.116       6     .0026   13.6
   3.19        .73        1.192        .32        .34        .36
    .06        .02          .          .          .          .
   4.11       1.44       1.485        .38        .50        .36
    .02          .          .          .          .          .
   5.37       1.95       1.719        .66        .88        .16
    .          .          .          .          .          .
   6.30       2.27       1.765      1.240        .96        .06
    .          .          .          .          .          .
   9.49       4.16       2.968       1.54        .80        .02
    .          .          .          .          .          .
  10.31       4.87       3.219       1.56        .66          .
    .          .          .          .          .          .
   9.36       3.76       3.36        1.60        .54          .
    .          .          .          .          .          .
   9.52       4.03       3.469       1.62        .40          .
    .          .          .          .          .          .
 0.000E 00 0.000E 00 1.400E 00 0.000E 00 0.000E 00
 0.125E 00 8.112E-02 1.250E 00 1.906E-01  .   E
 0.250E 00 1.192E-01 1.100E 00 0.300E 00 0.010E 00
 0.375E 00 0.138E 00 0.985E 00 0.386E 00 0.035E 00
 0.500E 00 1.411E-01 0.910E 00 4.468E-01 0.575E-01
 0.750E 00 0.134E 00 0.775E 00 0.547E 00 0.100E 00
 1.000E 00 1.159E-01 0.675E 00 0.618E 00 0.135E 00
 1.250E 00 0.096E 00 0.594E 00 0.674E 00 0.153E 00
 1.500E 00 7.867E-02 0.535E 00 7.175E-01 0.205E 00
 2.000E 00 0.050E 00 0.444E 00 0.783E 00 0.270E 00
 2.500E 00 3.101E-02 0.380E 00 8.273E-01 0.332E 00
 3.000E 00 0.188E-01 0.331E 00 0.859E 00 0.390E 00
 3.500E 00 1.157E-02 0.289E 00 8.841E-01 0.430E 00
 4.000E 00 0.682E-02 0.253E 00 0.904E 00 0.458E 00
 4.500E 00 4.094E-03 0.222E 00 9.178E-01 0.475E 00
 5.000E 00 2.435E-03 0.192E 00 9.288E-01 0.485E 00
 1          D2O              FIRST ORDER CORRECTION TO TRANSMISSION
    1    1  20.03       1.1017   10.
+           +           +          +          +     .
                                                                  .0001 50
0  +0.0000E+00+2.1300E+00-1.0000E+00+0.0000E+00+2.1300E+00+1.0000E+00+0.
                                                                  0000E 00
 1.  1.  1.  0.  1.  1.  0.  1.  1.    1
 116         BONDARENKO GROUP X-SECTIONS    TRANSPORT APPROX.   R-TABLES
    9                                 -1.000E+00 2
 1.050E+01 6.500E 00 4.000E 00 2.500E 00 1.400E 00 0.800E 00 0.400E 00 0
                                                                  .200E 00
```

```
 0.100E 00
    1      D2O      0.116        6     .0026    13.6
   3.19        .73        1.192        .32        .34        .36
    .06        .02          .          .          .          .
   4.11       1.44        1.485        .38        .50        .36
    .02          .          .          .          .          .
   5.37       1.95        1.719        .66        .88        .16
    .            .          .          .          .          .
   6.30       2.27        1.765       1.240       .96        .06

   9.49       4.16        2.968       1.54        .80        .02

  10.31       4.87        3.219       1.56        .66        .

   9.36       3.76        3.36        1.60        .54        .

   9.52       4.03        3.469       1.62        .40        .

 0.000E 00 0.000E 00 1.320E 00 0.000E 00 0.000E 00
 0.125E 00 0.068E 00 1.200E 00 1.906E-01  .   E
 0.250E 00 1.064E-01 1.090E 00 0.300E 00-0.015E 00
 0.375E 00 0.130E 00 0.990E 00 0.386E 00-0.033E 00
 0.500E 00 0.149E 00 0.920E 00 4.468E-01-0.050E 00
 0.750E 00 0.170E 00 0.800E 00 0.547E 00-0.086E 00
 1.000E 00 1.793E-01  .700E 00 0.618E 00-0.121E 00
 1.250E 00 0.185E 00 0.620E 00 0.674E 00- .157E 00
 1.500E 00 1.861E-01 0.555E 00 7.175E-01- .191
 2.000E 00 1.875E-01 0.450E 00 0.783E 00- .253E 00
 2.500E 00 1.881E-01 0.368E 00 8.273E-01- .305E 00
 3.000E 00 1.882E-01  .311E 00 0.859E 00-0.312E 00
 3.500E 00 1.883E-01 0.266E 00 8.841E-01-0.310E 00
 4.000E 00 1.883E-01  .227E    0.904E 00-0.300E 00
 4.500E 00 1.884E-01  .197E 00 9.178E-01- .290E 00
 5.000E 00 1.884E-01  .171E 00 9.288E-01- .280E 00
 1         D2O              FIRST ORDER CORRECTION TO TRANSMISSION
    1    2  20.03       1.1017   20.
+           +           +          +          +     .
                                                                .0001 50
0  +0.0000E+00+2.1300E+00-1.0000E+00+0.0000E+00+2.1300E+00+1.0000E+00+0.
                                                                0000E 00
 1.  1.  1.  0.  1.  1.  1.  1.  1.    1
 116         BONDARENKO GROUP X-SECTIONS    TRANSPORT APPROX.   T-TABLES
    9                                -1.000E+00 2
 1.050E+01 6.500E 00 4.000E 00 2.500E 00 1.400E 00 0.800E 00 0.400E 00 0
                                                                .200E 00
 0.100E 00
    1      D2O      0.116        6     .0026    13.6
   3.19        .73        1.192        .32        .34        .36
    .06        .02          .          .          .          .
   4.11       1.44        1.485        .38        .50        .36
    .02          .          .          .          .          .
   5.37       1.95        1.719        .66        .88        .16
    .            .          .          .          .          .
   6.30       2.27        1.765       1.240       .96        .06

   9.49       4.16        2.968       1.54        .80        .02

  10.31       4.87        3.219       1.56        .66        .

   9.36       3.76        3.36        1.60        .54        .
```

```
  9.52       4.03       3.469      1.62        .40        .

0.000E 00 0.000E 00 1.400E 00 0.000E 00 0.000E 00
0.125E 00 8.112E-02 1.250E 00 1.906E-01  .   E
0.250E 00 1.192E-01 1.100E 00 0.300E 00 0.010E 00
0.375E 00 0.138E 00 0.985E 00 0.386E 00 0.035E 00
0.500E 00 1.411E-01 0.910E 00 4.468E-01 0.575E-01
0.750E 00 0.134E 00 0.775E 00 0.547E 00 0.100E 00
1.000E 00 1.159E-01 0.675E 00 0.618E 00 0.135E 00
1.250E 00 0.096E 00 0.594E 00 0.674E 00 0.153E 00
1.500E 00 7.867E-02 0.535E 00 7.175E-01 0.205E 00
2.000E 00 0.050E 00 0.444E 00 0.783E 00 0.270E 00
2.500E 00 3.101E-02 0.380E 00 8.273E-01 0.332E 00
3.000E 00 0.188E-01 0.331E 00 0.859E 00 0.390E 00
3.500E 00 1.157E-02 0.289E 00 8.841E-01 0.430E 00
4.000E 00 0.682E-02 0.253E 00 0.904E 00 0.458E 00
4.500E 00 4.094E-03 0.222E 00 9.178E-01 0.475E 00
5.000E 00 2.435E-03 0.192E 00 9.288E-01 0.485E 00
1          D2O              FIRST ORDER CORRECTION TO TRANSMISSION
   1    3  20.03       1.1017   30.
+          +          +          +          +     .
                                                              .0001 50
0  +0.0000E+00+2.1300E+00-1.0000E+00+0.0000E+00+2.1300E+00+1.0000E+00+0.
                                                              0000E 00
 1.  1.  1.  0.  1.  1.  0.  1.  1.    1



316        BONDARENKO GROUP X-SECTIONS    TRANSPORT APPROX.
  26                                1.000E+00 2
1.050E+01 6.500E 00 4.000E 00 2.500E 00 1.400E 00 0.800E 00 0.400E 00 0
                                                              .200E 00
0.100E 00 0.465E-01 0.215E-01 0.100E-01 0.465E-02 0.215E-02 0.100E-02 0
                                                              .465E-03
0.215E-03 0.100E-03 0.465E-04 0.215E-04 0.100E-04 0.465E-05 0.215E-05 0
                                                              .100E-05
0.465E-06 0.215E-06
   2       AL     0.02467    7    .241     1.40
  1.34        .323       .187       .15        .25        .18
   .10        .04        .01        .          .          .
  1.47        .60        .174       .22        .11        .07
   .03        .01        .          .          .          .
  1.83       1.04        .506       .13        .10        .04
   .01        .          .          .          .          .
  2.17       1.50        .477       .19        .          .
   .          .          .          .          .          .
  2.39       1.98        .312       .06        .03        .01
   .          .          .          .          .          .
  3.27       2.93        .342       .          .          .
   .          .          .          .          .          .
  3.51       3.14        .371       .          .          .
   .          .          .          .          .          .
  4.92       4.40        .523       .          .          .
   .          .          .          .          .          .
  4.82       4.36        .46        .          .          .
   .          .          .          .          .          .
  7.20       6.50        .687       .          .          .
   .          .          .          .          .          .
   .98        .89        .094       .          .          .
   .          .          .          .          .          .
```

2.55	2.25	.238	.	.	.
.	.	.	.	.	.
1.38	1.25	.131	.	.	.
1.38	1.25	.131	.	.	.
1.38	1.25	.131	.	.	.
1.38	1.25	.131	.	.	.
1.38	1.25	.131	.	.	.
1.38	1.25	.131	.	.	.
1.38	1.25	.131	.	.	.
1.38	1.25	.131	.	.	.
1.38	1.25	.131	.	.	.
1.38	1.25	.131	.	.	.
1.38	1.25	.131	.	.	.
1.38	1.25	.131	.	.	.
1.38	1.25	.131	.	.	.

3	BI	0.00319	7	.034	9.03
3.02	.50	.074	.25	.75	.84
.66	.26	.10	.03	.	.
3.60	1.44	.07	.60	.60	.43
.18	.05	.01	.	.	.
4.36	3.14	.813	.18	.14	.06
.02	.01	.	.	.	.
4.32	3.81	.303	.17	.03	.01
.	.	.	.	.	.
3.98	3.82	.124	.03	.01	.
.	.	.	.	.	.
5.17	5.10	.071	.	.	.
.	.	.	.	.	.
6.76	6.67	.093	.	.	.
.	.	.	.	.	.
8.38	8.26	.115	.	.	.
.	.	.	.	.	.
9.75	9.63	.117	.	.	.
.	.	.	.	.	.
11.27	11.13	.139	.	.	.
.	.	.	.	.	.
16.	15.8	.197	.	.	.
.	.	.	.	.	.
9.5	9.383	.117	.	.	.
.	.	.	.	.	.
17.5	17.294	.216	.	.	.
.	.	.	.	.	.
9.5	9.383	.117	.	.	.
22.	21.729	.271	.	.	.
8.8	8.691	.109	.	.	.
.	.	.	.	.	.

9.	8.889	.111	.	.	.
9.	8.889	.111	.	.	.
9.	8.889	.111	.	.	.
9.	8.889	.111	.	.	.
9.	8.889	.111	.	.	.
9.	8.889	.111	.	.	.
9.	8.889	.111	.	.	.
9.01	8.889	.111	.	.	.
9.01	8.889	.111	.	.	.

ENC OF FILE

* END TAPE

A.1.4 GAUSSIAN INTEGRATION

The method used to evaluate a 1-dimensional integral is as follows:

$$I \equiv \int_A^B F(x)dx \quad \frac{B-A}{2} \Sigma_{j=1}^{N/2} H_j[f(x_j) + f(x_{N+1-j})] \tag{A.1}$$

where

$$x_j = \frac{B+A}{2} + a_j(\frac{B-A}{2})$$

$$x_{N+1-j} = \frac{B+A}{2} - a_j(\frac{B-A}{2}) \tag{A.2}$$

The coefficients H_j, a_j come from "Numerical Analysis", by Z. Copal, on p. 523. The order of integration is N(4, 6, or 8). For a two-dimensional integration,

$$I \equiv \int_A^B f(x)dx \int_C^D g(x,y)dy = \int_A^B f(x) \int_C^D g(x,y)\ dy\ \ dx$$

$$= \int_A^B f^1(x)dx \tag{A.3}$$

Consequently, what is done is to evaluate $f^1(x)$ for the appropriate x-values, as before; the only difference is that an inner integration over "y" takes place for each evaluation of $f^1(x)$. The extension to a triple integral is straightforward.

Table A.1 contains a_j, H_j for N = 4, 6, and 8, in one array AH(j) as used by MEDIPORT to evaluate gamma ray dose rates.

TABLE A.1 Gaussian Quadrature Weights

N	j	ENTRY	AH(j)
4	1	a_1	.86113631
	2	a_2	.33998103
	3	H_1	.34785485
	4	H_2	.65214515
6	5	a_1	.93246951
	6	a_2	.66120939
	7	a_3	.23861919
	8	H_1	.17132448
	9	H_2	.36076157
	10	H_3	.46791393
8	11	a_1	.96028986
	12	a_2	.79666647
	13	a_3	.52553241
	14	a_4	.18343464
	15	H_1	.10122854
	16	H_2	.22238103
	17	H_3	.31370664
	18	H_4	.36268377

A.1.5 NUMERICAL INTERPOLATION

A special subroutine known as SPINT was Fortran-coded to perform numerous tasks, such as the evaluation of the axial thermal flux $\phi(x)$ in a phantom, to obtain gamma-ray attenuation parameters $\mu, \mu_a, \alpha_1, a_2$, and A for an arbitrary energy gamma-ray, to interpolate fast neutron dose with depth, etc. The numerical method used follows Okazaki and Fowler. Given a table of entries $f_0, f_1, \ldots f_N$ evaluated at $x = x_0, x_0 + h, \ldots x_0 + Nh$ (N equally spaced intervals), this routine will find $f(x)$ for any given x. Extrapolation off the ends of the table is used if necessary.

1. Calculate $(x-x_0)/h = n+\theta$, where n is the integer and θ is the fraction.

2. If $2 \leq n \leq N - 3$, the modified Everett formula is used:

$$f(x) = \bar{\theta}\left[f_n + \frac{1}{6}(\bar{\theta}^2-1)(\delta^2 f_n - \mu\delta^4 f_n)\right] + \theta\left[f_{n+1} + \frac{1}{6}(\theta^2-1)(\delta^2 f_{n+1} - \mu\delta^4 f_{n+1})\right] \quad (A.4)$$

$$\bar{\theta} = 1 - \theta; \quad \mu = 0.184 \quad (A.5)$$

$$\delta^2 f_n = f_{n-1} - 2f_n + f_{n+1} \quad (A.6)$$

$$\delta^4 f_n = f_{n-2} - 4F_{n-1} + 6f_n - 4f_{n+1} + f_{n+2} \quad (A.7)$$

3. If $n = 1$ or $n = N-2$, the fourth differences $\delta^4 f_n$ lie outside the table; $\therefore$ μ is set to 0.

4. If $n < 0$, θ is replaced by $\theta^1 = n + \theta$ and $f(x) =$

$$\frac{(\theta^1-2)(\theta^1-1)}{2} f_0 - \theta^1(\theta^1-2)f_1 + \frac{\theta^1(\theta^1-1)}{2} f_2 \qquad (A.8)$$

5. If $n > N-1$, θ is replaced by $\theta^1 = 2+\theta-(N-2)$ and $f(x) =$

$$\frac{(\theta^1-2)(\theta^1-1)}{2} f_{N-2} - \theta^1(\theta^1-2)f_{N-1} + \frac{\theta^1(\theta^1-1)}{2} f_N \qquad (A.9)$$

A.2 TAR(N)

The name TAR(N) derives from Transmission, Absorption, and Reflection for N collisions. It solves the neutron transport equation in infinite slab geometry using a Gaussian quadrature method of numerical integration. Scattering is assumed to be isotropic in the laboratory system. It is coded largely in FORTRAN-II for the Fortran Monitor System as used by the IBM-7094 computer at the M.I.T. Computation Center. FAP-coded subroutines from the Share Library are:

1. SDA-3044, TAINT - Table Look Up and Interpolation,
2. SDA-3079, EXPI - Exponential Integrals,
3. SDA-1206, LEQ - Linear Equations Solution,
4. SDA-1124, MULLER - Polynomial Root Finder Subroutine.

Subroutines of TAR(N) perform the following functions:

1. QQQ: computes moments $\alpha_p(v)$ (Section 2.1.2),
2. WTS: computes Gaussian quadrature weights and abscissas which satisfy Equations (2.32),
3. EXN: evaluates the exponential integral functions $E_n(x)$,
4. TALLY: computes RT(k), RR(k), and tabulates all probabilities as a function of collision number, k,
5. QINT: selects number of steps to use in numerically evaluating the moments $\alpha_p(v)$.

Provision is made for using Gaussian quadratures of all

orders less than 40. Low order quadratures (3, 4, or 5) work satisfactorily for optical thicknesses less than about 5 mean free paths. Higher orders have not been tried. It is expected that the eight-figure accuracy of the code will limit its usefulness to low orders.

Input data to TAR(N) is given in the next section. The code is listed in Section A.2.2. Sample problem input/output is given in Section A.2.3 for a parallel neutron beam incident perpendicular to a slab for which $\Sigma_t L = 0.5$, $\Sigma_s/\Sigma_t = 0.8$. This problem was discussed in Section 3.1.2.

A.2.1 INPUT DATA FOR TAR(N)

Card 1: Format (4F10.5, 2F5.0, 4I5)

1. $c = \Sigma_s/\Sigma_t$ = mean number of secondaries per collision. Job terminates if $c \leq 0$.
2. SIGTT = $\Sigma_t L$ = optical thickness, mean free paths,
3. GMU = $\mu = \cos\theta$, where θ is the angle measured from the normal to the slab, for a parallel beam incident at angles θ. If SW1 > 0 set GMU = 1.0.
4. ERROR = convergence criterion. If $|T_n| / \sum_{i=1}^{n-1} T_i \leq$ ERROR then stop calculations and tabulate output. Otherwise, increment n and repeat for the next collision fluxes and probabilities. Usually, ERROR = .00010.
5. SW1 = switch describing neutron source. If SW1=0, the source is a parallel beam at angle $\cos^{-1}(GMU)$. The uncollided current inside the slab falls off as $\exp(-\Sigma_t x/\mu)$. If SW1 > 0, then the source angular distribution varies as $(GMU)^{SW1-1}$ and the uncollided current inside the slab as $E_{SW1}(\Sigma_t x)$.
6. SW2 = switch for flux interpolation. If ≤ 0, interpolate in flux table directly. If > 0, interpolate in table of logarithms of fluxes and exponentiate the result. Generally, direct interpolation is more accurate.
7. JJ = spare.

8. M = order of Gaussian quadrature.
9. N = Maximum number of collisions. Output is tabulated if n = N.
10. KK = Lagrangian interpolation order, used to find the k-th collision flux at an arbitrary point. If KK > 2M + 2, KK is automatically set to 2M + 2.

Card 2: Format (2I5,F10.5)

1. NSW = control switch. It operates as follows:
   <0, assume Gaussian quadrature weights and abscissas are in memory from a previous case,
   = 0, calculate new Gaussian quadrature weights and abscissas,
   >0, read from cards a previously calculated set of Gaussian quadrature weights and abscissas of order M = NSW.
2. MN = M + 1, if NSW > 0, for previously calculated set.
3. P = $\Sigma_t L$, if NSW > 0, for previously calculated set. The following set of Gaussian quadrature weights and abscissas are required only if NSW > 0. This set is punched automatically by TAR(N) upon completion of its calculation. Once obtained, it need not be recomputed. The first $3(M + 1)/5$ cards contain:
   1. A(K)=quadrature weight for integrand $E_2(\Sigma_t x)$,
   2. X(K) = quadrature abscissa for integrand $E_2(\Sigma_t x)$,
   3. XX(K) = $\Sigma_t L$ - X(K), K = 1...M + 1.

The next 4M/5 cards contain:

1. Y(K,J) = abscissa for calculation of flux at point X(J),
2. B(K,J) = quadrature weight for Y.
3. Z(K,J) = abscissa for calculation of flux at point XX(J),
4. G(K,J) = quadrature weight for Z.

For these parameters, K = 1...M and J = 1...M + 1.

A.2.2 LISTING OF TAR(N)

```
C       TAR(N)  TRANSMISSION ABSORPTION AND REFLECTION  FOR N COLLISIONS
        DIMENSION X(40),A(40),Y(40,40),B(40,40),Z(40,40),G(40,40),XX(40),
       1PHIT(40),  T(80),  AB(80),  R(80),PHI(40),PHIL(40),RT(40),RR(40),RA
       2B(40),NX(40),NXX(40),FB(80),XBAR(80),NLOC(80),PHB(40)
F       EXN
C       A P OLSON  AUGUST 1967
 1000 READ INPUT TAPE 4,100,C,SIGTT,GMU,ERROR,SW1,SW2,JJ,M,N,KK
  100 FORMAT(4F10.5,2F5.0,4I5)
        IF(C)1001,1001,1002
 1001 CALL EXIT
 1002 WRITE OUTPUT TAPE 2,101,C,SIGTT,GMU,ERROR,SW1,SW2,JJ,M,N,KK
  101 FORMAT(1H1,15H PROGRAM TAR(N),//,3H C=,F10.5,2X,6HSIGTT=,F10.5,2X,
      1  4HGMU=,F10.5,2X,6HERROR=,F10.5,2X,4HSW1=,F5.0,2X,4HSW2=,F5.0,2X,
      2   3HJJ=,I5,2X,2HM=,I2,2X,2HN=,I2,2X,3HKK=,I2)
        NK=KK
        L=2*M+2
        IF(NK-L)41,41,40
   40 NK=L
C       THESE ARE M MM SIGTT IF CARDS TO BE READ
   41 READ INPUT TAPE 4,104,NSW,MN,P
  104 FORMAT(2I5,F10.5)
C       LESS 0 MEANS REPEAT WITH NEW PARAMETERS USING MEMORY VALUES
C       =0 MEANS NEW CASE--CALCULATE WEIGHTS AND LOCATIONS
C       GREATER 0 MEANS INPUT PREVIOUSLY CALCULATED SET
        IF(NSW)1003,45,42
C       NOW READ WEIGHTS AND LOCATIONS
   42 M=NSW
        MM=MN
        SIGTT=P
        READ INPUT TAPE 4,105,(A(K),X(K),XX(K),K=1,MM)
  105 FORMAT(5E15.8)
        DO 43 K=1,M
        READ INPUT TAPE 4,105,(Y(K,J),B(K,J),Z(K,J),G(K,J),J=1,MM)
   43 CONTINUE
        WRITE OUTPUT TAPE 2,106,M,MM,SIGTT
  106 FORMAT(1H0,3H M=,I2,2X,3HMM=,I2,2X,6HSIGTT=,F10.5)
        GO TO 1003
C       CALC. MOMENTS T(I) FOR INTEGRAND E2(X) FROM 0 TO SIGTT
   45 M2=2*M
        K=2
        DO 20 I=1,M2
        L=I-1
        T(I)=QQQ(L,K,SIGTT,EXN)
   20 CONTINUE
        CALL WTS(T,M2,A,X,JJ)
C       WTS PROVIDES GAUSSIAN WEIGHTS A AND LOCATIONS X
        MM=M+1
        X(MM)=SIGTT
        DO 59 J=1,MM
   59 XX(J)=SIGTT-X(J)
C       NOW DO FOR INTEGRAND E1(W) OVER 0 TO TH AND 0 TO TH1
        DO 21 J=1,MM
        TH=X(J)
        TH1=XX(J)
        K=1
        DO 22 I=1,M2
        L=I-1
        T(I)=QQQ(L,K,TH,EXN)
```

```
      IF(J-MM)61,22,22
   61 R(I)=QQQ(L,K,TH1,EXN)
   22 CONTINUE
      CALL WTS(T,M2,RT,RR  ,JJ)
      IF(J-MM)91,92,92
   91 CALL WTS(R,M2,PHI,PHIL,JJ)
   92 DO 23 K=1,M
      Y(K,J)=TH-RR(K)
      B(K,J)=RT(K)
      IF(J-MM)93,99,99
   93 Z(K,J)=PHIL(K)+TH
      G(K,J)=PHI(K)
      GO TO 23
C     ONLY ONE SET FOR FLUX AT 0, SIGTT
   99 Z(K,J)=RR(K)
      G(K,J)=RT(K)
   23 CONTINUE
   21 CONTINUE
      WRITE OUTPUT TAPE 3,104,M,MM,SIGTT
      WRITE OUTPUT TAPE 3,105,(A(K),X(K),XX(K),K=1,MM)
      DO 44 K=1,M
      WRITE OUTPUT TAPE 3,105,(Y(K,J),B(K,J),Z(K,J),G(K,J),J=1,MM)
   44 CONTINUE
 1003 C2=C/2.
      M2=2*M
      MAX=2*M+2
      DO 70 J=1,M
      T(J)=X(J)
      L=J+M
      T(L)=XX(J)
      NLOC(J)=J
      NLOC(L)=L
   70 CONTINUE
      M1=2*M-1
   74 L=0
      DO 71 J=1,M1
      IF(T(J+1)-T(J))72,71,71
   72 P=T(J+1)
      T(J+1)=T(J)
      T(J)=P
      L=L+1
      K=NLOC(J+1)
      NLOC(J+1)=NLOC(J)
      NLOC(J)=K
   71 CONTINUE
      IF(L)75,75,74
   75 DO 76 J=1,M2
      XBAR(J+1)=T(J)
      K=NLOC(J)
      IF(K-M)77,77,78
   77 NX(K)=J+1
      GO TO 76
   78 L=K-M
      NXX(L)=J+1
   76 CONTINUE
      XBAR(1)=0.
      XBAR(MAX)=SIGTT
      N1=1
      MN=SW1+1.
      P=EXPF(-SIGTT/GMU)
C     THIS IS UNCOLLIDED TRANSMITTED CURRENT FOR A BEAM AT ANGLE THETA
```

```
C      NEUTRON LEAKAGE FROM SOURCE VARIES AS (COS THETA)**(SW1-1)
C         FOR SW1 POSITIVE
       IF(SW1)25,25,26
   26  P=EXN(MN,SIGTT)*SW1
   25  T(1)=P
       AB(2)=(1.-C)*(1.-P)
C      AB CONTAINS NEUTRON ABSORPTION PROBABILITIES AS FUNCTION OF
C        NUMBER OF COLLISIONS
       TOT=1.-P
C      R AND T CONTAIN REFLECTION AND TRANSMISSION PROBABILITES AS
C         FUNCTIONS OF COLLISION NUMBER
       R(1)=0.
       RR(1)=0.
       TT=T(1)
       AB(1)=0.
       RRR=0.
       ABS=AB(2)
       L=SW1
       DO 27 J=1,M
       PHI(J)=EXPF(-X(J)/GMU)
       PHB(J)=EXPF(-XX(J)/GMU)
       IF(SW1)28,28,29
   29  P=X(J)
       PHI(J)=EXN(L,P)*SW1
       P=XX(J)
       PHB(J)=EXN(L,P)*SW1
   28  K=NX(J)
       PHIL(K)=LOGF(PHI(J))
       FB(K)=PHI(J)
       PHIT(K)=PHI(J)
C      PHIT CONTAINS TOTAL FLUX FOR ALL NUMBERS OF COLLISIONS
       K=NXX(J)
       FB(K)=PHB(J)
       PHIT(K)=PHB(J)
       PHIL(K)=LOGF(PHB(J))
   27  CONTINUE
       P=0.
       FB(1)=EXN(L,P)*SW1
       FB(MAX)=EXN(L,SIGTT)*SW1
       IF(SW1)280,280,290
  280  FB(1)=1.
       FB(MAX)=EXPF(-SIGTT/GMU)
  290  PHIT(1)=FB(1)
       PHIT(MAX)=FB(MAX)
       PHIL(1)=LOGF(FB(1))
       PHIL(MAX)=LOGF(FB(MAX))
    5  WRITE OUTPUT TAPE 2,102,N1,R(N1),T(N1),AB(N1)
  102  FORMAT(1H0,3H N=,I5,5X,5HR(N)=,E13.6,5X,5HT(N)=,E13.6,5X,6HAB(N)=,
      1E13.6)
       WRITE OUTPUT TAPE 2,103,(J,XBAR(J),FB(J),PHIT(J),PHIL(J),J=1,MAX)
  103  FORMAT(I5,4E15.6)
       IF(GMU-1.)272,271,271
  272  IF(N1-1)270,270,271
  270  DO 273 J=1,MAX
       FB(J)=FB(J)/GMU
       PHIL(J)=LOGF(FB(J))
       IF(J-M)274,274,273
  274  PHI(J)=PHI(J)/GMU
       PHB(J)=PHB(J)/GMU
  273  CONTINUE
  271  Q=ABSF(T(N1)/TT)
```

```
C      DECIDE IF MORE COLLISIONS TO DO
       IF(Q-ERROR)4,4,10
   10  IF(N1-N)3,4,4
    3  N1=N1+1
       SUM1=0.
       SUM2=0.
       DO 8 J=1,M
       SUM1=SUM1+PHI(J)*A(J)
       SUM2=SUM2+PHB(J)*A(J)
    8  CONTINUE
       R(N1)=C2*SUM1
       T(N1)=C2*SUM2
       TOT=TOT-R(N1)-T(N1)-AB(N1)
       IF(TOT)81,82,82
   81  TOT=0.
   82  AB(N1+1)=(1.-C)*TOT
       RRR=RRR+R(N1)
       TT=TT+T(N1)
       ABS=ABS+AB(N1+1)
       DO 6 I=1,MM
       SUM1=0.
       SUM2=0.
       SUM3=0.
       SUM4=0.
       DO 7 J=1,M
       TH=Y(J,I)
       TH1=Z(J,I)
       TH2=SIGTT-TH
       TH3=SIGTT-TH1
       IF(I-MM)94,95,95
   95  TH2=TH
       TH3=TH1
   94  IF(SW2)33,33,34
   33  CALL TAINT(XBAR,  FB,TH ,P,MAX,NK,NERR,DMON)
       CALL TAINT(XBAR,  FB,TH1,Q,MAX,NK,NERR,DMON)
       CALL TAINT(XBAR,  FB,TH2,U,MAX,NK,NERR,DMON)
       CALL TAINT(XBAR,  FB,TH3,V,MAX,NK,NERR,DMON)
       GO TO 35
   34  CALL TAINT(XBAR,PHIL,TH ,P,MAX,NK,NERR,DMON)
       CALL TAINT(XBAR,PHIL,TH1,Q,MAX,NK,NERR,DMON)
       CALL TAINT(XBAR,PHIL,TH2,U,MAX,NK,NERR,DMON)
       CALL TAINT(XBAR,PHIL,TH3,V,MAX,NK,NERR,DMON)
       P=EXPF(P)
       Q=EXPF(Q)
       U=EXPF(U)
       V=EXPF(V)
   35  SUM1=SUM1+P*B(J,I)
       SUM2=SUM2+Q*G(J,I)
       SUM3=SUM3+U*B(J,I)
       SUM4=SUM4+V*G(J,I)
    7  CONTINUE
       IF(I-MM)96,97,97
   97  FB(1)=C2*SUM2
       FB(MAX)=C2*SUM1
       GO TO 6
   96  PHI(I)=C2*(SUM1+SUM2)
       PHB(I)=C2*(SUM3+SUM4)
    6  CONTINUE
C      UPDATE FLUXES
       DO 9 I=1,M
       L=NX(I)
```

```
      FB(L)=PHI(I)
      L=NXX(I)
      FB(L)=PHB(I)
    9 CONTINUE
      DO 85 I=1,MAX
      PHIL(I)=LOGF(FB(I))
      PHIT(I)=PHIT(I)+FB(I)
   85 CONTINUE
      GO TO 5
    4 ABS=ABS-AB(N1+1)
      CALL TALLY(T,R,RT,RR,AB,RAB,C2,TT,RRR,ABS,N1,M,MM,SIGTT,GMU)
      GO TO 1000
      END
*     LABEL
*     SUBROUTINE WTS
      SUBROUTINE WTS(T,M2,A,X,JJ)
C     CALCULATES GAUSSIAN QUADRATURE WEIGHTS AND ABSCISSAS FOR TAR(N)
C     QUADRATURE ORDER M NOT TO EXCEED 39
      DIMENSION A(40),X(40),C(40,40),R( 40),XX( 40),T( 80)
C     M2 MOMENTS ARE IN ARRAY T.  WTS GO IN A, AND LOCATIONS IN X
      CALL JOBTM(J1)
C     SUBROUTINE JOBTM GIVES RUNNING TIME
      M=M2/2
      DO 1 I=1,M
      K=I-1
      MI=M+I
      DO 2 J=1,M
      JK=J+K
      C(I,J)=T(JK)
    2 CONTINUE
      R(I)=-T(MI)
      R(MI)=0.
      WRITE OUTPUT TAPE 2,101,R(I),(C(I,J),J=1,M)
    1 CONTINUE
  101 FORMAT(1H0,E15.8,3X,(7E15.8))
      L=1
      I=40
      J=182
      K=M
      CALL JOBTM(J2)
      CALL LEQ(C,R,K,L,I,J,DET)
C     SUBROUTINE LEQ SOLVES A LINEAR MATRIX EQUATION AX=R AND PUTS
C     ANSWER VECTOR A IN R CONTAINS ABSCISSAS
      CALL JOBTM(J3)
C     COEFF. OF X**M IS 1.0 IN OUR POLYNOMIAL
      XX(1)=1.0
      DO 11 J=1,M
      M1=M+1-J
      XX(J+1)=R(M1)
   11 CONTINUE
      M1=M+1
      WRITE OUTPUT TAPE 2,102,(XX(J),J=1,M1)
  102 FORMAT(1H0,8E15.8)
C      NOW FIND RCOTS XX(J)
      K=M
      CALL JOBTM(J4)
C     SUBROUTINE MULLER EXTRACTS ROOTS OF A POLYNOMIAL
      CALL MULLER(XX,K,R,A)
      CALL JOBTM(J5)
      DO 12 J=1,M
      XX(J)=R(J)
```

```
   12 CONTINUE
      WRITE OUTPUT TAPE 2,102,(XX(J),J=1,M)
C     NOW PLACE ROOTS IN ASCENDING ORDER
      M1=M-1
    5 N=0
      DO 3 I=1,M1
      IF(XX(I+1)-XX(I))4,3,3
    4 AA=XX(I+1)
      XX(I+1)=XX(I)
      XX(I)=AA
      N=N+1
    3 CONTINUE
      IF(N)6,6,5
    6 DO 7 J=1,M
    7 C(1,J)=1.
      R(1)=T(1)
      R(M+1)=0.
      WRITE OUTPUT TAPE 2,102,(XX(J),J=1,M)
      WRITE OUTPUT TAPE 2,101,R(1),(C(1,J),J=1,M)
C     SET UP SECOND MATRIX EQUATION FOR LEQ
      DO 8 I=2,M
      MI=M+I
      DO 9 J=1,M
      C(I,J)=C(I-1,J)*XX(J)
    9 CONTINUE
      R(I)= T(I)
      R(MI)=0.
      WRITE OUTPUT TAPE 2,101,R(I),(C(I,J),J=1,M)
    8 CONTINUE
      I=40
      J=182
      K=M
      CALL LEQ(C,R,K,L,I,J,DET)
C     WTS ARE IN R
      WRITE OUTPUT TAPE 2,103
  103 FORMAT(1H4, 17H GAUSSIAN WEIGHTS,3X,9HLOCATIONS,5X,7HMOMENTS)
      DO 10 J=1,M
      MJ=M+J
      A(J)=R(J)
      X(J)=XX(J)
      WRITE OUTPUT TAPE 2,100, A(J),X(J),T(J),T(MJ)
   10 CONTINUE
  100 FORMAT(1H ,4E15.8)
      CALL JOBTM(J6)
      J6=J6-J1
      J5=J5-J4
      J4=J4-J3
      J3=J3-J2
      J2=J2-J1
      WRITE OUTPUT TAPE 2,104,J2,J3,J4,J5,J6
  104 FORMAT(1H ,5I10)
      RETURN
      END
*     LABEL
      FUNCTION QQQ(L,N,SIGTT,EXN)
D     DIMENSION X(11),W(11),DD(9)
C     21 POINT NUMERICAL INTEGRATION BY GAUSSIAN QUADRATURES
C     THIS SUBROUTINE OF TAR(N) EVALUATES MOMENTS OF EXPONENTIAL
C      INTEGRAL FUNCTIONS E(N).  N IS ARBITRARY.  L IS THE MOMENT
C       ORDER AND SIGTT IS THE OPTICAL THICKNESS(MFP).
      IF(SIGTT)5,5,6
```

```
    5 WRITE OUTPUT TAPE 2,100,SIGTT
  100 FORMAT(1HO,7H SIGTT=,E11.4)
      CALL EXIT
C     AN ERROR OCCURRED IF SIGTT NOT POSITIVE
    6 IF(X(11)-0.5)1,2,1
D   1 X(1)=.0021714184870960
D     X(2)=.0130467357414141
D     X(3)=.0349212543221459
D     X(4)=.0674683166555077
D     X(5)=.1095911367067916
D     X(6)=.1602952158504878
D     X(7)=.2186214326656977
D     X(8)=.2833023029353764
D     X(9)=.3528035686492699
D     X(10)=0.4255628305091844
D     X(11)=0.5
D     W( 1)=0.0058473194336859
D     W( 2)=0.0162790811539824
D     W( 3)=0.0273779482871760
D     W( 4)=0.0375198374054600
D     W( 5)=0.0465627272918488
D     W( 6)=0.0546935794011488
D     W( 7)=0.0617459881310329
D     W( 8)=0.0673546086557367
D     W( 9)=0.0713879692885300
D     W(10)=0.0738695524506692
D     W(11)=0.0373613885007292
    2 INT=QINT(L,SIGTT)
D     DD(1)=0.
      DD(2)=INT
      DD(4)=SIGTT/DD(2)
D     DD(2)=DD(4)
D     DD(9)=0.
      DO 7 J=1,INT
D     DD(3)=0.
      DO 8 K=1,11
D     DD(5)=DD(1)+DD(4)*X(K)
D     DD(6)=DD(2)-DD(4)*X(K)
      XP=DD(5)
      XM=DD(6)
      DD(7)=EXN(N,XP)
      DD(8)=EXN(N,XM)
D     DD(7)=DD(7)*DD(5)**L
D     DD(8)=DD(8)*DD(6)**L
D     DD(3)=DD(3)+(DD(7)+DD(8))*W(K)
    8 CONTINUE
D     DD(1)=DD(2)
D     DD(2)=DD(2)+DD(4)
D     DD(9)=DD(9)+DD(3)
    7 CONTINUE
D     DD(9)=DD(9)*DD(4)
      QQQ=DD(9)
      RETURN
      END
*     LABEL
      FUNCTION QINT(L,SIGTT)
C     SELECT NUMBER OF SUB-INTERVALS TO USE IN FINDING MOMENT L FOR
C      A SLAB OF OPTICAL THICKNESS SIGTT
      QINT=L
      QINT=QINT/3. + SIGTT/3. +1.
      RETURN
```

```
      END
*     LABEL
      FUNCTION EXN(M,XX)
C     FIND EXPONENTIAL INTEGRAL OF ORDER M EVALUATED AT XX
      N=M
      Z=1.
      X=ABSF(XX)
      IF(X-1.0E-10)7,8,8
    7 WRITE OUTPUT TAPE 2,9,X
    9 FORMAT(1H0,50H 1.0E-10 USED FOR ALL ARGUMENTS LESS THAN THIS. X=,
     1E15.8)
      X=1.0E-10
C     THE 1E-10 GETS AROUND LOGARITHMIC SINGULARITY IN E1
    8 W=EXPF(-X)
      E=-EXPIF(-X)
    4 IF(N-1)5,5,6
    5 EXN=E
      RETURN
C     USE RECURSION RELATION TO GET HIGHER ORDER EXPON. INTEGRALS
    6 E=(W-X*E)/Z
      Z=Z+1.
      N=N-1
      GO TO 4
      END
*     LABEL
*     SUBROUTINE TALLY
      SUBROUTINE TALLY(T,R,RT,RR,AB,RAB,C2,TT,RRR,ABS,N1,M,MM,SIGTT,GMU)
      DIMENSION T(80),R(80),RT(40),RR(40),AB(80),RAB(40)
C     COMPUTE RT(K) AND RR(K) ETC FOR TAR(N), AND TABULATE OUTPUT
      DO 9 J=3,N1
      L=J-1
      K=J-2
      RAB(K)=0.
      IF(AB(L))12,12,11
   11 RAB(K)=AB(J)/(AB(L)*C2)
   12 RT(K)=T(J)/(T(L)*C2)
      RR(K)=R(J)/(R(L)*C2)
    9 CONTINUE
      N=N1
      RAB(N-1)=C2
      RAB(N)=0.
      RT(N-1)=C2
      RT(N)=0.
      RR(N-1)=C2
      RR(N)=0.
      WRITE OUTPUT TAPE 2,106
  106 FORMAT(1H1,2H K,11X,4HT(K),11X,4HR(K),10X,5HAB(K),10X,5HRT(K),10X,
     15HRR(K),9X,6HRAB(K))
      WRITE OUTPUT TAPE 2,104,(K,T(K),R(K),AB(K),RT(K),RR(K),RAB(K),K=1,
     1N)
  104 FORMAT(1H0,I5,6E15.8)
      P=0.
      IF(AB(N-1))51,51,50
   50 P=AB(N)/AB(N-1)
      F1=AB(N)*P/(1.-P)
      ABS=ABS+F1
   51 P=R(N)/R(N-1)
      F2=R(N)*P/(1.-P)
      RRR=RRR+F2
      P=T(N)/T(N-1)
      F3=T(N)*P/(1.-P)
```

```
      TT=TT+F3
      P=TT+RRR+ABS
      WRITE OUTPUT TAPE 3,103,N,M,MM,SIGTT,GMU,P
  103 FORMAT(3I5,3F10.5)
      WRITE OUTPUT TAPE 3,102,(T(K),R(K),AB(K),K=1,N)
  102 FORMAT(5E15.8)
      WRITE OUTPUT TAPE 2,105,TT,F3,RRR,F2,ABS,F1,P
  105 FORMAT(1HO,19HTOTAL TRANSMISSION=,E15.8,26HINCLUDING EXTRAPOLATION
     1 OF,E15.8,/,18H TOTAL REFLECTION=,E15.8,26HINCLUDING EXTRAPOLATION
     2 OF,E15.8,/,18H TOTAL ABSORPTION=,E15.8,26HINCLUDING EXTRAPOLATION
     3 OF,E15.8,/,7H T+R+A=,E15.8)
      RETURN
      END
*     DATA
    .8          .5          1.          .0001     0.    0.     0     3    20     6
    0
              END OF FILE
```

A.2.3 SAMPLE PROBLEM FOR TAR(N)

```
 PROGRAM TAR(N)
C=     .80000  SIGTT=     .50000  GMU=    1.00000  ERROR=     .00010  SW1=    00  SW2=    00  OJ=     0  M= 3  N=20  KK= 6
 -.61849955E-02      .27839555E 00  .57288326E-01  .17401460E-01
 -.23897327E-02      .57288326E-01  .17401460E-01  .61849955E-02
 -.97194329E-03      .17401460E-01  .61849955E-02  .23897327E-02
  .10000000E 01 -.71533098E 00  .13288262E 00 -.48485519E-02
  .23107859E 00  .43614380E 00  .48108592E-01
  .48108592E-01  .23107859E 00  .43614380E 00
  .27839555E 00      .10000000E 01  .10000000E 01  .10000000E 01
  .57288326E-01      .48108592E-01  .23107859E 00  .43614380E 00
  .17401460E-01      .23144366E-02  .53397313E-01  .19022141E 00

 GAUSSIAN WEIGHTS   LOCATIONS      MOMENTS
  .10190429E 00  .48108592E-01  .27839555E 00  .61849955E-02
  .11991168E 00  .23107859E 00  .57288326E-01  .23897327E-02
  .56579579E-01  .43614380E 00  .17401460E-01  .97194329E-03
         2          1          0          3          13

 -.36762239E-05      .16742214E 00  .34587693E-02  .10489187E-03

 -.13899062E-06      .34587693E-02  .10489187E-03  .36762239E-05

 -.55056519E-08      .10489187E-03  .36762239E-05  .13899062E-06

  .10000000E 01 -.69281862E-01  .12417629E-02 -.42054867E-05

  .43968750E-02  .42242680E-01  .22642308E-01

  .43968750E-02  .22642308E-01  .42242680E-01

  .16742214E 00      .10000000E 01  .10000000E 01  .10000000E 01

  .34587693E-02      .43968750E-02  .22642308E-01  .42242680E-01

  .10489187E-03      .19332510E-04  .51267409E-03  .17844440E-02
```

```
GAUSSIAN WEIGHTS    LOCATIONS       MOMENTS
 .58802959E-01   .43968750E-02   .16742214E 00   .36762239E-05
 .70822401E-01   .22642308E-01   .34587693E-02   .13899062E-06
 .37796785E-01   .42242680E-01   .10489187E-03   .55056519E-08
       0           0           0           0          12

-.83118789E-02      .64456547E 00   .10156668E 00   .26487326E-01

-.28649721E-02      .10156668E 00   .26487326E-01   .83118789E-02

-.10445325E-02      .26487326E-01   .83118789E-02   .28649721E-02

 .10000000E 01 -.62273575E 00   .97466496E-01 -.26632239E-02

 .19748594E 00   .39073642E 00   .34513389E-01

 .34513389E-01   .19748594E 00   .39073642E 00

 .64456547E 00      .10000000E 01   .10000000E 01   .10000000E 01

 .10156668E 00      .34513389E-01   .19748594E 00   .39073642E 00

 .26487326E-01      .11911740E-02   .39000697E-01   .15267495E 00
```

```
GAUSSIAN WEIGHTS    LOCATIONS       MOMENTS
 .28389490E 00   .34513389E-01   .64456547E 00   .83118789E-02
 .25437777E 00   .19748594E 00   .10156668E 00   .28649721E-02
 .10629279E 00   .39073642E 00   .26487326E-01   .10445325E-02
       0           0           0          12          12

-.93673044E-03      .46173739E 00   .40993779E-01   .57036702E-02

-.16751386E-03      .40993779E-01   .57036702E-02   .93673044E-03

-.31539759E-04      .57036702E-02   .93673044E-03   .16751386E-03

 .10000000E 01 -.32479608E 00   .26851566E-01 -.40054772E-03

 .19048805E-01   .20127718E 00   .10447009E 00

 .19048805E-01   .10447009E 00   .20127718E 00

 .46173739E 00      .10000000E 01   .10000000E 01   .10000000E 01

 .40993779E-01      .19048805E-01   .10447009E 00   .20127718E 00

 .57036702E-02      .36285697E-03   .10914000E-01   .40512503E-01
```

```
GAUSSIAN WEIGHTS    LOCATIONS       MOMENTS
 .18495812E 00   .19048805E-01   .46173739E 00   .93673044E-03
 .18840358E 00   .10447009E 00   .40993779E-01   .16751386E-03
 .88375682E-01   .20127718E 00   .57036702E-02   .31539759E-04
       0             0              0              12

-.15556571E-02      .50125892E 00   .50868156E-01   .81734641E-02

-.32290983E-03      .50868156E-01   .81734641E-02   .15556571E-02

-.70628826E-04      .81734641E-02   .15556571E-02   .32290983E-03

 .10000000E 01 -.37657800E 00   .36008515E-01 -.61724024E-03

 .21840914E-01   .23392707E 00   .12081002E 00

 .21840914E-01   .12081002E 00   .23392707E 00

 .50125892E 00      .10000000E 01   .10000000E 01   .10000000E 01

 .50868156E-01      .21840914E-01   .12081002E 00   .23392707E 00

 .81734641E-02      .47702551E-03   .14595060E-01   .54721875E-01
```

```
GAUSSIAN WEIGHTS    LOCATIONS       MOMENTS
 .20460182E 00   .21840914E-01   .50125892E 00   .15556571E-02
 .20329970E 00   .12081002E 00   .50868156E-01   .32290983E-03
 .93357408E-01   .23392707E 00   .81734641E-02   .70628826E-04
       0             0              0              12

-.74379800E-02      .63459589E 00   .97134501E-01   .24519367E-01

-.24768648E-02      .97134501E-01   .24519367E-01   .74379800E-02

-.87215206E-03      .24519367E-01   .74379800E-02   .24768648E-02

 .10000000E 01 -.60180845E 00   .91099829E-01 -.24124868E-02

 .19102990E 00   .37730760E 00   .33470951E-01

 .33470951E-01   .19102990E 00   .37730760E 00

 .63459589E 00      .10000000E 01   .10000000E 01   .10000000E 01

 .97134501E-01      .33470951E-01   .19102990E 00   .37730760E 00

 .24519367E-01      .11203046E-02   .36492423E-01   .14236102E 00
```

```
GAUSSIAN WEIGHTS    LOCATIONS       MOMENTS
 .27787919E 00   .33470951E-01   .63459589E 00   .74379800E-02
 .25101396E 00   .19102990E 00   .97134501E-01   .24768648E-02
 .10570274E 00   .37730760E 00   .24519367E-01   .87215206E-03
       12            0               0              24

-.10285091E-04      .20463641E 00   .55373464E-02   .22171674E-03

-.51523798E-06      .55373464E-02   .22171674E-03   .10285091E-04

-.27057736E-07      .22171674E-03   .10285091E-04   .51523798E-06

 .10000000E 01 -.91681494E-01   .21699913E-02 -.96452158E-05

 .57573092E-02   .56017441E-01   .29906743E-01

 .57573092E-02   .29906743E-01   .56017441E-01

 .20463641E 00      .10000000E 01   .10000000E 01   .10000000E 01

 .55373464E-02      .57573092E-02   .29906743E-01   .56017441E-01

 .22171674E-03      .33146609E-04   .89441326E-03   .31379537E-02
```

```
GAUSSIAN WEIGHTS    LOCATIONS       MOMENTS
 .73121906E-01   .57573092E-02   .20463641E 00   .10285091E-04
 .86200108E-01   .29906743E-01   .55373464E-02   .51523798E-06
 .45314398E-01   .56017441E-01   .22171674E-03   .27057736E-07
       0               0               0              12

-.11373896E-01      .67292938E 00   .11507379E 00   .32915684E-01

-.43247399E-02      .11507379E 00   .32915684E-01   .11373896E-01

-.17410424E-02      .32915684E-01   .11373896E-01   .43247399E-02

 .10000000E 01 -.68638166E 00   .11812033E 00 -.35274548E-02

 .21705046E 00   .43168379E 00   .37647401E-01

 .37647401E-01   .21705046E 00   .43168379E 00

 .67292938E 00      .10000000E 01   .10000000E 01   .10000000E 01

 .11507379E 00      .37647401E-01   .21705046E 00   .43168379E 00

 .32915684E-01      .14173268E-02   .47110903E-01   .18635090E 00
```

```
GAUSSIAN WEIGHTS    LOCATIONS      MOMENTS
 .30152139E 00   .37647401E-01   .67292938E 00   .11373896E-01
 .26374521E 00   .21705046E 00   .11507379E 00   .43247399E-02
 .10766278E 00   .43168379E 00   .32915684E-01   .17410424E-02
        3            0             1             3            14

1.0E-10 USED FOR ALL ARGUMENTS LESS THAN THIS. X=  .00000000E 00

N=     1     R(N)=  .000000E 00     T(N)=  .606531E 00     AB(N)=  .000000E 00
   1    .000000E 00    .100000E 01    .100000E 01   -.000000E 00
   2    .481086E-01    .953030E 00    .953030E 00   -.481086E-01
   3    .638562E-01    .938140E 00    .938140E 00   -.638562E-01
   4    .231079E 00    .793677E 00    .793677E 00   -.231079E 00
   5    .268921E 00    .764203E 00    .764203E 00   -.268921E 00
   6    .436144E 00    .646525E 00    .646525E 00   -.436144E 00
   7    .451891E 00    .636423E 00    .636423E 00   -.451891E 00
   8    .500000E 00    .606531E 00    .606531E 00   -.500000E 00

N=     2     R(N)=  .915476E-01     T(N)=  .838283E-01     AB(N)=  .786939E-01
   1    .000000E 00    .229034E 00    .122903E 01   -.147389E 01
   2    .481086E-01    .276723E 00    .122975E 01   -.128474E 01
   3    .638562E-01    .284768E 00    .122291E 01   -.125608E 01
   4    .231079E 00    .304765E 00    .109844E 01   -.118821E 01
   5    .268921E 00    .299547E 00    .106375E 01   -.120548E 01
   6    .436144E 00    .244270E 00    .890794E 00   -.140948E 01
   7    .451891E 00    .235452E 00    .871876E 00   -.144625E 01
   8    .500000E 00    .195679E 00    .802210E 00   -.163128E 01

N=     3     R(N)=  .314259E-01     T(N)=  .304100E-01     AB(N)=  .278799E-01
   1    .000000E 00    .754169E-01    .130445E 01   -.258472E 01
   2    .481086E-01    .916933E-01    .132145E 01   -.238931E 01
   3    .638562E-01    .952051E-01    .131811E 01   -.235172E 01
   4    .231079E 00    .110478E 00    .120892E 01   -.220294E 01
   5    .268921E 00    .109684E 00    .117343E 01   -.221015E 01
   6    .436144E 00    .897983E-01    .980593E 00   -.241019E 01
   7    .451891E 00    .863029E-01    .958179E 00   -.244989E 01
   8    .500000E 00    .712448E-01    .873455E 00   -.264163E 01

N=     4     R(N)=  .110689E-01     T(N)=  .109335E-01     AB(N)=  .993675E-02
   1    .000000E 00    .262802E-01    .133073E 01   -.363894E 01
   2    .481086E-01    .319546E-01    .135340E 01   -.344344E 01
   3    .638562E-01    .332437E-01    .135136E 01   -.340389E 01
   4    .231079E 00    .395991E-01    .124852E 01   -.322895E 01
   5    .268921E 00    .394848E-01    .121292E 01   -.323184E 01
   6    .436144E 00    .325112E-01    .101310E 01   -.342617E 01
   7    .451891E 00    .312314E-01    .989410E 00   -.346633E 01
   8    .500000E 00    .257298E-01    .899185E 00   -.366010E 01

N=     5     R(N)=  .393767E-02     T(N)=  .391929E-02     AB(N)=  .354892E-02
   1    .000000E 00    .931620E-02    .134005E 01   -.467600E 01
   2    .481086E-01    .113228E-01    .136472E 01   -.448093E 01
   3    .638562E-01    .117849E-01    .136314E 01   -.444094E 01
   4    .231079E 00    .141584E-01    .126268E 01   -.425745E 01
   5    .268921E 00    .141423E-01    .122706E 01   -.425858E 01
   6    .436144E 00    .116849E-01    .102479E 01   -.444946E 01
   7    .451891E 00    .112246E-01    .100063E 01   -.448965E 01
   8    .500000E 00    .924185E-02    .908427E 00   -.468401E 01

N=     6     R(N)=  .140509E-02     T(N)=  .140258E-02     AB(N)=  .126774E-02
```

1	.000000E 00	.332033E-02	.134337E 01	-.570769E 01
2	.481086E-01	.403460E-02	.136876E 01	-.551285E 01
3	.638562E-01	.419971E-02	.136734E 01	-.547274E 01
4	.231079E 00	.506014E-02	.126774E 01	-.528636E 01
5	.268921E 00	.505791E-02	.123212E 01	-.528680E 01
6	.436144E 00	.418602E-02	.102897E 01	-.547600E 01
7	.451891E 00	.402117E-02	.100466E 01	-.551618E 01
8	.500000E 00	.331019E-02	.911737E 00	-.571075E 01

N= 7 R(N)= .501903E-03 T(N)= .501558E-03 AB(N)= .452661E-03

1	.000000E 00	.118552E-02	.134455E 01	-.673757E 01
2	.481086E-01	.144042E-02	.137020E 01	-.654282E 01
3	.638562E-01	.149941E-02	.136884E 01	-.650268E 01
4	.231079E 00	.180844E-02	.126955E 01	-.631529E 01
5	.268921E 00	.180814E-02	.123393E 01	-.631546E 01
6	.436144E 00	.149754E-02	.103047E 01	-.650393E 01
7	.451891E 00	.143858E-02	.100609E 01	-.654410E 01
8	.500000E 00	.118413E-02	.912921E 00	-.673875E 01

N= 8 R(N)= .179347E-03 T(N)= .179300E-03 AB(N)= .161437E-03

1	.000000E 00	.423561E-03	.134498E 01	-.776681E 01
2	.481086E-01	.514613E-03	.137071E 01	-.757210E 01
3	.638562E-01	.535694E-03	.136938E 01	-.753195E 01
4	.231079E 00	.646338E-03	.127019E 01	-.734419E 01
5	.268921E 00	.646296E-03	.123457E 01	-.734425E 01
6	.436144E 00	.535437E-03	.103101E 01	-.753243E 01
7	.451891E 00	.514360E-03	.100661E 01	-.757259E 01
8	.500000E 00	.423370E-03	.913344E 00	-.776726E 01

N= 9 R(N)= .640958E-04 T(N)= .640893E-04 AB(N)= .574199E-04

1	.000000E 00	.151365E-03	.134513E 01	-.879582E 01
2	.481086E-01	.183901E-03	.137090E 01	-.860111E 01
3	.638562E-01	.191435E-03	.136957E 01	-.856096E 01
4	.231079E 00	.231006E-03	.127042E 01	-.837307E 01
5	.268921E 00	.231000E-03	.123481E 01	-.837309E 01
6	.436144E 00	.191400E-03	.103120E 01	-.856114E 01
7	.451891E 00	.183866E-03	.100679E 01	-.860130E 01
8	.500000E 00	.151339E-03	.913496E 00	-.879599E 01

K	T(K)	R(K)	AB(K)	RT(K)	RR(K)	RAB(K)
1	.60653067E 00	.00000000E 00	.00000000E 00	.90691205E 00	.85818443E 00	.88570768E 00
2	.83828290E-01	.91547648E-01	.78693867E-01	.89884098E 00	.88055713E 00	.89103171E 00
3	.30409954E-01	.31425906E-01	.27879905E-01	.89616621E 00	.88935333E 00	.89287726E 00
4	.10933485E-01	.11068922E-01	.99367518E-02	.89466358E 00	.89208245E 00	.89304893E 00
5	.39192879E-02	.39376732E-02	.35489199E-02	.89399326E 00	.89300697E 00	.89265099E 00
6	.14025776E-02	.14050916E-02	.12677436E-02	.89371547E 00	.89333750E 00	.89159816E 00
7	.50155798E-03	.50190265E-03	.45266104E-03	.89360459E 00	.89345920E 00	.88920103E 00
8	.17930005E-03	.17934738E-03	.16143670E-03	.40000000E 00	.40000000E 00	.40000000E 00
9	.64089339E-04	.64095826E-04	.57419871E-04	.00000000E 00	.00000000E 00	.00000000E 00

TOTAL TRANSMISSION= .73780482E 00INCLUDING EXTRAPOLATION OF .35651575E-04
TOTAL REFLECTION= .14016623E 00INCLUDING EXTRAPOLATION OF .35646156E-04
TOTAL ABSORPTION= .12203040E 00INCLUDING EXTRAPOLATION OF .31697194E-04
T+R+A= .10000014E 01

A.3 LPF

LPF is an acronym for Legendre Polynomial Fits. Its purpose is to use tabulated differential angular scattering cross sections $\sigma_s(E,\mu)$ to evaluate the coefficients $F_n(E)$ of the following expansion:

$$\sigma_s(E,\mu) = \frac{\sigma_s(E)}{4\pi} \sum_{n=0}^{N} (2n + 1) F_n(E) P_n(\mu) \qquad (A.10)$$

where μ is the cosine of the scattering angle in the center of mass system and $\sigma_s(E)$ is the total (integrated over all solid angles) scattering cross section at energy E. Orthogonality of the legendre polynomials $P_n(\mu)$ gives the relations desired from the moments A_n:

$$A_n = \int_{-1}^{1} d\mu \, P_n(\mu) \, \sigma_s(E, \mu), \quad n = 0, 1, \ldots N$$

$$\sigma_s(E) = 2\pi A_0, \quad \text{with} \quad F_0(E) = 1.$$

$$F_n(E) = A_n/A_0 \qquad (A.11)$$

Subroutine QQQQQ, which numerically evaluates A_n, uses a 21-point Gaussian quadrature approximation for the integral. Provision has been made for subroutine QINT to choose the number of sub-intervals to use in evaluating the integral.

The $P_n(\mu)$ are evaluated by subroutine PLN using the recursion relation:

$$(n + 1)P_{n+1}(\mu) = \mu(2n + 1)\ P_n(\mu) - nP_{n-1}(\mu) \qquad (A.12)$$

starting with

$$P_0(\mu) = 1 \quad \text{and} \quad P_1(\mu) = \mu.$$

A test of PLN showed it to be accurate to seven decimal places for $n < 9$, and to have an error no larger than a digit in the seventh place for $n = 10$.

Numerical interpolation with the TAINT[15] subroutine provides $\sigma_s(E, \mu)$ at the nodes used by the quadrature formula.

An idea of the accuracy of the fit (Equation (A.10)) is provided by computing the root mean square percentage error evaluated at the tabulated μ-values. This is done for all N from one to nine.

Input data to LPF is given in the next Section. The code is listed in Section A.3.2. Sample input/output for deuterium is listed in Section A.3.3.

A.3.1 INPUT DATA FOR LPF

Card 1: Format (I5, A5, 3I5)

1. NE = number of E-values in tables of $\sigma_s(E, \mu)$. Job terminates if NE ≤ 0.
2. ISO = alphanumeric label for isotope.
3. N = order of highest Legendre polynomial in fit.
4. NT = order of numerical interpolation.
5. ITEST = output control digit. If > 0, output L, MM, NT during calculation of each moment, A_L. MM is the number of μ-values for that particular energy. The number of moments and coefficients evaluated is given by the least of MM or NI, where NI is the number of μ-values at which $\sigma_s(E, \mu)$ is tabulated.

Card 2: Format (8(F7.3, I3))

I E(I) = energy-value in table of $\sigma_s(E, \mu)$, MeV.

I + 1. NI(I) = number of μ-values at energy E(I).

For each energy E(I), I = 1...NE, the following is required:

Sufficient cards to contain NI(I) table pairs in Format (4(F10.5, E10.3)) of:

X(J,I) = J-th μ-value for energy E(I).

FX(J,I) = angular scattering cross section $\sigma_s(E(I), \mu_J)$, barns/steradian.

Other isotopes may be processes at the same time by placing data sets together. A final blank card (NE = 0) will terminate the job.

A.3.2 LISTING OF LPF

```
C      LPF -- LEGENDRE POLYNOMIAL FITTING TO ANGULAR SCATTERING CROSS
C         SECTIONS
C          ROUTINE FINDS BEST FIT IN LEAST SQUARES SENSE
       DIMENSION X(50,50),FX(50,50),XX(50),FFX(50),F(50,10),NI(50),E(50),
      1NM(10),RMS(10)
F      TAINT,PLN
   100 READ INPUT TAPE 4,20,NE,ISO,N,NT,ITEST
    20 FORMAT(I5,A5,3I5)
       IF(NE)101,101,102
   102 WRITE OUTPUT TAPE 2,21,NE,ISO,N,NT,ITEST
    21 FORMAT(1H1,4H NE=,I2,2X,8HISOTOPE=,A5,2X,2HN=,I2,2X,3HNT=,I2,2X,
      1  6HITEST=,I2)
       READ INPUT TAPE 4,22,(E(I),NI(I),I=1,NE)
       WRITE OUTPUT TAPE 2,23,(E(I),NI(I),I=1,NE)
    22 FORMAT(8(F7.3,I3))
    23 FORMAT(1HO,9H E, NI(I),/,(8(F7.3,I3)))
       DO 1 I=1,NE
       M=NI(I)
       READ INPUT TAPE 4,  24,(X(J,I),FX(J,I),J=1,M)
       WRITE OUTPUT TAPE 2,25,(X(J,I),FX(J,I),J=1,M)
     1 CONTINUE
    24 FORMAT(4(F10.5,E10.3))
    25 FORMAT(7H MU(CM),5X,15HDIFF. X-SECTION,/,(4(F10.5,E10.3)))
C      BEGIN POLYNOMIAL FITTING FOR EACH ENERGY
       DO 2 I=1,NE
       WRITE OUTPUT TAPE 2,26
    26 FORMAT(1H4,5H E(I),2X, 8HSIG(E,C),10X,7HF1...F9)
       DO 5 J=1,10
     5 F(I,J)=0.
       MM=NI(I)
       DO 3 J=1,MM
       XX(J)=X(J,I)
       FFX(J)=FX(J,I)
     3 CONTINUE
       M1=MM
       M=XMINOF(M1,N) + 1
C       FIT ONLY M   COEFFS IF M DATA POINTS, FOR M LESS N
       DO 4 L1=1,M
       L=L1-1
       IF(ITEST)30,30,31
    31 WRITE OUTPUT TAPE 2,32,L,MM,NT
    32 FORMAT(1H ,3I5)
    30 F(I,L1)=QQQQQ(PLN,XX,FFX,L,TAINT,MM,NT,ITEST)
       IF(L)4,4,6
     6 IF(F(I,1))13,13,12
    13 WRITE OUTPUT TAPE 2,29
    29 FORMAT(1H4,29H TOTAL X-SECTION NOT POSITIVE)
       F(I,1)=1.
       GO TO 4
    12 F(I,L1)=F(I,L1)/F(I,1)
     4 CONTINUE
       F(I,1)=F(I,1)*6.2831853
       WRITE OUTPUT TAPE 2,27,E(I),(F(I,L),L=1,10)
    27 FORMAT(1HO,F7.3,3X,10E10.3)
C      NOW FIND ERRORS IN FIT AND CHOOSE BEST NUMBER OF TERMS TO USE
       M=M-1
       DO 40 M1=1,M
```

```
      S=0.
      DO 7 J=1,MM
      SUM=0.
      W=XX(J)
      DO 8 L=1,M1
      V=2*L+1
    8 SUM=SUM+F(I,L+1)*PLN(L,W)*V
      SUM=0.25*F(I,1)*(1.+SUM)/3.1415927
      FFX(J)=100.*(FX(J,I)-SUM)/FX(J,I)
      S=S+FFX(J)**2.
    7 CONTINUE
      NM(M1)=M1
      RMS(M1)=SQRTF(S)
   40 CONTINUE
      WRITE OUTPUT TAPE 2,28,(NM(M1),M1=1,M)
      WRITE OUTPUT TAPE 2,41,(RMS(M1),M1=1,M)
   28 FORMAT(11H FIT ORDER=,10(5X,I5))
   41 FORMAT(11H RMS(PCT.)=,10F10.2)
    2 CONTINUE
      GO TO 100
  101 CALL EXIT
      END
*     LABEL
      FUNCTION QQQQQ(PLN,XX,FFX,L,TAINT,MM,NT,ITEST)
D     DIMENSION X(11),W(11),DD(11)
      DIMENSION XX(50),FFX(50)
      IF(L)5,6,6
    5 WRITE OUTPUT TAPE 2,100,L
  100 FORMAT(1H0,3H L=,I3)
      CALL EXIT
    6.IF(X(11)-0.5)1,2,1
D   1 X(1)=.0021714184870960
D     X(2)=.0130467357414141
D     X(3)=.0349212543221459
D     X(4)=.0674683166555077
D     X(5)=.1095911367067916
D     X(6)=.1602952158504878
D     X(7)=.2186214326656977
D     X(8)=.2833023029353764
D     X(9)=.3528035686492699
D     X(10)=0.4255628305091844
D     X(11)=0.5
D     W( 1)=0.0058473194336859
D     W( 2)=0.0162790811539824
D     W( 3)=0.0273779482871760
D     W( 4)=0.0375198374054600
D     W( 5)=0.0465627272918488
D     W( 6)=0.0546935794011488
D     W( 7)=0.0617459881310329
D     W( 8)=0.0673546086557367
D     W( 9)=0.0713879692885300
D     W(10)=0.0738695524506692
D     W(11)=0.0373613885007292
    2 INT=QINT(L)
      DMON=0.
D     DD(1)=-1.
      DD(2)=INT
      DD(4)=2./DD(2)
D     DD(2)=-1.+DD(4)
D     DD(9)=0.
      NN=NT
```

```
      IF(NT-MM)14,14,15
   15 NN=MM
   14 DO 7 J=1,INT
D     DD(3)=0.
      DO 8 K=1,11
D     DD(5)=DD(1)+DD(4)*X(K)
D     DD(6)=DD(2)-DD(4)*X(K)
      XP=DD(5)
      XM=DD(6)
      DD(7)=PLN(L,XP)
      DD(8)=PLN(L,XM)
      CALL TAINT(XX,FFX,XP,FXP,MM,NN,NERR,DMON)
      IF(NERR-1)10,11,10
   11 CALL TAINT(XX,FFX,XM,FXM,MM,NN,NERR,DMON)
      IF(NERR-1)10,12,10
   10 WRITE OUTPUT TAPE 2,13,NERR
   13 FORMAT(1H4,6H NERR=,I2)
      CALL EXIT
   12 DD(10)=FXP
      DD(11)=FXM
D     DD(7)=DD(7)*DD(10)
D     DD(8)=DD(8)*DD(11)
D     DD(3)=DD(3)+(DD(7)+DD(8))*W(K)
    8 CONTINUE
D     DD(1)=DD(2)
D     DD(2)=DD(2)+DD(4)
D     DD(9)=DD(9)+DD(3)
    7 CONTINUE
D     DD(9)=DD(9)*DD(4)
      QQQQQ=DD(9)
      IF(ITEST)20,20,21
   21 WRITE OUTPUT TAPE 2,18,QQQQQ
   18 FORMAT(1H ,E15.8)
   20 QQQQQ=DD(9)
      RETURN
      END
*     LABEL
      FUNCTION QINT(L)
      QINT=1.
      RETURN
      END
*     LABEL
      FUNCTION PLN(L,X)
D     DIMENSION DD(5)
      IF(L-1)1,2,3
    1 PLN=1.
      RETURN
    2 PLN=X
      RETURN
    3 DD(1)=X
D     DD(2)=1.
      DD(4)=X
      M=L-1
      DO 5 I=1,M
      DD(3)=I
D     DD(5)=((2.*DD(3)+1.)*DD(4)*DD(1) - DD(3)*DD(2))/(DD(3)+1.)
D     DD(2)=DD(1)
D     DD(1)=DD(5)
    5 CONTINUE
      PLN=DD(5)
      RETURN
      END
                ENC OF FILE
```

A.3.3 SAMPLE PROBLEM FOR LPF

```
*      DATA
   11    D      9     5
 14.1    18    .1     6    .2     11    .5    14    .75   11    1.    14    1.95   14    2.45   14
  3.27   15   4.5    14   5.5     15
   1.          .125E          .8          .100E          .6          .775E-01       .4          .584E-01
    .2         .041E          .0          .028E         -.2          .018E         -.3          .144E-01
   -.4         .012E         -.5          .107E-01      -.6          .107E-01      -.7          .014E
   -.75        .018E         -.8          .027E         -.85         .425E-01      -.9          .061E
   -.95        .087E        -1.           .118E          .            .    E        .            .    E
  -1.        +0.310E+00     -.6        +0.290E+00       -.2        +0.270E+00      0.2        +0.255E+00
   0.6       +0.242E+00      1.         +0.235E+00
 -1.         +0.380E+00     -.8        +0.352E+00       -.6        +0.324E+00      -.4        +0.297E+00
   -.2       +0.271E+00      0.         +0.249E+00        .2        +0.228E+00      .4         +0.210E+00
    .6       +0.190E+00       .8       +0.177E+00       1.         +0.161E+00
   1.00       0.093E+00      0.8          .114E 00       0.6          .135E          0.4          .158E
    .2          .180E         0.          .203E         -.2          .231E         -.4          .268E
   -.5          .292E        -.6          .325E         -.7          .370E         -.8          .437E
   -.9          .523E       -1.           .647E          .            .    E        .            .    E
   1.           .125E         .8          .135E          .6          .147E          .4          .160E
    .2          .177E         0.          .201E         -.2          .230E         -.4          .262E
   -.6          .296E        -.8          .333E        -1.           .370E          .            .    E
   1.           .140E         .8          .140E          .6          .140E          .4          .146E
    .2          .157E         .0          .172E         -.2          .196E         -.4          .237E
   -.5          .263E        -.6          .300E         -.7          .345E         -.8          .414E
   -.9          .517E       -1.           .675E          .            .    E        .            .    E
   1.           .227E         .8          .196E          .6          .170E          .4          .152E
    .2          .140E         .0          .136E         -.2          .141E         -.4          .163E
   -.5          .180E        -.6          .205E         -.7          .252E         -.8          .320E
   -.9          .425E       -1.           .640E          .            .    E        .            .    E
   1.           .325E         .8          .261E          .6          .207E          .4          .162E
    .2          .133E         .0          .117E         -.2          .116E         -.4          .129E
   -.5          .143E        -.6          .167E         -.7          .202E         -.8          .265E
   -.9          .335E       -1.           .425E          .            .    E        .            .    E
   1.           .310E         .8          .252E          .6          .200E          .4          .158E
    .2          .123E         .0          .100E         -.2          .088E         -.3          .088E
   -.4          .094E        -.5          .107E         -.6          .130E         -.7          .170E
   -.8          .230E        -.9          .296E        -1.           .380E          .            .    E
   1.           .295E         .8          .233E          .6          .178E          .4          .131E
    .2          .092E         .0          .061E         -.2          .042E         -.4          .044E
   -.5          .054E        -.6          .073E         -.7          .100E         -.8          .136E
```

```
-.9      .185E     -1.      .270E      .       .  E       .       .  E
1.       .340E       .8     .264E      .6     .197E       .4     .143E
 .2      .095E       .0     .060E     -.2     .042E      -.3     .040E
-.4      .042E      -.5     .050E     -.6     .065E      -.7     .088E
-.8      .125E      -.9     .170E    -1.      .230E       .      .  E
 0
```

END OF FILE

```
 NE=11  ISOTOPE=    D    N= 9  NT= 5  ITEST= 0

 E, NI(I)
14.100 18   .100  6   .200 11   .500 14   .750 11  1.000 14  1.950 14  2.450 14
 3.270 15  4.500 14  5.500 15
MU(CM)     DIFF. X-SECTION
  1.00000  .125E 00    .80000 1.000E-01    .60000  .775E-01    .40000  .584E-01
   .20000  .410E-01   0.       .280E-01   -.20000  .180E-01   -.30000  .144E-01
  -.40000  .120E-01   -.50000  .107E-01   -.60000  .107E-01   -.70000  .140E-01
  -.75000  .180E-01   -.80000  .270E-01   -.85000  .425E-01   -.90000  .610E-01
  -.95000  .870E-01  -1.00000  .118E 00
MU(CM)     DIFF. X-SECTION
 -1.00000  .310E 00   -.60000  .290E 00   -.20000  .270E 00    .20000  .255E 00
   .60000  .242E 00   1.00000  .235E 00
MU(CM)     DIFF. X-SECTION
 -1.00000  .380E 00   -.80000  .352E 00   -.60000  .324E 00   -.40000  .297E 00
  -.20000  .271E 00   0.       .249E 00    .20000  .228E 00    .40000  .210E 00
   .60000  .190E 00    .80000  .177E 00   1.00000  .161E 00
MU(CM)     DIFF. X-SECTION
  1.00000  .930E-01    .80000  .114E 00    .60000  .135E 00    .40000  .158E 00
   .20000  .180E 00   0.       .203E 00   -.20000  .231E 00   -.40000  .268E 00
  -.50000  .292E 00   -.60000  .325E 00   -.70000  .370E 00   -.80000  .437E 00
  -.90000  .523E 00  -1.00000  .647E 00
MU(CM)     DIFF. X-SECTION
  1.00000  .125E 00    .80000  .135E 00    .60000  .147E 00    .40000  .160E 00
   .20000  .177E 00   0.       .201E 00   -.20000  .230E 00   -.40000  .262E 00
  -.60000  .296E 00   -.80000  .333E 00  -1.00000  .370E 00
MU(CM)     DIFF. X-SECTION
  1.00000  .140E 00    .80000  .140E 00    .60000  .140E 00    .40000  .146E 00
   .20000  .157E 00   0.       .172E 00   -.20000  .196E 00   -.40000  .237E 00
  -.50000  .263E 00   -.60000  .300E 00   -.70000  .345E 00   -.80000  .414E 00
  -.90000  .517E 00  -1.00000  .675E 00
MU(CM)     DIFF. X-SECTION
  1.00000  .227E 00    .80000  .196E 00    .60000  .170E 00    .40000  .152E 00
   .20000  .140E 00   0.       .136E 00   -.20000  .141E 00   -.40000  .163E 00
  -.50000  .180E 00   -.60000  .205E 00   -.70000  .252E 00   -.80000  .320E 00
  -.90000  .425E 00  -1.00000  .640E 00
MU(CM)     DIFF. X-SECTION
  1.00000  .325E 00    .80000  .261E 00    .60000  .207E 00    .40000  .162E 00
   .20000  .133E 00   0.       .117E 00   -.20000  .116E 00   -.40000  .129E 00
  -.50000  .143E 00   -.60000  .167E 00   -.70000  .202E 00   -.80000  .265E 00
  -.90000  .335E 00  -1.00000  .425E 00
MU(CM)     DIFF. X-SECTION
  1.00000  .310E 00    .80000  .252E 00    .60000  .200E 00    .40000  .158E 00
   .20000  .123E 00   0.       1.000E-01   -.20000  .880E-01   -.30000  .880E-01
  -.40000  .940E-01   -.50000  .107E 00   -.60000  .130E 00   -.70000  .170E 00
  -.80000  .230E 00   -.90000  .296E 00  -1.00000  .380E 00
MU(CM)     DIFF. X-SECTION
  1.00000  .295E 00    .80000  .233E 00    .60000  .178E 00    .40000  .131E 00
   .20000  .920E-01   0.       .610E-01   -.20000  .420E-01   -.40000  .440E-01
  -.50000  .540E-01   -.60000  .730E-01   -.70000 1.000E-01   -.80000  .136E 00
  -.90000  .185E 00  -1.00000  .270E 00
MU(CM)     DIFF. X-SECTION
  1.00000  .340E 00    .80000  .264E 00    .60000  .197E 00    .40000  .143E 00
   .20000  .950E-01   0.       .600E-01   -.20000  .420E-01   -.30000  .400E-01
  -.40000  .420E-01   -.50000  .500E-01   -.60000  .650E-01   -.70000  .880E-01
  -.80000  .125E 00   -.90000  .170E 00  -1.00000  .230E 00
```

E(I)	SIG(E,C)	F1...F9								
14.100	.605E 00	.278E 00	.208E 00	-.703E-01	.425E-01	-.238E-01	.113E-01	-.319E-02	-.970E-03	.136E-02
FIT ORDER=	1	2	3	4	5	6	7	8	9	
RMS(PCT.)=	383.23	261.79	170.87	106.30	54.54	23.13	16.12	15.90	12.96	

E(I)	SIG(E,C)	F1...F9								
.100	.334E 01	-.494E-01	.530E-02	.187E-03	-.778E-04	.530E-03	-.107E-07	.000E 00	.000E 00	.000E 00
FIT ORDER=	1	2	3	4	5	6				
RMS(PCT.)=	4.40	1.03	.86	.88	.00	.00				

E(I)	SIG(E,C)	F1...F9								
.200	.323E 01	-.142E 00	.123E-01	.535E-03	-.942E-04	.434E-03	-.128E-03	-.512E-03	-.401E-03	-.117E-03
FIT ORDER=	1	2	3	4	5	6	7	8	9	
RMS(PCT.)=	11.82	1.90	2.30	2.19	2.80	2.55	1.39	.56	.61	

E(I)	SIG(E,C)	F1...F9								
.500	.301E 01	-.278E 00	.788E-01	-.382E-01	.151E-01	-.425E-02	.844E-03	.139E-03	-.489E-03	-.118E-03
FIT ORDER=	1	2	3	4	5	6	7	8	9	
RMS(PCT.)=	86.34	57.57	29.60	11.85	2.52	1.59	2.05	1.09	1.40	

E(I)	SIG(E,C)	F1...F9								
.750	.275E 01	-.189E 00	.294E-01	.132E-02	-.190E-02	-.687E-03	.242E-03	.493E-03	-.477E-04	-.689E-04
FIT ORDER=	1	2	3	4	5	6	7	8	9	
RMS(PCT.)=	32.46	2.99	3.71	1.10	1.74	1.24	.37	.25	.10	

E(I)	SIG(E,C)	F1...F9								
1.000	.286E 01	-.257E 00	.117E 00	-.430E-01	.181E-01	-.752E-02	.305E-02	-.154E-02	-.716E-04	.312E-03
FIT ORDER=	1	2	3	4	5	6	7	8	9	
RMS(PCT.)=	108.92	52.76	25.68	13.96	5.72	4.21	1.01	1.12	.78	

E(I)	SIG(E,C)	F1...F9								
1.950	.252E 01	-.139E 00	.159E 00	-.576E-01	.280E-01	-.126E-01	.556E-02	-.268E-02	.120E-02	-.116E-02
FIT ORDER=	1	2	3	4	5	6	7	8	9	
RMS(PCT.)=	133.83	65.16	35.69	19.24	10.07	5.84	3.74	3.33	3.04	

E(I)	SIG(E,C)	F1...F9								
2.450	.239E 01	.151E-02	.171E 00	-.334E-01	.131E-01	-.458E-02	-.111E-02	.230E-02	-.910E-03	.269E-03
FIT ORDER=	1	2	3	4	5	6	7	8	9	
RMS(PCT.)=	148.40	41.76	19.61	8.42	4.53	4.54	3.31	3.04	3.01	

E(I)	SIG(E,C)	F1...F9								
3.270	.213E 01	.419E-01	.186E 00	-.463E-01	.141E-01	-.108E-02	-.247E-02	.187E-02	-.869E-03	-.499E-03
FIT ORDER=	1	2	3	4	5	6	7	8	9	
RMS(PCT.)=	198.27	64.67	21.74	6.70	5.97	4.98	3.46	2.95	2.88	

E(I)	SIG(E,C)	F1...F9								
4.500	.157E 01	.169E 00	.221E 00	-.487E-01	.122E-01	-.153E-02	.134E-02	-.217E-02	.139E-02	-.663E-03
FIT ORDER=	1	2	3	4	5	6	7	8	9	
RMS(PCT.)=	278.27	80.42	19.05	6.95	6.95	6.31	4.12	2.52	2.02	

E(I)	SIG(E,C)	F1...F9								
5.500	.163E 01	.232E 00	.223E 00	-.359E-01	.863E-02	-.851E-03	.712E-03	.184E-03	-.142E-02	-.327E-03
FIT ORDER=	1	2	3	4	5	6	7	8	9	
RMS(PCT.)=	326.97	69.09	17.00	7.02	5.54	4.74	4.51	2.49	2.16	

A.4 STAR DATA REDUCTION

The STAR code has been modified (Section A.6) to punch on cards the total transmission and reflection matrices, $\underline{T}_t$ and $\underline{R}$, respectively. The reason for this is to find transmission and reflection for an arbitrary neutron source, not just an isotropic fission source as is given directly by STAR. The STAR DATA REDUCTION (SDR) code has been written to perform this important task, both to eliminate errors in hand calculations and to save about two man-hours per calculation. It is coded in FORTRAN-II for the IBM-7094 at the M.I.T. Computation Center.

It calculates angular group fluxes, n/cm^2-sec-MeV-unit incident cosine, scalar fluxes in n/cm^2-sec-MeV and n/cm^2-sec-unit lethargy, and dose rates in rad/min. The output reflected or transmitted flux from one case can be used as the source for the next case. For example, the flux transmitted through tissue irradiated by neutrons reflected from a scatterer is obtained by the following sequence of cases:

1. neutron source at core-reflector interface attenuated through Medical Beam Port;
2. special matrix to rotate coordinates by 45^o to give angular source as viewed by the scatterer;
3. reflection from the scatterer;
4. special matrix to rotate coordinates by 45^o to give angular source as viewed by the phantom;
5. transmission through various thicknesses of tissue phantom.

In STAR[17] the scalar flux is (per unit energy)

$$FLUX_m = \sum_{k=1}^{NEREG} FISS_k \; RHOXT_{m,k} \qquad (A.13)$$

where

$$RHOXT_{m,k} = \sum_{J=1}^{NMUREG} WMU_j \sum_{\ell=1}^{NMUREG} WMU_\ell \; T_t(SE_{\ell,m}; SI_{j,k})/4MU_\ell \cdot$$

(A.14)

Now define the fraction of the energy group k neutron source strength in angular group j and V_{jk}. Then redefine RHOXT as

$$RHOXT_{m,k} = \sum_{j=1}^{NMUREG} WMU_j \; V_{jk} \sum_{\ell=1}^{NMUREG} WMU_\ell \; T_t \; (SE_{\ell,m}; SI_{j,k})4MU_\ell \cdot$$

(A.15)

The scalar flux comes out as before, from Equation (A.13). Dose rates are simply found:

$$DOSE_m = FLUX_m*(CONV(m))*WE(m), \text{ rad/min}$$

$$DOSE = \sum_{m=1}^{NEREG} DOSE_m, \text{ rad/min.} \qquad (A.16)$$

Incident and exit states are defined as

$$\text{Incident state} = SI_{j,k} = (E_k, \mu_j);$$

$$\text{Exit state} \quad SE_{\ell,m} = (E_m, \mu_\ell) \qquad (A.17)$$

No subroutines are needed, as the calculations are a simple series of operations on vectors and matrices. Input to SDR is described in the following Section, with a listing in Section A.4.2. Section A.4.3 lists input/output for fission neutron penetration through 0 and 15 cm of polyethylene. Also given is the special matrix used for 45^{o} rotation.

A.4.1 INPUT FOR SDR

Set 1: Case Data

Card 1: Format (2I5)

1. NEREG = number of energy groups. If NEREG = 0, job terminates.
2. NMUREG = number of angular groups.

Card 2: Format (8F10.5)

L DU(L) = direction cosine assigned to group L.

L+1 WMU(L) = quadrature weight assigned to group L.

L = 1...NMUREG.

More cards may be needed if NS = NEREG*NMUREG > 8.

Card 3: Format (6E12.5)

J. S(J) = forward-directed flux in group J, where J = NEREG(I-1) + K for the I-th energy group and the K-th angular group. J = 1...NS.

More cards may be needed if NS > 6.

Card 4: Format (8F10.5)

I. WE(I) = width, MeV, of energy group I. Energy increases with I. I = 1...NEREG.

I+1. E(I) = energy, MeV, of group I.

More cards may be needed if NEREG > 4.

Card 5: Format (6E12.5)

I. CONV(I) = flux to dose conversion factor, rad/min per n/cm^2-sec. (Table 2.3). I = 1...NEREG.

Card 6: Format (14A5)

1. Descriptive alphanumeric title for the case, to appear on output.

Card 7: Format (2F10.4, I5, 10A5)

1. XT = thickness at which the transmission matrix applies.
2. XR = thickness at which the reflection matrix applies.
3. NQ = source switch. If $0 < NQ < 10$, existing S(J) in memory is to be used. If NQ = 10, set source for next problem to be the transmitted flux. If $NQ > 10$, set next source to be reflected flux. If $NQ \leq 0$, program control switches to read all data from Card 1 again, with a new S(J).
4. NAME = alphanumeric title for transmission and reflection matrices, to appear on output.

Set 2: Transmission and Reflection Matrices.

This set is normally punched by STAR, along with XT and XR of Card 7 as a title. The format is 6E12.5, with $\underline{T}_t$ and $\underline{R}$ individually close-packed. The sequence is:

1. $T_t(L,M)$, M = 1...NS, for each L = 1...NS,
2. R(L,M), M = 1...NS, for each L = 1...NS,

In STAR notation, the incident and exit states are M and L, where

$$M = NEREG(I-1) + K, \quad L = NEREG(I' - 1) + K',$$

for incident state (E_I, μ_K) and exit state $(E_{I'}, \mu_{K'})$.

A.4.2 LISTING OF SDR

```
C      STAR DATA REDUCTION FOR ARBITRARY ANGULAR SOURCES
C      S CONTAINS THE FORWARD DIRECTED SOURCE STRENGTH OF EACH STATE
C      DU CONTAINS COSINES MU IN STAR NOTATION
C      T IS ARRAY TTOT IN STAR NOTATION
       DIMENSION T(32,32),R(32,32),DU(32),S(32),ANGR(32),ANGT(32),SCALR(3
      12),SCALT(32),ITITLE(14),WE(32),CONV(32),DTJ(32),DRJ(32),
      2  WMU(32),WW(32),PHIUT(32),U(32),E(32),PHIUR(32),NAME(10)
 1000 READ INPUT TAPE 4,100,NEREG,NMUREG
       IF(NEREG)2000,2000,2001
 2000  CALL EXIT
 2001 READ INPUT TAPE 4,101,(DU(L), WMU(L), L=1,NMUREG)
       NS=NEREG*NMUREG
       JJ=0
       DO 60 J=1,NMUREG
       DO 61 I=1,NEREG
       K=JJ+I
       WW(K)=WMU(J)
   61 CONTINUE
       JJ=JJ+NEREG
   60 CONTINUE
       READ INPUT TAPE 4,102,(S(J),J=1,NS)
       READ INPUT TAPE 4,101,(WE(J),E(J),J=1,NS)
       READ INPUT TAPE 4,102,(CONV(J),J=1,NEREG)
       READ INPUT TAPE 4,150,ITITLE
  230 FORMAT(1HO, 46H DIMENSIONS OF SCALAR FLUXES ARE N/CM2/SEC/MEV,/,
      1 54H ANGULAR FLUXES ARE N/CM2/SEC/MEV/UNIT INCIDENT COSINE,/,
      2 59H PHIUT, PHIUR ARE N/CM2/SEC/UNIT LETHARGY,  DOSE IS RAD/MIN)
       WRITE OUTPUT TAPE 2,105,NEREG,NMUREG,(DU(L),WMU(L),L=1,NMUREG)
       WRITE OUTPUT TAPE 2,103,(S(J),J=1,NS)
       WRITE OUTPUT TAPE 2,113,(WE(J),E(J),J=1,NS)
       WRITE OUTPUT TAPE 2,114,(CONV(J),J=1,NEREG)
       DO 62 I=1,NEREG
       U(I)=LOGF(10./E(I))
   62 CONTINUE
       WRITE OUTPUT TAPE 2,210,(U(I),I=1,NEREG)
       WRITE OUTPUT TAPE 2,230
  210 FORMAT(1HO,6H U(I)=,/,(12F10.4))
  114 FORMAT(1HO,9H CONV(J)=,/,(10E12.5))
  113 FORMAT(1HO,7H WE, E=,/,(8F10.5))
  150 FORMAT(14A5)
  151 FORMAT(1HO,14A5)
 1001 READ INPUT TAPE 4,112,XT,XR,NQ,NAME
C      NQ GRTR 0 IMPLIES OLD SOURCE ETC IS OK
C      NQ .LE. 0 IMPLIES READ NEW SOURCE ETC.
       IF(NQ)1000,1000,1002
 1002 READ INPUT TAPE 4,102,((T(K,I),I=1,NS),K=1,NS)
       READ INPUT TAPE 4,102,((R(K,I),I=1,NS),K=1,NS)
       WRITE OUTPUT TAPE 2,110
       DO 2 K=1,NS
    2 WRITE OUTPUT TAPE 2,104,(T(K,I),I=1,NS)
       WRITE OUTPUT TAPE 2,111
       DO 3 K=1,NS
    3 WRITE OUTPUT TAPE 2,104,(R(K,I),I=1,NS)
  110 FORMAT(8H T(K,I)=,)
  111 FORMAT(8H R(K,I)=,)
  100 FORMAT(2I5)
  101 FORMAT(8F10.5)
  102 FORMAT(6E12.5)
```

```
  103 FORMAT(1HO,6H S(J)=,/,(10E12.5))
  104 FORMAT(1H ,10E12.5)
  105 FORMAT(1H1,7H NEREG=,I2,2X,7HNMUREG=,I2,/,(8F10.5))
  112 FORMAT(2F10.4,I5,10A5)
      KK=0
      DO 4 L=1,NMUREG
      X=1./(4.*DU(L))
      DO 5 K=1,NEREG
      M=K+KK
      DO 6 I=1,NS
      R(M,I)=R(M,I)*X
      T(M,I)=T(M,I)*X
    6 CONTINUE
    5 CONTINUE
      KK=KK+NEREG
    4 CONTINUE
      WRITE OUTPUT TAPE 2,110
      DO 7 K=1,NS
    7 WRITE OUTPUT TAPE 2,104,(T(K,I),I=1,NS)
      WRITE OUTPUT TAPE 2,111
      DO 8 K=1,NS
    8 WRITE OUTPUT TAPE 2,104,(R(K,I),I=1,NS)
      DO 9 I=1,NS
      X=S(I)/WW(I)
      DO 10 K=1,NS
      T(K,I)=T(K,I)*X/WW(K)
      R(K,I)=R(K,I)*X/WW(K)
   10 CONTINUE
    9 CONTINUE
      DO 11 K=1,NS
      SUMT=0.
      SUMR=0.
      DO 12 I=1,NS
      SUMT=SUMT+T(K,I)*WW(I)
      SUMR=SUMR+R(K,I)*WW(I)
   12 CONTINUE
      ANGT(K)=SUMT
      ANGR(K)=SUMR
C       ANGT(K) AND ANGR(K) ARE FLUX/MEV/UNIT INC. COSINE MU
   11 CONTINUE
      DOSET=0.
      DOSER=0.
      DO 13 J=1,NEREG
      SCALT(J)=0.
      SCALR(J)=0.
      DO 14 L=1,NMUREG
      LL=NEREG*(L-1)+J
      SCALT(J)=SCALT(J)+ANGT(LL)*WW(LL)
      SCALR(J)=SCALR(J)+ANGR(LL)*WW(LL)
   14 CONTINUE
      DTJ(J)=SCALT(J)*CONV(J)*WE(J)
      DRJ(J)=SCALR(J)*CONV(J)*WE(J)
      DOSET=DOSET+DTJ(J)
      DOSER=DOSER+DRJ(J)
      PHIUT(J)=SCALT(J)*E(J)
      PHIUR(J)=SCALR(J)*E(J)
   13 CONTINUE
      WRITE OUTPUT TAPE 2,120,XT,XR,NAME
  120 FORMAT(1H1,4H XT=,F10.4,4H XR=,F10.4,10A5)
      WRITE OUTPUT TAPE 2, 151, ITITLE
      WRITE OUTPUT TAPE 2,200,(ANGT(I),I=1,NS)
```

```
  200 FORMAT(1HO,14H ANGULAR FLUX=,/,(10E12.4))
      WRITE OUTPUT TAPE 2,201,(ANGR(I),I=1,NS)
  201 FORMAT(1HO,19H ANGULAR REF. FLUX=,/,(10E12.4))
      WRITE OUTPUT TAPE 2,202,(SCALT(J),J=1,NEREG)
  202 FORMAT(1HO,20H SCALAR TRANS. FLUX=,/,(10E12.4))
      WRITE OUTPUT TAPE 2,203,(SCALR(J),J=1,NEREG)
  203 FORMAT(1HO,18H SCALAR REF. FLUX=,/,(10E12.4))
      WRITE OUTPUT TAPE 2,204,DOSET,(DTJ(J),J=1,NEREG)
      WRITE OUTPUT TAPE 2,205,DOSER,(DRJ(J),J=1,NEREG)
      WRITE OUTPUT TAPE 2,208,(PHIUT(J),J=1,NEREG)
      WRITE OUTPUT TAPE 2,209,(PHIUR(J),J=1,NEREG)
  208 FORMAT(1HO,10H PHIUT(J)=,/,(10E12.4))
  209 FORMAT(1HO,10H PHIUR(J)=,/,(10E12.4))
      WRITE OUTPUT TAPE 2,206
  204 FORMAT(1HO, 7H DOSET=,E12.4,/,(10E12.4))
  205 FORMAT(1HO, 7H DOSER=,E12.4,/,(10E12.4))
  206 FORMAT(1H1)
C     IF NQ=10 SET SOURCE EQUAL TO TRANS. FLUX
C     IF NQ GRTR 10 SET SOURCE S=REF. FLUX
      IF(NQ-10)1001,1003,1004
 1003 DO 50 I=1,NS
      S(I)=ANGT(I)*WE(I)*WW(I)
   50 CONTINUE
      GO TO 1005
 1004 DO 51 I=1,NS
      S(I)=ANGR(I)*WE(I)*WW(I)
   51 CONTINUE
 1005 WRITE OUTPUT TAPE 2,207,(S(J),J=1,NS)
  207 FORMAT(1HO,12H NEW SOURCE=,/,(10E12.5))
C     S IS IN NEUTRONS/CM2-SEC, NOT DIFFERENTIAL FLUX
      GO TO 1001
      END
```

A.4.3 SAMPLE PROBLEM FOR SDR

```
*     DATA
    4    2
     .2113      .5         .7887      .5
 0.28270E 00 0.18505E 00 0.22345E-01 0.17895E-02 0.2827 E 00 0.18505E 00
 0.22345E-01 0.17895E-02
   1.722      0.7874     3.228      3.367      3.228      6.733      1.722      9.313
   1.722      0.7874     3.228      3.367      3.228      6.733      1.722      9.313
 1.45   E-07 2.83   E-07 4.04   E-07 4.30   E-07
  TEST OF POLY FOR FISSION SOURCE(ISOTROPIC)
    0.         0.         1        ZERO THICKNESS TEST
  .49082E 00 1.00000E-30 1.00000E-30 1.00000E-30 1.00000E-30 1.00000E-30
 1.00000E-30 1.00000E-30 1.00000E-32  .26183E 00 1.00000E-30 1.00000E-30
 1.00000E-32 1.00000E-30 1.00000E-30 1.00000E-30 1.00000E-32 1.00000E-32
  .26183E 00 1.00000E-30 1.00000E-32 1.00000E-32 1.00000E-30 1.00000E-30
 1.00000E-32 1.00000E-32 1.00000E-32  .49082E 00 1.00000E-32 1.00000E-32
 1.00000E-32 1.00000E-30 1.00000E-30 1.00000E-30 1.00000E-30 1.00000E-30
  .18321E 01 1.00000E-30 1.00000E-30 1.00000E-30 1.00000E-32 1.00000E-30
 1.00000E-30 1.00000E-30 1.00000E-32  .97732E 00 1.00000E-30 1.00000E-30

  .97732E 00 1.00000E-30 1.00000E-32 1.00000E-32 1.00000E-32 1.00000E-30
 1.00000E-32 1.00000E-32 1.00000E-32  .18321E 01

   15.0000    15.0000    1     POLY
  .37536E-03  .12049E-02  .17790E-02  .17137E-02  .31157E-02  .12843E-01
  .15315E-01  .13962E-01 1.00000E-32  .21633E-03  .56116E-03  .56195E-03
 1.00000E-32  .32251E-02  .68985E-02  .64971E-02 1.00000E-32 1.00000E-32
  .52723E-03  .54159E-03 1.00000E-32 1.00000E-32  .82413E-02  .88629E-02
 1.00000E-32 1.00000E-32 1.00000E-32  .80792E-04 1.00000E-32 1.00000E-32
 1.00000E-32  .13313E-02  .30482E-02  .84578E-02  .11351E-01  .10838E-01
  .25303E-01  .84490E-01  .87887E-01  .78878E-01 1.00000E-32  .31650E-02
```

```
 .52438E-02  .50023E-02 1.00000E-32  .47358E-01  .47618E-01  .40571E-01
1.00000E-32 1.00000E-32  .81366E-02  .82867E-02 1.00000E-32 1.00000E-32
 .15757E 00  .80363E-01 1.00000E-32 1.00000E-32 1.00000E-32  .13225E-02
1.00000E-32 1.00000E-32 1.00000E-32  .18171E 00
 .86828E-01  .37978E-01  .13140E-01  .11971E-01  .12204E 00  .58601E-01
 .23974E-01  .18885E-01 1.00000E-32  .28451E-01  .14013E-01  .10970E-01
1.00000E-32  .25957E-01  .11525E-01  .90979E-02 1.00000E-32 1.00000E-32
 .18549E-01  .18007E-01 1.00000E-32 1.00000E-32  .14980E-01  .15016E-01
1.00000E-32 1.00000E-32 1.00000E-32  .55264E-02 1.00000E-32 1.00000E-32
1.00000E-32 1.00000E-32  .12160E 00  .96081E-01  .53761E-01  .48309E-01
 .33629E 00  .22731E 00  .10738E 00  .85439E-01 1.00000E-32  .25864E-01
 .16681E-01  .14799E-01 1.00000E-32  .68807E-01  .29508E-01 1.00000E-32
1.00000E-32 1.00000E-32  .14924E-01  .15040E-01 1.00000E-32 1.00000E-32
 .28601E-01  .31565E-01 1.00000E-32 1.00000E-32 1.00000E-32 1.00000E-32
1.00000E-32 1.00000E-32 1.00000E-32 1.00000E-32


   0.          0.          11     45 DEGREE TRANSFER MATRIX
0.      E 00 0.      E 00 0.      E 00 0.      E 00 0.1227 E 00 0.      E 00

0.      E 00 0.06546E 00

                                                  0.06546E 00

             0.1227 E 00 0.91605E 00
1.1451 E 00                                                   0.48866E 00
                                      0.61082E 00
                         0.48866E 00
0.61082E 00                                                   0.91605E 00
                                      1.1451 E 00
0.      E 00 0.      E 00 0.      E 00 0.      E 00 0.1227 E 00 0.      E 00

0.      E 00 0.06546E 00

                                                  0.06546E 00

             0.1227 E 00 0.91605E 00
1.1451 E 00                                                   0.48866E 00
                                      0.61082E 00
                         0.48866E 00
0.61082E 00                                                   0.91605E 00
                                      1.1451 E 00
               END OF FILE
```

XT= 0. XR= 0. ZERO THICKNESS TEST 322

TEST OF POLY FOR FISSION SOURCE(ISOTROPIC)

ANGULAR FLUX=
.3283E 00 .1147E 00 .1384E-01 .2078E-02 .3283E 00 .1147E 00 .1384E-01 .2078E-02

ANGULAR REF. FLUX=
.0000E 00 .0000E 00 .0000E 00 .0000E 00 .0000E 00 .0000E 00 .0000E 00 .0000E 00

SCALAR TRANS. FLUX=
.3283E 00 .1147E 00 .1384E-01 .2078E-02

SCALAR REF. FLUX=
.0000E 00 .0000E 00 .0000E 00 .0000E 00

DOSET= .2063E-06
.8198E-07 .1047E-06 .1805E-07 .1539E-08

DOSER= .0000E 00
.0000E 00 .0000E 00 .0000E 00 .0000E 00

PHIUT(J)=
.2585E 00 .3860E 00 .9321E-01 .1936E-01

PHIUR(J)=
.0000E 00 .0000E 00 .0000E 00 .0000E 00

```
XT=   15.0000 XR=   15.0000    POLY

 TEST OF POLY FOR FISSION SOURCE(ISOTROPIC)

ANGULAR FLUX=
 .9457E-02   .1931E-02   .5035E-03   .5980E-05   .1749E-01   .6728E-02   .2448E-02   .2076E-03

ANGULAR REF. FLUX=
 .1841E 00   .2526E-01   .1913E-02   .2340E-04   .1224E 00   .1178E-01   .6694E-03   .6237E-32

SCALAR TRANS. FLUX=
 .1347E-01   .4329E-02   .1476E-02   .1068E-03

SCALAR REF. FLUX=
 .1533E 00   .1852E-01   .1291E-02   .1170E-04

DOSET=   .9323E-08
 .3365E-08   .3955E-08   .1924E-08   .7909E-10

DOSER=   .5688E-07
 .3827E-07   .1692E-07   .1684E-08   .8664E-11

PHIUT(J)=
 .1061E-01   .1458E-01   .9936E-02   .9947E-03

PHIUR(J)=
 .1207E 00   .6235E-01   .8693E-02   .1090E-03
```

A.5 MODIFICATIONS TO CSDP

Cross section data preparation for STAR is performed by CSDP. It was coded in MAD by Mathews[17] for the M.I.T. Computation Center Fortran Monitor System as used by an I.B.M.-7094 computer. Section 5 of CSDP, known as SEC5, is a subroutine that averages the inelastic contribution to the transfer probability SCS over each incident and exit state. Input to SEC5 consists of:

1. The microscopic total inelastic scattering cross section SIGIN(1,1)...SIGIN(NN,NE),
2. NEIN = the number of incident energy values the inelastic scattering energy distribution function G(I,K,M) is non-zero. I is the nuclide, K is the incident energy, and M is the scattering energy.
3. G(1,NE-NEIN + 1,1)...G(NN,NE,NE).

The original SEC5 required that

$$\int_0^\infty G(I,K,M)\,dE_M = 1, \quad \text{all } I \text{ and } K. \tag{A.18}$$

The probability $P(K \rightarrow M)$ of an inelastically scattered neutron from group K transfering to group M is, for nuclide I:

$$P(K \rightarrow M) = \frac{\int_{\text{group } K} \phi(E_K)\,dE_K \int_{\text{group } M} dE_M\, G(I,K,M)}{\sigma_{in}} = \frac{\sigma_{in}(K \rightarrow M)}{\sigma_{in}} \tag{A.19}$$

Trapezodal integration is used to evaluate Equation (A.19). It turns out to be convenient for the user to be able to use an arbitrary normalization on G, rather than that of Equation (A.18). The only difference is a new definition of the total inelastic scattering cross section:

σ_{in} = total inelastic scattering cross section for a scattered neutron energy not less than the lower bound of the lowest energy group.

SEC5 has been modified to automatically normalize G, and is listed in Section A.5.1.

A.5.1 LISTING OF SEC5 FOR CSDP

```
*       MAD
 SEC5      R SECTION 5
           R   REVISED BY A P OLSON TO AUTOMATICALLY NORMALIZE G TO 1
            EXTERNAL FUNCTION
            ENTRY TO SEC5.
            START=6
            INTEGER MTL,MTH
            PROGRAM COMMON ETA,W,N,K,DE,NMUREG ,NEREG,EL,EH,
           1 CC1,E,WE,MUL,MUH,J,MU,WMU,NE,ET,KT,KTL,KTH,DT,NN,AD,SIGT,TCS
           2,I,CC2,FLUX,PRINT,SIGF,SIGS,SIGN2N,NU,C,CC3,DG,DS,NS,SIGIN,NE
           3IN,G,K1,K2,SI,L,M,SO,SCS,MT,DF,AF,TF,E1,E2,H,S1,S2,FISS(32),F
           4LC,DFL,LC,A,START,NPL,NIT
            INTEGER N,K,DE,NMUREG,NEREG,J,NE,KT,KTL,KTH,DT,NN,I,PRINT,DG,
           1DS,NS,NEIN,K1,K2,SI,L,M,SO,MT,DF,NPL,NIT,DFL,LC,START,MAXT,NI
           2T,N1,N2
            DIMENSION ETA(137,DE),W(137,DE),DE(2),EL(32),EH(32),E(32),WE(
           132),MUL(32),MUH(32),MU(32),WMU(32),ET(100),KTL(32),KTH(32),DT
           2(2),AD(5),SIGT(500,DT),TCS(32),SIGF(500,DT),SIGS(500,DT),SIGN
           32N(500,DT),NU(500,DT),C(32),DG(3),DS(2),SIGIN(500,DT),G(7500,
           4DG),SCS(2048,DS),DF(2),AF(5),TF(5),FLC(1200,DFL),DFL(3),A(5),
           5FLUX(100),LP(6)
            VECTOR VALUES DG=3,1,0,6
            VECTOR VALUES DS=2,1,0
            NS=NEREG*NMUREG
            DS(2)=2*NS
            THROUGH QQ1,FOR SO=1,1,SO.G.2*NS*NS
 QQ1        SCS(SO)=0.
            PRINT COMMENT $0TYPE VALUE OF NEIN$
            READ DATA
            PRINT RESULTS NEIN
            WHENEVER NEIN.E.0
            PRINT COMMENT $0NEIN.E.0, NO INELASTIC SCATTER$
            TRANSFER TO QQ140
            END OF CONDITIONAL
            DG(2)=NE
            PRINT COMMENT $0TYPE VALUES OF SIGIN(1,1)...SIGIN(NN,NE) AND
           1G(1)...G(NN*NE*NE)$
            READ DATA
            DG(3)=NE
            THROUGH QQ20,FOR I=1,1,I.G.NN
            THROUGH QQ20,FOR KT=NE-NEIN+1,1,KT.G.NE
            GSUM=0.
            THROUGH QQ5,FOR MT=KT+1,1,MT.G.NE
 QQ5        GSUM=GSUM+G(I,KT,MT)
            WHENEVER .ABS.(GSUM) .G. 1.E-10
            PRINT COMMENT $0ERROR IN SEC5,INELASTIC ENERGY DISTRIBUTION F
           1UNCTION IMPLIES ENERGY INCREASES$
            PRINT RESULTS I,KT,G(I,KT,KT+1)...G(I,KT,NE)
            PRINT COMMENT $0TYPE NEW VALUES OF G(I,KT,KT+1)...G(I,KT,NE)
           1 NOW,IF DESIRED, OTHERWISE QUIT$
            READ DATA
            END OF CONDITIONAL
            WHENEVER KT.E.1
            GSUM=G(I,1,1)
            TRANSFER TO QQ9
            END OF CONDITIONAL
            GSUM=0.
            CC1=G(I,KT,1)
            THROUGH QQ10,FOR MT=1,1,MT.GE.KT
```

```
          CC2=G(I,KT,MT+1)
          GSUM=GSUM+(ET(MT+1)-ET(MT))*(CC1+CC2)
QQ10      CC1=CC2
          GSUM=.5*GSUM
QQ9       GS=1.
          WHENEVER .ABS.(GSUM-GS) .G. .001
          PRINT COMMENT $0INTEGRAL OVER MT OF G(I,KT,MT) .NE. ONE$
          THROUGH QQ11,FOR MT=1,1,MT.G.KT
QQ11      G(I,KT,MT)=G(I,KT,MT)*GS/GSUM
          END OF CONDITIONAL
QQ20      PRINT RESULTS I,KT,GSUM,G(I,KT,1)...G(I,KT,KT)
          INTERNAL FUNCTION DET.(DV1)=ET(DV1+1)-ET(DV1)
          INTERNAL FUNCTION SIGINF.(DV2,DV3)=(SIGIN(DV2,DV3)+SIGN2N(DV2
         1,DV3))*E2I.(DV2,DV3)/CSIGT.(DV2,DV3)
          INTEGER DV1,DV2,DV3
          INTERNAL FUNCTION(DV4,DV5)
          INTEGER DV4,DV5
          ENTRY TO E2I.
          PRINT RESULTS DV4,DV5,MTL
          WHENEVER MTL.G.DV5,FUNCTION RETURN 0.
          WHENEVER DV5.E.1
             WHENEVER MTL.E.1
                 FUNCTION RETURN G(DV4,1,1)
             OTHERWISE
                 FUNCTION RETURN 0.
          END OF CONDITIONAL
          OTHERWISE
          DIMENSION GSUMV(100)
          GSUMV(DV5)= .5*DET.(DV5-1)*G(DV4,DV5,DV5)
          WHENEVER MTL.E.DV5,FUNCTION RETURN GSUMV(DV5)
          THROUGH QQ31,FOR MT=DV5-1,-1,MT.L.2 .OR. MT.L.MTL
QQ31      GSUMV(MT)= .5*(ET(MT+1)-ET(MT-1))*G(DV4,DV5,MT)
          GSUMV(1)= .5*DET.(1)*G(DV4,DV5,1)
          GSUM=0.
          THROUGH QQ32, FOR MT=MTL,1,MT.G.MTH .OR. MT.G.DV5
QQ32      GSUM=GSUM+GSUMV(MT)
          PRINT RESULTS GSUM
          FUNCTION RETURN GSUM
          END OF CONDITIONAL
          END OF FUNCTION
          INTERNAL FUNCTION(DV9)
          INTEGER DV9
          ENTRY TO E1I.
          WHENEVER KTH.E.KTL
          DV10=SIGINF.(DV9,KTL)
          OTHERWISE
          DV10=0.
          DV11=SIGINF.(DV9,KTL)*FLUX(KTL)
          THROUGH QQ40,FOR KT=KTL,1,KT.GE.KTH
          DV12=SIGINF.(DV9,KT+1)*FLUX(KT+1)
          DV10=DV10+DET.(KT)*(DV11+DV12)
QQ40      DV11=DV12
          DV10= .5*DV10
          END OF CONDITIONAL
          FUNCTION RETURN DV10
          END OF FUNCTION
          THROUGH QQ45,FOR SI=1,1,SI.G.NS
QQ45      SUMSCS(SI)=0.
          DIMENSION SUMSCS(32)
          THROUGH QQ70,FOR K=NEREG,-1,K.L.1 .OR. KTH(K).L.NE-NEIN+1
          CC1=FLUXI.(K)*2.*AD
```

```
            PRINT RESULTS K,CC1
            KTL=KTL(K)
            KTH=KTH(K)
            WHENEVER KTL.L.NE-NEIN+1,KTL=NE-NEIN+1
            WHENEVER KTH.L.KTL,TRANSFER TO QQ70
            THROUGH QQ70,FOR M=K,-1,M.L.1
            MTL=KTL(M)
            MTH=KTH(M)
            WHENEVER MTH.L.MTL,TRANSFER TO QQ70
            CC2=CC1*WE(M)
            PRINT RESULTS CC2
            CC3=0.
            THROUGH QQ50,FOR I=1,1,I.G.NN
QQ50        CC3=CC3+E1I.(I)*AD(I)
            PRINT RESULTS CC3
            THROUGH QQ60,FOR J=1,1,J.G.NMUREG
            SI=NEREG*(J-1)+K
            THROUGH QQ60,FOR L=1,1,L.G.NMUREG
            SO=NEREG*(L-1)+M
            SCS(SO,SI)=CC3/CC2
            SCS(SO,SI+NS)=CC3/CC2
QQ60        SUMSCS(SI)=SUMSCS(SI)+(SCS(SO,SI)+SCS(SO,SI+NS))*WE(M)*WMU(L)
QQ70        CONTINUE
            PRINT RESULTS SIGIN(1,1)...SIGIN(NN,NE)
            PRINT RESULTS SUMSCS(1)...SUMSCS(NS)
            PRINT RESULTS SCS(1,1)...SCS(NS,2*NS)
QQ140       FUNCTION RETURN
            END OF FUNCTION
                END OF FILE
```

A.6 MODIFICATIONS TO STAR

Program STAR is a multigroup shielding code which solves the neutron transport equation in infinite slab geometry by the Method of Invariant Imbedding. Two changes have been made to STAR. The first modification is concerned with the exponential predictor, Equation (3.32) in Mathews' [17] thesis. It was found that, for a laminated Bi-D_2O shield, some group transfers possible in D_2O were impossible in Bi. This meant that some matrix elements in $\underline{R}$ and $\underline{T}$ which remained zero through Bi had to become finite in D_2O. Unfortunately, the exponential predictor is self-starting only if all matrix elements of $\underline{R}$ and $\underline{T}$ are initially zero. Tests were coded to detect this condition, and to linearly integrate the troublesome matrix elements. The integration step was examined and modified as required to keep the value of the matrix elements less than 0.001. From this point on, the exponential predictor again applied. If Δx is the step in the numerical integration of matrix element R, then the solution to

$$\frac{d}{dx} R(x,I,J) = B(x,I,J) + K_r(x,I,J)$$

with the initial condition

$$R(0,I,J) = 0$$

is

$$R(\Delta x, I, J) \simeq R(0, I, J) + (B(0, I, J) + K_r(0, I, J))\Delta X.$$

A similar method is used for the elements of $\underline{T}$.

The second modification to STAR consisted of adding two small subroutines to punch out and read XT, XR, $\underline{R}$, and $\underline{T}_t$ at each step where print-out occurs. Data cards are punched by APO and read by CMO. A control card has been added at the end of normal input to STAR which indicates when an old case is to be restarted be reading in XT, XR, $\underline{R}$, and $\underline{T}_t$. An integer variable, NEWJOB, indicates special input of XT, XR, $\underline{R}$, and $\underline{T}_t$ if it is greater than zero.

A.6.1 LISTING OF STAR MODIFICATIONS

```
*       MAD
 STAR       R PROGRAM STAR
            R  MODIFIED MAY/67 TO ENABLE RESTARTING A CASE.  NEW FUNCTIONS
            R  ARE CMO, TO READ EXTRA DATA, AND APO, TO PUNCH IT
             PROGRAM COMMON ATE,B,C,CC,DR,DRMIN,DRMINS,E,EXPTH,EXPTX,
            1 EXPWH,F,FISS,FOPT,H,HOPT,HR,HRMAX,HRMIN,HRN,HT,HTMAX,HTMIN,
            2 HTN,I,IP,ITC,ITCE,J,JRHOP,K,MAXNIT,MU,MWI,MWJ,NEREG,
            3 NHIT,NITR,NITT,NMUREG,NOR,NS,NSSQ,NXCREG,NXSREG,PSIP,R,RO,
            4 RD,RK,RKO,RT,S,SCS,SD,T,TO,TCS,TCSMUI,TCSMUJ,TD,TER,TERA,
            5 TERS,TET,TETA,TETS,TK,TKO,TMAX,TMAXS,TNON,TONLY,TTOT,VR,
            6 VRI,VS,VSI,VT,VTI,W,WE,WMU,WR,WRO,WT,WTO,XC,XMAX,XPR,XPRINT,
            7 XPU,XPUNCH,XR,XS,XT
             DIMENSION C(32),E(32),FISS(32),MU(32),R(1024,RD),RO(1024,RD),
            1 RD(2),RK(1024,RD),RKO(1024,RD),RT(1024,RD),SCS(2048,SD),SD(2
            2 ),T(1024,TD),TO(1024,TD),TCS(32),TD(2),TK(1024,TD),TKO(1024,
            3 TD),TNON(32),TTOT(1024,TD),VR(64),VS(32),VT(32),W(32),WE(32)
            4 ,WMU(32),XC(256),XS(16)
             INTEGER HOPT,I,IP,ITC,ITCE,J,JRHOP,K,MAXNIT,NEREG,NHIT,NITR,
            1 NITT,NMUREG,NOR,NS,NSSQ,NXCREG,NXSREG,PSIP,S,TONLY,VR,VRI,
            2 VS,VSI,VT,VTI,FOPT
QQ0          EXECUTE TIM.(0)
             EXECUTE INPUT.
             EXECUTE CMO.
QQ10         EXECUTE TIM.(10)
             EXECUTE RHS.
             EXECUTE EXCHAN.(TKO,TK,RKO,RK)
QQ15         WHENEVER HT.L.HTMIN
             PRINT COMMENT $1HT.L.HTMIN.$
             TRANSFER TO END1
             OR WHENEVER HT.G.HTMAX
             HT=HTMAX
             END OF CONDITIONAL
             WHENEVER HR.L.HRMIN
             PRINT COMMENT $1HR.L.HRMIN.$
             TRANSFER TO END1
             OR WHENEVER HR.G.HRMAX
             HR=HRMAX
             END OF CONDITIONAL
             WHENEVER XT+HT.G.XC,HT=XC-XT+1.0E-06
             WHENEVER XR+HR.G.XC,HR=XC-XR+1.0E-06
             WHENEVER HT.G.HR
             HT=HR
             OTHERWISE
             HR=HT
             END OF CONDITIONAL
             PRINT RESULTS HR,HT
QQ25         THROUGH QQ30,FOR I=1,1,I.G.NS
             VSI=VS(I)
             VTI=VT(I)
             TCSMUI=TCS(I)/MU(I)
             EXPTH=EXP.(-TCSMUI*HT)
             THROUGH QQ30,FOR J=1,1,J.G.NS
             VS=VSI+J
             VT=VTI+J
             TO=TO(VT)
             WHENEVER TO.L.1.E-31,TRANSFER TO QQ30
             WTO=TKO(VT)/TO
             WHENEVER WTO*HT .G. 88.
             PRINT COMMENT $OWTO*HT .G. 88.$
```

```
          PRINT RESULTS TKO(VT), TO, HT
         R  EXPONENTIAL APPROX. FAILS TO START R OR T FROM ZERO IF
         R  ENTIRE R OR T MATRIX NOT ZERO, SUCH AS IN MULTI-SLAB
         R  PROBLEMS.  USE ORDINARY INTEGRATION TO GET STARTED.
          F=.ABS.(TKO(VT)*HT)
          WHENEVER F .G. 0.0011
          HT=HT*0.001/F
          HR=HR*0.001/F
          TRANSFER TO QQ25
          END OF CONDITIONAL
          WTO=0.
          TO=TO+TKO(VT)*HT
          PRINT RESULTS I,J,TO
          END OF CONDITIONAL
          EXPWH=EXP.(WTO*HT)
          F=MU(J)*SCS(VS)/W(J)
          T(VT)=EXPWH*TO+F*TNON(I)*(EXPWH-EXPTH)/(TCSMUI+WTO)
QQ30      CONTINUE
          WHENEVER TONLY.E.1,TRANSFER TO QQ50
          THROUGH QQ40,FOR I=1,1,I.G.NS
          VRI=VR(I+NS)
          VSI=VS(I)
          MWI=2.*MU(I)/W(I)
          THROUGH QQ40,FOR J=1,1,J.G.NS
          VR=VRI+J
          VS=VSI+J+NS
          RO=RO(VR)
          WHENEVER RO.L.1.E-31,TRANSFER TO QQ40
          WRO=RKO(VR)/RO
          WHENEVER WRO*HR .G. 88.
          PRINT COMMENT $OWRO*HR .G. 88.$
          PRINT RESULTS RKO(VR),RO,HR
          B=MWI*MU(J)*SCS(VS)/W(J)
          F=.ABS.((RKO(VR)+B)*HR)
          WHENEVER F .G. 0.0011
          HR=HR*0.001/F
          HT=HT*0.001/F
          TRANSFER TO QQ25
          END OF CONDITIONAL
          R(VR)=RO+(RKO(VR)+B)*HR
          PRINT RESULTS R,B
          TRANSFER TO QQ40
          END OF CONDITIONAL
          EXPWH=EXP.(WRO*HR)
          B=MWI*MU(J)*SCS(VS)/(W(J)*WRO)
          R(VR)=EXPWH*(RO+B)-B
QQ40      CONTINUE
QQ50      EXECUTE RHS.
          H=0.5*HT*HT
          TET=0.
          THROUGH QQ60,FOR S=1,1,S.G.NSSQ
          WHENEVER T(S).L.1.E-29
          T(S)=1.E-32
          TRANSFER TO QQ60
          END OF CONDITIONAL
          WTO=TKO(S)/TO(S)
          WHENEVER WTO .G. 1.E+10
          TRANSFER TO QQ60
         R  THIS TRANSFER OCCURS ONLY IF ORDINARY INTEGRATION USED
          END OF CONDITIONAL
          WT=TK(S)/T(S)
```

```
      TETS=-H*WTO*(WT-WTO)
      WHENEVER .ABS.(TETS).G..ABS.(TET),TET=TETS
QQ60  CONTINUE
      TETA=.ABS.(TET)
      WHENEVER TONLY.E.1,TRANSFER TO QQ80
      H=0.5*HR*HR
      TER=0.
      THROUGH QQ70,FOR S=1,1,S.G.NSSQ
      WHENEVER R(S).L.1.E-29
      R(S)=1.E-32
      TRANSFER TO QQ70
      END OF CONDITIONAL
      WRO=RKO(S)/RO(S)
      WHENEVER WRO .G. 1.E+10
      TRANSFER TO QQ70
     R  THIS TRANSFER OCCURS ONLY IF ORDINARY INTEGRATION USED
      END OF CONDITIONAL
      WR=RK(S)/R(S)
      TERS=-H*WRO*(WR-WRO)
      WHENEVER .ABS.(TERS).G..ABS.(TER),TER=TERS
QQ70  CONTINUE
      TERA=.ABS.(TER)
QQ80  WHENEVER HOPT.E.1 .OR. ATE.L.0.,TRANSFER TO QQ110
      WHENEVER TONLY.E.1,TRANSFER TO QQ100
      HTN=((CC/TETA).P..33)*HT
      HRN=((CC/TERA).P..33)*HR
      WHENEVER TETA.G.2.*CC .OR. TERA.G.2.*CC
      NHIT=NHIT+1
      EXECUTE TIM.(90)
      PRINT RESULTS XR,XT,NITR,NITT,HR,HRN,HT,HTN,TER,TET,NHIT
      ITCE=0
      EXECUTE END.
      HT=HTN
      HR=HRN
      TRANSFER TO QQ15
      END OF CONDITIONAL
      XT=XT+HT
      NITT=NITT+1
      XR=XR+HR
      NITR=NITR+1
      EXECUTE OUTPUT.
      ITCE=1
      EXECUTE END.
      EXECUTE EXCHAN.(TO,T,RO,R)
      EXECUTE EXCHAN.(TKO,TK,RKO,RK)
      WHENEVER HTN.L.HTMIN
      PRINT COMMENT $1HTN.L.HTMIN.$
      TRANSFER TO END1
      OR WHENEVER HTN.G.HTMAX
      HTN=HTMAX
      END OF CONDITIONAL
      WHENEVER HRN.L.HRMIN
      PRINT COMMENT $1HRN.L.HRMIN.$
      TRANSFER TO END1
      OR WHENEVER HRN.G.HRMAX
      HRN=HRMAX
      END OF CONDITIONAL
      WHENEVER XR+HRN.GE.XC,HRN=XC-XR+1.0E-06
      WHENEVER XR+HRN.GE.XPR,HRN=XPR-XR+1.0E-06
      WHENEVER ATE.LE.0.
      HOPT=1
```

```
          WHENEVER HTN.G.HRN
          HR=HRN
          HT=HRN
          OTHERWISE
          HR=HTN
          HT=HTN
          END OF CONDITIONAL
          WHENEVER NOR.E.1, TONLY=1
          TRANSFER TO QQ25
          END OF CONDITIONAL
          NHT=HRN/HTN
          INTEGER NHT
          NHT=NHT+1
          HTN=HRN/NHT
          HT=HTN
          HR=HRN
          ITC=0
          WHENEVER NHT.GE.2
          TONLY=1
          OTHERWISE
          TONLY=0
          END OF CONDITIONAL
          WHENEVER NOR.E.1, TONLY=1
          TRANSFER TO QQ25
QQ100     XT=XT+HT
          NITT=NITT+1
          WHENEVER NOR.E.1 .AND. HT.L..99*HTMAX,HTN=((CC/TETA).P..33)
         1*HT
          EXECUTE OUTPUT.
          EXECUTE EXCHAN.(TO,T,RO,R)
          EXECUTE EXCHAN.(TKO,TK,RKO,RK)
          ITCE=1
          EXECUTE END.
          ITC=ITC+1
          WHENEVER ITC.GE.NHT-1,TONLY=0
          WHENEVER NOR.E.1,TONLY=1
          WHENEVER NOR.E.1 .AND. HTN.G.HT
          HT=HTN
          WHENEVER HT.G.HTMAX,HT=HTMAX
          WHENEVER HT.L.HTMIN
          PRINT COMMENT $1HT.L.HTMIN.$
          TRANSFER TO END1
          END OF CONDITIONAL
          END OF CONDITIONAL
          WHENEVER NOR.E.1 .AND. XT+HT.G.XC,HT=XC-XT+1.0E-06
          TRANSFER TO QQ25
QQ110     XT=XT+HT
          NITT=NITT+1
          WHENEVER TONLY.E.1, TRANSFER TO QQ120
          XR=XR+HR
          NITR=NITR+1
QQ120     EXECUTE OUTPUT.
          EXECUTE EXCHAN.(TO,T,RO,R)
          EXECUTE EXCHAN.(TKO,TK,RKO,RK)
          ITCE=1
          EXECUTE END.
          WHENEVER NOR.E.1, TONLY=1
          TRANSFER TO QQ25
          INTERNAL FUNCTION(TT,TTO,RR,RRO)
          ENTRY TO EXCHAN.
          THROUGH EX1,FOR S=1,1,S.G.NSSQ
```

```
EX1         TT(S)=TTO(S)
            WHENEVER TONLY.E.1, TRANSFER TO EX3
            THROUGH EX2, FOR S=1,1,S.G.NSSQ
EX2         RR(S)=RRO(S)
EX3         FUNCTION RETURN
            END OF FUNCTION
            INTERNAL FUNCTION
            ENTRY TO END.
            WHENEVER NHIT.L.20,TRANSFER TO END2
            PRINT COMMENT $2COULD NOT FIND STEP SIZE YIELDING ACCEPTABLE
           1ERROR IN 20 ATTEMPTS. END OF PROBLEM.$
END1        XPR=0.
            TONLY=0
            EXECUTE OUTPUT.
            EXECUTE APO.
            TRANSFER TO QQO
END2        WHENEVER ITCE.E.0,TRANSFER TO END6
            WHENEVER XT.GE.XMAX .OR. XR.GE.XMAX
            PRINT COMMENT $2DESIRED VALUE OF X REACHED. END OF PROBLEM.$
            TRANSFER TO END1
            OR WHENEVER NITT.GE.MAXNIT .OR. NITR.GE.MAXNIT
            PRINT COMMENT $2MAXIMUM NUMBER OF ITERATIONS (STEPS) REACHED.
           1 END OF PROBLEM.$
            TRANSFER TO END1
            END OF CONDITIONAL
            TMAXS=0.
            THROUGH END3,FOR S=1,1,S.G.NS
            TMAXS1=T(S,S)
END3        WHENEVER TMAXS1.G.TMAXS, TMAXS=TMAXS1
            WHENEVER TMAXS.L.TMAX
            PRINT COMMENT $2DESIRED VALUE OF T REACHED. END OF PROBLEM.$
            TRANSFER TO END1
            END OF CONDITIONAL
            WHENEVER NOR.E.1 .OR. TONLY.E.1, TRANSFER TO END5
            DRMINS=0.
            THROUGH END4,FOR S=1,1,S.G.NS
            DR=.ABS.(R(S+NS,S)-RO(S+NS,S))/HR
END4        WHENEVER DR.G.DRMINS,DRMINS=DR
            WHENEVER DRMINS.L.DRMIN
            PRINT COMMENT $0DR.L.DRMIN. PROCEEDING WITH THE CALCULATION
           1  OF T ONLY AFTER A COMPLETE PRINT OUT OF ALL VARIABLES AT TH
           2IS POINT.$
            XXX1=XPR
            XPR=0.
            XXX2=XPRINT
            XPRINT=0.
            XXX3=HT
            HT=0.
            EXECUTE OUTPUT.
            HT=XXX3
            XPRINT=XXX2
            XPR=XXX1
            NOR=1
            END OF CONDITIONAL
END5        EXECUTE DATA.
            WHENEVER VR.G.0 .OR. VT.G.0
            TONLY=0
            NOR=0
            WHENEVER ATE.GE.0.,HOPT=0
            TRANSFER TO QQ10
            END OF CONDITIONAL
```

```
END6        FUNCTION RETURN
            END OF FUNCTION
            END OF PROGRAM
*       MAD
 CMO        RCMO, FOR STAR -- SPECIAL RESTART INPUT ROUTINE
            EXTERNAL FUNCTION
            ENTRY TO CMO.
            PROGRAM COMMON ATE,B,C,CC,DR,DRMIN,DRMINS,E,EXPTH,EXPTX,
           1 EXPWH,F,FISS,FOPT,H,HOPT,HR,HRMAX,HRMIN,HRN,HT,HTMAX,HTMIN,
           2 HTN,I,IP,ITC,ITCE,J,JRHOP,K,MAXNIT,MU,MWI,MWJ,NEREG,
           3 NHIT,NITR,NITT,NMUREG,NOR,NS,NSSQ,NXCREG,NXSREG,PSIP,R,RO,
           4 RD,RK,RKO,RT,S,SCS,SD,T,TO,TCS,TCSMUI,TCSMUJ,TD,TER,TERA,
           5 TERS,TET,TETA,TETS,TK,TKO,TMAX,TMAXS,TNON,TONLY,TTOT,VR,
           6 VRI,VS,VSI,VT,VTI,W,WE,WMU,WR,WRO,WT,WTO,XC,XMAX,XPR,XPRINT,
           7 XPU,XPUNCH,XR,XS,XT
            DIMENSION C(32),E(32),FISS(32),MU(32),R(1024,RD),RO(1024,RD),
           1 RD(2),RK(1024,RD),RKO(1024,RD),RT(1024,RD),SCS(2048,SD),SD(2
           2 ),T(1024,TD),TO(1024,TD),TCS(32),TD(2),TK(1024,TD),TKO(1024,
           3 TD),TNON(32),TTOT(1024,TD),VR(64),VS(32),VT(32),W(32),WE(32)
           4 ,WMU(32),XC(256),XS(16)
            INTEGER HOPT,I,IP,ITC,ITCE,J,JRHOP,K,MAXNIT,NEREG,NHIT,NITR,
           1 NITT,NMUREG,NOR,NS,NSSQ,NXCREG,NXSREG,PSIP,S,TONLY,VR,VRI,
           2 VS,VSI,VT,VTI,FOPT
            INTEGER NEWJOB
            PRINT COMMENT $ONEWJOB$
            READ DATA
            WHENEVER NEWJOB .LE. 0, TRANSFER TO QQ1
            PRINT COMMENT $ARRAYS R, T,TNON, RT, AND VARIABLES VR,VT,TON
           1LY,NOR,RO,XR,XT$
            READ DATA
QQ1         FUNCTION RETURN
            END OF FUNCTION
*       MAD
 APO        RAPO, FOR STAR -- SPECIAL RESTART OUTPUT ROUTINE
            EXTERNAL FUNCTION
            ENTRY TO APO.
            PROGRAM COMMON ATE,B,C,CC,DR,DRMIN,DRMINS,E,EXPTH,EXPTX,
           1 EXPWH,F,FISS,FOPT,H,HOPT,HR,HRMAX,HRMIN,HRN,HT,HTMAX,HTMIN,
           2 HTN,I,IP,ITC,ITCE,J,JRHOP,K,MAXNIT,MU,MWI,MWJ,NEREG,
           3 NHIT,NITR,NITT,NMUREG,NOR,NS,NSSQ,NXCREG,NXSREG,PSIP,R,RO,
           4 RD,RK,RKO,RT,S,SCS,SD,T,TO,TCS,TCSMUI,TCSMUJ,TD,TER,TERA,
           5 TERS,TET,TETA,TETS,TK,TKO,TMAX,TMAXS,TNON,TONLY,TTOT,VR,
           6 VRI,VS,VSI,VT,VTI,W,WE,WMU,WR,WRO,WT,WTO,XC,XMAX,XPR,XPRINT,
           7 XPU,XPUNCH,XR,XS,XT
            DIMENSION C(32),E(32),FISS(32),MU(32),R(1024,RD),RO(1024,RD),
           1 RD(2),RK(1024,RD),RKO(1024,RD),RT(1024,RD),SCS(2048,SD),SD(2
           2 ),T(1024,TD),TO(1024,TD),TCS(32),TD(2),TK(1024,TD),TKO(1024,
           3 TD),TNON(32),TTOT(1024,TD),VR(64),VS(32),VT(32),W(32),WE(32)
           4 ,WMU(32),XC(256),XS(16)
            INTEGER HOPT,I,IP,ITC,ITCE,J,JRHOP,K,MAXNIT,NEREG,NHIT,NITR,
           1 NITT,NMUREG,NOR,NS,NSSQ,NXCREG,NXSREG,PSIP,S,TONLY,VR,VRI,
           2 VS,VSI,VT,VTI,FOPT
            NS=NMUREG*NEREG
            PUNCH FORMAT FRM20
            PUNCH FORMAT FORM1
            PUNCH FORMAT FORM2,R(NS+1,1)...R(2*NS,NS)
            PUNCH FORMAT FORM4
            PUNCH FORMAT FORM2,T(1,1)...T(  NS,NS)
            PUNCH FORMAT FORM6
            PUNCH FORMAT FORM2,TNON(1)...TNON(NS)
            PUNCH FORMAT FRM11
```

```
 PUNCH FORMAT FORM2,RT(NS+1,1)...RT(2*NS,NS)
 PUNCH FORMAT FRM14,VR,VT,TONLY,NOR,RO,XR,XT
 VECTOR VALUES FORM1=$8HR(   ,1)=*$
 VECTOR VALUES FORM2=$4(E15.8,1H,)*$
 VECTOR VALUES FORM4=$7HT(1,1)=*$
 VECTOR VALUES FORM6=$8HTNON(1)=*$
 VECTOR VALUES FRM11=$9HRT(   ,1)=*$
 VECTOR VALUES FRM14=$3HVR=,I3,4H,VT=,I3,7H,TONLY=,
1   I2,5H,NOR=,I2,4H,RO=,E11.4,4H,XR=,F9.4,4H,XT=,F9.4,1H**$
 VECTOR VALUES FRM20=$9HNEWJOB=1**$
 FUNCTION RETURN
 END OF FUNCTION



     END OF FILE
```

APPENDIX B

BIBLIOGRAPHY

1. Locher, G. L., Am. J. Roentgenology and Radium Therapy 36, 1(1936).
2. Sweet, W. H. and M. Javid, J. Neurosurgery 9, 200 (1952).
3. Farr, L. E., Science 130, 1067 (1959 and J. C. A. E. Hearings, Wash. D. C. (1961); Asbury, A. K. and Ojemann, R. J., Journal of Neuropathology and Experimental Neurology 24, 157 (1965).
4. Brownell, G. L., A. H. Soloway and W. H. Sweet, "Boron Capture Therapy", Modern Trends in Radiotherapy 1, 132 (1967).
5. Soloway, A. H., G. L. Brownell, R. G. Ojemann, and W. H. Sweet, "Boron-Slow Neutron Capture Therapy: Present Status", Report EUR-2200C, EURATOM (1965).
6. Soloway, A. H., H. Hatanaka, and M. A. Davis, J. Med. Chem. Vol. 10, 4, 714 (1967).
7. Aronson, R. and D. L. Yarmush, J. Math. Phys. 7, 221 (1966).
8. Eaton, M. L. and C. M. Huddleston, "A Markov Matrix Treatment of Neutron Diffusion in Slabs", Nuc. Sc. and Eng., Vol. 27 2, 475 (Feb. 1967).
9. Chandrasekhar, S., Radiative Transfer, Oxford, (1950).
10. Kronrod, Aleksandr Semenovich, Nodes and Weights of Quadrature Formulas, Consultants Bureau, New York (1965).
11. SDA-3079 - EXPI - Exponential Integrals, Share Library, M.I.T. Computation Center.

12. SDA-1206, LEQ - Linear Equations, Share Library, M.I.T. Computation Center.

13. SDA-1514 F, RTSCH - Roots of a Polynomial, Share Library, M.I.T. Computation Center.

14. SDA-1124 F, MULLER - Polynomial Root Finder Subroutine Share Library, M.I.T. Computation Center.

15. SDA-3044, TAINT - Table Look Up and Interpolation, Share Library, M. I. T. Computation Center.

16. Bondarenko, I.I. (Ed.) Group Constants for Nuclear Reactor Calculations, Consultants Bureau, New York (1964).

17. Mathews, Donald Richard, Calculation of the Deep Penetration of Radiation by the Method of Invariant Imbedding, Ph.D. Thesis, M.I.T. Dept. of Nuclear Engineering, (June 1966).

18. Bellman, R.E., R.E. Kalaba, and G. M. Wing, "Invariant Imbedding and Mathematical Physics I, Particle Processes", J. Math. Phys., 280 (1960).

19. SDA-1171, RKS3 - Fortran Floating-Point Runge-Kutta (or Simpson's Rule) Integration With Simpson's Rule Check. Share Library, M.I.T. Computation Center.

20. Avery, A. F., D. E. Bendall, J. Butler, and K. T. Spinney, "Method of Calculation for Use in the Design of Shields for Power Reactors." AERE-R-3216 (1960).

21. Ridley, E. C., "A Numerical Method of Solving Second-Order Linear Differential Equations with Two-Point Boundary Conditions." Proc. Camb. Phil. Soc., Vol. 53, p. 442 (1957).

22. Snyder, W. S. and J. Neufeld, Brit. J. Radiol. 28:324 (1955).

23. N.B.S. Handbook 63. Protection Against Neutron Radiation up to 30 Million Electron Volts, U.S. G.P.O. (1957).

24. Rydin, Roger Alan, Fast Neutron Spectroscopy and Dosimetry of the M.I.T. Reactor Medical Therapy Facility Beam, Ph.D. Thesis, M.I.T. Dept. of Nuclear Engineering, (June 1964).

25. Etherington, Harold (Ed.) Nuclear Engineering Handbook, McGraw-Hill Book Co., New York (1958).

26. Okazaki, E. A. and J. K. Fowler, "Library Programs for the AECL G-20 Computer", AECL-1744 (Part A), (1963).

27. Bellman, R.E., and R. E. Kalaba, Editors, Invariant Imbedding and Radiative Transfer in Slabs of Finite Thickness. American Elsevier Publ. Co., New York (1963).

28. Allen, F. J., A. T. Futterer, and W. P. Wright, "Neutron Transmission Versus Thicknesses for Some Common Materials", BRL-1174, Ballistic Research Laboratories, Aberdeen Proving Ground, Maryland (1962).

29. Goldstein, H. "Neutron Cross Sections for Neutron Attenuation Problems Proposed by the A.N.S. Shielding Division". TID - 21294 (1963).

30. "Angular Distributions in Neutron-Induced Reactions", BNL-400 (2nd Edition), Office of Technical Services, Dept. of Commerce, Washington, D.C. (1964).

31. "Neutron Cross Sections", BNL-325 (and Edition) Supp. 2, Vol. I, Office of Technical Services, Dept. of Commerce, Washington, D.C. (1964).

32. Godel, Jules B., "Description of Facilities and Mechanical Components Medical Research Reactor" BNL - 600, Office of Technical Services, Dept. of Commerce, Washington, D.C. (1960).

33. Fairchild, R. G., "The Development of an 'Epithermal' Neutron Beam for Possible Use in Neutron Capture Therapy". Physics in Medicine and Biology, Vol.10, 4, 491 (1965).

34. Schermer, R. I. and Gordon Brownell, Nuc. Sc. and Eng. 11 (1961).

35. Mathews, R. L. Flux Distributions in the M.I.T. Reactor, Ph.D. Thesis, M.I.T. Dept. of Nuclear Engineering (1964).

36. SDA-1230, GAS4-4 Point Gaussian Integration, Share Library, M.I.T. Computation Center.